# GEO-3900

## MASTER'S THESIS IN GEOLOGY

---

# First-order estimation of in-place natural gas resources at the Nyegga gas hydrate prospect, mid-Norwegian Margin

Kim Senger

November, 2009

FACULTY OF SCIENCE
Department of Geology
University of Tromsø

GEO-3900

MASTER'S THESIS IN GEOLOGY

# First-order estimation of in-place natural gas resources at the Nyegga gas hydrate prospect, mid-Norwegian Margin

Kim Senger

November, 2009

## Abstract

Gas hydrates are solid compounds of a guest gas molecule (primarily methane) enclosed in a lattice of host water molecules, occurring under specific pressure-temperature (P-T) conditions in both natural and man-made environments. Traditionally gas hydrates were considered more as a nuisance, due to their tendency to plug hydrocarbon pipelines. However, in the past decade, gas hydrates are increasingly investigated as a potential new energy source. Globally, it is estimated that hydrate may contain as much as 1 to $5 \times 10^{15} m^3$ of gas (Milkov 2004), an order of magnitude higher than all conventional gas fields combined.

In order to consider methane hydrate as an unconventional gas resource, it is vital to quantify its presence in the regional setting. This thesis presents an integrated evaluation of the gas bound within the hydrate province of the Nyegga area, located in the southern Norwegian Sea on the north slope of the Storegga slide scar. Gas hydrates have long been inferred in the region on the basis of bottom simulating reflections (BSRs), and were physically sampled in 2006 (Ivanov *et al.* 2007). Furthermore, modelling of the hydrate stability zone suggests that the BSR is most likely related to the acoustic contrast between the solid gas hydrate and the underlying free gas zone. This is confirmed by numerous ocean bottom seismic (OBS) experiments, revealing a decrease in P-wave velocity across the BSR (Bünz and Mienert 2004, Bünz *et al.* 2005b, Westbrook *et al.* 2008a, Faverola *et al.* 2009).

This approach, making use of all the available data and standard industry tools (Petrel, GeoX), calculates the in-place gas bound within the solid gas hydrate zone, the underlying free gas zone and a localised chimney zone. A prospect, defined by the BSR-extent, is evaluated with focus on the uncertainty of the various reservoir parameters. The lateral variation in reservoir parametes, particularly the 3D reservoir extent and gas saturation, is poorly constrained using the available data and thus results in a large range of input parameters. A stochastic Monte Carlo-type calculation was conducted to give a probability range of in-place resources. Reservoir parameters are primarily based on a multitude of geophysical models and one shallow geotechnical borehole, as well as global analogues. Different parameters were assigned to three different zones, comprising a regionally extensive gas hydrate zone, its associated free gas zone and a chimney zone assumed to contain solid gas hydrate.

The Nyegga prospect appears to hold approximately $615 GSm^3$ of gas in the mean case, roughly comparable to the recoverable Ormen Lange gas reserves. The uncertainty related to the input parameters gives a wide spread of in-place volumes of ca. $150 GSm^3$ (P90) to $>1400 GSm^3$ (P10). The majority of the resources appear to be bound in the solid gas hydrate zone, followed by the free gas zone and the chimney zone. The average resource density ($0.2\, GSm^3/km^2$) is roughly comparable to similar hydrate provinces. It is notable that potential exists for proving additional resources both in the immediate area around the Nyegga prospect, as well as in other regions on the Norwegian continental shelf.

# Contents

## Acknowledgments

This project was undertaken in partial fulfillment of a Master of Science (MSc) degree at the University of Tromsø, under the guidance of Dr Jürgen Mienert and Dr Stefan Bünz. I am primarily indebted to the aforementioned gas hydrate experts for allowing me to undertake this thesis within the stimulating Geology Department in Tromsø, offering advice and discussions throughout.

The work was supported, both financially and through knowledge transfer, by Bayerngas Norge AS, which I am extremely grateful for. I particularly wish to thank Mr Arne Westeng, Dr Gregor Neunzert, Ms Catherine Holter and Ms Nina Dahl for allowing me to complete the MSc during my employment at Bayerngas Norge AS. Furthermore, Dr Karsten Schütz, Dr Branimir Cvetkovic and Dr Birger Dahl have played a vital role in schooling me in the wide world of the oil & gas industry. Ms Siri Clemet has aided me in compiling the necessary well and seismic database. Bayerngas Norge AS also provided access to the licenses to the key software used in this thesis, notably Petrel, GeoX, Seismic Toolkit and Grapher.

Data used in this integrated project come from a wide array of sources. Full references are given within the text, but I would like to especially thank Dr Reidar Lien at StatoilHydro for granting me access to the long-lost wireline and VSP data for the 6404/5 GB1 geotechnical borehole and allowing me to use it in this thesis. I am also indebted to Dr Anders Solheim for helping me in the quest of finding these data. Oceanographic data, particularly time-series data collected as part of the Ormen Lange development project, have been generously provided by StatoilHydro through Fugro Geos. The SEABED consortium provided much of the critical data of this study, particularly the geotechnical reports on the shallow drilling project. Dr Graham Westbrook and Ms Andreia Plaza Faverola are thanked for granting access to their OBS studies, while Dr Haflidi Haflidason is acknowledged for providing recent literature.

Discussions with fellow students, especially Dr Jörg Petersen and Dr Steinar Hustoft, served to direct this study. Dr Steinar Hustoft and Mr Wiktor Weibull are further acknowledged for generously making their previous study of the Nyegga gas chimneys available. Furthermore, Dr Tim Collett, Dr Dendy Sloan and Dr Charles Paull are acknowledged for sharing their insight into specific aspects of hydrate formation and production.

Apart from this MSc thesis, I have had, thanks to my supervisors Dr Jürgen Mienert and Dr Stefan Bünz, the chance to participate in the GEO-3144 research cruise to the West Svalbard hydrate province. While none of the data collected during this cruise is used in this thesis, the cruise served as an extremely educative and fruitful experience with respect to understanding methane fluxes in the subsurface.

Last but not least, I'd like to thank Dr Andrew Gorman who originally introduced me to gas hydrates.

---

0

*This document has been written in TEXNic Center, typeset with LaTeX 2ε, compiled using MikTeX and referenced using BibTeX.*

# Chapter 1

# Introduction

## 1.1 Objectives

The main objective of this Master's thesis is to: ***provide a best technical estimate for the total in-place natural gas encaged within the gas hydrate and free gas zones of the Nyegga area and discuss the possibility of its potential economic extraction.***

This is systematically addressed through the following sub-objectives:

- Constraining the regional three-dimensional gas hydrate stability zone through the modeling of ocean bottom temperatures, geothermal gradients and hydrate composition.
- Identifying the 2D areal extent of the gas-hydrate related BSR[1] using both existing high-density 3D seismic information and new regional 2D seismic interpretation.
- Developing a 'sub-regional' 3D model of the concentration of gas hydrates and free gas to gain a better understanding of the total amount of gas stored in such a geological setting.
- Utilizing previous work to constrain the nature of relevant features (e.g. chimneys) and incorporate them into the 3D model, along with relevant uncertainty ranges.
- Conducting a volumetric calculation of in-place hydrate resources, together with relevant

[1] BSR = bottom simulating reflection

uncertainties.

- Demonstrating possible development concepts.
- Considering an economic evaluation of extracting hydrates from the Nyegga system.
- Commenting on possible data acquisition that could reduce the uncertainty of the presented results.

## 1.2 Thesis structure and outline

To fulfill the above aims and objectives, I have structured the thesis into 8 chapters:

1. ***Introduction:*** Apart from investigating the objectives and structure of this thesis, the introduction reveals the motivation of looking at producing gas hydrate in Norway.
2. ***Gas Hydrates:*** A review chapter on gas hydrate research is, while solely literature-based, important in understanding the complex processes that drive hydrate formation and dissociation.
3. ***Nyegga area study site:*** A chapter to introduce the study site in terms of its physical evolution.
4. ***Database and Methods:*** An overview of the data used in this thesis, as well as a review of the methods applied.
5. ***Results:*** The main body of the thesis, namely the prospect evaluation of the Nyegga gas hydrate prospect. This chapter also includes a section on the hydrate stability modeling as well as an overview of the seismic interpretation conducted.
6. ***Development & Economics:*** A brief outline of how the Nyegga prospect may be produced, and a brief speculative investigation in how much such a development may cost.
7. ***Discussion:*** Overview of the significance of the calculated in-place results, including comparison with other hydrate provinces.
8. ***Conclusions:*** The accomplishments of the Master's thesis are given here.

Apart from the main body of the Master's thesis, the appendix provides further thesis-related data including high resolution plots and illustrations. A general evaluation of possible environmental side-effects of a hydrate development offshore Norway is provided in the HSE section of the appendix. Interpretations and the underlying data sets are provided on the accompanying DVD.

## 1.3 Motivation

Looking at gas hydrates from the development point of view is a challenging idea on the Norwegian continental margin. The 'Norwegian' gas hydrates have, however, been intensely studied, both in terms of flow assurance (Gudmundsson 2002, Ilahi 2005) but also due to their possible implications in submarine landslides (Bryn *et al.* 2005b, De Blasio *et al.* 2005, Forsberg and Locat 2005, Mienert *et al.* 2005a;b, Løvholt *et al.* 2005, Kvalstad *et al.* 2005, Nadim *et al.* 2005, Solheim *et al.* 2005a, Bryn *et al.* 2005a, Solheim *et al.* 2005b). Resource estimates so far have, however, been limited to regional investigations of the Barents Sea (Laberg *et al.* 1998) and the West Svalbard province (Hustoft *et al.* 2009, Hustoft 2009).

### 1.3.1 Forecasting demand for natural gas

Global demand for energy is increasing, nearly doubling in the period 1970-2006 (Figure 1.1).

Demand for natural gas will fundamentally depend on the global energy requirements. Virtually all scenarios (Bentley 2002, IEA 2006; 2008, MPE/NPD 2008, Holditch and Chianelli 2008) predict an increased use of energy, fundamentally driven by economic growth in highly populated regions such as Asia and Africa.

There is a strong correlation between a country's gross domestic product (GDP) and its fossil fuel consumption (Figure 1.2). Note that both of the most populated countries in the world, China and India, plot on the lower left of the graph. Development of such countries towards even the European Union average of ~10 b.o.e./year[2] will inevitably put a strain on global energy supplies.

[2]b.o.e. = barrels of oil equivalents. This refers to the standard measure of quantifying energy demand from a range of petroleum products. Please note that 1 barrel of oil equates to 0.159 standard cubic metres.

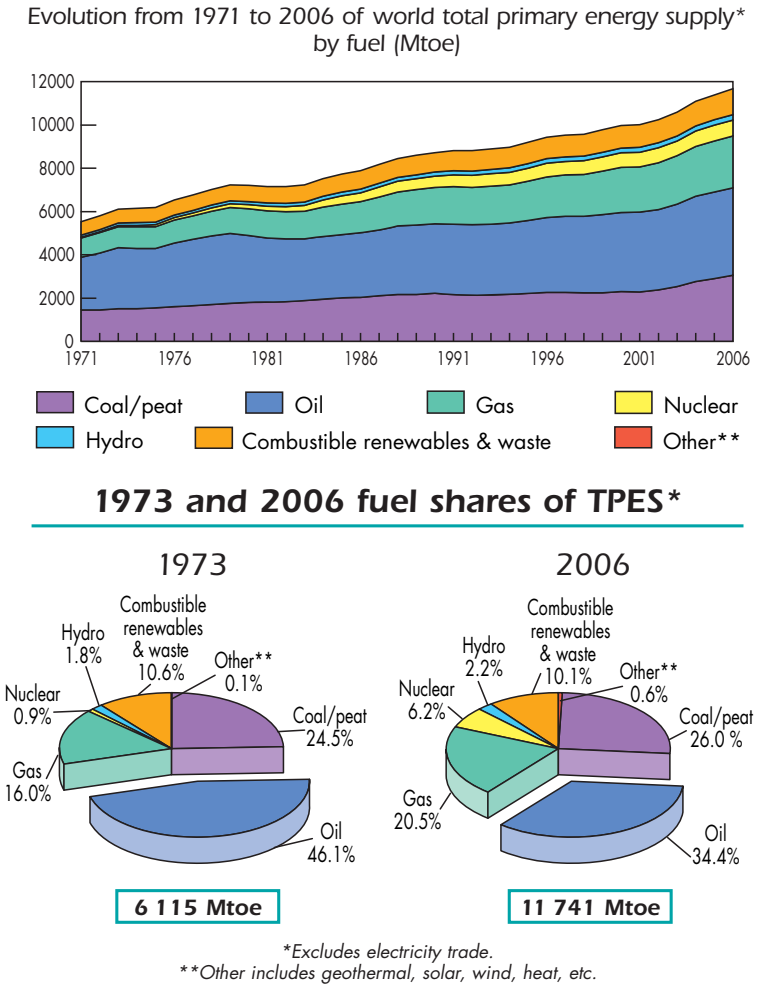


Figure 1.1: Global energy usage subdivided into its sources. It is notable that energy production from crude oil is falling at the expense of natural gas, nuclear and coal. Note the nearly constant share of renewable supplies. Data source: IEA (2008).

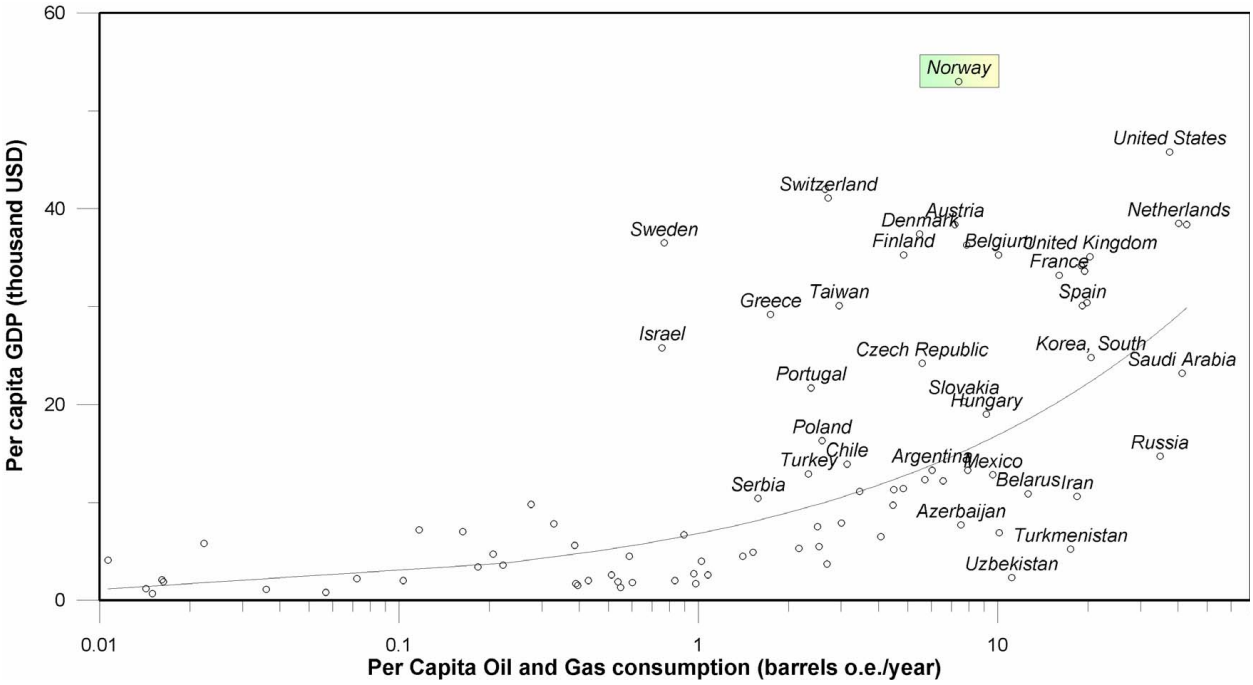


Figure 1.2: Graph comparing per capita oil & gas consumption with the per capita GDP. Please note that, for clarity, countries with less than 5 million inhabitants or with a per capita consumption lower than 0.01 barrels of oil equivalents (b.o.e.) have not been included. Note the logarithmic x-axis. Data source: CIA (2008).

Estimates further suggest a 50-60% increase in global energy demand between 2008 and 2030, primarily due to a rising global population and an increase in the energy-intensive standard of living (Holditch and Chianelli 2008).

Strong focus on environmental-friendly renewable energy sources has the potential to reduce this strain, as seen by the development of the Scandinavian countries, but it remains to be seen whether such a concept is viable in highly populated countries with heavy industries. In addition, renewable energy provided a nearly constant 10% supply for the past 30 years, and a valid argument concerns the plausibility of increasing this to the '20% by 2020' as stipulated by a recent EU Directive (2008), given current technical, environmental, social, political and economical challenges.

| | Parameter | Reservoir classes according to gas recoverability | | | | |
|---|---|---|---|---|---|---|
| | | Class 1 (Sweet spots) | Class 2 | Class 3 | Class 4 | Class 5 |
| Geological parameters | Permeability | **> 0.1 mD** | **< 0.1 mD** | **> 0.1 mD** | **> 0.1 mD** | **> 0.1 mD** |
| | Natural gas share in gas phase | **> 80 %** | **> 80 %** | **< 80 %** | **> 80 %** | **> 80 %** |
| | Reservoir depth | **< 4.5 km** | **< 4.5 km** | **< 4.5 km** | **> 4.5 km** | **< 4.5 km** |
| Technological parameters | Recoverable gas reserves density in reservoir(s) | **> 0.2 GSm$^3$/km$^2$** | **> 0.2 GSm$^3$/km$^2$** | **> 0.2 GSm$^3$/km$^2$** | **> 0.2 GSm$^3$/km$^2$** | **< 0.2 GSm$^3$/km$^2$** |
| | Gas flowrate per vertical well with usual perforation | **> 20 000 m$^3$/day** | **> 20 000 m$^3$/day** | **> 20 000 m$^3$/day** | **> 20 000 m$^3$/day** | **< 20 000 m$^3$/day** |
| | Wellhead pressure | **> 2MPa** | **> 2MPa** | **> 2MPa** | **> 2MPa** | **< 2 Mpa** |
| Types of UGR | | Coalbed methane, gas hydrates, gas shales | Tight sands, coalbed methane, gas hydrates, gas shales | Gas hydrates, coalbed methane | Deep reservoir | All sources except deep reservoirs. Production for local needs (non-industrial) |

Figure 1.3: Geological and technological criteria for classifying unconventional gas resources. Note that gas hydrates can occur in any of the mentioned classes, with the exception of the deep reservoir more than 4.5 km deep. Flow rates are primarily a function of saturation. Also note that the Nyegga province has a resource density range of 0.08 to 0.62,$GSm^3/km^2$. Figure adapted from Yakushev (2008). Units: mD = milli Darcy; GSm$^3$ = billion standard cubic meters; MPa = mega Pascal.

### 1.3.2 Gas hydrate as an unconventional gas resource

Gas hydrate can be regarded as an unconventional gas resource, along with shale gas, tight sands and coal bed methane (Figure 1.3). These resources are, along with conventional gas, competitors to gas hydrates in terms of providing energy at an acceptable cost.

#### 1.3.2.1 Why are gas hydrates considered as a potential resource?

The development of any natural gas resource, conventional or unconventional, is much more market-dependent than the development of oil provinces. This is mostly due to the higher transportation cost of gas, on a per-unit-energy basis, compared to that of oil (Max *et al.* 2006). Expensive infrastructure, such as Trans-Canada's 2750 km Alaska pipeline project (Trans Canada 2008), need to be constructed to make gas development feasible. Gas has therefore traditionally been considered more as a flareable nuisance, especially in countries with large reserves and few customers. As recently as 2004, a World Bank report estimated a global annual flaring volume of 110 GSm$^3$ of natural gas, equivalent to the combined annual consumption of Germany and France (World Bank

Group 2004) and more than the annual Norwegian gas export of 2007[3].

If pipelines are not feasible for gas transportation, natural gas can be compressed (Demirbas 2002), liquefied (Abdalla and Abdullatef 2005) or hydrated (Gudmundsson and Borrehaug 1996, Kanda 2006) for oceanic transport. Liquefied natural gas (LNG) currently seems the most popular method, but requires expensive LNG plants to be built. Even though the price tag of an LNG plant (US$1.5-2 billion, EIA (2003)) remains high, LNG is increasingly popular due to the manageable risk and the adequate level of technical know-how and expertise. In comparison, developing gas hydrates would require high-risk investments with limited know-how and expertise, but with potentially very high rewards.

Norwegian infrastructure and export routes already exist for parts of the Norwegian continental margin. Future hydrate developments, provided they are undertaken within the lifetime of existing and potential new installations, may be able to use both the facilities themselves and the local know-how gathered during 50 years of the Norwegian oil adventure.

Public opinion in most of the Western world nevertheless dictates a shift towards more environmentally-friendly fuels, partly in response to the debated threat of global warming (Lindzen 1990, Victor 2001, Root *et al.* 2003). Natural gas, with its lower 'per-unit-energy' carbon emissions than all other fossil fuels (Figure 1.4), is seen by many as a bridge towards a renewable energy-dominated society within the next 100 years (Moessner, pers. comm. 2008).

In Norway, for example, pressure is put on oil & gas producing companies to electrify their offshore platforms from non-$CO_2$ emitting energy sources on land (Energy Current 2008). In addition, major projects on $CO_2$ sequestration and storage are creating value in a technology that may have large short-term benefits on reducing atmospheric $CO_2$ emissions (Braathen 2009). With the possibility of a global $CO_2$ tax and a subsequent $CO_2$ storage market, natural gas is arguably becoming the most important fossil fuel of the next 50 years.

[3]In 2007, Norway exported 86.7 $GSm^3$, third only to Russia (199.5 $GSm^3$) and Canada (87.3 $GSm^3$) in terms of global gas export.

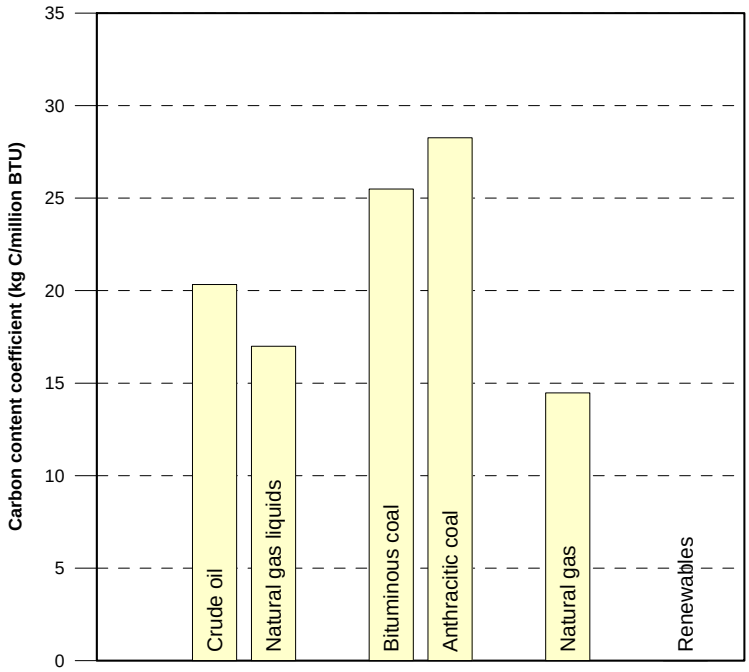


Figure 1.4: Emission coefficients for various fossil fuels. The figure illustrates the amount of carbon produced in order to generate energy equivalent to one million BTUs (British Thermal Units) from a range of fuels. Note particularly the lower carbon emissions from natural gas compared to both coal and crude oil, the main reason why natural gas is regarded as a 'bridge' to a fossil fuel free future. Data source: EIA (2008a) and EPA (2009).

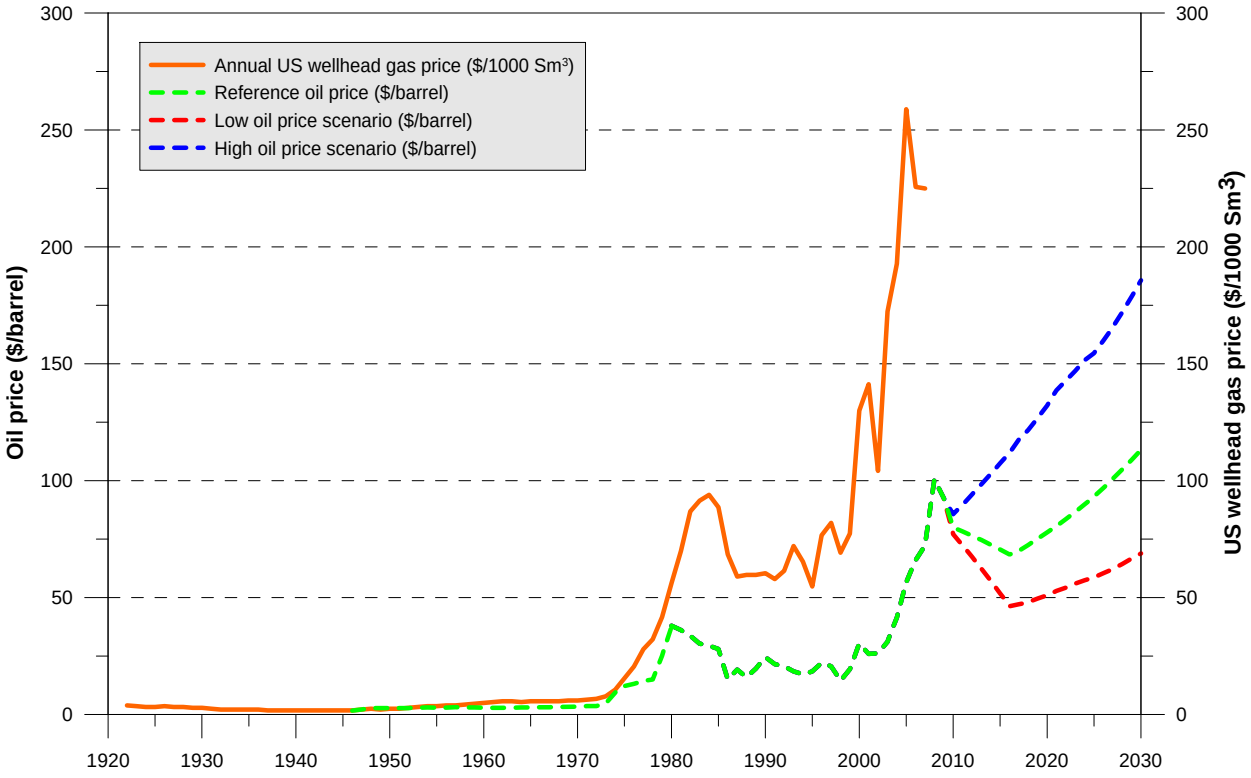


Figure 1.5: Historical and prognosed annual oil (dashed) and gas (solid) prices, illustrating that the gas price generally follows the trend of oil price development. This development is a function of market dynamics (supply and demand), which is strongly affected by world events such as the Gulf War. Historical oil & gas data is provided by EIA (2008c;b), while oil price predictions are provided by IEA (2008). Please note that energy prices are not adjusted for inflation. The two axes have the same range to ease readability, and reflect the energy price for oil (in $ per barrel on the left axis) and gas (in $ per thousand cubic metres on the right axis).

### 1.3.3 Production of unconventional gas resources

Unconventional gas resources are already readily produced, with gas production from shale gas, tight sands and coal bed methane in the USA rising from 17% of total domestic gas production in 1990 to 32% in 2003 (Max *et al.* 2006). This rapid increase is driven both by advancement in applied technologies, government incentives and a steadily rising cost of energy (Figure 1.5). As with LNG, the economic risks are now manageable.

Unconventional resources are currently developed primarily in the United States, though the

interest is slowly spreading globally. Projects in Canada, Australia and Saudi Arabia are amongst those developed in the past 10 years (NPR 2007). Estimates for global in-place resources indicate 255 000 $GSm^3$ in coal bed methane, 453 000 $GSm^3$ as shale gas and 210 000 $GSm^3$ in tight gas sands, mostly within North America and the former Soviet Union (Holditch 2006).

Examples of successful integration of those unconventional gas resources into the North American gas supply are outlined by Max *et al.* (2006). The development of hydrates will require much the same approach, through developing reliable exploration and production technologies while at the same time considering factors such as the investment required, natural gas demand and the environmental consequences. As seen with other unconventional resources, availability and sharing of geological and engineering knowledge will be as important as government-level natural gas policies in lieu of the general state of the gas market in developing the gas hydrate resource.

### 1.3.4 The Norwegian hydrocarbon industry

Norway ranks as the world's $5^{th}$ largest oil producer and as the world's $3^{th}$ largest gas producer (MPE/NPD 2008). For a country of less than 5 million inhabitants (CIA 2008), this makes the petroleum industry one of the key pillars of Norwegian society. Through its 58% share in total exports the industry provided 31% of Norway's 2007 state revenues (MPE/NPD 2008). Production has traditionally been from the giant oil fields Ekofisk, Statfjord, Oseberg and Gullfaks, though gas production is becoming increasingly more significant (Figure 1.6).

In comparison with the majority of the other major petroleum exporting countries, Norway has been concerned about developing its petroleum resources in a sustainable and environmentally-conscious way. The $CO_2$ tax, implemented in 1991, is an example of how government policies can shift focus to developing new technologies that cut back on emissions. Due to advanced technology, such as $CO_2$ injection and combined cycle power plants on platforms, as well as the strict environmental legislation, Norway now emits less than 50% of the global average emission per unit energy produced (MPE/NPD 2008).

The industry's scenario-based outlook towards 2046, as outlined by the Norwegian Petroleum

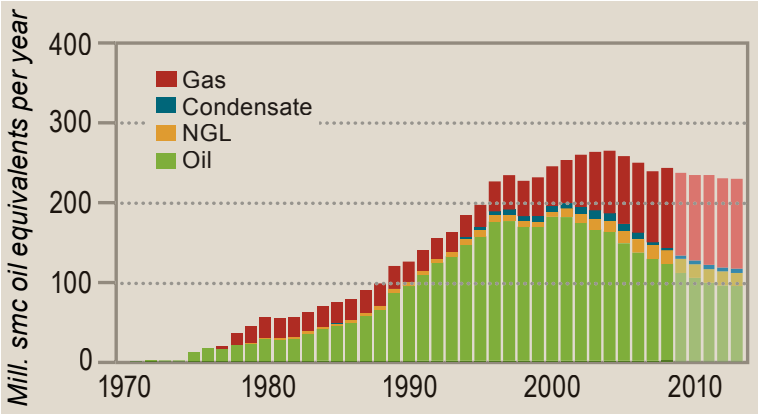


Figure 1.6: Historical gas and liquid production (in million standard cubic metres oil equivalents per year) on the Norwegian continental shelf, with a five-year production forecast. It is notable that natural gas is, since the year 2000, steadily becoming Norwegian's major export hydrocarbon. Infrastructure developed for this purpose could eventually be used in developing gas hydrate deposits. Figure from NPD (2009c).

Directorate (NPD 2007), shows definite production decline within the next 10 years (Figure 1.7). The most pessimistic scenario predicts a steep decline in production to a quarter of present-day by 2020. The most optimistic scenario, on the other hand, maintains production in excess of 200 $MSm^3$ o.e. per year[4]. This scenario incidentally involves the production of gas from gas hydrates (NPD 2007).

### 1.3.5 When will hydrate be developed?

No obvious show-stoppers to hydrate development have been identified (Bil 2003). The global hydrate-bound resource base is deemed significant even if only considering the conservative estimates (Lee and Holder 2001, Collett 2002, Beauchamp 2004, Sloan and Koh 2008). While technology needs to be refined, production tests in the Canadian Arctic have proven the feasibility of using conventional gas recovery equipment for hydrate extraction (Dallimore and Collett 2005). Extensive offshore campaigns in the Nankai Trough and the Gulf of Mexico have penetrated many

[4]Please note that volumes in this thesis are given according to the Norwegian Petroleum Directorate standards, available at www.npd.no and in the appendix. $MSm^3$ refers to millions of standard cubic metres of oil ($*10^6$), while $GSm^3$ refers to billions of standard cubic metres of gas ($*10^9$). Volumes comprising both oil and gas are traditionally given in oil equivalents (o.e.).

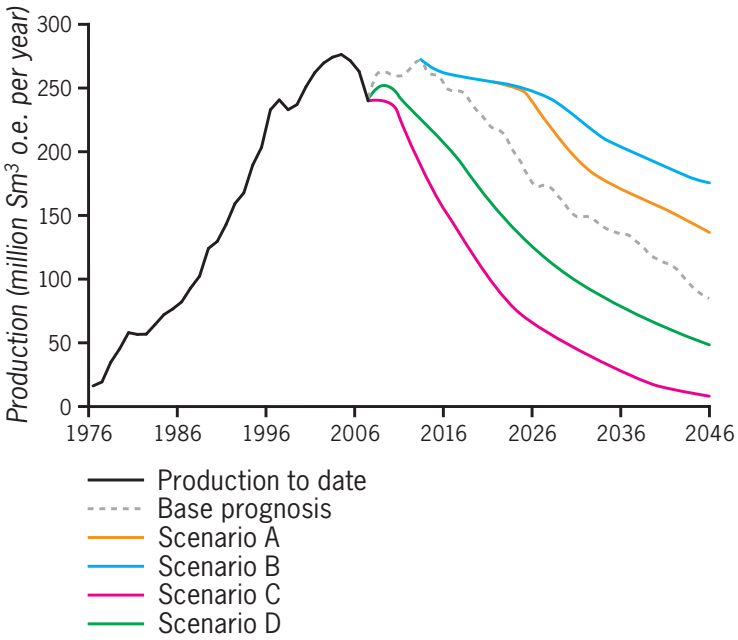


Figure 1.7: Graph showing predicted total annual production from the Norwegian continental shelf based on four different scenarios, as compared to historical production in the period 1976-2007. Note that production is given in oil equivalents (o.e.) and comprises both oil and gas fields. Note that the most optimistic scenario, 'Scenario B', includes the production of gas from hydrate deposits. Figure from (NPD 2007).

hydrate-saturated reservoirs and demonstrated the use of conventional offshore drilling tools for hydrate resource assessment (Juichiro *et al.* 2002, MH21 2008, Ruppel *et al.* 2008).

In 1992, the National Petroleum Council benchmarked the cost of gas hydrate production and found it to be uneconomical in the competitive global energy market (Collett 2002). During the 1990s, with low oil prices plummeting to below 10$ per barrel (EIA 2008d), Hovland *et al.* (1997) also concluded that the gas hydrates within the Niger Delta are too dispersed to be economically producible. New technologies and adaptations of existing technologies, coupled with the increased global demand for energy, have since made gas hydrate development more feasible. Makogon *et al.* (2007) argue that costs related to gas hydrate production in permafrost regions are only 15-20% higher than developing the associated gas field. These authors particularly point to the lower drilling costs of accessing shallow hydrate in comparison to deep conventional gas resources. Depressurisation-induced hydrate production has been shown to be economic over a 15-year production period (Howe *et al.* 2004), though the model and assumptions used were highly simplistic.

Collett (2002) argues that significant worldwide gas hydrate production is unlikely to occur within the next 30-50 years, though he admits that certain motivations could significantly reduce this time, possibly to less than 10 years. Johnson and Max (2006), assume an increasing price of natural gas and the emergence of gas hydrate as a commercial resource by 2011.

Political and economic motivations are particularly important for net energy-importing countries. Both India and Japan are prime examples of implementing highly ambitious and well-funded hydrate research programs at the national level in order to make use of their indigenous resources. For Japan, which is currently importing ~97% of its consumed gas (Milkov and Sassen 2002), the development of the Nankai Trough gas hydrate province would be as much a question of economics as that of national energy security.

It is most likely that hydrates will initially be developed in conjunction with conventional gas, as was the case with Messoyakha and North Slope Borough (Collett and Ginsburg 1998, Makogon *et al.* 2004; 2007, Singh *et al.* 2008). The access to markets via well developed infrastructure, coupled with subsurface and technical competence in a region, would make the North Slope of

Alaska a possible candidate for permafrost-hydrate production.

Political motivations, essentially driven by public opinion, are forcing a shift from polluting to renewable energies. With its lower carbon dioxide emissions than crude oil, natural gas from methane hydrates may act as a bridge towards a cleaner energy source. Subsidies through taxation and regulations would allow willing governments to focus research efforts into hydrate production.

In Norway, NPD refers to hydrates as a possible unconventional petroleum resource, elaborating that 'the technological challenges and costs are expected to be great' (NPD 2007). On the positive side, the Norwegian continental shelf has a reasonably well developed conventional infrastructure which could be used for the future development of hydrates.

### 1.3.6 The case for gas hydrate

Gas hydrate has, as a resource, several key advantages that may fast-track its development. It is essentially a global resource, occurring in vast quantities also in territories of countries traditionally reliant on importing energy. Furthermore, its main product, the natural gas methane, can be handled using existing gas infrastructure and produces less harmful emissions than both oil or coal (Englezos and Lee 2005). It may thus form a natural bridge to a more sustainable and environmentally-conscious energy industry. Finally, production tests have proven the viability of producing gas hydrates with only slight modifications to conventional technologies.

# Chapter 2

# Gas hydrates

The growing interest in gas hydrates is perhaps best exemplified by Figure 2.1, illustrating that approximately four new papers on hydrates are currently published every day.

This chapter aims to introduce the reader to gas hydrates. It is structured in order to form the foundation for the following chapters, with focus on gas hydrate distribution, exploration techniques and maturing hydrates towards producible resources.

## 2.1 Introduction to gas hydrates

### 2.1.1 What are gas hydrates?

Gas hydrates are solid non-stoichiometric compounds of small gas molecules set in a rigid cage of water molecules (Kvenvolden 1998; 2000; 2002, Sloan and Koh 2008). Occasionally, natural gas hydrates are found in shallow cores, dredge samples or by scientific submarines in marine and lacustrine environments (Figure 2.2a). More frequently, hydrates are found as an unwanted solid and flow-blocking blob in hydrocarbon pipelines (Figure 2.2b). In physical appearance hydrates somewhat resemble snow, but a quick experiment with a match will determine the true nature of this 'burning snowball' (Figure 2.2c).

Terminology distinguishes between traditional hydrates, in which water molecules are bound

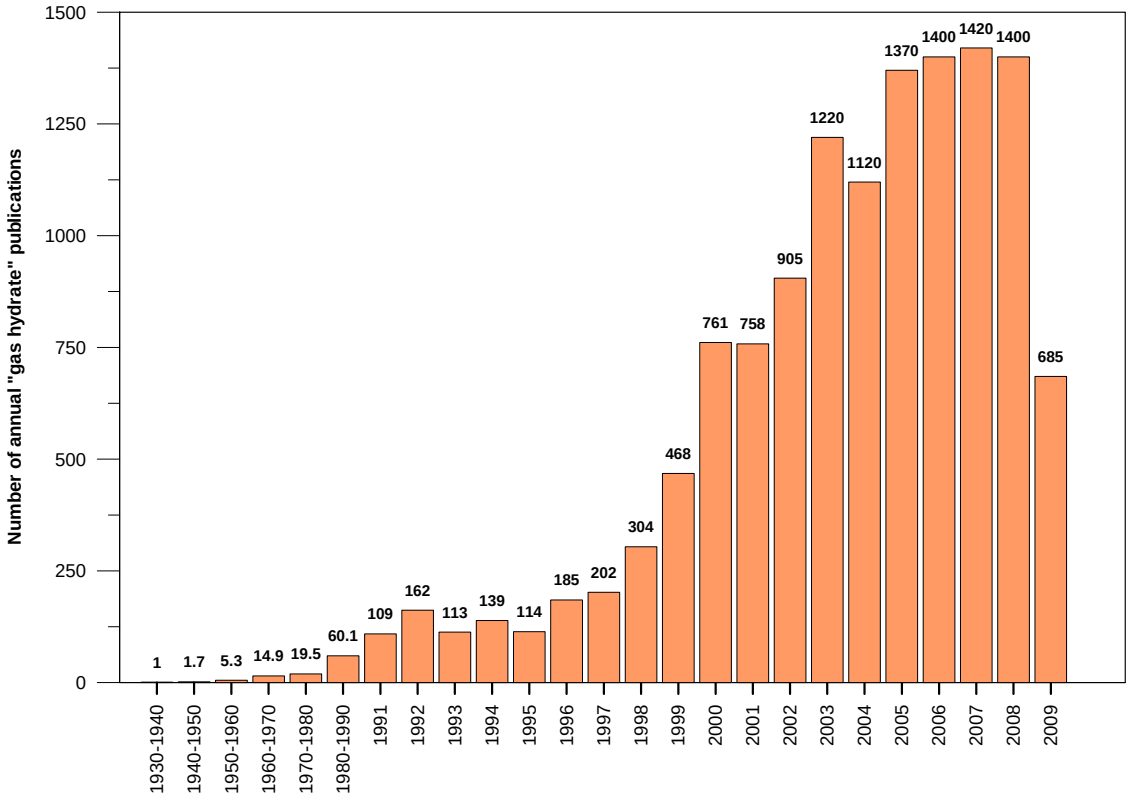


Figure 2.1: Publications with the word 'gas hydrate(s)' used. Data was compiled on the 5th of October 2009. Data source: Google Scholar (2008).

a) Natural gas hydrate *(Source: NOAA)* b) Hydrate plug *(Source: Petrobras)* c) Burning snow *(Source: DOE)*

Figure 2.2: Gas hydrate in its many environments. (A) Blake Ridge hydrate sample recovered during ocean drilling programme (ODP) Leg 164. (B) A hydrate plug in a pipeline. (C) Synthetic gas hydrate in a laboratory.

with another molecule, and clathrates, a crystallographic term referring to a configuration in which a guest molecule is enclosed in a lattice of host molecules. It follows that the correct term for gas hydrate should be 'natural gas clathrate hydrate', though the more colloquial term 'gas hydrate' is commonly used as a synonym. This term is used throughout this thesis.

### 2.1.2 Significance of gas hydrates

Gas hydrates can be examined in a wide array of settings, occurring both as a nuisance and as a potential resource (Figure 2.3). Furthermore, the sheer volume of hydrate-bound methane makes them a potential climatic forcer. The following four are the pillars of modern-day hydrate research:

- ***Flow assurance:*** The non-flowing crystalline nature of hydrates causes them to plug pipes, delaying oil and gas production. The hydrocarbon industry is driving the vast majority of research on flow assurance (Sloan 2003b), unsurprising given the daily cost of US$2 million spent on keeping pipes hydrate-free (Makogon *et al.* 2004). Costly inhibitors or even more costly pipeline heaters must be used to both prevent and dissociate the blockage (Mehta *et al.* 2003). Future solutions, such as SINTEF's ColdFlow concept, may allow for the controlled formation of gas hydrates, thus reducing the need for environmentally harmful inhibitors (Gudmundsson 2002, Ilahi 2005, Larsen 2008).

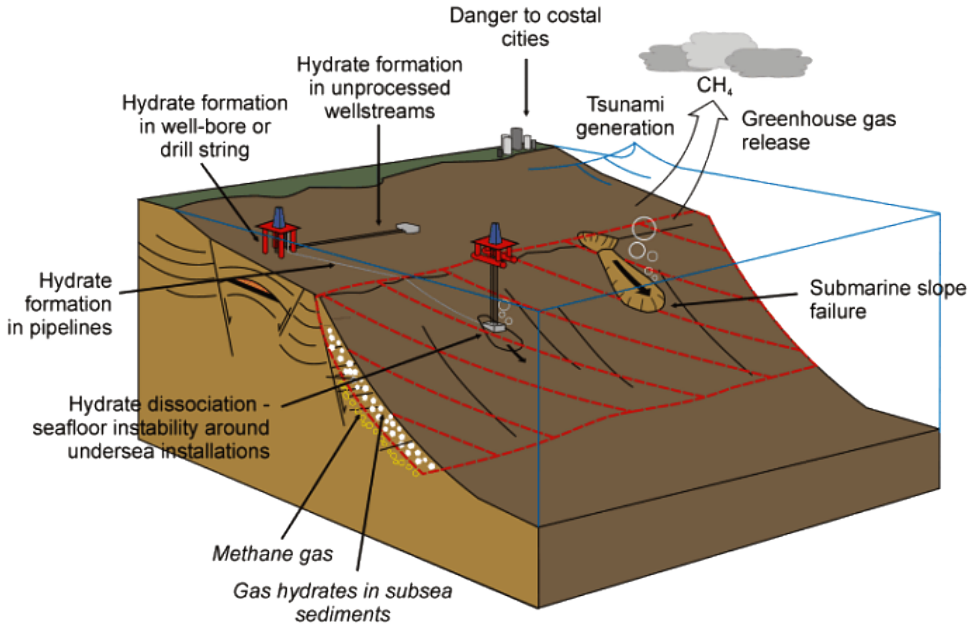


Figure 2.3: A summary of hydrate-associated issues. The main topic of this thesis is the quantification of methane in subsea sediments, potentially important as an energy source. Courtesy of the Center for Gas Hydrate Research (HWU 2008).

Rapid dissociation of hydrate blockages, whether by the use of an inhibitor or by the natural removal from the hydrate stability zone, can lead to pipeline blowouts and failures. Given a large enough pressure gradient across the blockage, the solid hydrate can reach speeds of up to 300 km/h (Sloan 2000; 2003b).

- ***Climate change:*** Kennett *et al.* (2003) have published a hypothesis regarding the climatic effect of substantial methane release during hydrate dissociation. Their 'Clathrate Gun Hypothesis', suggesting that oceanic hydrate dissociation was responsible for rapid global warming of up to 8°C 15,000 years ago, sparked a heated scientific debate culminating in suggestions that the 'Clathrate Gun is firing blanks' (Maslin and Thomas 2003a;b). These authors suggested that oceanic methane is responsible for only a 20-30% increase in atmospheric methane between 18,000 and 8,000 years ago, with the majority of atmospheric methane increase being driven by changes in the extent of tropical and temperate wetlands.

  Dickens *et al.* (1995) have proposed a slightly less controversial hypothesis, which still suggests that massive hydrate dissociation during the Late Paleocene Thermal Maximum (at ca. 55.5 My[1]) was responsible for global temperature elevations of 4-8°C (Dickens *et al.* 1995; 1997, Dickens 2003). Catastrophic releases of methane have even been linked to major mass extinctions (Padden and Weissert 2001, Kennett *et al.* 2003). All the above publications nonetheless agree on the fact that oceanic hydrates are one of the major, if maybe not the most important, regulators of the carbon cycle.

- ***Slope stability:*** Due to the strengthening effect gas hydrate has on its host sediment, hydrate dissociation may lead to a loss of integrity and thus increase the potential for sediment slumping (Locat and Lee 2002; 2005, Mienert *et al.* 2005b, Solheim *et al.* 2005a;b). Kvenvolden (1999) rates the submarine geohazard as an 'immediate' threat to humankind, especially given the ever-increasing exploitation of seabed resources in ever-deepening waters. Subaqueous slumps can also have adverse effects on sub-sea structures such as trans-oceanic

[1] My = million years

fiber-optic cables or offshore installations (Yakushev 2008, Peters *et al.* 2008). Furthermore, submarine landslides, hydrate-related or otherwise, may initiate tsunamis threatening coastal populations (Driscoll *et al.* 2000, Tappin *et al.* 2001, Haugen *et al.* 2005, Bondevik *et al.* 2005, Walters *et al.* 2006).

- ***Energy recovery:*** Even the most conservative estimates (Kvenvolden 1998) place global hydrate resources at the same level as that of all other fossil fuels combined (Figure 2.21). Given the dense hydrate structure, one volume of hydrate would dissociate to ~164 volumes (STP[2]) of gas (Sloan 2003a, Max *et al.* 2006). Hydrate may have already been produced from permafrost at both the Messoyakha field in Siberia and the North Slope Borough in Alaska (Makogon 1965, Collett and Ginsburg 1998, Makogon *et al.* 2007). A recent project at Mallik, in the Canadian Arctic, has proven the concept of producing hydrate from beneath the permafrost (Dallimore and Collett 2005, Sloan and Koh 2008). Marine hydrate production appears theoretically possible but as yet economically unprofitable and represents an exploration frontier (Max and Lowrie 1996). Even so, both the Japanese and American programs predict that stand-alone oceanic hydrate production could begin by 2015 (Sloan 2003a).

  The debate on when, how and where gas hydrate will first be commercially produced is ongoing and the reader is referred to a number of articles dealing with the issue (Lee and Holder 2001, Collett 2002, Moridis and Collett 2003, Beauchamp 2004, Makogon *et al.* 2004, Chatti *et al.* 2005, Dawe and Thomas 2007, Ruppel 2007, Makogon *et al.* 2007, Holditch and Chianelli 2008, Walsh *et al.* 2008).

[2]STP refers to conditions of standard temperature and pressure conditions. Similar to conventional gas being naturally compressed with depth, squeezing more gas into the same amount of porosity, a cubic metre of hydrate will give 164 volumes of methane upon dissociation.

### 2.1.3 A brief history of gas hydrates

Research on gas hydrates began in 1778 when Joseph Priestley obtained the first recorded sample of hydrate by bubbling $SO_2$ through 0℃ at atmospheric pressures (Makogon *et al.* 2007). In the early $19^{th}$ century the term 'hydrate' was first defined during the experiments of Sir Humphrey Davy and Michael Faraday on chlorine hydrates (Faraday and Davy 1823). These early scientists utilized a 'long spell of cold weather' to grow chlorine crystals. In the process, they realized that an ice-like solid formed above the freezing point of water.

Throughout the latter half of $19^{th}$ century, scientists such as Villard (1896) and de Forcrand (1902) were interested in which components could form hydrates and what range of pressure and temperature conditions were required. They were able to measure hydrates of many gases, including $CH_4$, $CO_2$, $C_2H_6$, $C_2H_4$, $C_2H_2$, and $N_2O$. This study continues to the present day, with even $H_2$ now having been shown to occur in clathrate structures with $H_20$ (Mao *et al.* 2002).

The theoretical world of hydrate research became immediately applicable in the 1930s when engineers discovered that gas hydrates were blocking hydrocarbon pipelines and experimented with various inhibitors to remove the hydrate plugs (Hammerschmidt 1934).

Throughout the 1940s and 1950s interest was centered primarily on permafrost hydrates in Siberia (Makogon 1965). The Messoyakha gas field in western Siberia was developed for both conventional natural gas and permafrost hydrate in the 1970s (Kvenvolden 2000). While hydrate production at Messoyakha has subsequently been shown to be little more than a by-product of conventional gas production (Collett and Ginsburg 1998), it is still notable in lieu of upcoming hydrate production. At the same time as $CH_4$ was being extracted from hydrates in Siberia, the hydrate structures known at present were being studied in laboratories worldwide (Ripmeester *et al.* 1987, Sloan 1998a, Sloan and Koh 2008).

It was not until the late 1970s, during a DSDP[3] cruise, that the first bottom simulating reflection (BSR) was identified in the Bering Sea (Hein *et al.* 1978). At the time, it was interpreted as the

[3]DSDP = Deep Sea Drilling Programme

| | |
|---|---|
| **1978** | First bottom-simulating reflection identified |
| **1995** | ODP dedicates Leg 164 to hydrate drilling on the Blake Ridge |
| **1998** | Mallik 2L-38 pilot drilling and characterization project |
| **2002** | Mallik 5L international field-scale production experiment |
| **2002** | ODP Leg 204 drills hydrates off Hydrate Ridge off Oregon |
| **2003** | Nankai Trough drilling expedition |
| **2005** | IODP Expedition 311 drills hydrates on Cascadia Margin |
| **2005** | Chevron/DOE JIP, Gulf of Mexico |
| **2006** | Indian National Gas Hydrate Program Expedition 1, Bay of Bengal |
| **2006** | R/V Tangaroa Gas Hydrate Research cruise, Hikurangi Margin, New Zealand |
| **2007** | Mt Elbert prospect drilled and analysed on Alaskan North Slope |
| **2007** | R/V Sonne Gas Hydrate Research cruise, Hikurangi Margin, New Zealand |
| **2007** | Mallik production test continues |
| **2007** | Chinese Guangzhou Marine Geological Survey Expedition 1, South China Sea |
| **2007** | Korean Ulleung Basin Gas Hydrate Expedition 1, East Sea |
| **2008** | Mallik production test continues |
| **2009** | Gulf of Mexico JIP, 3-week hydrate drilling expedition |
| **2010** | ? ConocoPhillips and BP to work with DOE and partners on production tests of permafrost hydrate |

Table 2.1: Table listing a selection of the major gas hydrate achievements and milestones, 1978-2010.

upper portion of a silicification surface, though the same scientists returned to the scene a decade later to find one of the largest hydrate provinces and demonstrate that the BSR was, in fact, hydrate-related (Scholl and Hart 1993).

Even as late as 1980, most research into the natural occurrences of hydrate was permafrost-based, summed up in the IPOD[4] proposal of Curray (1980): "Virtually nothing is known of the distribution of hydrates on the outer continental margin". Only 15 years later, the Ocean Drilling Programme (ODP) dedicated a full leg to hydrate research on the Blake Ridge (Paull and Matsumoto 1995). Other hydrate expeditions quickly followed (Table 2.1).

In the past decade, hydrate research has shifted to identifying hydrates with more sophisticated methods than merely mapping BSRs, including hydrate-specific acoustic acquisition campaigns (Wood and Gettrust 2001, Chapman *et al.* 2002, Talukder *et al.* 2007), detailed seismic velocity analyses (Andreassen *et al.* 1995; 1997, Posewang and Mienert 1999a, Bünz *et al.* 2005b, Westbrook *et al.* 2008a;b, Faverola *et al.* 2009), electro-magnetic surveys (Yuan and Edwards 2000, Schwalen-

[4]IPOD = International Programme for Ocean Drilling

berg *et al.* 2005b; 2009b), geochemical studies (Paull and Matsumoto 1995, Paull *et al.* 2008b;a) and both onshore (Dallimore and Collett 2005, Williams *et al.* 2005) and offshore drilling campaigns (Ichikawa and Yonezawa 2002, MH21 2008). Short-term production tests have been conducted at several sites including the successful campaigns at Mallik in 2002, 2007 and 2008 (MH21 2008). Longer term production tests are planned for 2010/2011 (Bradner 2009).

## 2.2 Fundamental science of gas hydrates

### 2.2.1 Hydrate crystal structures

Gas hydrates generally form by the interaction of water and small (<0.9 nm) 'guest' molecules at moderate pressures (>0.6 MPa) in temperatures below 273 K (Sloan 2003a) [5]. Depending on the actual guest molecules' repulsions[6], three different structural types form (Figure 2.4). A hydrate structure refers to the construction of the $H_20$ lattice, and fundamentally controls the internal space available for guest molecules to inhabit. All three structures are repetitive, but hydrate deposits may contain both occupied and unoccupied cages. Structures I and II have been known from both natural and man-made environments since the 1950s (von Stackelberg and Müller 1951, von Stackelberg and Jahns 1954), but structure H was only discovered in the late 1980s (Ripmeester *et al.* 1987).

The most common natural structure, structure I, forms in conjunction with small (0.4-0.55 nm) guest molecules. Anything smaller than propane will be able to be incorporated into this body-centered cubic structure. Structure II, more widespread in pipelines and other man-made environments, forms with larger (0.6 - 0.7 nm) guests, with sizes greater than that of ethane but smaller than pentane. The general framework is that of a diamond lattice (Figure 2.4). Structure H may form in both environments, requiring either a small or large occupant. Both common structures, I and II, have multiple cavity sizes that can be occupied by various guests.

[5] Note that the P-T conditions at which gas hydrate remains stable also depend on the gas composition.

[6] Guest molecules generally consists of methane, though other compounds like ethane, propane, iso-butane etc. may make up a significant portion of the gaseous phase.

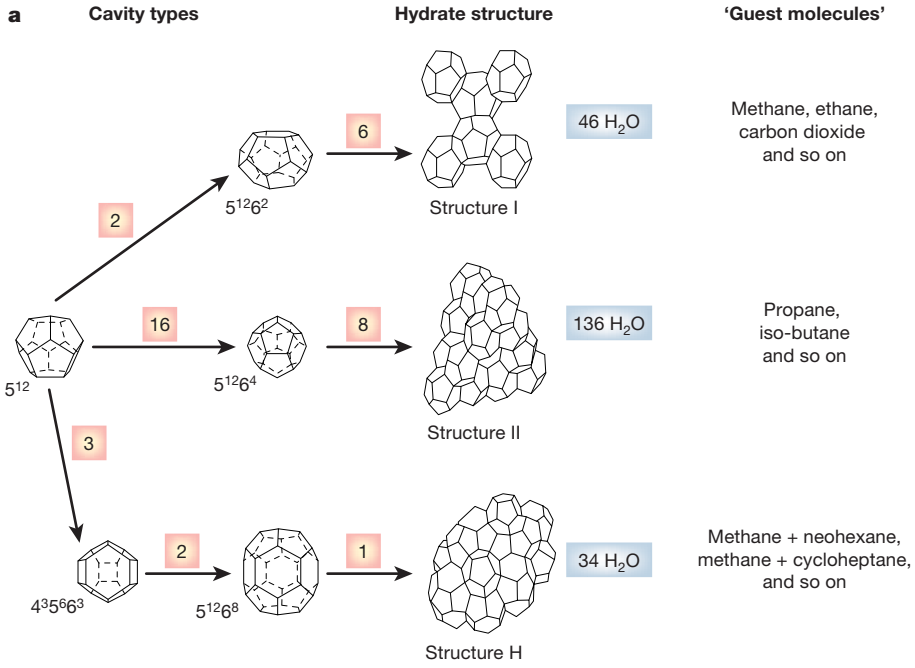


**b**

| Hydrate crystal structure | I | | II | | H | | |
|---|---|---|---|---|---|---|---|
| Cavity | Small | Large | Small | Large | Small | Medium | Large |
| Description | $5^{12}$ | $5^{12}6^2$ | $5^{12}$ | $5^{12}6^4$ | $5^{12}$ | $4^35^66^3$ | $5^{12}6^8$ |
| Number of cavities per unit cell | 2 | 6 | 16 | 8 | 3 | 2 | 1 |
| Average cavity radius (Å) | 3.95 | 4.33 | 3.91 | 4.73 | 3.91† | 4.06† | 5.71† |
| Coordination number* | 20 | 24 | 20 | 28 | 20 | 20 | 36 |
| Number of waters per unit cell | 46 | | 136 | | 34 | | |

*Number of oxygens at the periphery of each cavity.
†Estimates of structure H cavities from geometric models.

Figure 2.4: Diagram of hydrate structures. (A) The three hydrate structures. The crystal structure descriptors refer to the number of quadrant, pentagonal and hexagonal faces. Numbers in squares refer to the number of cage types. (B) Summary of the main properties of the three hydrate structures. Figure from Sloan (2003a).

Hydrate structure determines the concentration of gas molecules within a volume of hydrate, shown to match that of compressed gas (Sloan 2003a, Max *et al.* 2006, Sloan and Koh 2008). It also defines the heat of dissociation ($\Delta H_d$), defined as the enthalpy change required to dissociate the hydrate phase to free gas and a liquid (Sloan 1998a). $\Delta H_d$ is a function of the number of crystal hydrogen bonds (Sloan and Fleyfel 1992), and thus crystal structure will exert a control on hydrate dissociation.

Further details on hydrate structures can be found in Crutchley's excellent summary (Crutchley 2004) or in comprehensive books (Sloan 1998a, Sloan and Koh 2008).

#### 2.2.1.1 Properties of gas hydrates and ice

The physical properties of hydrates, fundamentally defined by their structure, play a central role in detecting and classifying *in situ* natural gas hydrates. Furthermore, it is important to be able to distinguish between ice and hydrate in the permafrost environment. A listing of the key properties of both hydrate and ice is given in Table 2.2. It is notable that, apart from defining which structure will form, the composition of the hydrate forming gas does not contribute significantly to hydrate properties. The composition of the hydrate-forming gas is, however, fundamental in defining the HPB[7].

The mechanical strength of hydrate has previously been shown to be roughly comparable to that of ice (Stern *et al.* 1996, Parameswaran *et al.* 1989, Cameron *et al.* 1990, Sloan and Koh 2008).

Using real geological samples, Winters *et al.* (2007) have demonstrated the increased shear strength of a hydrated sediment compared to that of one without hydrate. Hyodo *et al.* (2005) further demonstrated the positive correlation of an increase in methane hydrate saturation and the mechanical strength of the sediment. However, depending on the components and the nature of sample preparation, a minimum cut-off saturation may need to be reached for the effect to be registered (Sloan and Koh 2008).

The difference in elastic properties of hydrates in comparison to their surroundings, essentially

[7]HPB = hydrate phase boundary

**Comparison of Properties of Ice, sI, and sII Hydrates***

| Property | Ice | Structure I | Structure II |
|---|---|---|---|
| Structure and dynamics | | | |
| Crystallographic unit cell space group | $P6_3/mmc$ | Pm3n | Fd3m |
| No. of $H_2O$ molecules | 4 | 46 | 136 |
| Lattice parameters at 273 K (Å) | $a = 4.52$, $c = 7.36$ | 12.0 | 17.3 |
| Dielectric constant at 273 K | 94 | ~58 | ~58 |
| Far infrared spectrum | Peak at 229.3 $cm^{-1}$ | Peak at 229.3 $cm^{-1}$ | with others |
| $H_2O$ reorientation time at 273 K (μs) | 21 | ~10 | ~10 |
| $H_2O$ diffusion jump time (μs) | 2.7 | >200 | >200 |
| Mechanical properties | | | |
| Isothermal Young's modulus at 268 K ($10^9$ Pa) | 9.5 | 8.4[est] | 8.2[est] |
| Poisson's ratio | 0.3301[a] | 0.31403[a] | 0.31119[e] |
| Bulk modulus (GPa) | 8.8; 9.097[a] | 5.6; 8.762[a] | 8.482[a] |
| Shear modulus (GPa) | 3.9; 3.488[a] | 2.4; 3.574[a] | 3.6663[a] |
| Compressional velocity, $V_p$ (m/s) | 3870.1[a] | 3778[a,b] | 3821.8[a] |
| Shear velocity, $V_S$ (m/s) | 1949[a] | 1963.6 | 2001.14[b] |
| Velocity ratio (comp/shear) | 1.99 | 1.92 | 1.91 |
| Thermal properties | | | |
| Linear thermal expansion at 200 K ($K^{-1}$) | $56 \times 10^{-6}$ | $77 \times 10^{-6}$ | $52 \times 10^{-6}$ |
| Thermal conductivity ($Wm^{-1}K^{-1}$) | 2.23 | $0.49 \pm 0.02$; | $0.51 \pm 0.02$ |
| at 263 K | $2.18 \pm 0.01$[c] | $0.51 \pm 0.01$[c] 0.587[d] | $0.50 \pm 0.01$[c] |
| Adiabatic bulk compression at 273 K (GPa) | 12 | 14[est] | 14[est] |
| Heat capacity ($Jkg^{-1}K^{-1}$) | $1700 \pm 200$[c] | 2080 | $2130 \pm 40$[c] |
| Refractive index (632.8 nm, −3°C) | 1.3082[e] | 1.346[e] | 1.350[e] |
| Density ($g/cm^3$) | 0.91[f] | 0.94 also see Example 5.2 | 1.291[g] |

* *Note:* Unless indicated, values are from Davidson (1983), Davidson et al. (1986b) and Ripmeester et al. (1994).

[a] Helgerud et al. (2002 ) at 253–268 K, 22.4–32.8 MPa (ice, Ih), 258–288 K, 27.6–62.1 MPa ($CH_4$,sI), 258–288 K, 30.5–91.6 MPa ($CH_4$–$C_2H_6$, sII).
[b] Helgerud et al. (2003) at 258–288 K, 26.6–62.1 MPa.
[c] Waite et al. (2005) at 248–268 K (ice Ih), 253–288 K ($CH_4$, sI), 248–265.5 K (THF, sII).
[d] Huang and Fan (2004) for $CH_4$, sI.
[e] Bylov and Rasmussen (1997).
[f] Fractional occupancy (calculated from a theoretical model) in small (S) and large (L) cavities: sI = $CH_4$: 0.87 (S) and $CH_4$: 0.973 (L); sII = $CH_4$: 0.672 (S), 0.057 (L); $C_2H_6$: 0.096 (L) only; $C_3H_8$: 0.84 (L) only.
[g] Calculated for 2,2-dimethylpentane $5(Xe,H_2S)\cdot 34H_2O$ (Udachin et al., 1997b); est = estimated.

Table 2.2: Comparison of the physical properties of ice and hydrate structures I and II. Note particularly the compressional velocity ($V_p$) of pure hydrate, compared with the measured $V_p$ of hydrated sediments listed in Table 2.4. Figure from Sloan and Koh (2008).

its compressional ($V_p$) and shear ($V_s$) velocities, allow them to be imaged through seismic methods. These properties can be theoretically estimated if the crystal structure is known (Whalley 1980). Calculations have also shown that an empty hydrate lattice has a lower velocity than one which is fully occupied (Shpakov *et al.* 1988). Laboratory measurements, both of synthetic hydrates (Whiffen *et al.* 1982, Bathe *et al.* 1984, Shimizu *et al.* 2002) and geological samples (Lee and Collett 2001, Winters *et al.* 2005; 2007) have generally confirmed those theoretical calculations, though the effect of gas hydrate concentration within the sediment also needs to be considered. In fact, the difference between the $V_p$ of a hydrate-bearing sand with 30% hydrate saturation (2.7 km/s) and the same hydrate-bearing sand with 60% hydrate saturation (3.3 km/s) can be applied to quantify the hydrate saturation using the sonic log and, to some extent, seismic attributes (Winters *et al.* 2007). In essence, this approach assumes that an increase in a sediment's $V_p$, given that all other factors (e.g. lithology) remain unchanged, is directly related to the presence of gas hydrates.

The thermal conductivity of gas hydrate ($0.49 \pm 0.02\ Wm^{-1}\ K^{-1}$ for structure I and $0.51 \pm 0.02\ Wm^{-1}\ K^{-1}$ for structure II) has been shown to be about a fifth of that of ice ($2.23\ Wm^{-1}\ K^{-1}$ (Sloan and Koh 2008)). In fact, it more closely resembles that of liquid water ($0.605\ Wm^{-1}\ K^{-1}$ (Sloan and Koh 2008)). Numerous studies have confirmed this (Asher *et al.* 1986, Waite *et al.* 2006), though the over-use of the synthetic tetrohydrofuran (THF) hydrate as an analogue for natural gas hydrate has been criticized (Sloan and Koh 2008). Early work on the thermal conductivity of hydrates by Asher *et al.* (1986) has resulted in the development of the thermal conductivity needle probe as a means of distinguishing between ice and hydrate at *in situ* conditions.

Pure methane hydrate is a complete insulator (Schwalenberg *et al.* 2005b), a property that is exploited by electro-magnetic surveying further explained in Section 2.4.1.3.

### 2.2.2 Formation and dissociation of gas hydrates

A hydrate deposit requires four basic prerequisites to form:

1. Pressure-temperature (P-T) conditions within the hydrate stability zone.
2. An adequate and steady supply of hydrate-forming gas.
3. The presence of water.
4. A suitable host rock for hydrate to grow in.

While time-independent phenomena such as thermodynamics and structure are relatively well understood, the time-dependent phenomena of hydrate nucleation, growth and dissociation are substantially more challenging to comprehend. In order to understand a hydrate's 'life cycle', three key questions need to be answered: (1) When do hydrates nucleate?, (2) How quickly will they grow once nucleated?, (3) What are the key factors and time frames for dissociation?

It is possible to address the first two questions by examining a laboratory experiment (see Sloan and Koh (2008) for set-up description) recording the gas consumption over time at constant pressure-temperature (P-T) conditions (Figure 2.5a). The idealistic result shows an induction time during which hydrate does not form due to metastability (Sloan and Koh 2008). Once detectable amounts of gas are consumed, the hydrate enters the growth period and gas is rapidly concentrated in the hydrate cages. Eventually, the consumption of available water reduces hydrate growth past the growth period (Sloan and Koh 2008).

Another experiment, illustrating the same concept and depicted by Figure 2.5b, involves a closed-system with no addition of water and/or gas and measuring the corresponding hydrate formation pathway on a pressure-temperature (P-T) plot. From A to B, the hydrate is in its induction period and no hydrate forms. Upon reaching Point B, pressure drops rapidly as hydrates form and the catastrophic growth period continues to Point C. As the cell is heated at Point C, hydrates begin to dissociate towards Point D along a path of increasing pressure.

As seen from the experiments, there is a fundamental difference between hydrate growth and dissociation. The initial hydrate formation requires a long induction period while dissociation initiates rather quickly when outside the hydrate stability zone. This has been explained by Sloan and Koh (2008) as the effect of entropy favoring disorder over order, in that disorderly gas and

liquid will take longer to arrange itself into an orderly hydrate structure than to destroy it.

#### 2.2.2.1 Hydrate nucleation and growth

Sloan and Koh (2008) provide a comprehensive review of hydrate nucleation process. In this context, it suffices to review their main points.

Hydrate nucleation, happening at infinitely small scales on the gas-fluid boundaries, is initiated during the induction period. Nucleation is dependent on the size and composition of the gas guest molecule, its geometry in relation to the fluids, surface area exposure, impurities in and history of the fluids as well as the degree of inherent turbulence. Importantly, the rate of nucleation is proportional to the displacement from equilibrium conditions (Sloan and Koh 2008). The stochastic nucleation process is difficult to predict, though the stochasticity is considerably lower with high driving forces and constant cooling and predictions correspondingly better.

A 'memory effect' is observed if the hydrate is melted with a temperature close to that of the dissociation temperature. Fundamentally this leads to rapid formation of hydrate in the future unless the hydrate has been heated for a prolonged time or beyond 28°C (Sloan and Koh 2008).

In general, growth of gas hydrates appears more predictive than its nucleation. Experimental growth appears to be linear for as much as 100 min (Englezos *et al.* 1987, Englezos 1993, Sloan and Koh 2008).

There is a consensus that hydrate formation is primarily controlled by heat and mass transfer, implying that kinetics generally plays a minor role (Sloan and Koh 2008).

#### 2.2.2.2 Hydrate dissociation

Dissociation is important both in producing gas hydrate from natural gas hydrate deposits and removing plugs from pipelines. The dissociation process is an endothermic reaction, requiring the external supply of heat to break the hydrogen bonds between the water molecules and the van der Waals forces coupling guest to lattice (Sloan and Koh 2008). Laboratory dissociation measurements

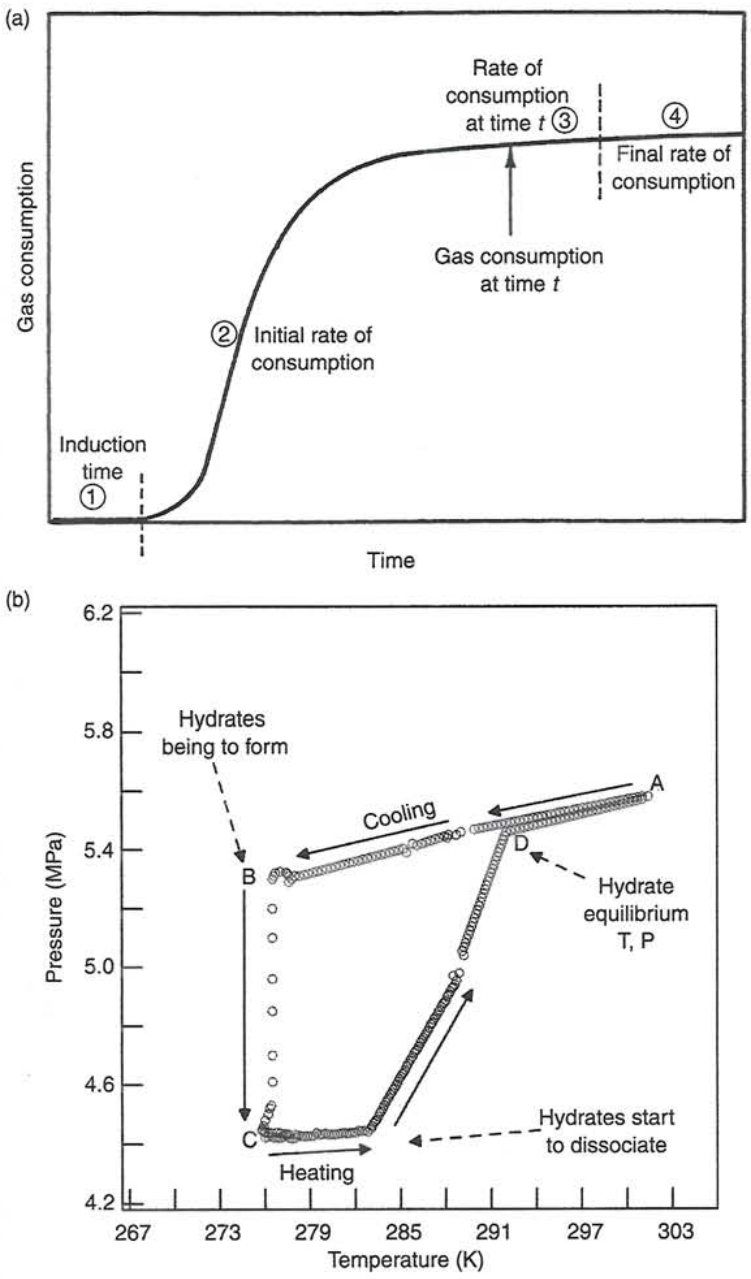


Figure 2.5: Experiments to help understand hydrate nucleation, growth and dissociation. (A) Gas consumption vs time at constant P-T conditions. Note that no dissociation is illustrated in this graph. From Sloan and Koh (2008), Lederhos *et al.* (1996). (B) A temperature and pressure trace for the formation of simple methane hydrates. Please refer to Section 2.2.2 for a detailed description of the experiments. From Sloan and Koh (2008).

utilizing X-ray CT scans confirmed that hydrates dissociate radially and not axially (Gupta 2007, Sloan and Koh 2008; Figure 2.6).

It should be emphasized that hydrates will not occur outside the thermodynamic restrictions of the respective hydrate phase boundary (HPB). It follows that a decrease in pressure (e.g. Messoyakha, Mallik), an increase in temperature (e.g. Mallik) or the addition of an inhibitor (e.g. Messoyakha) can shift the hydrate outside this zone (Figure 2.7).

*In situ* dissociation has been well studied by pressure stimulation tests at Mallik (Hancock *et al.* 2005a;b, Sloan and Koh 2008). Modular Formation Dynamics Tester (MDT) tests during the 2002 campaign investigated the hydrate response following depressurization. In the actual test, gas was produced from two reservoirs within the hydrate zone, leading to hydrate dissociation and associated build up of pressure. It is notable that gas from hydrates was produced immediately following depressurization, not after 2 years as indicated for Messoyakha (Makogon *et al.* 2007, Sloan and Koh 2008).

It should not be forgotten that hydrate dissociation, apart from releasing gas, also releases water. In some cases, especially with single-well configurations, water can actually account for up to 98% of the produced mass (Moridis and Collett 2003). Reinjecting the produced warm water may be a way of avoiding expensive surficial water management facilities while, at the same time, improving the recovery factor through thermal stimulation.

### 2.2.3 Phase equilibria for natural gas hydrates

As outlined above, a specific envelope of correct pressure and temperature conditions is required to form gas hydrates. This envelope is calculated on the basis of the guest composition, the presence of inhibitors (e.g. salts), the presence of water and the P-T conditions. It is routinely calculated using software packages such as CSMHYD (Sloan 1998b, Sloan and Koh 2008) or HWHydrate (Mohammadi 2001). The resulting plot illustrates the hydrate phase boundary for the given scenario (Figure 2.8).

The extent of the hydrate stability zone (HSZ) will be determined by the ocean bottom temper-

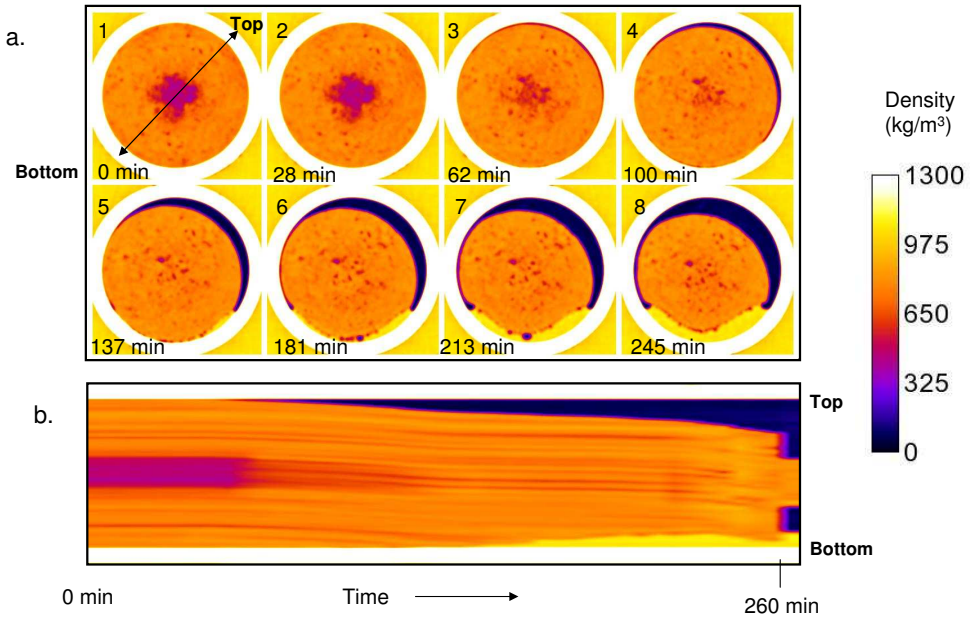


Figure 2.6: Radial dissociation of hydrate, as illustrated by laboratory experiments of Gupta (2007). a) CT images at one location showing the radial nature of hydrate dissociation. b) Temporal changes showing the increased dissociation from the top of the synthetic hydrate sample. While this work helps to understand the dissociation process of homogeneous synthetic hydrate samples, it is important to consider preferential dissociation induced by increased fluid flux along features such as faults.

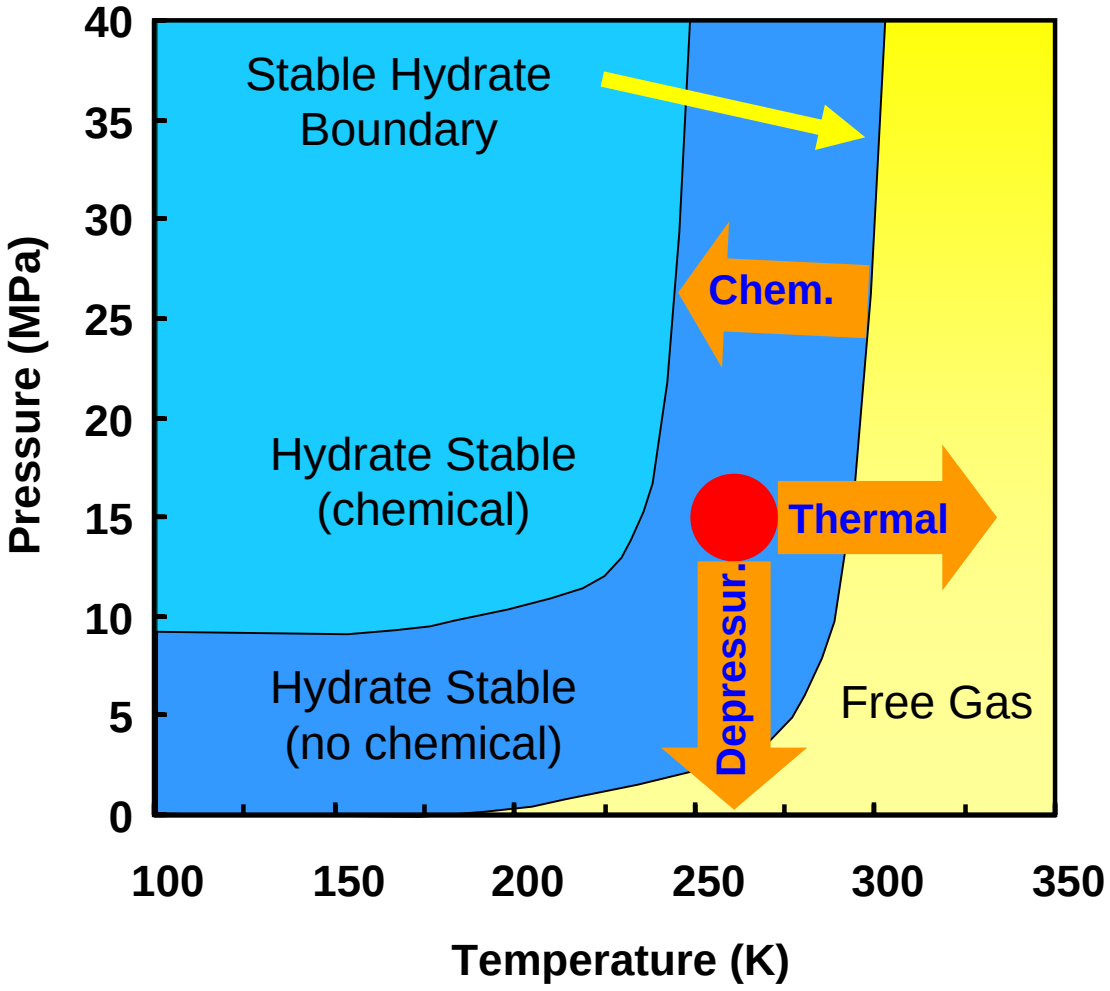


Figure 2.7: Effect of the different production techniques on the hydrate stability zone. Both depressurisation and thermal stimulation allow for the production of the deposit (represented by the red circle) by moving it outside the hydrate stability zone. Chemical inhibition, on the other hand, directly shifts the phase boundary by adding an inhibitor. Figure from Zitha *et al.* (2008).

ature, the local geothermal gradient and the hydrate phase boundary (HPB). The HPB, in turn, depends on the composition of the hydrate former, the proportion of water and the presence of any inhibitors.

These fundamental controls on hydrate formation have been studied as early as the first half of the $20^{th}$ century (e.g. Hammerschmidt 1934), while ongoing work is aimed at redefining the hydrate formation zone with regard to other factors, including salinity (Zatsepina and Buffett 1998) and host rock properties (Clennell *et al.* 1999). Contrary to conventional gas fields, initiation and stabilization of hydrates requires a sufficient and stable supply of methane throughout 'field life' (Kvenvolden 1999).

An example binary plot of a methane-water system, as discussed by Kobayashi and Katz (1949), allows for a check of the formation of hydrate of a given composition (Figure 2.9). The system, as outlined by Sloan and Koh (2008), works as follows:

1. A 60 mol% $CH_4$ + 40% $H_20$ mixture is cooled at constant pressure. The single-vapour mixture hits the dew point at Point 1. At this point, the composition of the equilibrium liquid water with minor methane dissolved is defined by Point 5.
2. Further cooling to Point 2 causes three phases ($L_w$-H-V) to coexist. The calculated methane mole fractions for the aqueous, sI hydrate and vapor phases are defined by Points 6, 7 and 8, respectively.
3. Still further cooling completely converts the free water phase to hydrate, with the same initial composition of 60% methane.
4. Further heat removal towards Point 3 will cause the condensation of some of the vapor to liquid methane. Points 9, 10 and 11 define the relative compositions of the three phases (H-V-$L_M$).
5. Cooling beyond Point 4 traverses across the solidification point of pure methane, at which the liquid methane phase disappears.

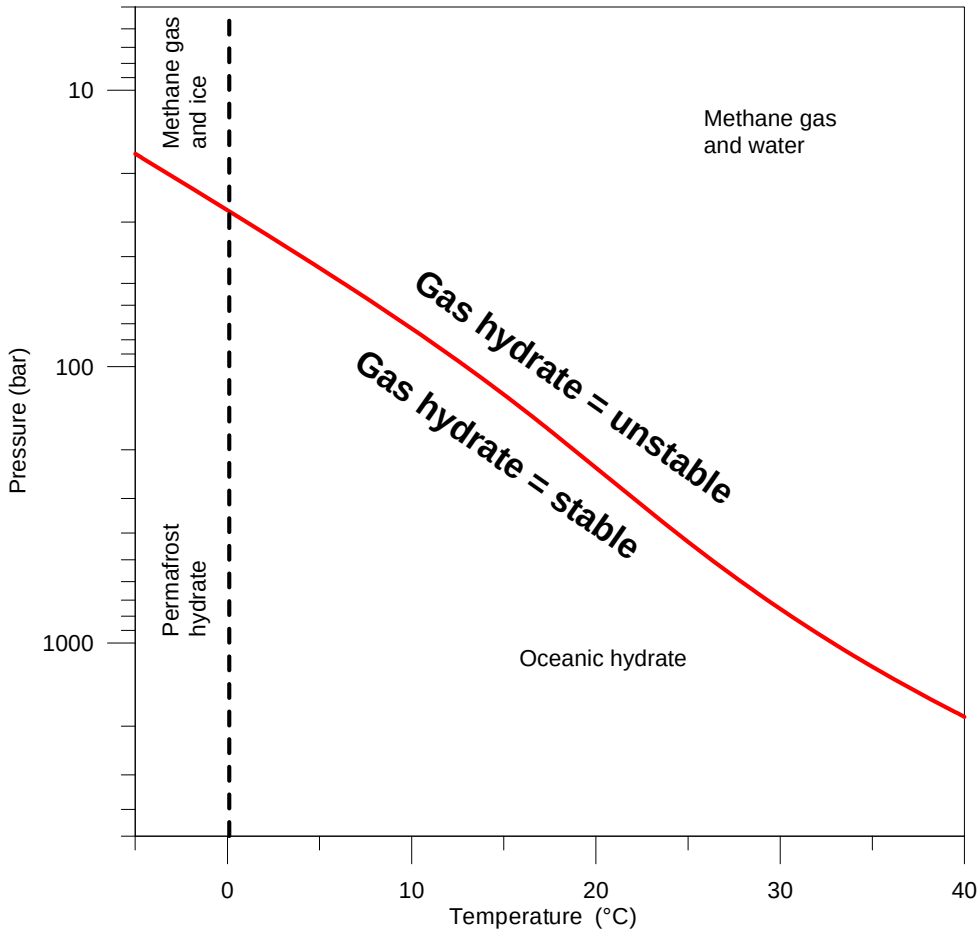


Figure 2.8: A diagram showing the pressure-temperature conditions of methane hydrate formation. Note the uncorrected freezing point and diffuse boundary between oceanic and permafrost hydrate. The hydrate dissociation curve was calculated using HWHYD (Mohammadi 2001), using a 100% methane composition.

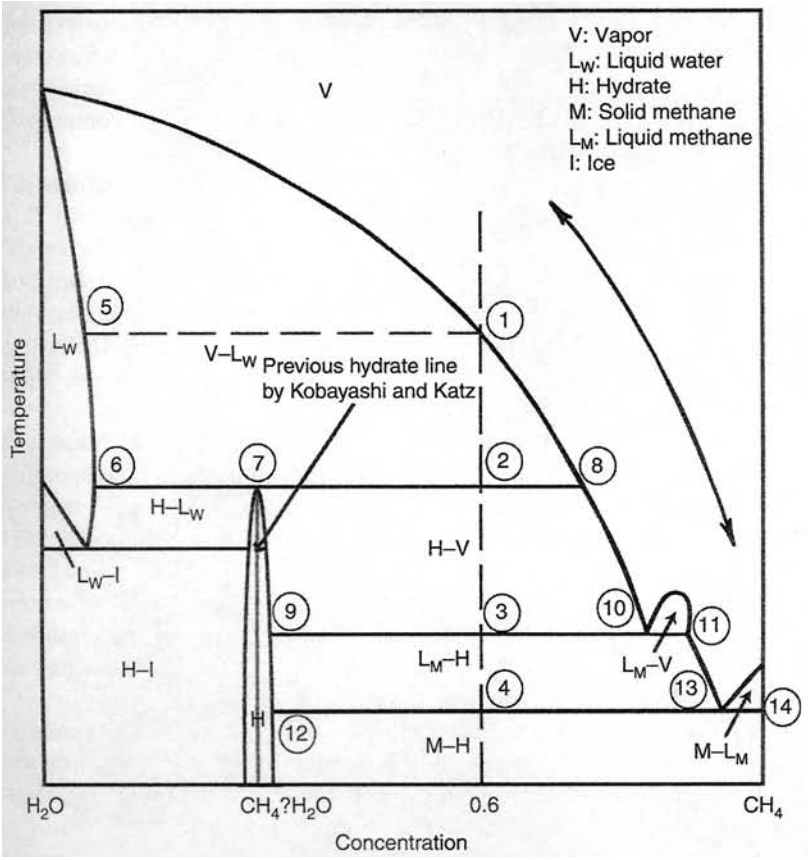


Figure 2.9: Temperature-composition diagram for methane and water. Figure from Sloan and Koh (2008), originally published in Huo *et al.* (2003). For an explanation of the illustrated process, please refer to Section 2.2.3.

## 2.3 The gas hydrate petroleum system

As outlined in Chapter 1, gas hydrates can be considered as an unconventional gas resource. In some aspects, the 'gas hydrate petroleum system' resembles that of the conventional gas deposits in that it consists of a source and a reservoir including an accumulation mechanism. Exploring for gas hydrates (using the methods considered in Section 2.4) will need to make use of the widely used petroleum approach to qualitatively define areas of interest (e.g. continental margins) and further evaluate those in terms of suitable gas sourcing, reservoir rocks, migration histories and trapping mechanisms. In addition, the dynamic nature of the hydrate system needs to be considered in much more detail than for conventional systems.

### 2.3.1 Distribution and occurrence of natural gas hydrates

Globally, natural gas hydrates form at cool temperatures and/or higher pressures. It is precisely these two characteristics that allow us to subdivide the two types of hydrates into the mostly temperature-driven permafrost hydrates (Collett and Dallimore 2000) and the predominantly pressure-driven oceanic hydrates (Dillon and Max 2000).

A thorough and updated review of hydrate localities is given by Sloan and Koh (2008). Based primarily on Kvenvolden's work, Sloan and Koh (2008) list 89 global hydrate sites (Figure 2.10). Modeling of the global occurrence of gas hydrates by Klauda and Sandler (2005) fits this distribution reasonably well (Figure 2.11), though such large-scale extrapolation using a set of essentially global reservoir parameters inevitably leads to large uncertainties.

### 2.3.2 Gas hydrate versus conventional gas

A classic conventional gas field will be sourced from an organic-rich source rock that will generate and expel hydrocarbons at a time determined by the basin's thermal maturation history (Figure 2.12). Hydrocarbons will subsequently migrate through permeable pathways to a suitable reservoir, often exhibiting porosities in excess of 20%. The reservoir rock is overlain by an imperme-

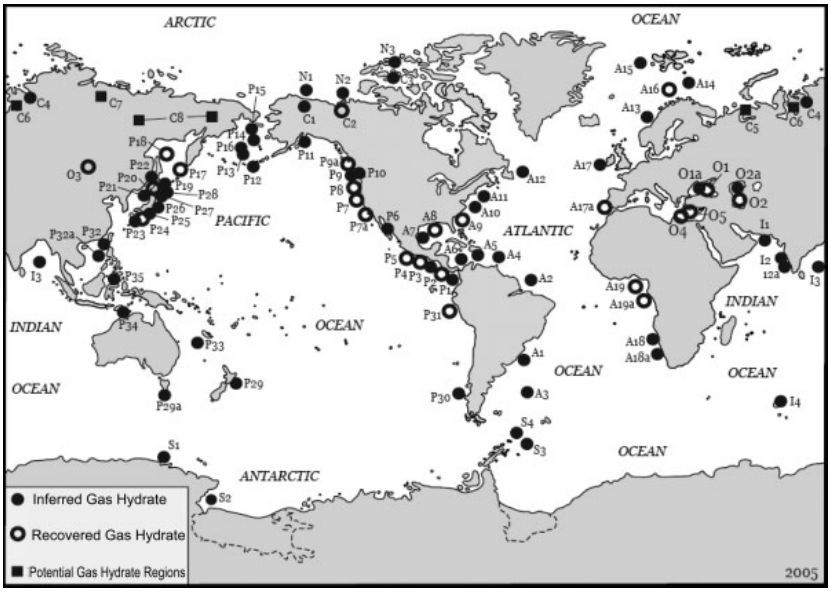


Figure 2.10: The worldwide distribution of gas hydrates. From Sloan and Koh (2008), updated from Kvenvolden and Loreson (2001). Please note that site A13, the study site at Nyegga, has recently had physical hydrate recovered as reported by Ivanov *et al.* (2007) and Haflidason *et al.* (2008).

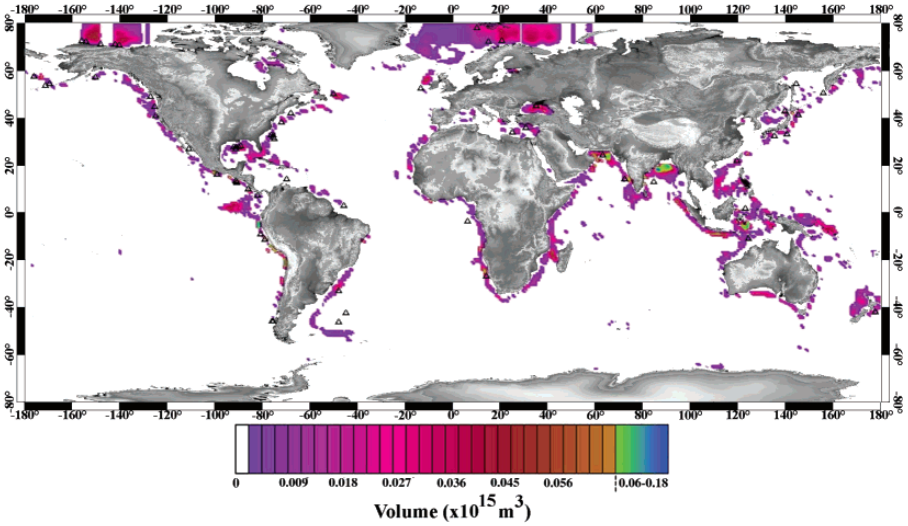


Figure 2.11: Modeled deposits of oceanic gas hydrate in water depths of <3000m. The authors, Klauda and Sandler (2005), first modeled the thickness of the global HSZ before modeling the hydrate amounts, using input parameters such as methane production, BSR locations, water properties, pore space distribution and hydrate saturation. The partial usage of essentially global reservoir parameters inevitably leads to large uncertainties. Note the model's good fit to the sites where hydrate has actually been recovered, shown above in Figure 2.10.

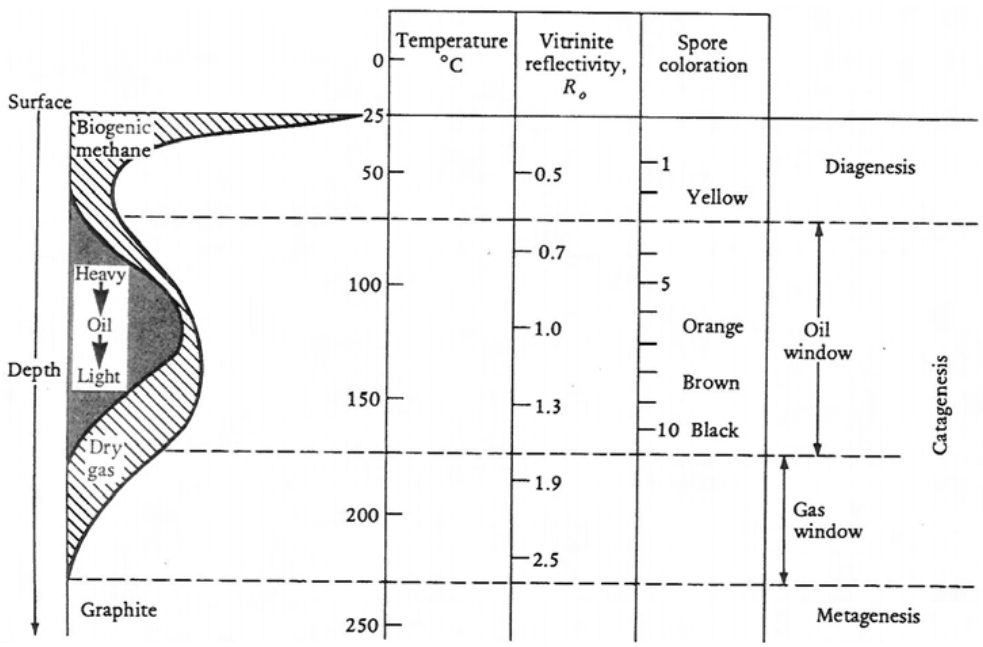


Figure 2.12: Maturation curves for hydrocarbons. Note that biogenic gas, the major constituent of most gas hydrate deposits, forms at relatively low temperatures while thermogenic gas (sometimes referred to as 'dry gas') forms at much higher temperatures below the oil window. Figure from Selley (1998).

able layer (often a shale) which, with the help of a suitable pre-existing structural or stratigraphic configuration, traps hydrocarbons.

Once trapped, the hydrocarbons only move in response to renewed tectonic activity that destroys their trap or by large-scale changes to the pore pressure regime (van Balen and Skar 2000). Both processes often lead to leakage and potential development of gas columns above the paleo-trap. A typical hydrocarbon column generally contains density-driven zonation of gas-oil-water (from top to bottom), with a considerable dissolved gas component in the oil zone. The pressure is maintained from the water zone below, and production of hydrocarbons leads to water replacement and no structural damage to the reservoir. Due to the thermal maturation required to generate thermogenic gas and crude oil, conventional reservoirs are typically in hardened sediments.

In contrast, 99% of hydrate deposits are biogenic in origin (Kvenvolden 1995, Kvenvolden and Loreson 2001) and occur in shallow and unconsolidated sediments. Hydrate deposits are typically

not trapped as such, but owe their presence to the phase boundary at the base of the HSZ. The formation of impermeable hydrates thus also creates a trap for the underlying free gas. Due to the nature of hydrate growth, it has the potential to become an integral part of the host sediment's framework and increase its mechanical strength. In contrast to production of conventional gas fields, hydrate dissociation during production may actually increase the reservoir pressure (Max *et al.* 2006, Sloan and Koh 2008).

A specific type of hydrate deposits in the permafrost environment (e.g. Mt Elbert) occurs where a conventional gas deposit has been 'hydrated' by a shift in P-T conditions (Boswell *et al.* 2008). In essence, the deposit has been frozen. Such hydrate deposits tend to be far off the hydrate phase boundary, thus making their production more energy-demanding.

### 2.3.3 Source

Gas hydrates require a steady supply of gas to form. This gas, typically methane, may be either biogenic or thermogenic in origin. Furthermore, abiogenic methane may be generated in hydrothermal systems during the hydrothermal reduction of $CO_2$ (Sherwood Lollar *et al.* 2006, Fiebig *et al.* 2007). 99% of all naturally occurring hydrate is thought to be biogenic in origin (Kvenvolden and Loreson 2001). However, in areas such as the Gulf of Mexico and the Caspian Sea significant proportions of the hydrate-forming gas may consist of deeply-sourced thermogenic gases (Sassen *et al.* 1999, Milkov and Sassen 2002, Tréhu *et al.* 2006, Lorenson *et al.* 2008).

#### 2.3.3.1 Biogenic methane formation

Organic diagenesis, the low temperature biogenic conversion of organic matter to methane, occurs in six stages (Figure 2.13). In the first stage, organic matter[8] is oxidized. Burial brings on reduction by nitrates. From the third stage, both the stagnant and ventilated basins follow similar mechanisms, including sulfate ion reduction. In the fourth stage of carbonate reduction, methane is generated

[8]Organic matter is typically composed of carbon, nitrogen and phosphorus.

by the following (simplified) reaction:

$$(CH_2O)_{106}(NH_3)_{16}(H_3PO_4) \rightarrow 53CO_2 + 53CH_4 + 16NH_3 + H_3PO_4 \tag{2.1}$$

Deeper stages below that of the methane production include fermentation and thermocatalytic decarboxylation (Sloan and Koh 2008). Further details about the biogenic process is provided by Hesse (1986), while thermogenic gas generation has been reviewed by Selley (1998).

To distinguish between a thermogenic and biogenic gas, it is possible to use both the ratio between carbon's isotopes $^{12}C$ and $^{13}C$ and the ratio of methane to the sum of ethane and propane[9] (Sloan and Koh 2008). Carbon isotopes fractionate during carbonate reduction since the generated methane is approximately 70‰ lighter than the carbon of the parent material (Hesse 1986). Collected gas samples, compared to the carbon content of the standard sample of Pee Dee Belemnite (PDB), are used to calculate the ratio difference by:

$$\delta^{13}C \equiv \left[ \frac{[^{13}C] \,/\, [^{12}C]_{sample}}{[^{13}C] \,/\, [^{12}C]_{PDB}} - 1 \right] \times 10^3 \tag{2.2}$$

Typical values for $\delta^{13}C$ are from -60‰ to -85‰ for biogenic gas, and from -25‰ to -55‰ for thermogenic gas. Typical values for C1/(C2+C3) are $10^3$ for biogenic gas and $< 100$ for thermogenic gas (Sloan and Koh 2008).

#### 2.3.3.2 Implications for sourcing

Tréhu *et al.* (2006) identify two styles of natural hydrate concentration, linked to two end-member modes of hydrate formation:

1. The diffuse-gas flow model often leads to broadly distributed distributed low flux (DLF)

[9] This ratio, $[methane/(ethane + propane)]$, is commonly expressed as C1/(C2+C3), and is widely referred to as the wetness index.

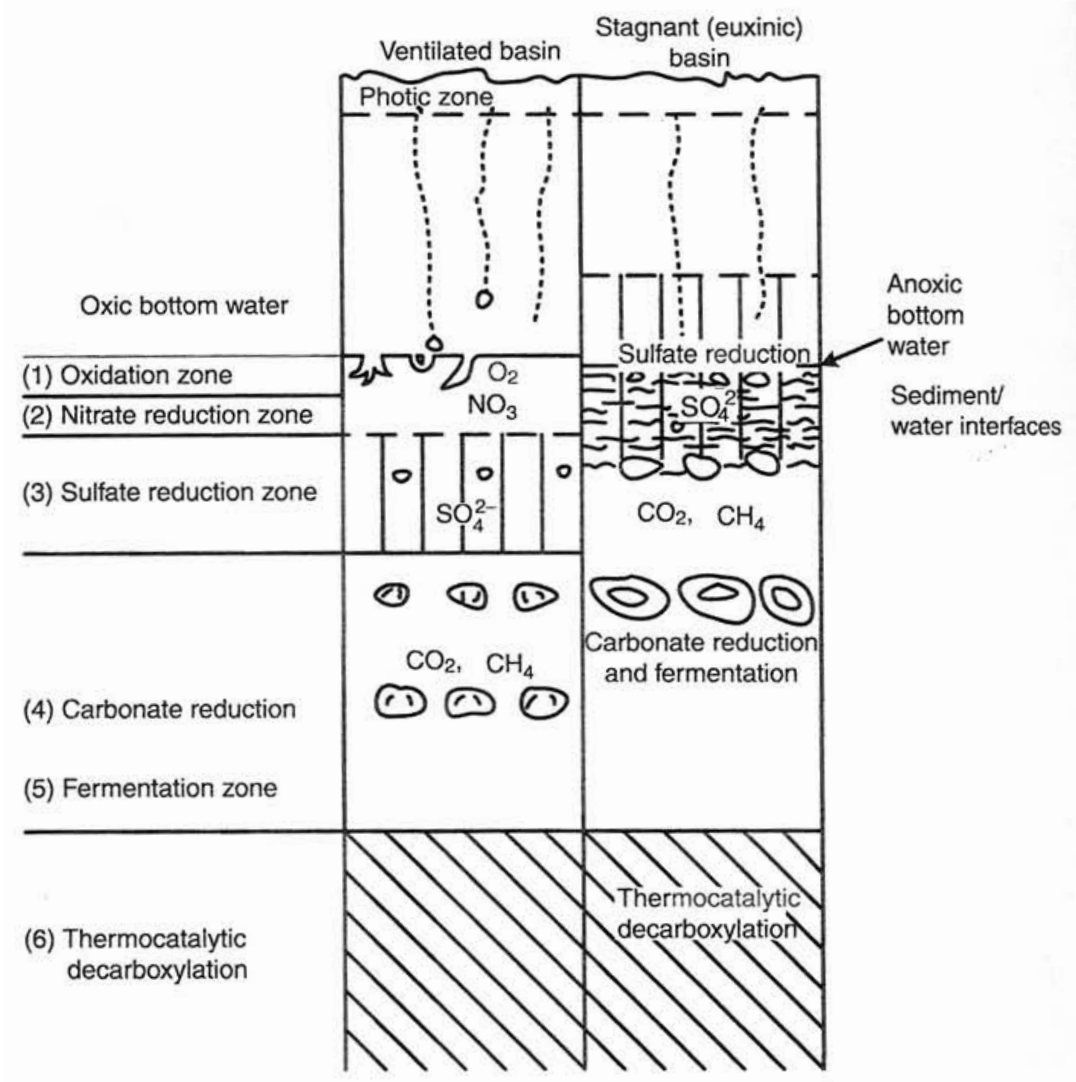


Figure 2.13: The six stages of organic matter oxidation in anoxic sediments. Note particularly the difference between the sulfate reduction zone in a stagnant basin compared to a ventilated basin. Figure from Sloan and Koh (2008).

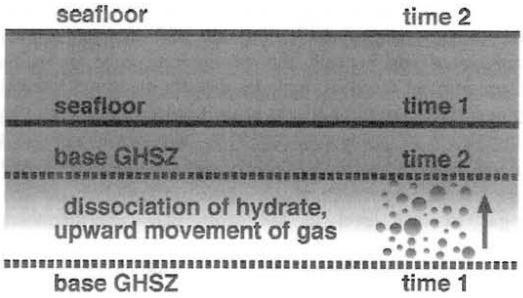


Figure 2.14: The effect of seafloor accretion on hydrated sediment. The illustration highlights the dynamic nature of the hydrate stability zone (HSZ), adjusting to sedimentation on the seafloor. In the period between 'time 1' and 'time 2' hydrate dissociation is initiated by the upward movement of the base of the HSZ. Figure from Max *et al.* (2006).

hydrate manifested as pore fillings in sandy reservoir and veins in shaly reservoirs.

2. The focused gas-flow model forms highly concentrated focussed high flux (FHF) hydrate accumulations along fluid migration pathways.

Biogenic gas is primarily responsible for forming hydrates in the first model, often referred to as distributed low flux (DLF) gas hydrates. Most scientists agree that hydrates generally form at the base of the HSZ, being sourced from upward-moving gas. This gas may in itself be sourced from hydrates due to the accretion of the seafloor and subsequent shift in the thermo-baric conditions (Figure 2.14). DLF gas hydrates form from biogenic methane generated in the immediate vicinity. In addition, they tend to be associated with shales and are generally more dispersed (Sloan and Koh 2008).

Focussed high flux (FHF) gas hydrates, on the other hand, are typically deeply sourced, possibly containing higher-order gases and are frequently restricted to sandy units (Sloan and Koh 2008). At the Nyegga study site, FHF hydrates may occur within the acoustic chimneys described by Weibull (2008) and Hustoft (2009). These chimneys, typically associated with pockmarks on the seafloor, are thought to be formed in areas of focussed fluid flux, and could thus potentionally represent a sweet spot gas hydrate deposit. Stoian *et al.* (2008) found velocities to be higher within similar chimney structures in the Korean Ulleung basin, compared to both the background profile

| FHF gas hydrates | DLF gas hydrates |
|---|---|
| *Rich, localised hydrate deposits* | *Broadly distributed, lean hydrate deposits* |
| *Related to mounds, vents, pockmarks* | *Related to dispersed, low concentrations* |
| *CH4/H20 from kilometres below seafloor* | *CH4 generated near hydrate deposit* |
| *High-permeability conduits* | *Low-permeability flow* |
| *Frequently are deposited in sands* | *Frequently are deposited in shales* |
| *Forming flow rapid: convective and diffusive* | *Forming flow is slow; frequently diffusive* |
| *Form within tens of metres of mud line* | *Form deeper in occurrence zone* |
| *Represent a small amount of hydrates* | *Represent the majority of hydrate* |
| *Not normally predicted by models* | *Frequently modelled* |
| *Can be massive gas hydrates* | *Hydrates dispersed, < 5% of pore volume* |
| *Found by seafloor imaging and protrusions* | *Found by BSR mapping* |
| *Can be structure I, II or H hydrates* | *Usually structure I, biogenic gas hydrate* |
| *Can have complex fauna with them* | *Usually associated with shales, not fauna* |
| *Represented by Barkley Canyon hydrates* | *Represented by Blake Ridge hydrates* |

Table 2.3: The two end-member types of hydrate deposits, the distributed low flux (DLF) and the focussed high flux (FHF) gas hydrates. Adapted from Sloan and Koh (2008).

and the hydrate zone presumed to be above the BSR (Figure 2.15). Furthermore, shallow coring has successfully recovered solid hydrate from Nyegga's G11 pockmark (Hjelstuen *et al.* 2009, Jose *et al.* 2007), even though the origin of the seismic pull-up at Nyegga has been contested (Paull *et al.* 2008b, Paull, pers. comm. 2008).

The major characteristics of these two end-members are listed in Table 2.3.

### 2.3.4 Reservoir

As outlined above, distributed low flux (DLF) gas hydrates tend to be associated with regionally deposited lower permeability unconsolidated hemipelagic sediments while focussed high flux (FHF) gas hydrates typically occur within chimneys or fault zones. Hydrate behaves opportunistically, in that it favors growth in areas of least resistance. Permeable unconsolidated sands are thus favored reservoirs (Sloan and Koh 2008).

An analysis of regional geological control on hydrate formation within the Nyegga study area

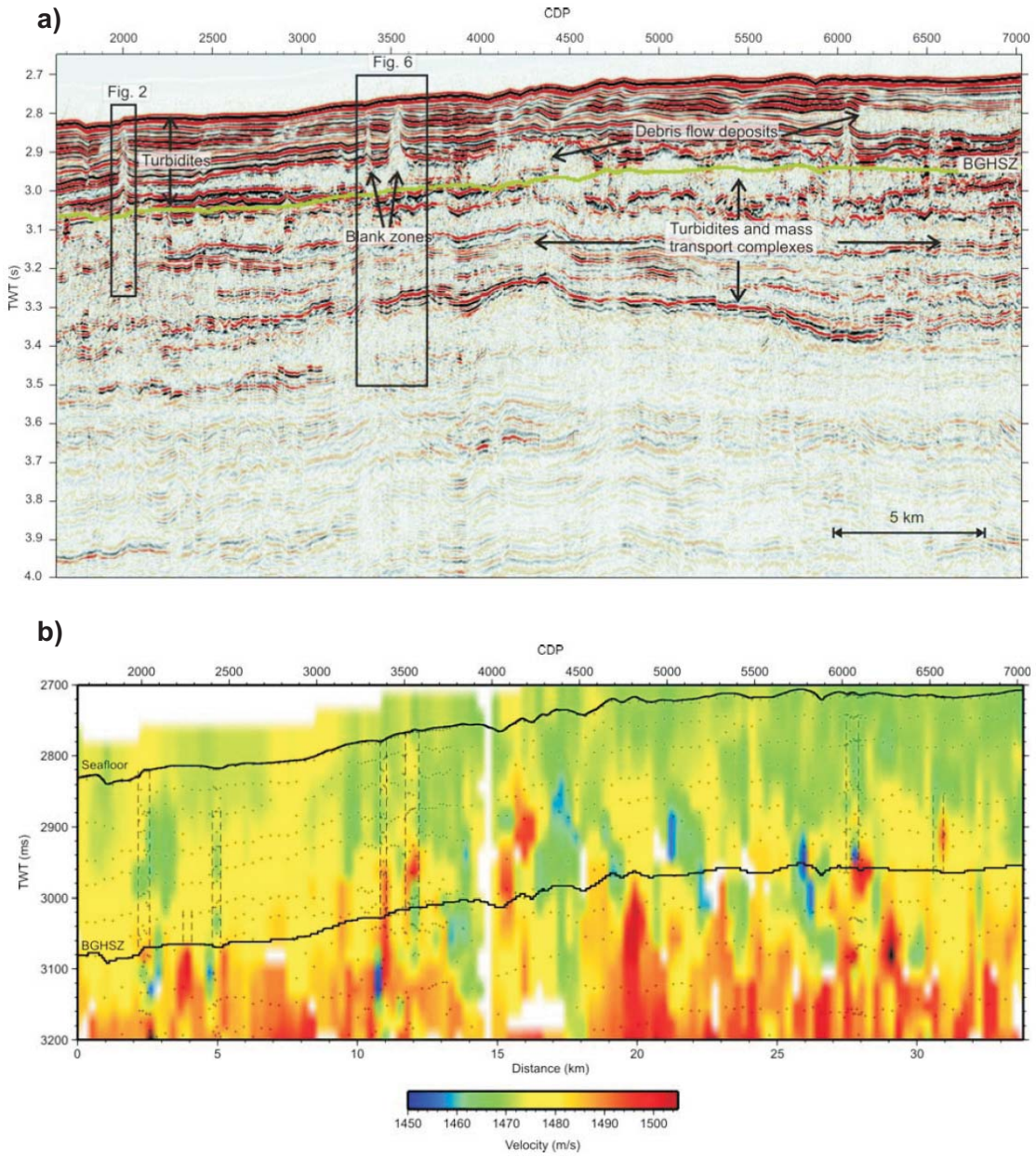


Figure 2.15: An example of chimney structures from the Ulleung Basin off Korea. (A) Time migrated section from multi-channel seismic data. (B) Gridded stacking velocities obtained by semblance analysis. Note the higher velocities within the chimney zones (stippled lines) compared to the surroundings. Figure from Stoian *et al.* (2008).

.

by Bünz *et al.* (2003) has shown that hydrates are unlikely to form within the impermeable and fine glacigenic debris flow (GDF). The GDF sediments typically exhibit reduced pore space, a lower water content and fine-grained sediment composition, culminating in the pinch-out of the BSR against the toe of the GDF deposits (Bünz *et al.* 2003; Figure 2.16)

### 2.3.5 Migration

Migration into the reservoir is essentially pressure and density driven. Free gas, or gas-saturated water, is less dense than water and thus percolates upwards into the region of gas hydrate stability (Sloan and Koh 2008). Upon reaching the base of the HSZ, gas hydrates will start forming provided that a suitable reservoir rock exists. In contrast to conventional gas reservoirs, methane hydrate may not require an impermeable boundary to stop its upward migration. The hydrate itself forms the top seal, and thus traps migrating gas below it. This gas then subsequently may form gas hydrate.

Thermogenic gas, by definition generated at depth, has much longer migration pathways to the hydrate stability zone. Focused migration occurs via faults, pipes and other high-permeability migration pathways. The local occurrence of such fault-associated gas hydrate deposits may explain the lack of BSRs associated with such focused hydrate deposits (Paull *et al.* 2005).

### 2.3.6 Trapping and accumulation mechanism

The fundamental difference between DLF and FHF gas hydrates has been discussed above.

Focusing of gas migration via faults, chimneys, pipes or other highly permeable pathways is well studied by the conventional gas industry, as well as hydrate researchers (Minshull *et al.* 1994, Hustoft *et al.* 2007, Paull *et al.* 2008a). FHF gas hydrates are readily supplied through these pathways by rising gas and gas-saturated fluids (Hyndman and Davis 1992, Sloan and Koh 2008).

DLF gas hydrates will, on the other hand, typically form by local *in situ* hydrate formation, as proposed by Kvenvolden and Barnard (1983). This mechanism is, however, unlikely to produce hydrate saturations higher than ca. 3 % (Klauda and Sandler 2005, Sloan and Koh 2008).

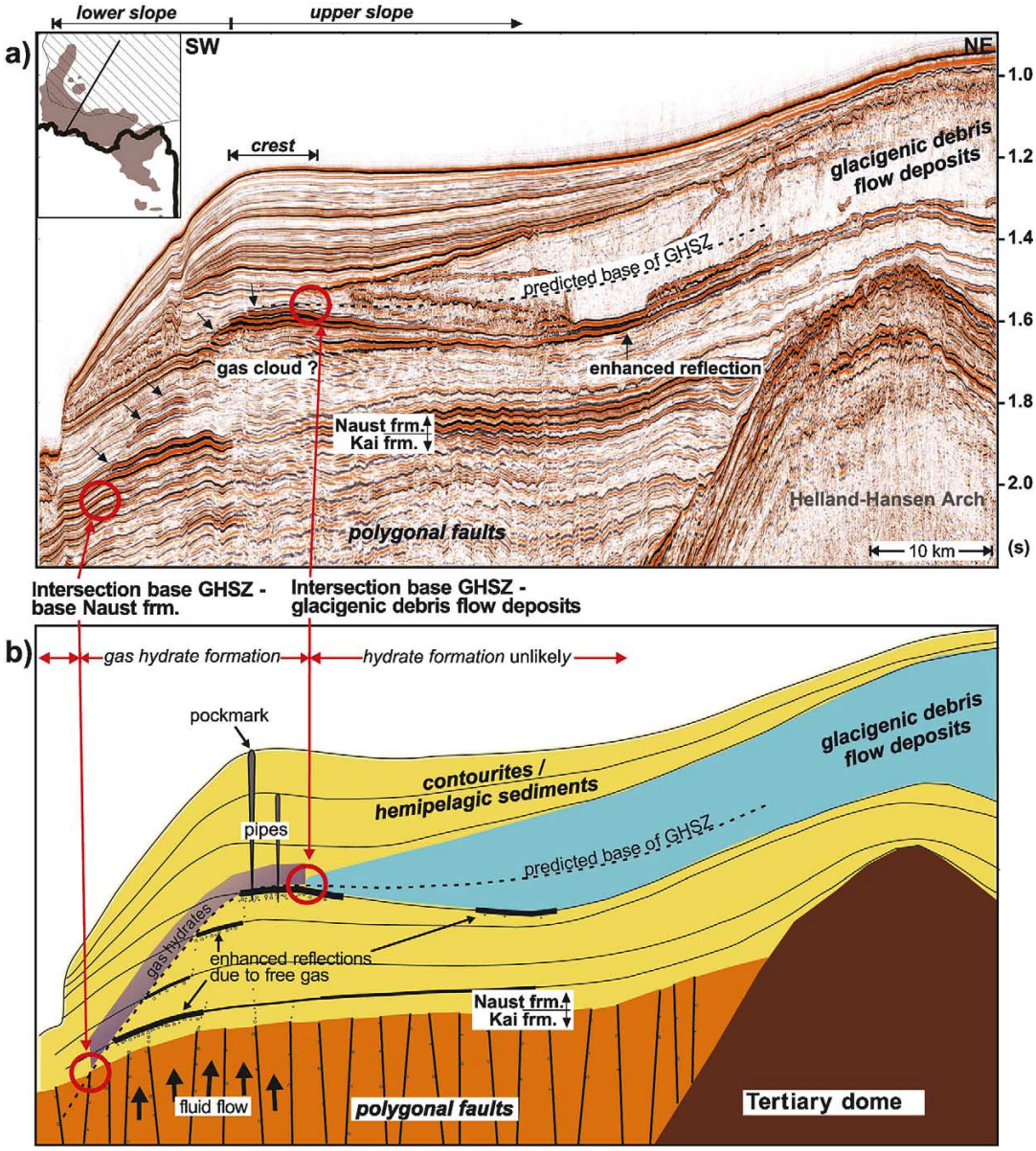


Figure 2.16: The effect of lithology on the Nyegga gas hydrate system. The illustration serves to highlight the preferential formation of gas hydrates within the contourites and hemipelagic sediments of the Naust Formation. In contrast, gas hydrates do not appear to be present within the fine sediments of the glacigenic debris flow deposits. Enhanced reflections beneath both the presumed gas hydrate zone and the glacigenic debris flow is deemed to be caused by free gas trapped beneath these impermeable zones. Figure from Bünz *et al.* (2003).

In the study area, DLF hydrates prevail, though FHF hydrates may be important consituents in the chimney zone (Hustoft *et al.* 2007, Faverola *et al.* 2009).

### 2.3.7 Hydrate system dynamics

In comparison to a conventional gas system, the hydrate system also requires a steady continuous flow of gas through the HSZ (Kvenvolden and Barnard 1983, Max *et al.* 2006). It is important to regard the HSZ as a dynamic system which will adjust to changing pressure (e.g. eustatic shifts) and temperature (e.g. annual variability and changing bottom currents). Eustatic changes are especially important in upper slope and shallow-water shelf regions, such as the Norwegian continental margin (Mienert and Posewang 1999, Posewang and Mienert 1999b, Mienert *et al.* 2000).

At the Nyegga study area, both the regional eustatic changes and the rapid shift in P-T conditions following the release of the Storegga slide (Solheim *et al.* 2005b) are to be considered.

## 2.4 Exploring for gas hydrates

The geophysical signature of gas hydrates allows them to be identified using both remote sensing as well as wireline logging tools. In addition, well sidewall coring and shallow coring provide means of collecting physical samples. Geochemical studies defining the sulfate-methane interface (SMI) as well as regional heat flow mapping assist in determining the regions of highest fluid flux suitable for hydrate formation. The occurrence of associated seabed features, notably pockmarks, may indicate areas of increased fluid expulsion. As with successful conventional gas exploration, integration of all available methods is critical to understanding the subsurface gas hydrate system.

### 2.4.1 Remote sensing

#### 2.4.1.1 Seismic

The most common, cost-effective and accurate method of identifying the presence of gas hydrates over large areas is by acoustic methods. Seismic methods are able to image the bottom simulating reflection (BSR), at the base of the hydrate stability zone. The BSR is generally a strong negative-polarity reflection dividing the upper high-velocity gas hydrate-cemented sediments from the underlying low velocity gas bearing sediments (Singh *et al.* 1993, Andreassen *et al.* 1995; 2000, Posewang and Mienert 1999b;a, Yuan *et al.* 1999, Haacke *et al.* 2007; 2008). BSRs in the Bering Sea have initially been identified as sedimentary features (Hein *et al.* 1978), and velocity profiles across BSRs are essential in identifying hydrates solely from acoustic methods.

The compressional P-wave ($V_p$) velocity decrease across the BSR gives the characteristic negative polarity seen on seismic profiles (Katzman *et al.* 1994, Andreassen *et al.* 1995, Minshull *et al.* 1993; 1994). On seismic profiles, the BSR can be most easily recognized by its tendency to cut across dominant stratigraphy. In addition, the temperature-governed spatial extent of the HSZ results in a mimicking of the seafloor, hence the name *bottom-simulating* reflection.

**2.4.1.1.1 The hydrate effect on sediment** Hydrate properties have been reviewed in Section 2.2.1.1. The formation of hydrate has a strengthening effect on its host sediment by incorporating pore water into its structure and replacing it with solid hydrate. This alters both the bulk ($K$) and shear moduli ($\mu$) and thus the P-wave velocity, $V_p$:

$$V_p = \sqrt{\frac{K + \frac{4\mu}{3}}{\rho}} \tag{2.3}$$

Laboratory experiments on coarse-grained sediments have confirmed an increase in $V_p$ from gas to water to hydrate to ice (Table 2.4). This effect is not so apparent in fine-grained sediments,

| | Coarse-grained sediment | | | | Fine-grained sediment | Source |
|---|---|---|---|---|---|---|
| | *Gas-charged* | *Water-saturated* | *Hydrate-saturated* | *Frozen sediment* | *Hydrate-saturated* | |
| $V_p$ | **< 1 km/s** | **1.77–1.94 km/s** | **2.91–4.00 km/s** | **3.88–4.33 km/s** | **1.97 km/s** | Winters et al 2007 |
| $V_p$ | | | | | **1.56-1.90 km/s** | Winters et al 2008 (INGH 2006 expedition) |
| $V_p$ | | | **2.73-2.80 km/s** | | | Winters et al 1999 (Mallik 1998 well) |
| $V_p$ | | | **2.70-3.30 km/s** | | | Lee & Collett 2001 |

Table 2.4: Laboratory-derived properties of hydrated sediments. The range of velocities is primarily a function of hydrate saturation. Based on data from Lee and Collett (2001), Winters *et al.* (1999; 2007; 2008).

as confirmed by the recent Indian Gas Hydrate Expedition (Winters *et al.* 2008). Additionally, different morphologies will exhibit different physical properties even at the same hydrate saturation (Holland *et al.* 2008).

Further discussion on the seismic response of gas hydrate is provided by Chand and Minshull (2003).

**2.4.1.1.2 Multichannel seismic data** Multichannel seismic reflection data can lead to the determination of high P-wave velocities and reduced amplitudes in a lens overlying the bottom-simulating reflection (BSR), as well as identification of 'bright spots' from concentrated hydrate layers, providing direct acoustic-only detection of hydrates (Hornbach *et al.* 2003).

The strength of the BSR is fundamentally controlled by the presence, and nature, of underlying gas (Figure 2.17). Based on a combination of single-channel seismic and wide-angle ocean bottom seismometers, Korenaga *et al.* (1997) determine free gas of low saturation ($< 10\%$) below the BSRs of the Blake and Carolina Ridges. A full waveform inversion determined that the strength of the BSR correlates with a low-velocity (~1.4 km/s) zone of trapped free gas below a thin, high-velocity (~2.3 km/s) wedge of possibly hydrate-bearing sediments (Korenaga *et al.* 1997).

On the Cascadia margin of Canada, hydrate deposits lacking a BSR have been mapped successfully through an electromagnetic survey (Yuan and Edwards 2000).

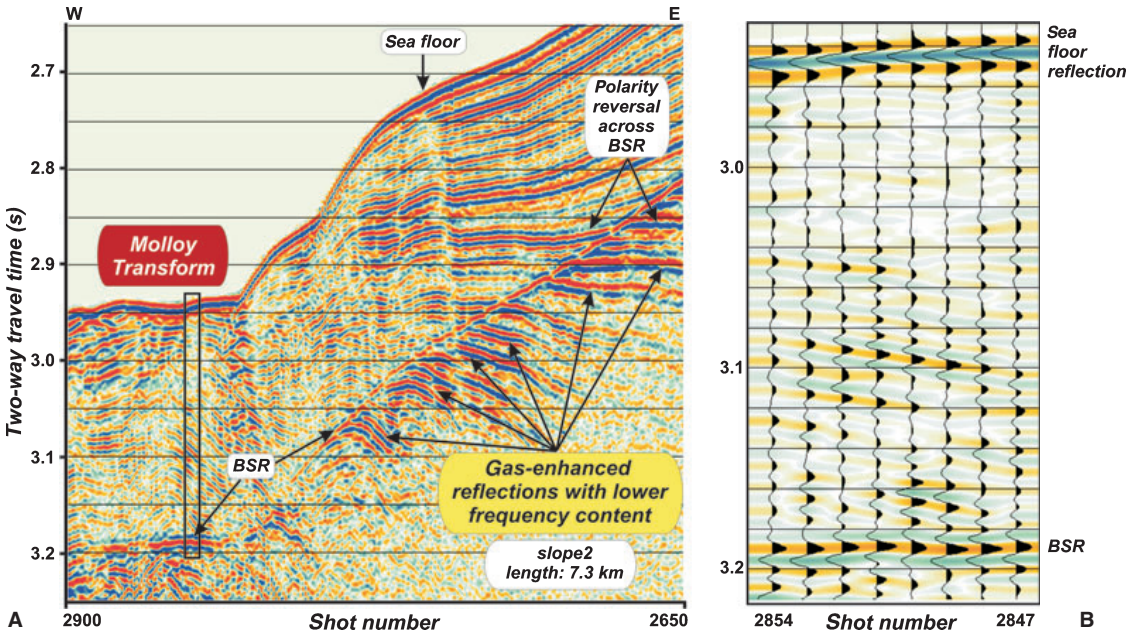


Figure 2.17: An example of a bottom-simulating reflection (BSR) from the West Svalbard continental slope. Note particularly the resemblance of the BSR to the seafloor, the polarity reversal across the BSR and the negative polarity compared to the seafloor. Figure from Vanneste *et al.* (2005).

**2.4.1.1.3 Alternative seismic methods** More detailed seismic analyses can be undertaken to provide more than a simple BSR outline map. Seismic determination of velocities (e.g. Minshull *et al.* 1993; 1994, Korenaga *et al.* 1997, Berndt *et al.* 2004a, Bünz *et al.* 2005b) is the first step towards proving the existence of hydrates, and may be used to estimate its concentration (Gorman *et al.* 2002, Ecker *et al.* 2000, Zillmer *et al.* 2005, Carcione *et al.* 2005, Westbrook *et al.* 2008a;b, Faverola *et al.* 2009). Ocean-bottom seismometer (OBS) data is especially useful for this purpose (Mienert *et al.* 2005a). Ocean-bottom cable (OBC) data, as discussed by Bünz *et al.* (2005a), is able to acquire S-wave data by deploying an ocean bottom cable with a series of multi-component sensors. This allows for the measurement of converted (PS) waves, which serve to identify hydrate accumulations. AVO[10] analysis, as applied by Andreassen *et al.* (1995) is particularly useful in understanding the free gas effect on the BSR.

A deep-towed seismic system, outlined by Wood and Gettrust (2001), provides the added benefit of flexibility while keeping a high resolution in the shallow surface. This system will become especially useful in ever-deepening waters.

High-resolution, high-frequency systems targeting the shallow subsurface are essential for hydrate studies, particularly if 3D acquisition can be achieved. The P-cable system currently used aboard R/V Jan Mayen (Rasmussen *et al.* 2007) may serve as an example of such systems.

#### 2.4.1.2 Seafloor acoustic imagery

High-flux gas hydrate systems manifest themselves onto the seafloor by forming both positive and negative landscape features. Common examples of these gas-escape features include pockmarks (Paull *et al.* 2008a, Mazzini *et al.* 2006, Hovland *et al.* 2005), submarine pingos (Hovland and Svensen 2006), mud volcanoes (Ginsburg *et al.* 1999, Bohrmann *et al.* 2003, Sauter *et al.* 2006, Tinivella *et al.* 2008) and craters (Solheim and Elverhoi 1993).

By utilizing multibeam, sidescan or high-resolution 3D seismic data, detailed maps of the seafloor can be generated. One example is the 10 * 10 m terrain model constructed for the Håkon

[10] AVO = amplitude versus offset

Mosby mud volcano (Beyer *et al.* 2005). This tool is especially powerful when accompanied by submarine photography, as in the Gulf of Mexico (Hart *et al.* 2008).

#### 2.4.1.3 Electromagnetic imaging

Electrical resistivity data have traditionally been, prior to the commercialization of this technology by Norway's EMGS[11], almost exclusively applied on wireline logging tools (Constable and Weiss 2006). At present, electro-magnetic (EM) surveys are more routinely used, coupled with seismic profiles, to aid in determining reservoir fluids (oil, gas or water). The principle remains the same as for wireline tools, in that it utilizes the high contrast between the background resistivity (1.1 Ωm to 1.5 Ωm (Schwalenberg *et al.* 2005b)), hydrocarbon resistivities (~50 Ωm (Eidesmo *et al.* 2002)) and gas hydrate resistivities (pure gas hydrate is a complete insulator, (Ellis *et al.* 2008, Yuan and Edwards 2000, Schwalenberg *et al.* 2005b;a; 2009a)). The major limitation remains the electrical penetration, which makes this method mostly suitable for shallow prospects within the uppermost 2 km of sediments (Ellingsrud, pers. comm. 2007).

Given the near-surface deep-water habitat of gas hydrates it is not a surprise that controlled-source EM was applied early on in hydrate exploration (Yuan and Edwards 2000, Schwalenberg *et al.* 2005b;a). Pure methane hydrate is a complete insulator that displaces conductive seawater during its growth, thus allowing for estimating gas hydrate saturation based on the EM method.

### 2.4.2 Downhole logging

Ground truth from wells and shallow cores can provide the only direct evidence of the physical properties of *in situ* hydrates. Before ODP Leg 164, only three hydrate zones were characterized by logging tools. One was the permafrost deposit of Alaska's North Slope (Collett 1993); the other two being from the coasts off Guatemala and western Canada (Collett and Ladd 2000). The ODP recognized the need for further information with its 'special holes' program, with Leg 164 concentrating on hydrates within Blake Ridge (Paull and Matsumoto 1995).

[11] EMGS = Electro-Magnetic Geo Services

The presence of hydrates on the Blake Ridge was detected both by electrical resistivity (Collett and Ladd 2000) and acoustic logs (Lee 2000). Physical detection, by recovery of hydrate during coring, allows the identification of hydrate-rich zones and subsequent development of a hydrate fingerprint. The following list of properties is based upon the Blake Ridge example (Collett and Ladd 2000), with modifications based on Sloan and Koh (2008):

- ***Mud log:*** gas from dissociating hydrates increases the gas content of the drilling mud. Most modern rigs have real-time gas chromatographs measuring the gas content of the circulating mud, and are thus additionally able to distinguish methane from higher-order hydrocarbons.
- ***Dual induction/Electrical Resistivity:*** higher electrical resistivity in the hydrate zone than in the water-saturated zone.
- ***Spontaneous Potential:*** lower spontaneous potential in the hydrate zone compared to the free gas zone.
- ***Caliper Log:*** generally higher borehole instability and collapse in the hydrate zone.
- ***Acoustic Transit-Time Log:*** faster velocities in the hydrate zone compared to both the free gas and water-saturated zones.
- ***Neutron Porosity:*** slight increase in neutron porosity in the hydrate zone compared to the free gas zone.
- ***Density Log:*** slight decrease in density in the hydrate zone compared to the water-saturated zone.
- ***Nuclear Magnetic Resonance:*** the NMR tool, coupled with the density log, can provide a good estimate for hydrate saturation.
- ***Drilling rate:*** drilling rate is lower in the hydrated zone, though not significantly different from that in ice.
- ***Gamma ray:*** The standard tool for distinguishing sand bodies within a shale sequence, thus useful for defining porous reservoirs.

### 2.4.3 The Sulfate Methane Interface

Due to the anaerobic oxidation of methane, gas hydrate is often absent from the upper few meters of the sediment (Borowski *et al.* 1996; 1999, Boetius *et al.* 2000, Borowski 2004, Lapham *et al.* 2008, Martin *et al.* 2009). Exceptions occur in areas with an extremely high methane flux (Milkov *et al.* 2000, Chapman *et al.* 2002, Hovland and Svensen 2006, Sauter *et al.* 2006, Riedel *et al.* 2006a, Hustoft *et al.* 2007). Methane and sulfate react at the sulfate-methane interface (SMI) to define the local top of the hydrate stability zone:

$$CH_4 + SO_4^{2-} \rightarrow CO_3^{2-} + H_2S + H_2O \tag{2.4}$$

It has been argued that a steep sulfate gradient represents a high methane-flux area (Borowski *et al.* 1999). Paull *et al.* (2005) proposed the 'SMI Rule of 10', which states that 'the methane concentration is insufficient to form hydrates until a depth 10 times the SMI depth´. In practice this means that in an area where the average SMI lies at 20 mbsf[12], hydrates will not be forming until a depth of 200 mbsf.

Authigenic carbonates are often associated with gas hydrate deposits, in a wide range of geologic settings. They form as methane-rich fluids oxidize and precipitate in the shallow subsurface (Johnson *et al.* 2003, Bojanowski 2007, Hovland 2002, Hovland *et al.* 2005). Bohrmann *et al.* (1998) and Aloisi *et al.* (2000) both provide examples of the interplay of hydrate and authigenic carbonate formation. Due to their *in situ* formation and no pressure-driven dissociation as for methane hydrate, authigenic carbonates are able to record (in their isotopic composition) the prevalent physical conditions at the time of formation. In the Nyegga study area, Paull *et al.* (2008a) argue on the basis of such isotopic information that the chimneys have previously served as fluid flux conduits only to be later sealed by such authigenic carbonates.

[12]mbsf = metres below seafloor

### 2.4.4 Heat flow

Globally, heat flow is highest along the tectonic plate boundaries, such as the Mid-Atlantic ridge. Local variations in fluid flow will affect the regional geothermal gradient.

In hydrate exploration, heat flow determinations are useful for two reasons:

1. They define a first-order estimate of the local geothermal gradient for subsequent modeling of depth to the base of the HSZ.
2. Regional and local scale heat flow maps may indicate gas venting through anomalies.

Heat flow may be coupled to the geothermal gradient provided that information on the thermal conductivity of the sediments is known (Pribnov *et al.* 2000). Geothermal gradients may either be extrapolated from shallow (up to 5 m) heat flow probe measurements or calculated from deeper borehole temperature measurements. In addition, in frontier basins with limited ground truth, the depth to the thermally-controlled BSR may be used to estimate heat flow (Townend 1997, Grevemeyer and Villinger 2001, Henrys *et al.* 2003, Vanneste *et al.* 2005; 2002). This is particularly useful in frontier oil and gas provinces, where BSRs may be used to provide input to the initial thermal basin modeling (Grauls 2001).

As might have become apparent in this section, the identification of oceanic hydrate requires an integration of a wide range of disciplines, including marine geology, geochemistry and geophysics.

## 2.5 From hydrate resources to produced reserves

Resources and reserves are two key terms when quantifying and classifying quantities of petroleum products. Resources cover all petroleum volumes, and may be subdivided into *undiscovered resources* thought to be present in a prospect before exploration drilling and *contingent resources* which are proven recoverable quantities whose recovery has not been clarified (NPD 2005). *Reserves* applies to petroleum products whose recovery has been decided and approved by the relevant authorities.

Both resources and reserves are, through the application of a recovery factor, given as technically recoverable quantities. Most hydrate estimates to date, are, however, given as in-place volumes.

### 2.5.1 Classifying gas hydrate resources

Hydrates may be seen as either a mineral or an unconventional petroleum deposit. On the one hand, its production involves the production of conventional methane and higher-order gases produced and sold in much the same way as conventional gas. On the other hand, it is a crystalline solid with methane as the economic material, which has been called an 'ore' of natural gas (Max *et al.* 2006), implying the continuous and well-defined nature of the economically extractable mass. At the same time gas hydrate deposits form an integral and highly dynamic part of the bio- and lithosphere, which places them somewhere between the realms of petroleum and economic geology.

Numerous hydrate classification schemes have been proposed (Figure 2.18). All involve a certain element of economic feasibility of the deposit's production as well as the geological understanding of the system. What is perhaps more important to consider than the classification of hydrate resources is their nature of occurrence (Figure 2.19). It quickly becomes apparent that most of the dispersed marine hydrate resources will never be produced. Even so, both permafrost and marine hydrates are abundant enough near existing infrastructure to be developed in the foreseeable future.

### 2.5.2 Classifying hydrate reservoirs

On the broadest scale, hydrate deposits may be classified on the basis of their formation, as outlined in Section 2.3.3.2. The end-member distributed low flux (DLF) and focussed high flux (FHF) gas hydrates can be related to two respective end-member economic hydrate accumulation types, namely the structural and stratigraphic types. In addition, hydrate morphologies will locally vary based on lithology, fluid flux and pore space availability.

#### 2.5.2.1 Economic hydrate accumulations

Milkov and Sassen (2002) define three types of economic gas hydrate accumulations:

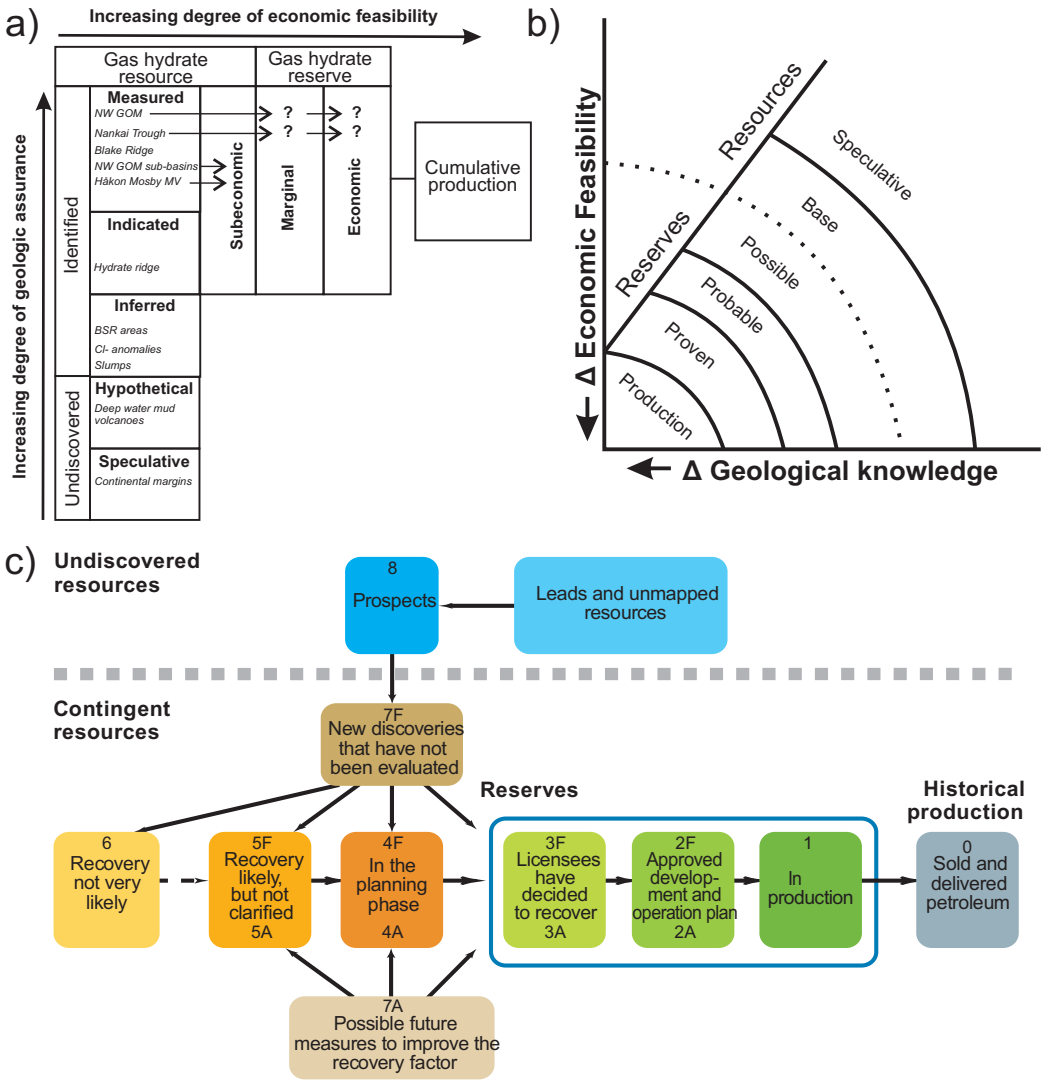


Figure 2.18: Three possibilities of classifying gas hydrate resources. (A) Hydrate classification developed by Milkov and Sassen (2002). (B) Similar hydrate classification proposed by Max *et al.* (2006). (C) Conventional oil & gas classification used by the Norwegian Petroleum Directorate (NPD 2005). Option (a) is used throughout this thesis.

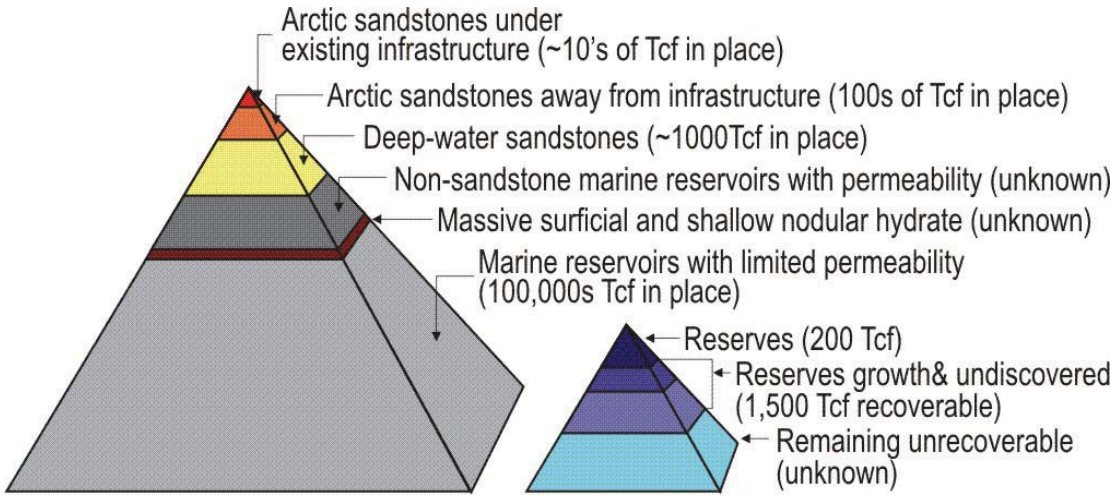


Figure 2.19: Gas hydrate resource pyramid developed by Boswell *et al.* (2007), with comparison to volumes within conventional gas reservoirs. The Nyegga prospect covers both the marine reservoir with permeability (regional BSR associated deposit) and the massive surficial hydrate (chimneys).

1. Structural accumulations
    - Associated with fault system
    - Associated with a mud volcano
2. Stratigraphic accumulations
3. Combination accumulations

Combination accumulations may incorporate elements of both end-members, the structural and stratigraphic deposits. A structural accumulation is characterized by high gas hydrate concentration, high resource density and high recovery factors. Correspondingly low development and production costs make structural accumulations the prime exploration target (Milkov and Sassen 2002).

Stratigraphic accumulations, on the other hand, typically exhibit low hydrate concentration, poor recovery factors, a low resource density and high cost of development and production. Sweet spots, such as the high gas hydrate-concentration sand layers of the Nankai Trough, may nonetheless still be considered as viable exploration targets (Milkov and Sassen 2002).

#### 2.5.2.2 Hydrate morphologies

Natural gas hydrates occur in sediments in two end-member type morphologies:

1. Grain-displacing
2. Pore-filling

Further subdivision of these small-scale morphologies requires borehole pressure coring tools, such as HYACINTH (Schultheiss *et al.* 2006), to study gas hydrates at *in situ* conditions. It is important to distinguish the inequivalent subdivision of 'massive' and 'disseminated' gas hydrates from 'grain-displacing' and 'pore-filling' morphologies. The former are typically associated with negative thermal anomalies measured on conventional cores, where recent endothermic hydrate dissociation reactions resulted in cold regions (Holland *et al.* 2008).

Grain-displacing hydrate forms layers, veins and lenses of highly concentrated hydrate. It does not occupy pore space and Archie's calculations of hydrate saturation are therefore unsuitable, as they assume a uniform medium with conductive seawater and resistive hydrate particles. The wide range of sizes, ranging from thin veins to massive hydrate blocks, further complicates hydrate saturation calculations, especially when no ground truth exists.

Pore-filling hydrates, on the other hand, form in the pore space of sediment where it may or may not cement the host sediment. Pore-filling hydrates typically occur in coarser sedimentary layers (sand - silt) within a fine-grained matrix, and have been recovered from numerous geological settings (Riedel *et al.* 2005, Winters *et al.* 2008).

Different hydrate morphologies will have a fundamental impact on geophysically-derived measurements, using both remote sensing and borehole logging methods. The widespread assumption that gas hydrate occurs as a pore-filling, uniform and isotropic element of the subsurface is invalid and morphologies need to be considered when modeling the hydrate system (Holland *et al.* 2008).

| Class | Hydrate | Bounded | Materials in contact beneath hydrate | Geological situation | Groundwater system |
|---|---|---|---|---|---|
| 1 | Concentrated | Permeability boundaries/geological strata/faults | Gas over water | Oceanic | Unconfined |
| | | | | Permafrost | Confined |
| 2 | | | Mobile water | Oceanic, Normal (2-OU) | Unconfined |
| 3 | | | No gas or water | Trap | No mobile fluids |
| 4 | Dispersed | No effective permeability boundaries | Pore water | Undifferentiated marine sediments | Unconfined |

Table 2.5: An attempt at classifying gas hydrate deposits with respect to their production chracteristics, after Max *et al.* (2006).

#### 2.5.2.3 Hydrate production classes

Moridis and Collett (2003) define four classes of hydrate deposits on the basis of their production strategies (Figure 2.5).

A Class 1 deposit consists of an impermeable hydrate zone underlain by a two-phase fluid zone with free gas. The base of the hydrate stability zone (HSZ) typically lies in close proximity to the hydrate phase boundary (HPB), and production is thus typically less energy-demanding than for other classes (Moridis and Collett 2003).

A Class 2 deposit involves a hydrated layer overlying a mobile water zone with no gas.

A Class 3 deposits involves only a hydrate-bearing zone, with no contact to underlying mobile zones.

Class 4 deposits, typically dissemiated and exhibiting low hydrate saturation ($< 0.1\%$), have been evaluated by Moridis and Sloan (2007).

Both Classes 2 and 3 may be located well away from the HPB, and their production may thus be rather energy-demanding (Moridis and Collett 2003).

### 2.5.3 Global hydrate estimates

Global hydrate-bound methane estimates, even though greatly reduced from the overly optimistic estimates of the early 1970s (Figure 2.20), still lie an order of magnitude higher than global conventional gas reserves (BP 2008, OPEC 2008).

The latest estimates place the total global methane hydrate amount, converted to standard atmospheric temperature and pressure, on the order of 1-5x$10^{15}$ $m^3$, equivalent to approximately 500-2,500 giga tonnes of methane carbon (Milkov 2004)[13]. The highest estimate places it at ~75,000 GT (Klauda and Sandler 2005). The Klauda & Sandler model (Figure 2.11) is able to predict 68 of 71 known gas hydrate sites, but may be affected by overly optimistic assumptions such as the 3.4% global hydrate saturation within the HSZ (Klauda and Sandler 2005).

Total global hydrate-bound methane estimates merely provide an academic exercise in uncertainty management. However, the aforementioned studies reveal the vast dominance of marine hydrates in comparison with permafrost hydrates. Notably, a 1% error in the marine hydrate-bound methane is so large that it easily encompasses the whole permafrost hydrate-bound methane (Sloan and Koh 2008). This is primarily attributable to the higher carbon flux in oceans (Dillon and Max 2000).

As with conventional gas resources, the hydrate-bound gas resource may be subdivided by its occurrence. Only a small percentage (10's of TCF[14]) occurs under existing infrastructure (e.g. Alaskan North Slope, Mackenzie Delta) while the vast majority of possible resources lies within the marine environment dispersed as non-economic resources. A comparison with conventional gas resources reveals that the hydrate-bound methane in deep water sandstones and non-sandstone marine reservoirs with ample permeabilities for production approximate the total conventional gas resources (Figure 2.19).

#### 2.5.3.1 Regional hydrate estimates

Regional hydrate estimate were calculated for both the Gulf of Mexico region (MMS 2008) and the Alaskan North Slope (Collett *et al.* 2008). While the final number of hydrates bound in sandstone reservoirs (190 000 $GSm^3$ in the Gulf of Mexico, 2 400 $GSm^3$ on the Alaskan North Slope)

[13]This is equivalent to 10 times the global conventional gas reserves, and represents approximately 800 years of the global gas consumption (CIA 2008).

[14]1 TCF (trillion cubic foot) equates to 0.028 TCM (trillion cubic meters) at standard conditions (@ 14.73 psia and $60^0F$).

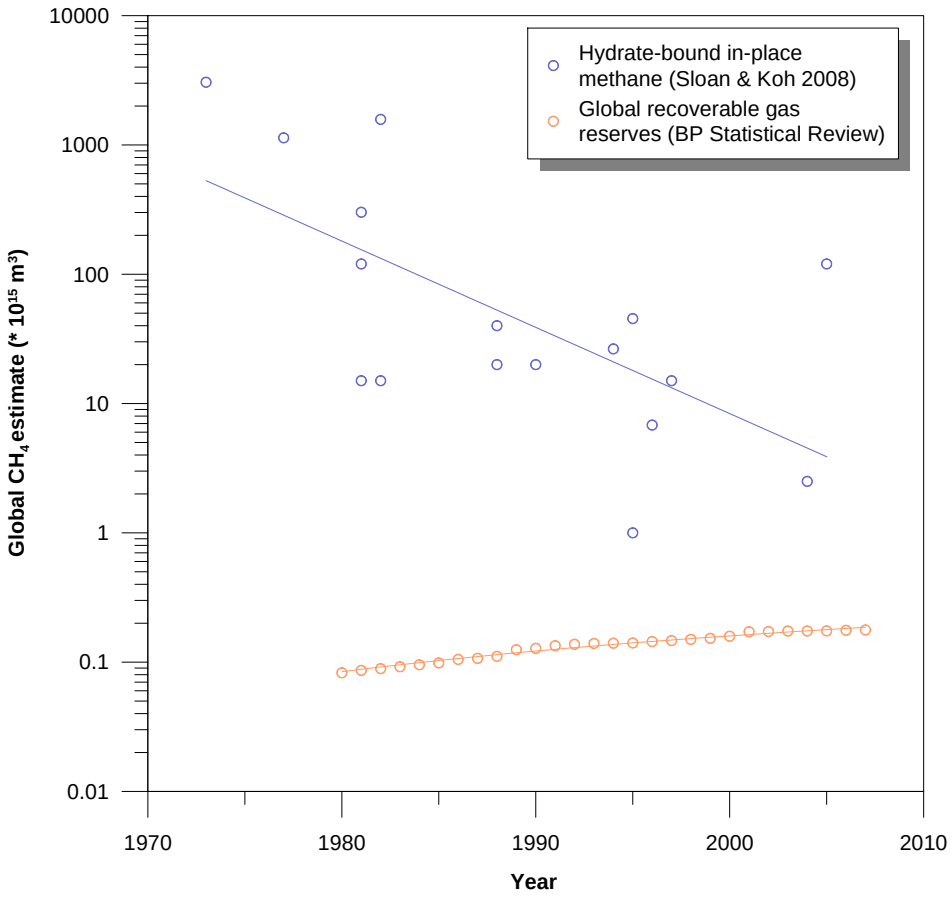


Figure 2.20: Estimates of global gas hydrate resources. The conventional recoverable gas reserves are plotted for comparison. A large range of currently published global hydrate estimates highlights the large uncertainty of characterizing hydrate provinces. The increase in conventional reserves is primarily related to ongoing exploration and development of technologies that allow for the production of non-conventional gas deposits (e.g. shale gas, tight sands, coalbed methane). Note the logarithmic y-axis. Data from BP (2008) and Sloan and Koh (2008).

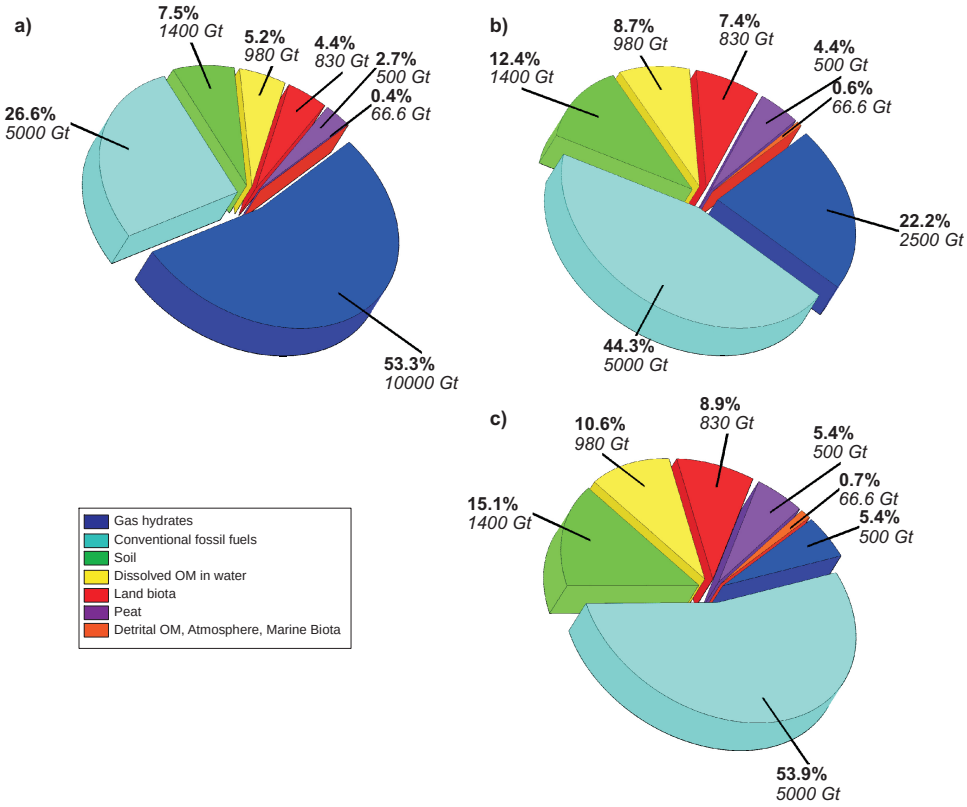


Figure 2.21: The distribution of organic carbon in the Earth's reservoirs, plotted using data from USGS and Milkov (2004). Organic carbon in rocks and sediments is unaccounted for and would account for more than 1,000 times the total amount depicted here. 'Gas hydrates' refers to known and inferred oceanic and permafrost hydrate reservoirs. Conventional fossil fuels include oil, natural gas and coal. The land component includes peat, soil, detritus and biota. The ocean component includes dissolved organics and biota. Carbon dioxide is responsible for the bulk of the atmosphere. (A) USGS best-estimate. (B) Upper bound calculated by Milkov (2004). (C) Lower bound calculated by Milkov (2004).

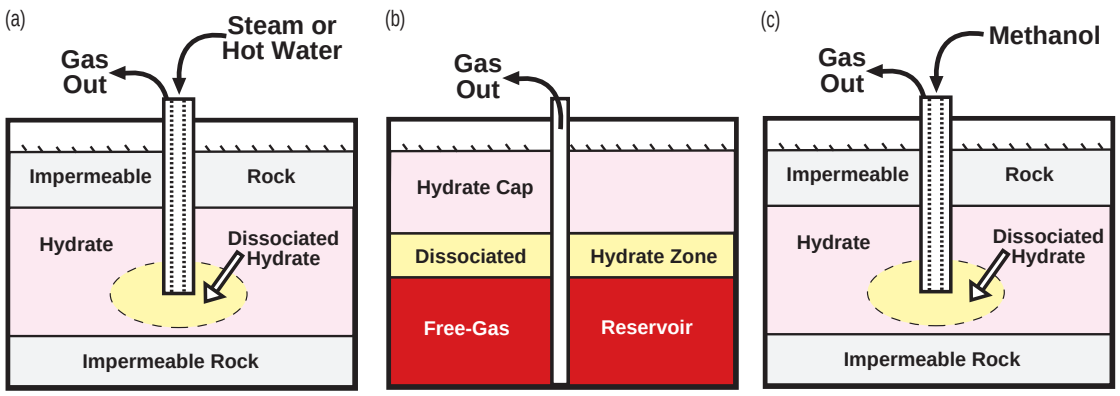


Figure 2.22: Sketch of the three main production scenarios for hydrate extraction. (A) Thermal stimulation, dissociating hydrate by injection of hot brines. (B) Depressurisation, allowing for hydrate dissociation by producing the underlying free gas zone and thus drawing down the pressure. (C) Inhibitor injection, requiring the injection of methanol to break down hydrate and allow for the production of released methane. Figure from Collett (2002).

is interesting in itself, the work provides an approach for assessing hydrate potential on a regional scale. A summary of similar regional studies is covered as a comparison to the Nyegga area in Table 7.1.

### 2.5.4 Production of gas hydrate and associated free gas

To dissociate gas hydrate, one can either lower the pressure, increase the temperature or add an inhibitor (Figure 2.7). Combinations of the above can also be applied. The production strategy will ultimately depend on the geological setting and the hydrate reservoir properties (Moridis and Collett 2003). The three main potential production methods reflect the above dissociation mechanisms (Figure 2.22).

#### 2.5.4.1 Depressurisation

Depressurisation fundamentally involves the production of free gas or water from beneath the gas hydrate zone.

Production of free gas, in contrast to the dissociation of gas hydrates, decreases the reservoir

pressure. The resulting lower pressure will effectively cause gas hydrates to dissociate, with an added gas influx into the production wells. This is thought to be the method by which hydrates have already been produced at Messoyakha (Makogon 1965, Makogon *et al.* 2004; 2007), North Slope Borough (Singh *et al.* 2008) and the initial Mallik test of 2002 (Hancock *et al.* 2005a). The method is particularly well suited to Class 1W and Class 1G (see Table 2.5) deposits, in which the gas hydrate deposit lies at the base of its stability zone. A limited amount of energy is thus required to move the deposit outside its stability zone.

Depressurisation was fully tested at the Mallik site during the 2007 and 2008 production tests. In 2008, continuous gas flow was achieved over a 139 hour period (Numasawa *et al.* 2008). While technical problems regularly hamper operations, depressurization is currently deemed to be the most promising method for dissociating *in situ* hydrates (Max *et al.* 2006).

Reservoir modeling using the TOUGH-Fx/HYDRATE simulator has shown that hydrates contribute significantly to both production rate (65-75%) and cumulative produced volume (45-54%) for modelled Class 1W and 1G reservoirs (Moridis and Kowalsky 2006).

#### 2.5.4.2 Thermal stimulation

Thermal stimulation involves the externally-forced heating of the reservoir, warming it up to a level outside the hydrate stability zone. Hot saline aqueous brines, a by-product of conventional oil and gas operations, are best suited for this purpose. Other techniques, including steam injection, cyclic steam injection and fire flooding, suffer from high heat loss (Max *et al.* 2006).

Thermal stimulation was the method employed at the first research-oriented Mallik production test in 2002, producing a modest 468 $Sm^3$ of gas during its 124 hour test duration (Dallimore and Collett 2005, Hancock *et al.* 2005b).

Experimental studies conducted by Tang *et al.* (2005) suggest an increasing-decreasing gas production rate during a 300 min experiment. The water production remained constant during the same test. The authors concluded that the efficiency of the process is a function of the inlet brine temperature, the injection rate and the initial hydrate saturation (Tang *et al.* 2005). Most

favorable conditions for the highest energy recovery ratios appear to be lower injection temperatures and rates coupled with higher initial hydrate concentrations (Tang *et al.* 2005). The disadvantage of this concept is the need for energy to recover energy, with typical energy ratio values of 1.0 (White *et al.* 2005). In essence, this requires 50 % of the recovered energy to be used to heat the injected brine.

Thermal simulation has, through numerical simulations (Moridis and Collett 2003), been shown to be more appealing in hydrates of Class 2 and 3 rather than Class 1.

#### 2.5.4.3 Inhibition

The inhibitor injection, effectively the chemical manipulation of the hydrate phase boundary, has been applied with good short-term results at the Messoyakha field (White *et al.* 2005, Makogon *et al.* 2007, Sloan and Koh 2008). The method has been examined both numerically (Sung *et al.* 2002) and experimentally (Sung and Kang 2003) and it follows that inhibition by methanol[15] lowers the hydrate formation temperature and thus potentially releases encaged methane. Dissolved salts (e.g. NaCl, $CaCl_2$, KCl, NaBr) may also function as inhibitors and, for this reason, mainly brines are used in the thermal stimulation method.

The knowledge of using inhibitors for assuring flow in pipelines is high (Carroll 2003). However, on a field-scale, hydrate production by inhibition is prohibitive due to its high cost, the thermal self-regulation of gas hydrates and the environmental impact on the subsurface (Max *et al.* 2006, Sloan and Koh 2008).

#### 2.5.4.4 Alternative methods

Research is ongoing to identify alternative hydrate production methods, including gas phase exchange (Ohgaki *et al.* 1994, Kvamme *et al.* 2007), electromagnetic heating (Islam 1994, Tang *et al.* 2005), exothermic heating (Chatterji and Griffith 1998), geothermal heating (Ning *et al.* 2008) or subsurface mining (Max *et al.* 2006). Gas exchange, essentially the injection of $CO_2$ and subsequent

[15]Other inhibitors frequently used include monoethylene glycol (MEG).

exchange of $CH_4$ by $CO_2$ as the main guest molecule, is of particular interest given the added benefit of storing the greenhouse gas $CO_2$ underground in a relatively safe and stable hydrated form. Furthermore, experiments verified by reservoir modeling suggest a possible three-fold increase in gas recovery by utilizing $CO_2$ injection as part of gas hydrate recovery (McGrail *et al.* 2007).

# Chapter 3

# The Nyegga area

## 3.1 Location

The study area lies in the Norwegian Sea offshore Mid-Norway approximately 100 km north of the Ormen Lange gas field (Figure 3.1). The area covers the whole of Quad 6404 and most of Quad 6405, as well as parts of Quads 6503, 6504, 6505, 6403, 6304 and 6305[1]. One of the world's largest submarine slides, the Storegga slide, lies in the southern part of the study area.

The center of the largest mapped gas hydrate accumulation, referred to as the 'Nyegga' prospect, lies 136 km north of the Ormen Lange gas field, 83 km south-west-west of the Kristin gas/condensate field and 239 km from the nearest onshore facility at Tjeldbergodden.

## 3.2 Geological development of the mid-Norwegian margin

The mid-Norwegian margin has been shaped by a combination of lasting tectonically-driven processes and more recent glacial activity.

[1] The exact boundaries for the study site are defined by Universal Transverse Mercator (UTM) coordinates 255 000-350 000 (East) and 7 067 500-7 250 000 (North). The complete study site lies in UTM zone V32.

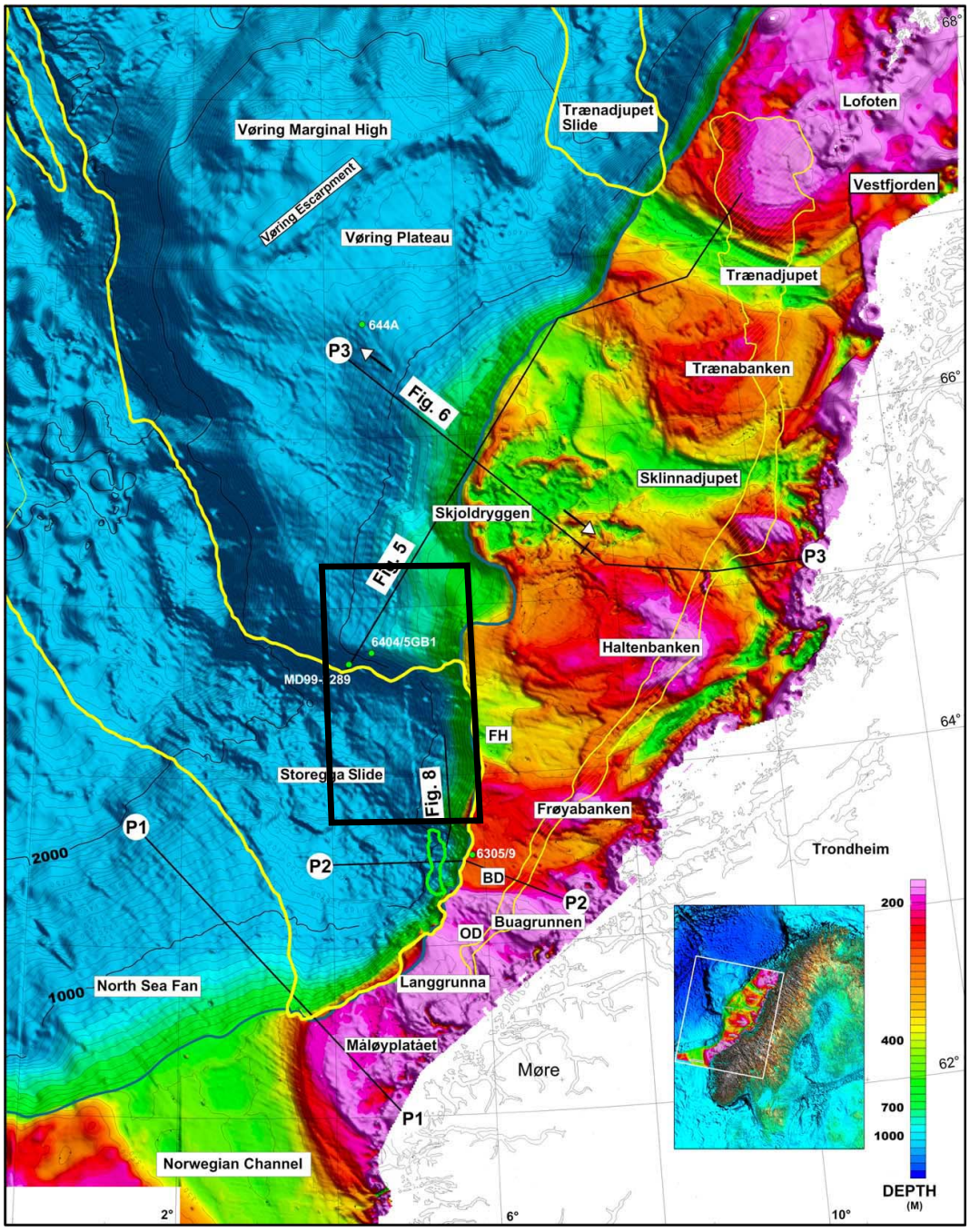


Figure 3.1: Study area location, as outlined by the black rectangle, in the context of the regional bathymetry of Rise *et al.* (2005). Note the profile locations P1, P2 and P3 plotted on Figure 3.4. FH: Frøyabankhola, BD: Buadjupet, OD: Onadjupet. The blue line marks the shelf break, while the green line indicates the Ormen Lange gas field.

### 3.2.1 Tectonic evolution

The passive mid-Norwegian continental margin developed during several rifting episodes since the Permian. Three main tectonic phases have been identified; Late Paleozoic, Late Mid-Jurassic-Early Cretaceous and Late Cretaceous-Early Tertiary (Brekke 2000). All these events were controlled by two major structural trends: NE-SW and NW-SE. The transverse NW-SE trend is manifested through a series of lineaments (Brekke 2000). The final continental break-up in the Early Eocene (~ 55 My) resulted in the opening of the Norwegian-Greenland Sea and was accompanied by thermal subsidence that led to the development of the Møre and Vøring sedimentary basins (Bjørnseth *et al.* 1997, Brekke 2000).

During the strike-slip compression of Late Eocene and Mid-Miocene time, N-S trending anticlinal structures, such as the Ormen Lange Dome, developed (Doré 1996, Brekke 2000, Lundin and Doré 2002). The growth of these tectonic features was typically governed by the reactivation (and reversal) of pre-existing faults (Brekke 2000). These structures presently act as structural-stratigraphic traps with both leaking (e.g. Helland-Hansen Arch) and producible hydrocarbon systems (e.g. Ormen Lange gas field).

Rift-associated sedimentation exhibits large spatial and temporal variations due to changes in tectonic deformation, sediment supply and climate (Ravnas *et al.* 2000). In contrast, sedimentation within the past ~3 My was primarily a function of glacial activity and associated sediment supply.

### 3.2.2 Glacial evolution

Uplift of the Norwegian mainland during the past 4 My provided additional sediment supply from the east (Hjelstuen *et al.* 1999). However, it was primarily the glacial activity that began ~3 My ago that shaped the present-day continental shelf.

The last ~3 My have been characterized by extensive deposition of glacially derived material transported westwards from the Norwegian mainland and the inner part of the continental shelf. These deposits, well over 1000 m thick over a wide area, are defined as the Naust Formation (Dalland

| Property | Diamicton | Marine clay |
|---|---|---|
| Clay content | 30–40% | 50–60% |
| Water content | 10–20% | 25–35% |
| Unit weight | 20–22 kN/m$^3$ | 18–19 kN/m$^3$ |
| Sensitivity | Lower | Higher |
| Plasticity | 15–25 | 30–35 |
| Geotechn. behaviour | Dilatant | Contractant |

Table 3.1: Summary of the physical property characteristics for the two prevalent sediment types in the study site. Table from Berg *et al.* (2005).

*et al.* 1988, Rise *et al.* 2005).

The variation between glacial and interglacial regimes resulted in a fluctuating depositional environment, from shelf-wide deposition of glacigenic debris flow (GDF) deposits during glaciations and predominantly glacimarine/hemipelagic deposition during interglacials. The Fennoscandian Ice Sheet has reached the shelf edge on multiple occasions[2], most recently during the Last Glacial Maximum (LGM; Hjelstuen *et al.* (2005), Larsen and Sejrup (1990)). Cyclical variations within each glaciation further affected depositional patterns.

Two main modes of deposition have been identified by Berg *et al.* (2005). During peak glaciations, basal tills have been deposited on the shelf, partially reworked on the shelf edge into glacigenic debris flows on the continental slope (Figure 3.2). In the more frequent and longer-lasting interglacial periods, normal marine and distal glacial marine conditions prevailed (Berg *et al.* 2005).

The two resulting broad classes of sediment, diamicton and marine clay respectively, exhibit very different properties (Table 3.1). These, in conjunction with loading, are highly important with respect to slope stability (Rise *et al.* 2005, Nadim *et al.* 2005). All major glide planes on the Norwegian margin are, for example, initiated within the weak zone of the marine clay (Berg *et al.* 2005).

It is generally agreed that the first major ice advance occurred in the Early Pleistocene at ca. 1.1 My (Sejrup *et al.* 1995, Hjelstuen *et al.* 2005, Rise *et al.* 2005). However, in the period from 2.6 My to 0.5 My, ice sheets were largely restricted to fjords and the inner shelf (Figure 3.3).

[2]Specifically during Marine Isotope Stages 12, 10, 8, 6 and 2, please refer to Figure 3.3 for timing of the individual stages.

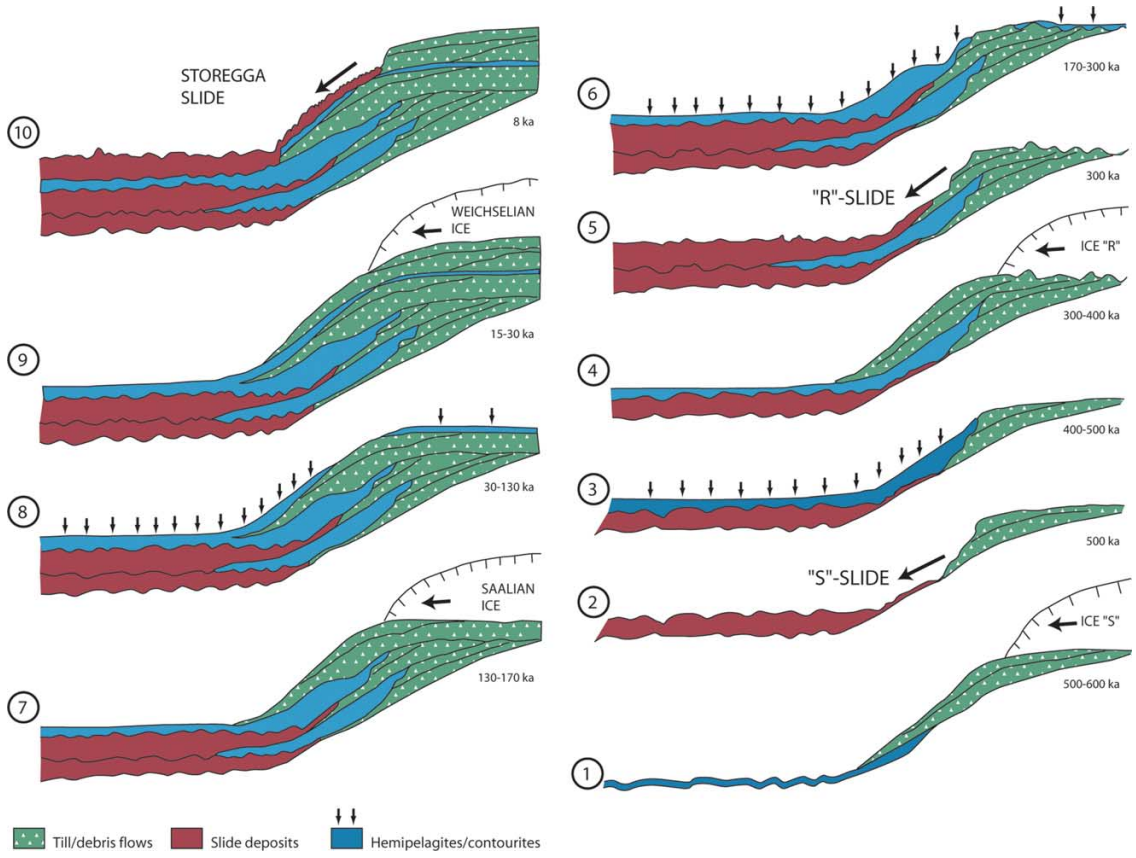


Figure 3.2: Processes associated with Plio-Pleistocene glaciations on the Norwegian Continental Shelf. The figure illustrates the area's development during the last half a million years. It is notable that the three main slides, the 'S', 'R' and 'Storegga' slides appear to be cyclic events occuring after major glaciations provided extensive sediment input to the shelf break. Also note the alternating deposition of glacigenic debris flows and hemipelagic muds. Figure from Rise *et al.* (2005).

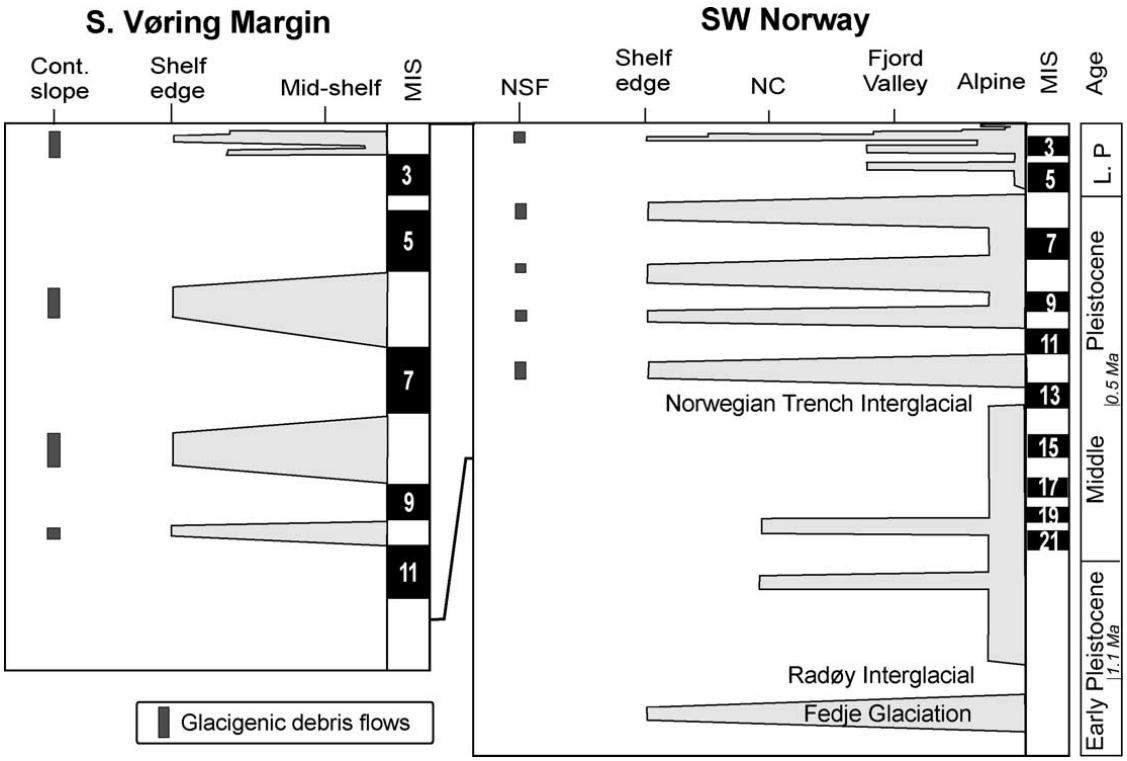


Figure 3.3: The spatial and temporal extent of Pleistocene glaciations on the Norwegian Continental Margin. Note particularly the glacigenic debris flows associated with major glaciations reaching the shelf edge. Figure from Hjelstuen *et al.* (2005).

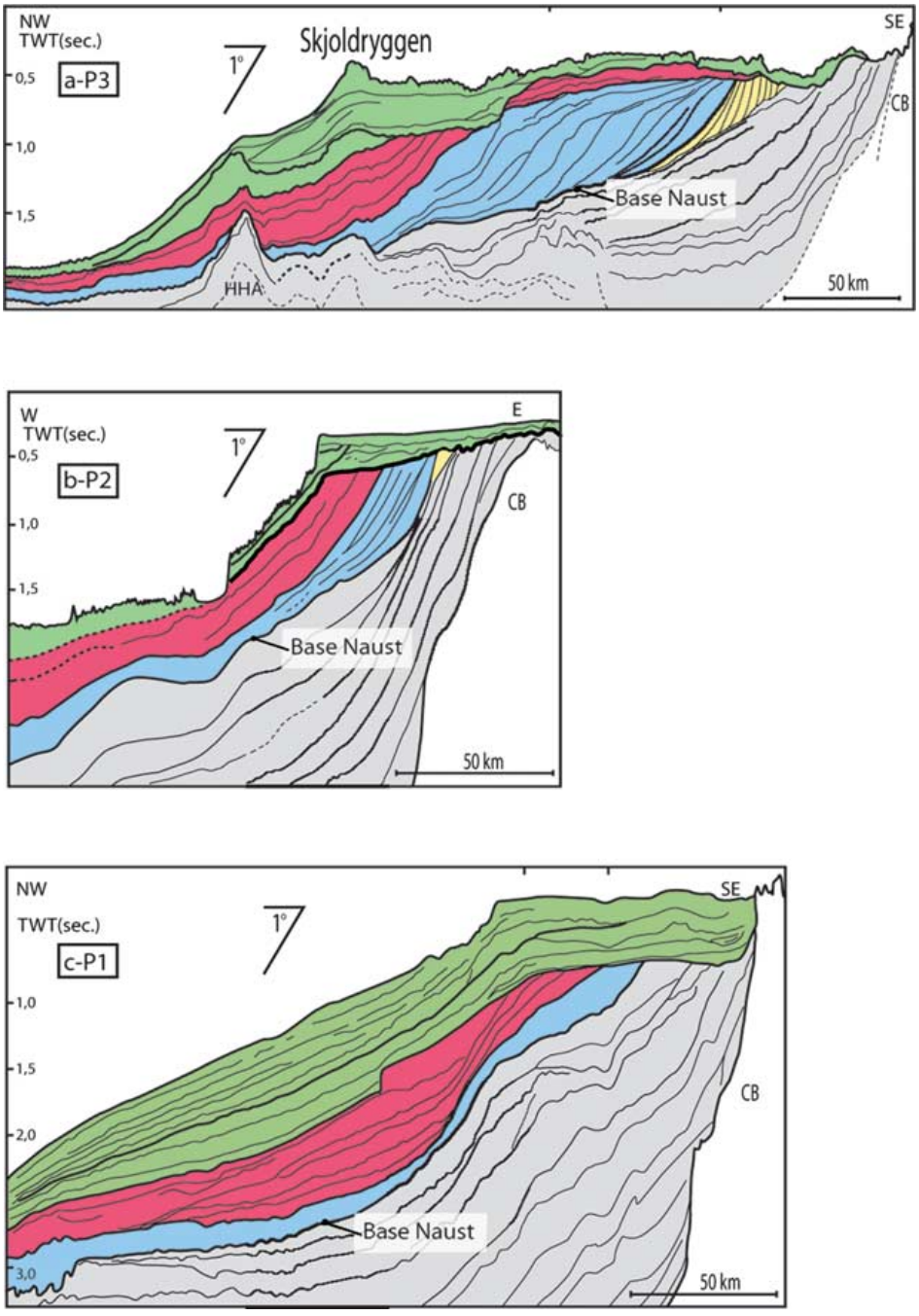


Figure 3.4: Regional deposition patterns of the Naust Formation. Note the distinct 'packages' associated with the major glaciations, as well as the prograding wedges. For location of the profiles refer to Figure 3.1. HHA = Helland-Hansen Arch. Figure from Rise *et al.* (2005).

## 3.3 Lithostratigraphy

The regional stratigraphy is illustrated by Figure 3.5, and is primarily based on Rise *et al.* (2006).

The Nyegga gas hydrate system is fundamentally linked to the two youngest sedimentary successions: the Miocene/earliest Pliocene Kai Formation and the Plio-/Pleistocene Naust Formation. Contourites are important constituents of both these formations.

### 3.3.1 Kai Formation

The Kai Formation[3] is a regionally extensive marine formation comprising claystones, silstone and locally varying amounts of sandstone with limestone stringers (Dalland *et al.* 1988). Fine-grained hemipelagic ooze is the main constituent of the Kai Formation (Rokoengen *et al.* 1995, Evans *et al.* 1996).

Its contraction during rapid sedimentation, coupled with pore fluid extraction, is thought to be responsible for the development of an extensive network of layer-bound non-tectonic polygonal faults (Cartwright and Lonergan 1996, Berndt *et al.* 2003). These small-offset non-tectonic faults, seen in their distinctive polygonal shape through the use of 3D time-slice seismic data, commonly occur in two tiers of the uppermost Brygge Formation and within the Kai Formation (Berndt *et al.* 2003). The extent of these faults is primarily controlled by the thickness of the host Kai Formation (Berndt *et al.* 2003).

Polygonal fault systems have been previously shown to be important conduits for regional fluid flow as well as providers of a local fluid source suitable for the formation of gas hydrates (Henriet *et al.* 1991, Berndt *et al.* 2003, Hustoft *et al.* 2007).

### 3.3.2 Naust Formation

The Naust Formation[4] is defined as the glacial-interglacial sediment package deposited during the Plio-Pleistocene climate-driven cycles (Sejrup *et al.* 2004, Hjelstuen *et al.* 2005, Rise *et al.*

[3]Type well: 6407/1-2, in Dalland *et al.* (1988).
[4]Type well: 6507/12-1, in Dalland *et al.* (1988).

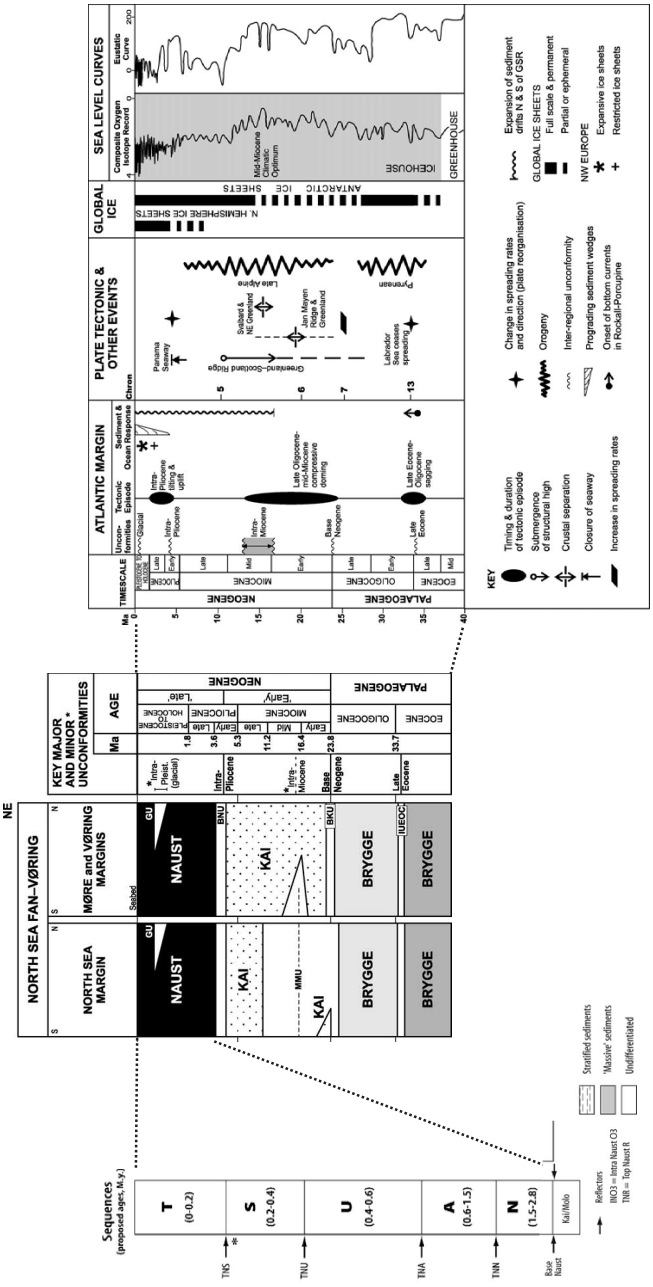


Figure 3.5: Subdivision of the Naust Formation units as seen in the overall Neogene stratigraphic framework proposed by Stoker *et al.* (2005). Note particularly the setting of the Naust Formation, as defined by the Plio-Pleistocene glaciations. Figure compiled with components from Rise *et al.* (2005), Rise *et al.* (2006), Bryn *et al.* (2005b) and Stoker *et al.* (2005).

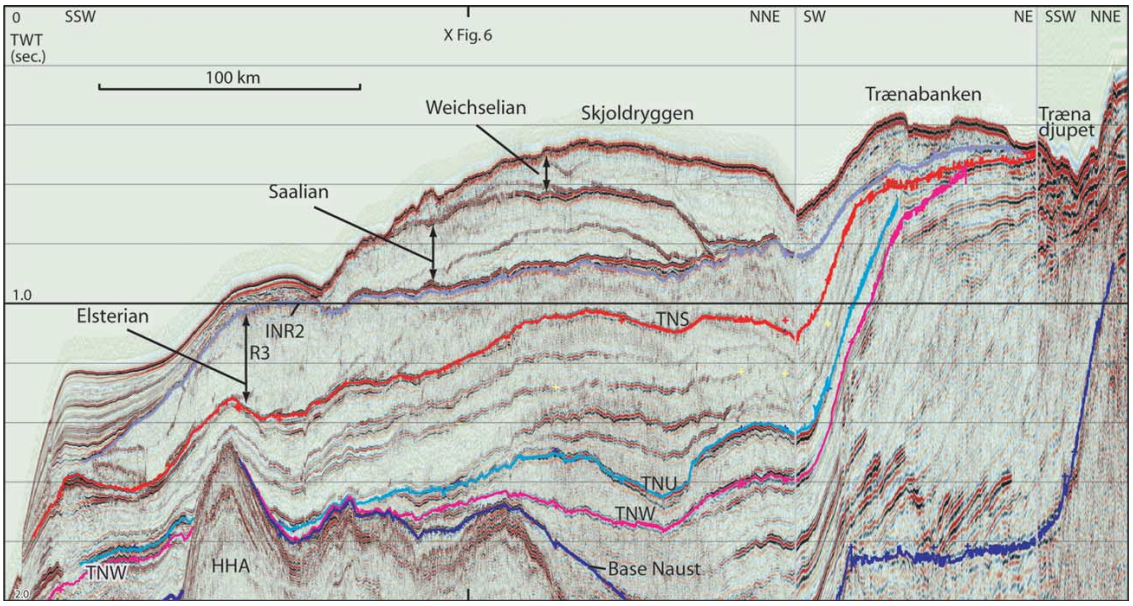


Figure 3.6: Naust Formation subdivisions. Please refer to Figure 3.5 for definition of seismic horizons. For location please refer to line marked 'Fig. 5' on Figure 3.1. From Rise *et al.* (2005).

2006). The lithologically heterogeneous formation consists of glacigenic debris flows, basal tills and hemipelagic/glaciomarine oozes.

The Naust Formation can, on the basis of a shallow geotechnical borehole (6404/5GB1) and seismic correlation (Hjelstuen *et al.* 2004, Rise *et al.* 2005; 2006), be further subdivided into 5 units: N, A, U, S and T (Figures 3.5 and 3.6, Rise *et al.* (2006)).

No polygonal faulting has been identified in the Naust Formation, though hints of deformation have been described above zones of intense faulting in the underlying Kai Formation (Berndt *et al.* 2003).

### 3.3.3 Contourites

Drift deposits[5] are common along the Norwegian continental margin (Laberg *et al.* 2001). Drift deposits form an important sediment group within both the Kai and Naust Formations.

Drifts may be subdivided and classified into six main classes on the basis of their morphology.

[5]Drift deposits are sometimes also referred to as contouritic oozes.

Their detailed description is beyond the scope of this thesis, but interested readers are referred to Stow *et al.* (2002) and references therein.

Sedimentation due to bottom-water activity has been most prevalent between 12 and 4-3 My, though even in the last 3 My contourite processes prevailed to infill mass wasting scars (Bryn *et al.* 2005b). They typically exhibit high sedimentation rates (up to 1.2 m/ky on the Norwegian continental margin, Laberg *et al.* (2001)), especially if close to the sediment source area. The Lofoten Drift, in contrast, exhibits relatively low sedimentation rates of 0.036 m/ky (Laberg *et al.* 2001), probably due to the reduced downslope sediment input from the barrier-like Lofoten Islands (Laberg *et al.* 2002). The Storegga contourites experience relatively stable sedimentation rates of ~1-2 m/ky over the past 8000 years (Bryn *et al.* 2005b).

Within the Kai Formation sediment drifts developed predominantly without the influence of downslope processes through deep-water basinal sedimentation (Bryn *et al.* 2005b). These drifts, with sediment unit weights of ~14-15kN/m$^3$, are typically not affected by mass wasting processes (Bryn *et al.* 2005b).

In contrast, the Naust Formation sediment drifts are affected by mass wasting processes as well as exerting an effect on those. Primarily, they deposit within the large-scale depressions of the Lofoten and Storegga regions, forming an infill of old slide scars (Bryn *et al.* 2003; 2005b, Solheim *et al.* 2005a). In addition, their 'weaker' physical properties relative to the coarser glacial debris flow deposits (Kvalstad *et al.* 2005), make them a prime candidate as failure planes (Bryn *et al.* 2005b, Leynaud *et al.* 2007).

## 3.4 Oceanography

The study area lies within the Norwegian-Greenland Sea (Figure 3.7), in which oceanic circulation is governed by the northward-flowing waters of the NAC[6]. Studies of benthic microfossil assemblages during ODP[7] Leg 104 have confirmed that the modern-day oceanic conveyor system was established

[6]NAC = Norwegian Atlantic Current
[7]ODP = Ocean Drilling Programme

already during the mid-Miocene (Eldholm *et al.* 1987).

The NAC transports warm saline waters into the Nordic Seas. In addition, the NCC[8] (3-18℃, Klitgaard-Kristensen *et al.* (2001)) flows along the Norwegian coast.

The main branch of the Norwegian Atlantic Current (NAC) continues northward, eventually mixing with southward-flowing polar water and sinking to contribute in forming the NSDW[9] water mass ($< 0.5$℃, salinity of 34.91 psu, Alendal *et al.* (2005)). An intermediate water mass, defined as the NSAIW[10], forms in between the NAC and the Norwegian Sea Deep Water (NSDW). With temperatures ranging from 0.5℃ to -0.5℃, this water mass is responsible for the negative bottom water temperatures around Ormen Lange at depths below 500-600 m (Alendal *et al.* 2005).

Seasonal variability has, due to increased ocean-atmosphere interaction, the highest impact on the uppermost ~200 m of water masses (Furevik 2001). Inter annual variability, on the order of 1℃, has the largest amplitudes at depths exceeding 400 m (Furevik 2001). On the geologically miniscule timescale of the last 18 000 years since the LGM, large fluctuations between warm surface conditions of ~9℃ and extensive ice cover have been proposed (Klitgaard-Kristensen *et al.* 2001).

For the Ormen Lange area, Alendal *et al.* (2005) describe the temporal and spatial variability of near seabed currents. Currents are strongly affected by winds and atmospheric pressures in the uppermost ~150 m, with topography most important in the near-seabed environment (Alendal *et al.* 2005).

## 3.5 Gas hydrates at Nyegga

Gas hydrates have initially been inferred on the Vøring Plateau through BSRs (Bugge *et al.* 1988, Mienert and Bryn 1997, Posewang and Mienert 1999b, Andreassen *et al.* 2000, Bouriak *et al.* 2000; 2003, Berndt *et al.* 2003). It was, however, not until an UNESCO cruise in 2006 that physical hydrate samples were actually recovered (Ivanov *et al.* 2007).

[8]NCC = Norwegian Coastal Current
[9]NSDW = Norwegian Sea Deep Water
[10]NSAIW = Norwegian Sea Arctic Intermediate Water

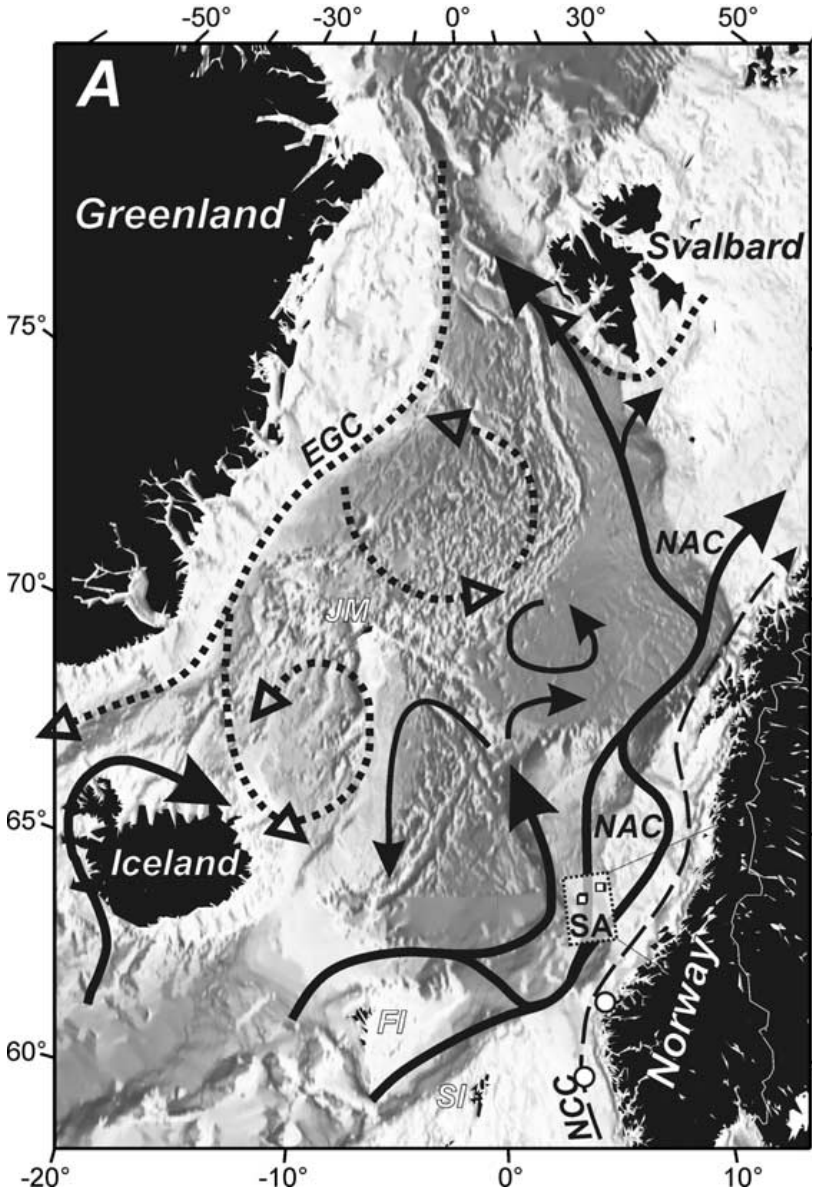


Figure 3.7: The general oceanic circulation in the Norwegian-Greenland Sea. Note the key oceanic currents, including the Norwegian Coastal Current (NCC) and the North Atlantic Current (NAC). The study area is marked with 'SA'. Figure from Mienert *et al.* (2005b).

The Nyegga gas hydrate system has also been intensively studied in terms of submarine pingoes (Hovland and Svensen 2006), authigenic carbonates (Mazzini *et al.* 2006), seafloor instability (Bugge *et al.* 1988, Sultan *et al.* 2004, Berndt *et al.* 2004b, Bünz *et al.* 2005c, Leynaud *et al.* 2007), fluid flow (Hustoft *et al.* 2007), host rock constraints (Bünz *et al.* 2003), concentration estimation (Westbrook 2004, Bünz *et al.* 2005c, Mienert *et al.* 2005a, Westbrook *et al.* 2008a, Faverola *et al.* 2009) and the link to climate change (Mienert and Posewang 1999, Posewang and Mienert 1999b, Mienert *et al.* 2005b).

## 3.6 Exploration history

The sedimentary basins of the Norwegian Sea were initially documented by coarse geophysical studies in the early 1970s (Eldholm 1970, Dalland *et al.* 1988). Furthermore, seismic ties from the North Sea, coupled with dredged samples of pre-Quaternary sediments, revealed more detailed stratigraphic information (Bugge *et al.* 1975, Sellevoll 1975). The first well offshore Mid-Norway, Saga Petroleum's 6507/12-1, was drilled in 1980 (Dalland *et al.* 1988, MPE/NPD 2008). The Ormen Lange field was discovered in 1997.

Traditionally, a small group of major companies[11] held stakes in the area of interest. These were primarily clustered around, and on trend with, Ormen Lange and the 6405/10-1 (Midnattsol) and 6405/7-1 (Ellida) discoveries. Recent activity in the 2006 and 2007 APA[12] rounds has also seen newcomers showing an interest in the area. In June 2009, Production License 281 containing both the Ellida and Midnattsol discoveries was relinquished (NPD 2009d).

The Ormen Lange gas field is Norway's second largest gas field. Producing since September 2007 (NPD 2009d), this deep-water field (water depth between 850 and 1000 m) still contains the majority of its original recoverable reserves[13]. The hydrocarbons occur primarily in the Paleocene turbidite sands of the Egga Formation, sealed by a shale in what essentially constitutes an enormous

[11] ExxonMobil, Norske Shell, BP, which later sold its share to DONG Energy, and (Statoil)Hydro.

[12] APA = awards in pre-defined areas

[13] The official total reserves of the field are estimated at 393.70 $GSm^3$ of gas and 28.50 $MSm^3$ of condensate (NPD 2009d).

stratigraphic trap some 15 km wide and 60 km long (WoodMackenzie 2008b).

An in-depth assessment of potential geohazards in the Storegga Slide area, beneath which the Ormen Lange dome lies, has been undertaken as part of the field development planning (Solheim *et al.* 2005b). This highly integrated project has been a success, both in its multi-disciplinarity and high-quality results. Furthermore, it demonstrated that developing the Ormen Lange gas field is safe with respect to future submarine sliding (Solheim *et al.* 2005a, Gauer *et al.* 2005, Nadim *et al.* 2005).

# Chapter 4

# Database and methods

The sub-regional geomodel of the Nyegga prospect is based on seismic, well and oceanographic data (Figure 4.1). Furthermore, previous work on the Nyegga area, particularly that of Bünz *et al.* (2005c), Westbrook *et al.* (2008a), Hustoft (2009), Weibull (2008) and Faverola *et al.* (2009), provide necessary constraints for the volumetric calculation.

## 4.1 Seismic database

Numerous 2D and 3D surveys were used for interpretation (Table 4.1). The JMF97 2D survey, due to its quality and coverage of the area of interest proved to be most useful. Nevertheless, this key survey has a line spacing of 5 by 10 km, making this study clearly a regional one. Furthermore, high-resolution surveys acquired with focus on the shallow subsurface are clearly more suited to hydrate exploration (Figure 4.1).

## 4.2 Well database

Conventional oil and gas exploration boreholes, research boreholes as well as shallow geotechnical boreholes were used to tie seismic horizons and provide ground truth (Table 4.2). The stratigraphy

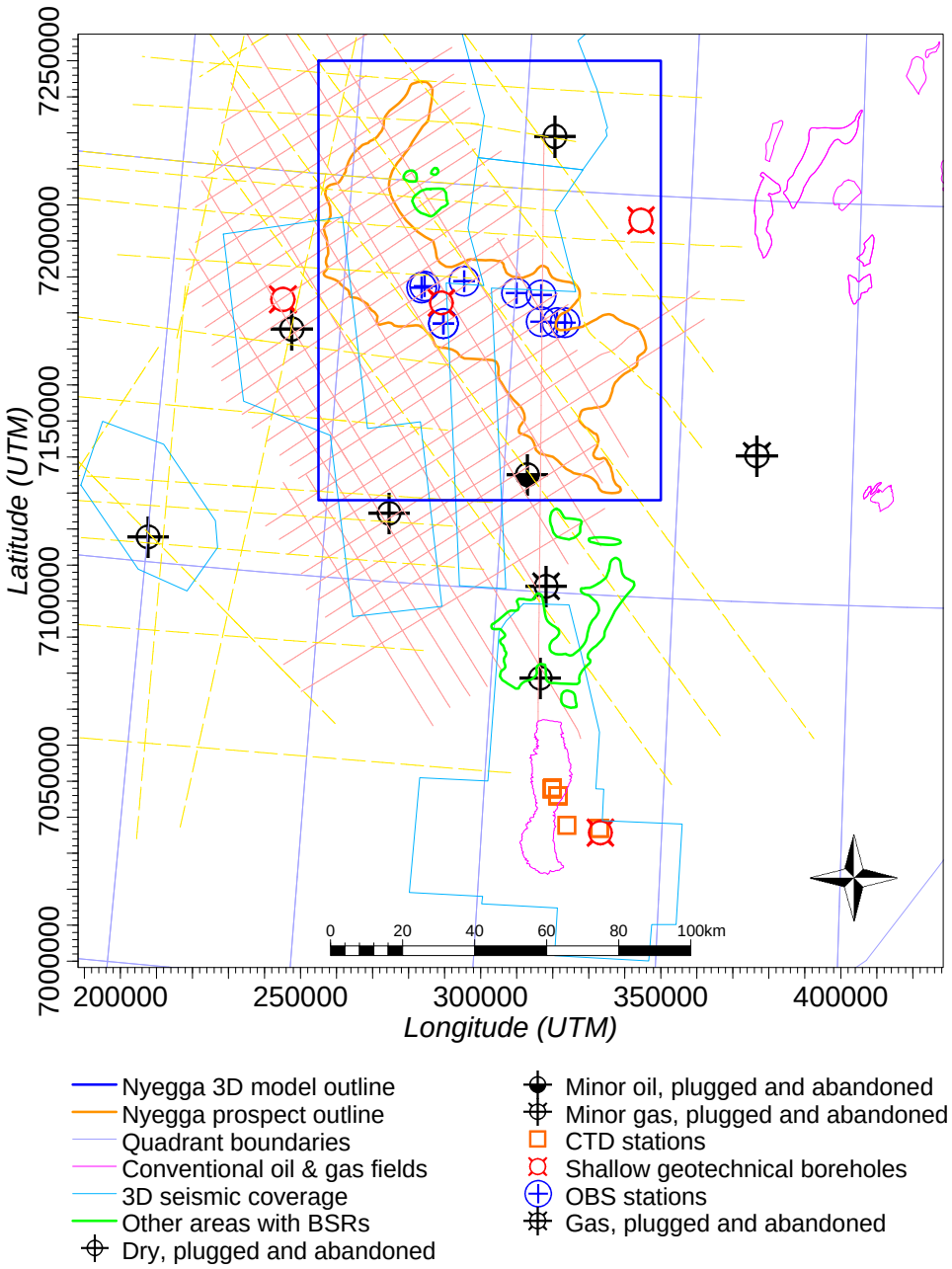


Figure 4.1: Location map showing the data used, including seismic, borehole and oceanographic data used to generate the 3D model. Please note that the stippled yellow lines indicate 2D seismic data used to tie the key 2D seismic data set, JMF97 (pink solid lines), to the wells. For a map view highlighting the conventional and geotechnical boreholes, please refer to Figure 4.3. Coordinates of the oceanographic CTD stations are listed in Table 4.3, while OBS stations are summarized in Table 5.8. Details related to conventional and geotechnical boreholes can be found in Table 5.2.

| Seismic survey | Type | CDP spacing | Comments |
|---|---|---|---|
| PGS MegaMerge Vøring 3 | 3D | 12.5 m | Merge of several 3D surveys, both |
| PGS MegaMerge Vøring 4 | 3D | 12.5 m | public and commercial. |
| GH2001 (Grip High) | 3D | 12.5 m | used by Hustoft et al 2007 |
| NH9208 | 2D | 12.5 m | |
| NH9303 | 2D | 12.5 m | |
| NPD-MB-91 | 2D | 12.5 m | |
| NPD-MB-91/NPD-VRB-91 | 2D | 12.5 m | |
| NPD-MB-92 | 2D | 12.5 m | |
| JMF97 | 2D | 12.5 m | key survey for Nyegga prospect |
| SG9711 | 2D | 12.5 m | |
| SG9618 | 2D | 12.5 m | |
| V2R96 | 2D | 12.5 m | |
| WG96GRH | 2D | 12.5 m | |

Table 4.1: Listing of seismic surveys used. The majority of the surveys, including the key JMF97 data set, is in the public domain.

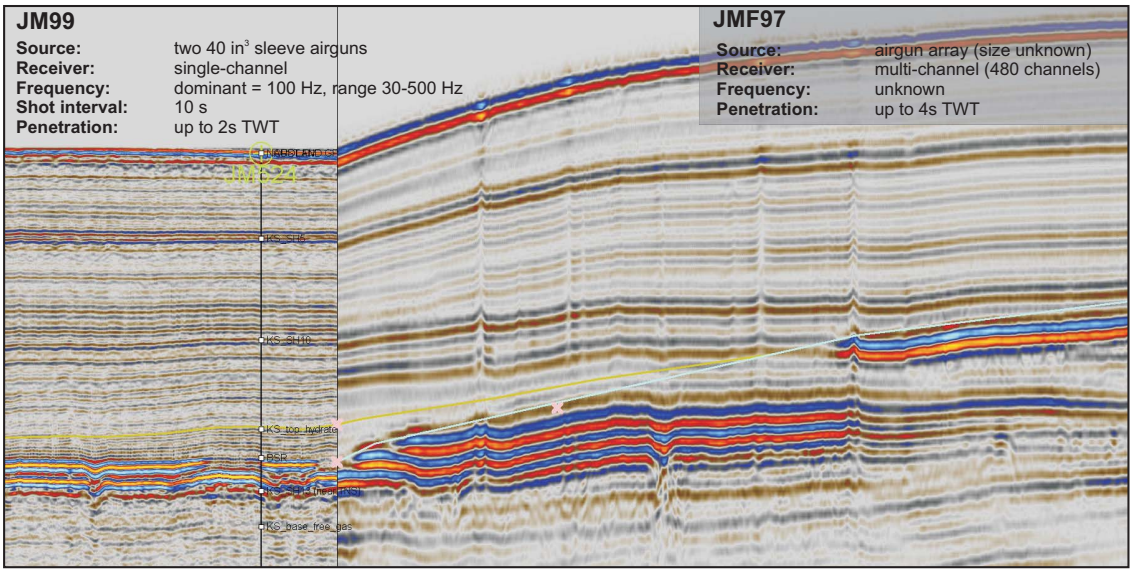


Figure 4.2: Example of the quality contrast between high-resolution shallow-target seismic acquired by R/V Jan Mayen in 1999 (left) and the conventional deeper-target JMF97 survey (right). Note particularly the imaging of thinner layers which fall below the vertical resolution of the conventional JMF97 survey.

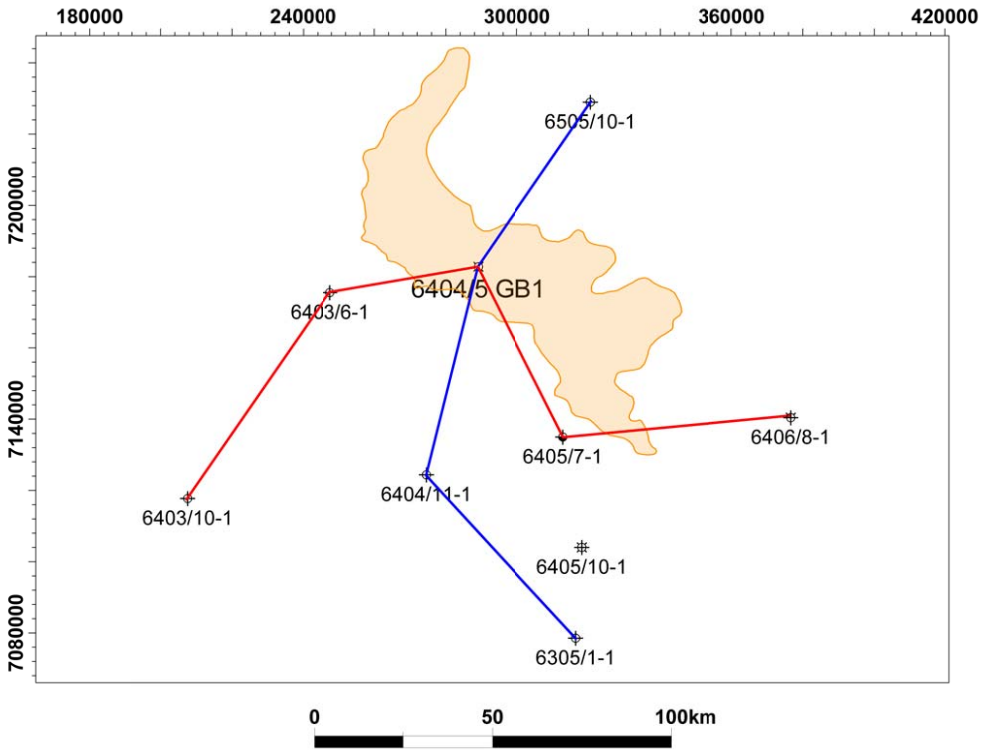


Figure 4.3: Map showing the key conventional wells around the Nyegga prospect. The red line depicts the east-west correlation panel illustrated in Figure 4.4 and the blue line marks the north-south correlation panel depicted in Figure 4.5.

of the study area is based on Rise *et al.* (2006), Faverola *et al.* (2009) and Hustoft (2009).

A well correlation panel (Figure 4.3) shows the data available from the most relevant wells used to tie the seismic interpretation.

## 4.3 Oceanographic database

Table 4.3 lists the key data of the key CTD stations used. These are shown in map view on Figure 4.1.

| Well | Year | Comment | Final vertical depth (mss TVD) | Oldest penetration | Operator | Data |
|---|---|---|---|---|---|---|
| **Nearby wells** | | | | | | |
| 6405/7-1 | 2003 | Ellida oil discovery | 4300 m | Late Cretaceous Lysing Fm | Statoil | Yes |
| 6404/11-1 | 2002 | Dry wildcat | 3650 m | Late Cretaceous Nise Fm | BP Amoco | Yes |
| 6405/10-1 | 2007 | Midnattsol gas discovery | 3181 m | Late Cretaceous | Statoil | None |
| 6403/6-1 | 2006 | Dry wildcat | 4120 m | Late Cretaceous Lysing Fm | Statoil | Yes |
| 6403/10-1 | 2002 | Dry wildcat | 3397 m | Late Cretaceous Kvitnos Fm | Norsk Hydro | Yes |
| 6305/1-1 | 1998 | Dry wildcat | 4546 m | Late Cretaceous Lysing Fm | Norsk Hydro | Yes |
| 6505/10-1 | 1998 | Dry wildcat | 5026 m | Late Cretaceous Lange Fm | Norske Shell | Yes |
| **Regional wells** | | | | | | |
| 6302/6-1 | 2005 | Minor Tertiary gas discovery | 4234 m | Late Cretaceous Springar Fm | Statoil | |
| 6205/3-1 | 1989 | Dry wildcat | 4292 m | Early Cretaceous Åsgard Fm | Norsk Hydro | |
| 6205/3-1 R | 1990 | Dry wildcat with shows | 5253 m | Late Jurassic Spekk Fm | Norsk Hydro | |
| 6305/12-1 | 1991 | Wildcat with shows | 4296 m | Late Triassic Red Beds | Norsk Hydro | |
| 6305/12-2 | 1993 | Wildcat with shows | 3161 m | Pre-Devonian basement | Norsk Hydro | |
| 6305/9-1 | 2001 | Dry wildcat | 2654 m | Late Cretaceous Springar Fm | Norsk Hydro | |
| 6306/10-1 | 1990 | Wildcat with shows | 3183 m | Pre-Devonian basement | Norske Shell | |
| 6306/6-1 | 1994 | Dry wildcat | 1317 m | Pre-Devonian basement | Statoil | |
| 6406/5-1 | 2004 | Gas discovery | 5077 m | Early Jurassic Åre Fm | Norske Shell | |
| 6406/8-1 | 1987 | Wildcat with shows | 4914 m | Early Jurassic Åre Fm | Elf | |
| 6406/8-2 | 2006 | Dry wildcat | 4722 m | Early Jurassic | Total | |
| 6406/9-1 | 2004 | Gas discovery | 5077 m | Early Jurassic Åre Fm | Norske Shell | |
| 6406/9-2 | 2007 | Appraisal for 6406/9-1 | 5349 m | Early Jurassic | Norske Shell | |
| 6406/11-1 S | 1990 | Oil discovery | 4131 m | Late Triassic Red Beds | Saga Petroleum | |
| 6406/12-1 S | 1990 | Dry wildcat | 3891 m | Middle Jurassic Melke Fm | Statoil | |
| 6406/12-2 | 1995 | Dry wildcat | 4363 m | Middle Jurassic Melke Fm | Statoil | |
| **ODP/DSDP wells** | | | | | | |
| 644 A | 1987 | Ref Eldholm et al 1987 | 1479 m | | ODP | Yes |
| DSDP338 | 1974 | Ref Talwani et al 1974 | 1734 m | | DSDP | Yes |
| DSDP341 | 1974 | Ref Talwani et al 1974 | 1895 m | | DSDP | Yes |
| **Geotechnical boreholes** | | | | | | |
| 6404/5 GB1 | 1997 | Ref NGI 1997 | 1276 m | Naust Fm | NGI/Norsk Hydro | Yes |
| 6404/2 | 1997 | Ref NGI 1997 | 596 m | Naust Fm | NGI/Norsk Hydro | Partial |

Only used for geothermal gradient calculation

Table 4.2: Listing of wells used. For details on well locations, please refer to Table 5.2.

| Station | Latitude (UTM) | Longitude (UTM) | Water depth (m) | Instrument height in water column (m) | Instrument depth (m) | First measurement | Last measurement | Days | Sampling interval (min) |
|---|---|---|---|---|---|---|---|---|---|
| *Station 8A* | 7 045 940 | 321 485 | 874 | 234 | 640 | 5/20/2002 | 1/13/2004 | 593 | 10 |
| *Station 8B* | 7 045 940 | 321 485 | 874 | 131 | 743 | 5/20/2002 | 12/27/2003 | 577 | 10 |
| *Station 8C* | 7 045 940 | 321 485 | 874 | 30 | 844 | 5/20/2002 | 1/13/2004 | 593 | 10 |
| *Station 8D* | 7 047 691 | 319 922 | 874 | 9 | 865 | 7/19/2002 | 1/7/2004 | 528 | 10 |
| *Station B12* | 7 023 773 | 341 340 | 190 | 3 | 187 | 6/27/2003 | 1/9/2004 | 192 | 10 |
| *TH8_RCM1_PH7* | 7 048 185 | 319 930 | 860 | 190 | 670 | 1/25/2005 | 5/12/2005 | 107 | 10 |
| *TH8_RCM3_PH7* | 7 048 185 | 319 930 | 860 | 10 | 850 | 1/25/2005 | 5/13/2005 | 108 | 10 |
| *TH8_RCM4_PH1* | 7 047 932 | 319 734 | 860 | 10 | 850 | 1/13/2004 | 3/2/2004 | 49 | 10 |
| *TH11_RCM_PH2* | 7 037 682 | 323 974 | 300 | 3 | 297 | 3/2/2004 | 4/29/2004 | 57 | 10 |
| *TH11_RCM_PH3* | 7 036 860 | 332 935 | 312 | 3 | 309 | 4/29/2004 | 7/2/2004 | 63 | 10 |

Table 4.3: Summary of CTD stations used to plot Figure 5.3. Data provided by Fugro Geos, property of Norwegian Deepwater Programme. Locations of CTD stations are illustrated by Figure 4.1.

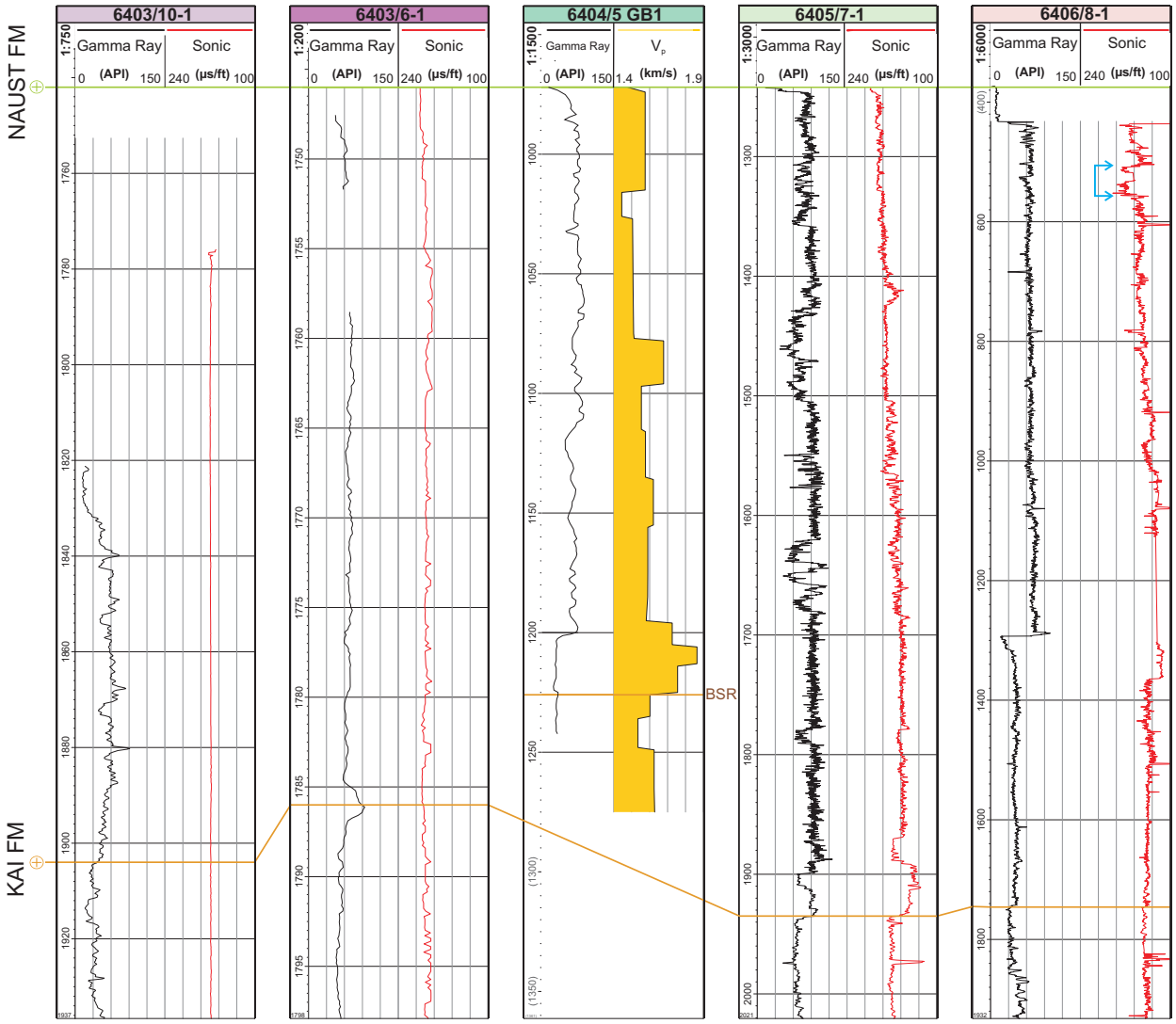


Figure 4.4: East-west well correlation panel, showing the scarce data available for the Naust Formation. Note particularly the sonic (DT) log, registering velocity variations within the Naust Formation. The blue arrow indicates a lower velocity zone in the upper Naust Formation. Please note that the depth scale is different for each well to optimally illustrate the Naust Formation. For location, please refer to Figure 4.3.

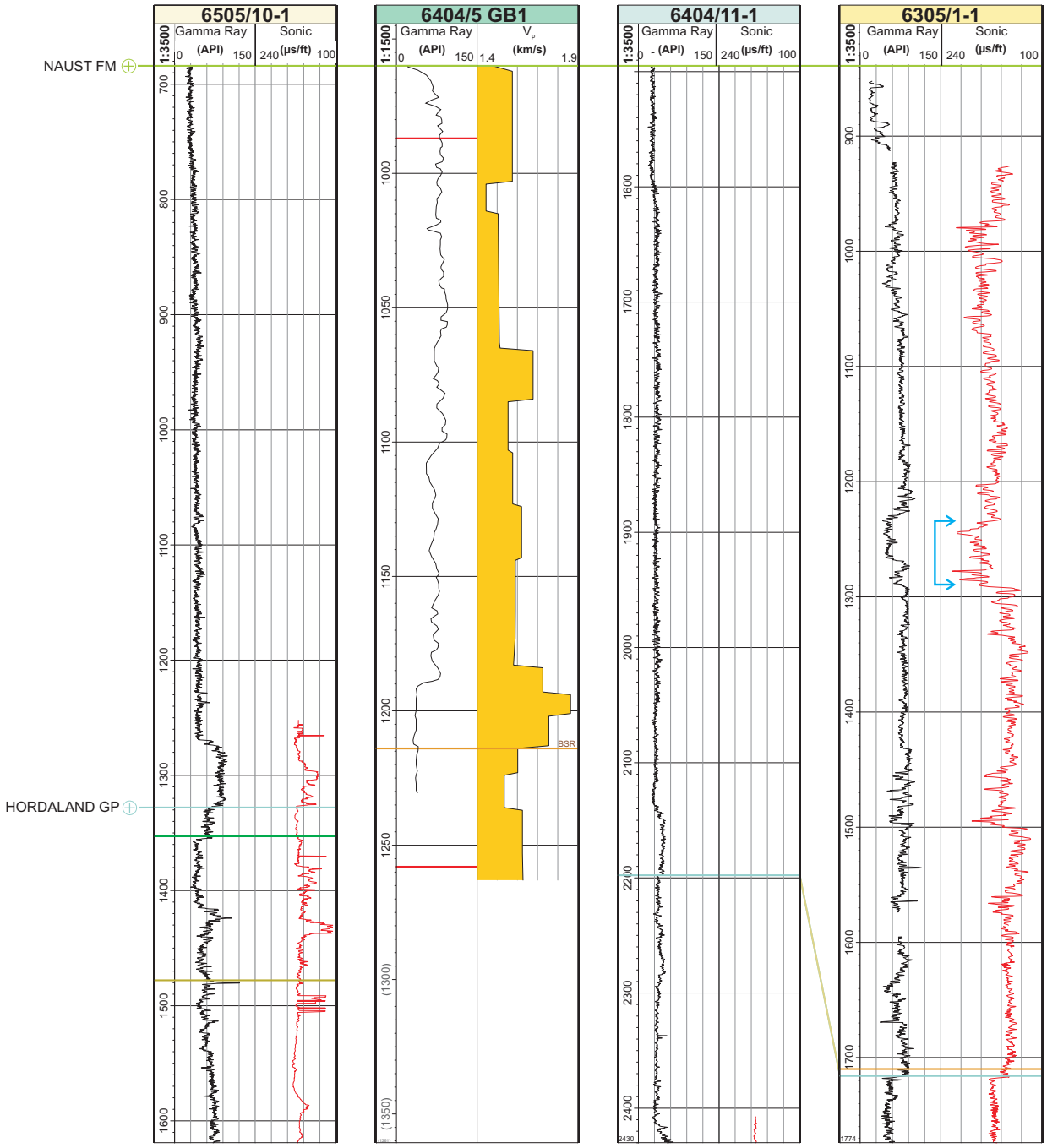


Figure 4.5: North-south well correlation panel. The blue arrow on well 6305/1-1 indicates a low velocity zone within the Naust Formation. For location, please refer to Figure 4.3.

## 4.4 Prospect evaluation

The Nyegga prospect is a gas hydrate accumulation, defined primarily on the basis of a bottom simulating reflection, on the north flank of the Storegga Slide. It comprises a solid gas hydrate zone, as well as the underlying free gas zone. The former is further subdivided into a regionally extensive solid gas hydrate zone, and a localized higher-concentration chimney zone.

The core of this thesis involves the calculation of in-place gas volumes at this prospect, achieved through the building of a regional 3D model populated with regional seismic interpretation and a range of probable reservoir parameters.

The volumetric calculation considers the Nyegga prospect as a 3-segment unit (Figure 4.6), with each segment assigned a different range of reservoir parameters (Table 5.6 in Section 5.4.1).

Petrel and GeoX are two industry-standard tools used for the volumetric calculation. Both calculations rely on the areal extent of the BSR to provide the initial spatial constraint (Figure 4.7). The thickness of both the hydrate and the free gas zone, sourced primarily from OBS experiments (Bünz and Mienert 2004, Bünz *et al.* 2005b, Westbrook *et al.* 2008a, Faverola *et al.* 2009), are subsequently added to give a 'gross rock volume'. The volume of the chimney structures is provided by extrapolating the result of Weibull (2008). A hydrocarbon pore volume (HCPV) volume is obtained by accounting for the net-to-gross (NTG) ratio, porosity and gas saturation. Gas initially in place (GIIP) relates to the physical amount of gas present, defined by the HCPV multiplied with the expansion factor $B_G$. Only a fraction of this gas is ultimately recoverable, depending on the recovery factor used. The GeoX calculation additionally includes a depandancy argument, which prevents the free gas zone to be filled in cases where the gas hydrate zone not being present. In this way, the hydrate zone's sealing property, with respect to the underlying free gas zone, is ensured. A distribution of values for the aforementioned input parameters was assigned to account for the uncertainty of the various parameters.

The calculation follows the general pathway illustrated graphically by Figure 4.7 and mathematically by Equation 4.1. The calculation was performed in both a deterministic fashion, using

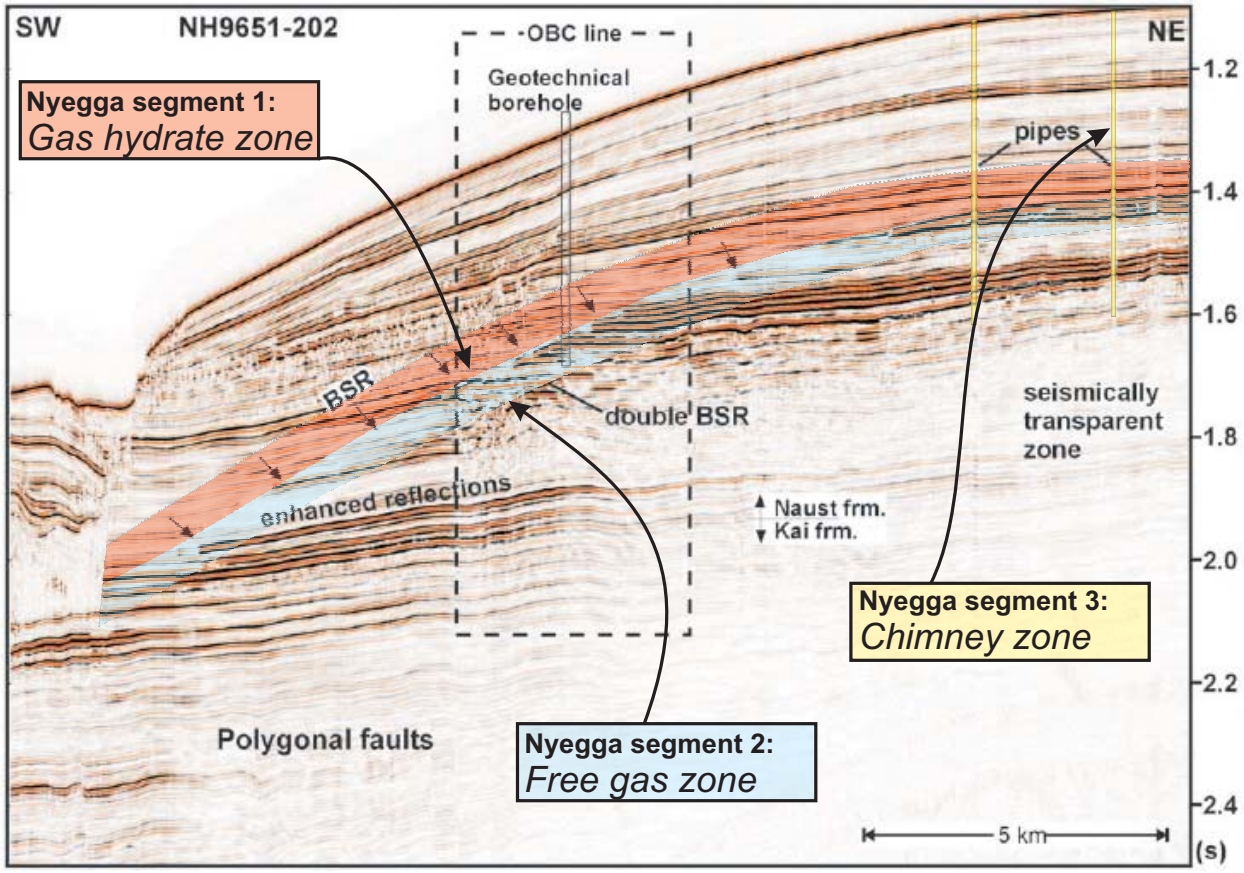


Figure 4.6: A geo-seismic cartoon sketch of the Nyegga prospect based on seismic line NH9651-202, showing its three main segments; 1. The gas hydrate zone, 10-120 m thick; 2. The free gas zone, 20-80 m thick; 3. The chimney zone, on average 200 m wide. Figure modified from Bünz and Mienert (2004).

only the base case input parameters, and stochastically. Stochastic methods use, instead of a single base case deterministic value, a range of probable input parameters to calculate a range of probable results. In this way, the spread of parameters related to their uncertainties is accounted for in the calculation. For both approaches, the volumetric calculation was repeated for all three segments (gas hydrate, free gas and chimney zones) and added together to give the total in-place/recoverable volumes.

$$Q_{hydrate} = GRV * \phi * N/G * (1 - S_W) * \frac{1}{B_G} * RF \tag{4.1}$$

where:

$GRV$ = Gross rock volume, $m^3$

$\phi$ = porosity, given as a fraction of 1

$N/G$ = net to gross ratio of sand, given as a fraction of 1

$S_W$ = Water saturation, given as a fraction of 1

$B_G$ = Compressibility of gas, defined by volume at reservoir/volume at STP

$RF$ = Recovery factor, given as a fraction of 1. Not used when calculating in-place resources.

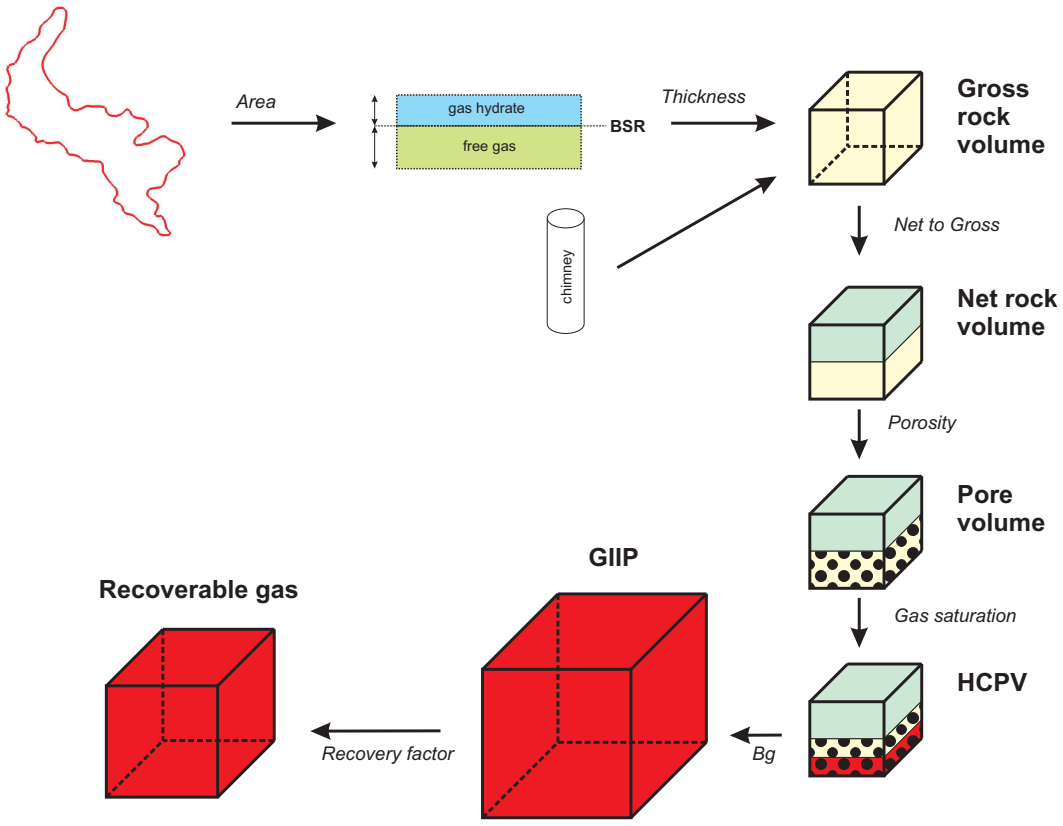


Figure 4.7: A sketch illustrating the Nyegga volumetric calculation. The three-dimensional reservoir extent is calculated based on the areal extent of the bottom-simulating reflection (BSR) and the thickness of the hydrate and free gas zones, based on ocean bottom seismometer (OBS) experiments. For the chimney zone, the gross rock volume (GRV) is directly defined by the study of Weibull (2008). Net-to-gross (NTG), porosity and gas saturation is applied to give a hydrocarbon pore volume (HCPV). Upon application of an expansion factor, $B_G$, a gas initially in place (GIIP) volume is calculated. Only a fraction of the GIIP is technically producable, depending on the recovery factor, to give the final recoverable gas. Please note that GIIP equates in-place volumes, a term widely used in this thesis.

# Chapter 5

# Results

The results chapter includes the main achievements of this thesis, including the regional hydrate stability modeling, seismic interpretation and the volumetric calculation.

## 5.1 Hydrate stability zone modeling

The hydrate stability zone (HSZ) is modeled based on publicly available oceanographic, geothermal and geochemical data. Since the HSZ model is data-driven, and fundamentally relies on the underlying data sets, these are presented in this section for clarity. The data source is referenced throughout.

### 5.1.1 Ocean temperatures

A large publicly available data set (ICES 2008) allows the examination of 1070 CTD[1] casts within the study area over a period of 20 years[2] (Figure 5.1). The data clearly show the largest variation within the uppermost 200 m of the water column. At depths exceeding approximately 750 m,

[1] CTD = Conductivity-Temperature-Depth

[2] The oceanographic study area is somewhat larger than the model outline due to the ability of using data acquired in the vicinity of the Ormen Lange field. It is geographically bounded by the following co-ordinates: 63 - 65.75 dd N and 3 - 6.5 dd E.

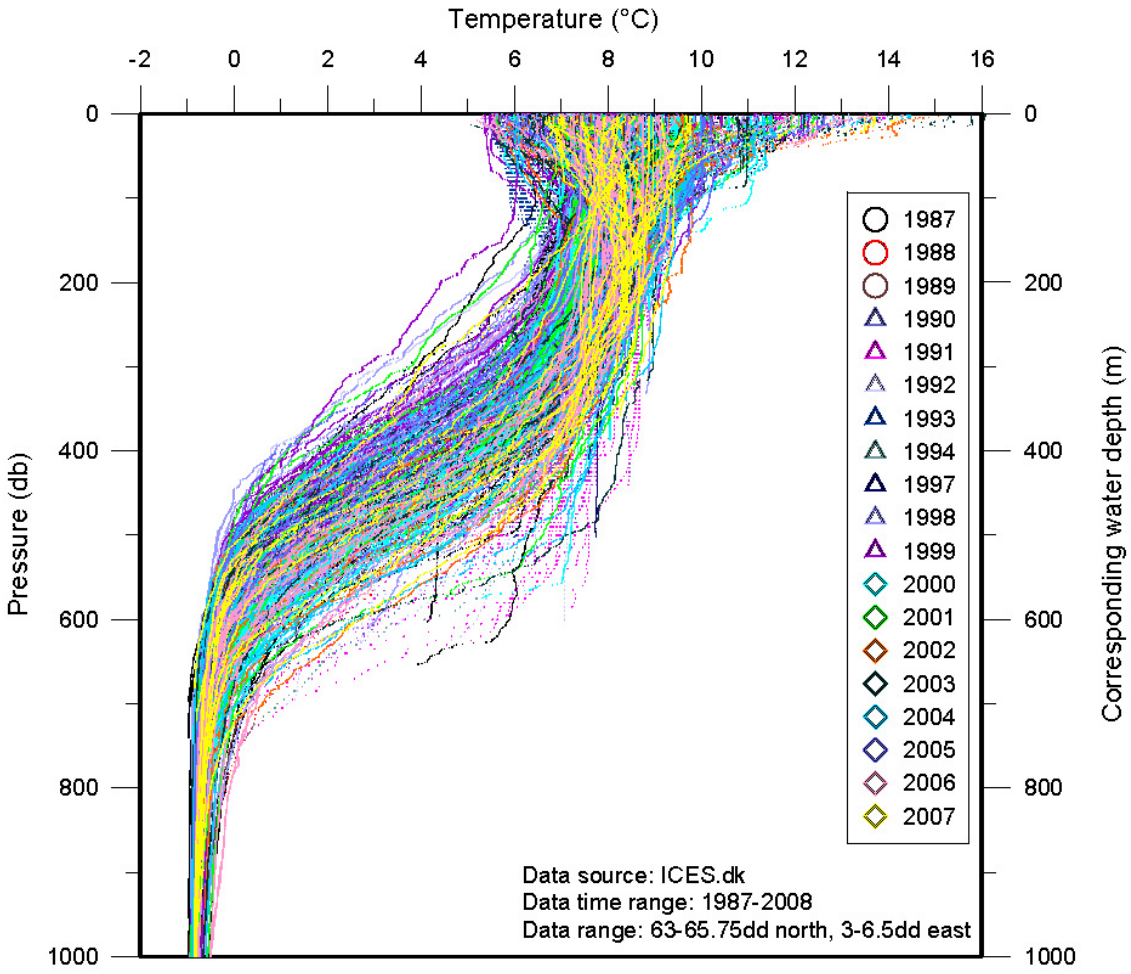


Figure 5.1: Conductivity-Temperature-Depth (CTD) data from the study area showing all publicly available CTD casts (1070 casts) in the period 1987-2007, grouped by the year the data was collected. The data shows a consistent pattern over the past 20 years, over the relatively large extent of the study area. Data is geographically restricted to the oceanographic study area. Data from ICES (2008).

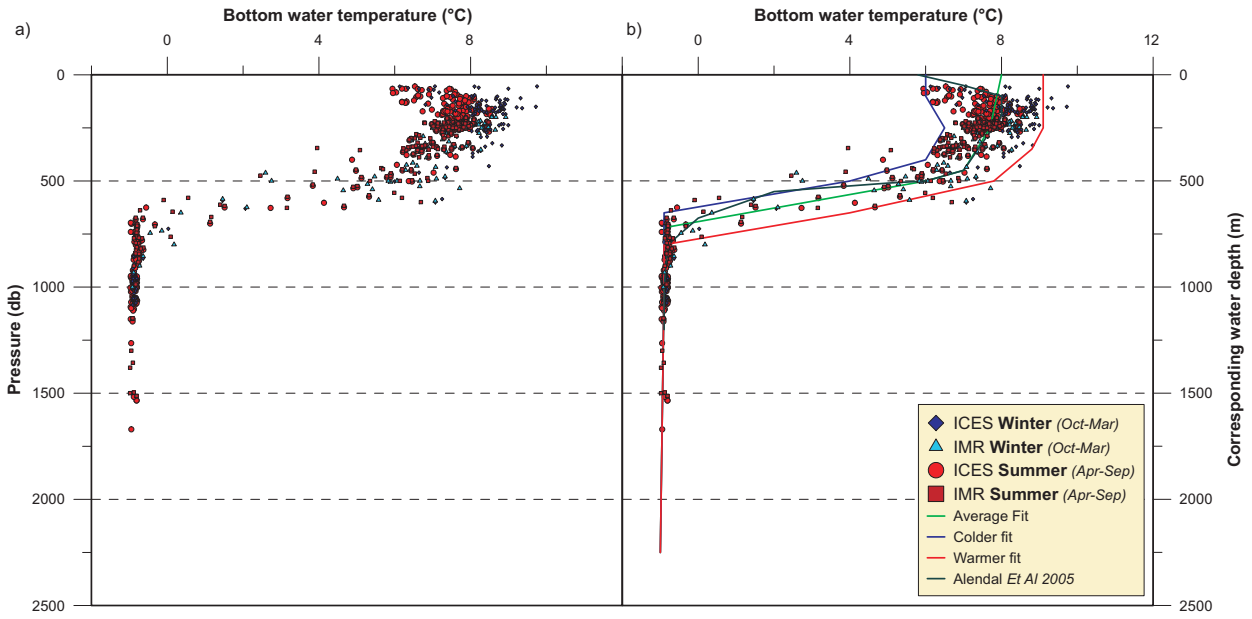


Figure 5.2: Two CTD data sets from the study area showing summer and winter bottom hole temperatures during the period 1987-2008. The left graph visualizes only the data set, while the right graph defines the interpreted upper and lower fits. Data from ICES (2008) and IMR (2008), compared with average gradient extracted from Alendal *et al.* (2005). Data is geographically restricted to the oceanographic study area.

temperatures are stable at approximately -1°C. Between ~250 m and ~750 m there is a large variation in oceanic temperatures between 4°Cto 8°C.

Examining only bottom water temperatures measured within 50 m of the seabed, obtained from two independent databases (ICES 2008, IMR 2008), this variation is reduced to approximately 4°C between the colder and warmer fit at any particular depth (Figure 5.2). Temperatures appear to be somewhat warmer during the winter months, especially in the uppermost 500 m of the water column. This is also confirmed by time series temperature data (Figure 5.3). It is notable that the oceanic thermal gradient (OTG) appears to be practically constant below 750 m and to some extent above 500 m. In between, there appears to be a linear and rapid shift between ~7.5°C and ~-1°C. The data fits well to the average profile for Ormen Lange published by Alendal *et al.* (2005).

Time-series data provided by Fugro Geos reiterate this general picture (Figure 5.3, Table 4.3).

| Depth interval | Temperature | Uncertainty |
|---|---|---|
| *0-450 m* | 7.5°C | ± 1.5°C |
| *450-750 m* | 7.5°C to -1°C | ± 2°C |
| *750-2250 m* | -1°C | ± 0.1°C |

Table 5.1: Depth subdivision with associated temperatures and uncertainty in the bottom water temperature used for modeling the Nyegga gas hydrate system.

Two stations, measuring temperature at 640 m and 670 m (at a water depth of 874 m), display large variation in temperature with a range up to 7℃. In contrast, stations measuring at 845 m and 865 m practically always fall within the 0 to -1℃ window. Shallow stations in the uppermost ~300 m display reasonable constant temperatures with a maximum variation of ~2℃.

For developing the Nyegga gas hydrate system model, an average oceanic profile was used (Figure 5.2b). This profile combines three distinct oceanographic intervals with specified average temperatures and uncertainties (Table 5.1).

### 5.1.2 Geothermal gradients

In the study area, regional geothermal gradients as calculated from the closest conventional exploration wells fall, with two exceptions, within an approximate 30-50℃/km window (Table 5.2, Figure 5.4). The six most proximal wells average to 42.80℃/km. The error range on these measurements, given that they are based on one unverifiable bottom hole temperature reading, is substantial (Forster *et al.* 1997).

In contrast, shallow DSDP[3], ODP[4] and NGI[5] boreholes display a much larger variation in gradients, ranging from 90℃/km in DSDP 341 to 41℃/km in NGI hole 6404/2. Bottom simulating reflection (BSR)-inferred gradients by Bouriak *et al.* (2000) plot at approximately 55℃/km.

The geothermal gradient is fundamental in defining the base of the hydrate stability zone (BHSZ). The BHSZ, coinciding with the BSR, has been penetrated by NGI borehole 6404/5 GB1. This borehole included multiple temperature measurements with depth, illustrating the near-

[3]DSDP = Deep Sea Drilling Programme
[4]ODP = Ocean Drilling Programme
[5]NGI = Norwegian Geotechnical Institute

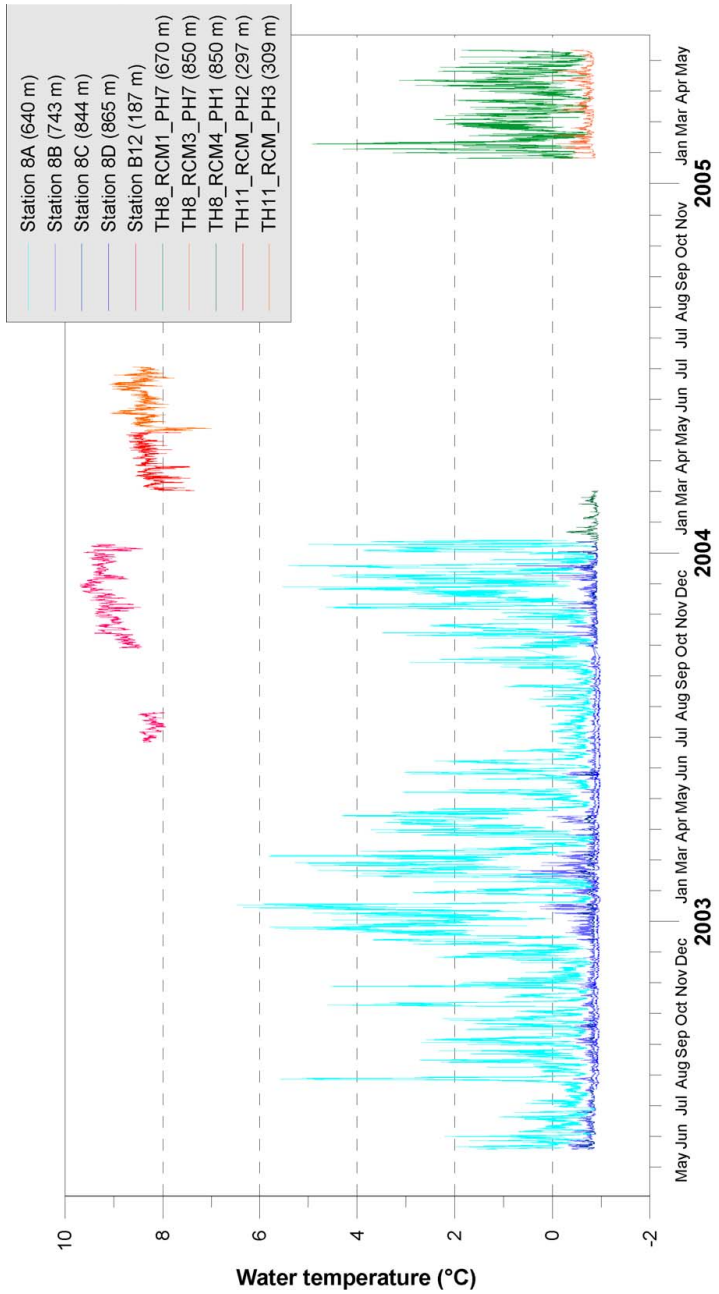


Figure 5.3: Time-series data showing variability in ocean bottom and water column temperatures from 10 stations in the study area. It is notable that the stations nearest to the seabed experience least variation in this setting. This is hypothesised to be an effect of the strong stratification of the water masses in the region, as shown by Figure 5.1. Data provided by Fugro Geos, property of Norwegian Deepwater Programme. For station locations and details please refer to Table 4.3.

| Well | Easting | Northing | UTM Zone | Water depth (m) | Final vertical depth (mssTVD) | Sediment penetration | Bottom water temperature (°C) | Bottom hole temperature (°C) | Geothermal gradient (°C/km) |
|---|---|---|---|---|---|---|---|---|---|
| *nearby wells:* | | | | | | | | | |
| 6405/7-1 | 603234.55 | 7131003.11 | 31 | 1206 | 4300 | 3094 | -1 | 129 | 42.02 |
| 6404/11-1 | 566124.46 | 7116837.72 | 31 | 1495 | 3650 | 2155 | -1 | 93 | 43.62 |
| 6405/10-1 | 611431.76 | 7100698.16 | 31 | 928 | 3181 | 2253 | -1 | no data | |
| 6403/6-1 | 534417.98 | 7165192.95 | 31 | 1721 | 4120 | 2399 | -1 | 118 | 49.60 |
| 6403/10-1 | 500148.05 | 7103974.07 | 31 | 1717 | 3397 | 1680 | -1 | 80 | 48.21 |
| 6305/1-1 | 611981.31 | 7075028.48 | 31 | 840 | 4546 | 3706 | -1 | 141 | 38.32 |
| 6505/10-1 | 602035.97 | 7225243.08 | 31 | 684 | 5026 | 4342 | -1 | 151 | 35.01 |
| *regional wells:* | | | | | | | | | |
| 6302/6-1 | 488277.59 | 7044540.65 | 31 | 1261 | 4234 | 2973 | -1 | 112 | 38.01 |
| 6205/3-1 | 649328.84 | 6983872.90 | 31 | 159 | 4292 | 4133 | 7.5 | 107 | 24.07 |
| 6205/3-1 R | 649328.84 | 6983872.90 | 31 | 159 | 5253 | 5094 | 7.5 | 155 | 28.96 |
| 6305/12-1 | 641178.97 | 6991476.94 | 31 | 177 | 4296 | 4119 | 7.5 | 146 | 33.62 |
| 6305/12-2 | 635050.51 | 6990772.25 | 31 | 146 | 3161 | 3015 | 7.5 | 121 | 37.65 |
| 6305/9-1 | 649731.56 | 7022673.85 | 31 | 187 | 2654 | 2467 | 7.5 | 86 | 31.82 |
| 6306/10-1 | 365416.35 | 7006088.05 | 32 | 83 | 3183 | 3100 | 7.5 | 114 | 34.35 |
| 6306/6-1 | 391515.49 | 7043364.00 | 32 | 284 | 1317 | 1033 | 7.5 | 43 | 34.37 |
| 6406/5-1 | 385280.80 | 7168587.93 | 32 | 286 | 4684 | 4398 | 7.5 | 165 | 35.81 |
| 6406/8-1 | 376765.25 | 7140372.60 | 32 | 348 | 4914 | 4566 | 7.5 | 172 | 36.03 |
| 6406/8-2 | 372069.05 | 7153423.09 | 32 | 365 | 4722 | 4357 | 7.5 | no data | |
| 6406/9-1 | 394862.07 | 7148739.49 | 32 | 308 | 5077 | 4769 | 7.5 | 184 | 37.01 |
| 6406/9-2 | 394369.15 | 7152101.68 | 32 | 299 | 5349 | 5050 | 7.5 | no data | |
| 6406/11-1 S | 383011.32 | 7104524.70 | 32 | 315 | 4131 | 3816 | 7.5 | 150 | 37.34 |
| 6406/12-1 S | 389379.24 | 7106932.34 | 32 | 329 | 3891 | 3562 | 7.5 | 147 | 39.16 |
| 6406/12-2 | 395821.77 | 7110509.23 | 32 | 334 | 4363 | 4029 | 7.5 | 146 | 34.38 |
| *ODP/DSDP wells:* | | | | | | | | | |
| 644 A | 569310.00 | 7395499.00 | 31 | 1226.3 | 1479.1 | 252.8 | -1 | 15.48 | 65.19 |
| DSDP338 | 600842.00 | 7521192.00 | 31 | 1297 | 1734 | 437 | -1 | | 86.00 |
| DSDP341 | 372650.00 | 7397569.00 | 32 | 1439 | 1895 | 456 | -1 | | 90.00 |
| *geotechnical boreholes:* | | | | | | | | | |
| 6404/5 GB1 (DGP) | 575078.90 | 7176334.00 | 31 | 966 | 1275.5 | 309.5 | -1 | | 51.54 |
| 6404/5 GB1 (CT) | 575078.90 | 7176334.00 | 31 | 966 | 1275.5 | 309.5 | -1 | | 55.00 |
| 6404/2 (DGP) | 627896.00 | 7204356.00 | 31 | 532 | 596 | 64 | | 2.65 | 41.41 |
| *literature:* | | | | | | | | | |
| Mienert et al 2005 | | | | | | | | | 50-56 |
| Bouriak et al 2000 | | | | | | | | | 51.58-55.8 |
| **Chosen geothermal gradient** | | | | | | | | | **50°C/km** |

Table 5.2: Geothermal gradients in the study area, as calculated from the bottom hole temperatures of nearby exploration, DSDP, ODP and NGI wells. For the 6404/5 GB1 borehole, two methods (DGP = deepwater gas probe and CT = cone testing) were used to measure downhole temperature, giving a slightly different result. Data from Talwani *et al.* (1974), The Shipboard Scientific Party (1974), Eldholm *et al.* (1987), NGI (1997), Bouriak *et al.* (2000), Mienert *et al.* (2005a), Pribnov *et al.* (2000), Gosnold (2008) and NPD (2009d).

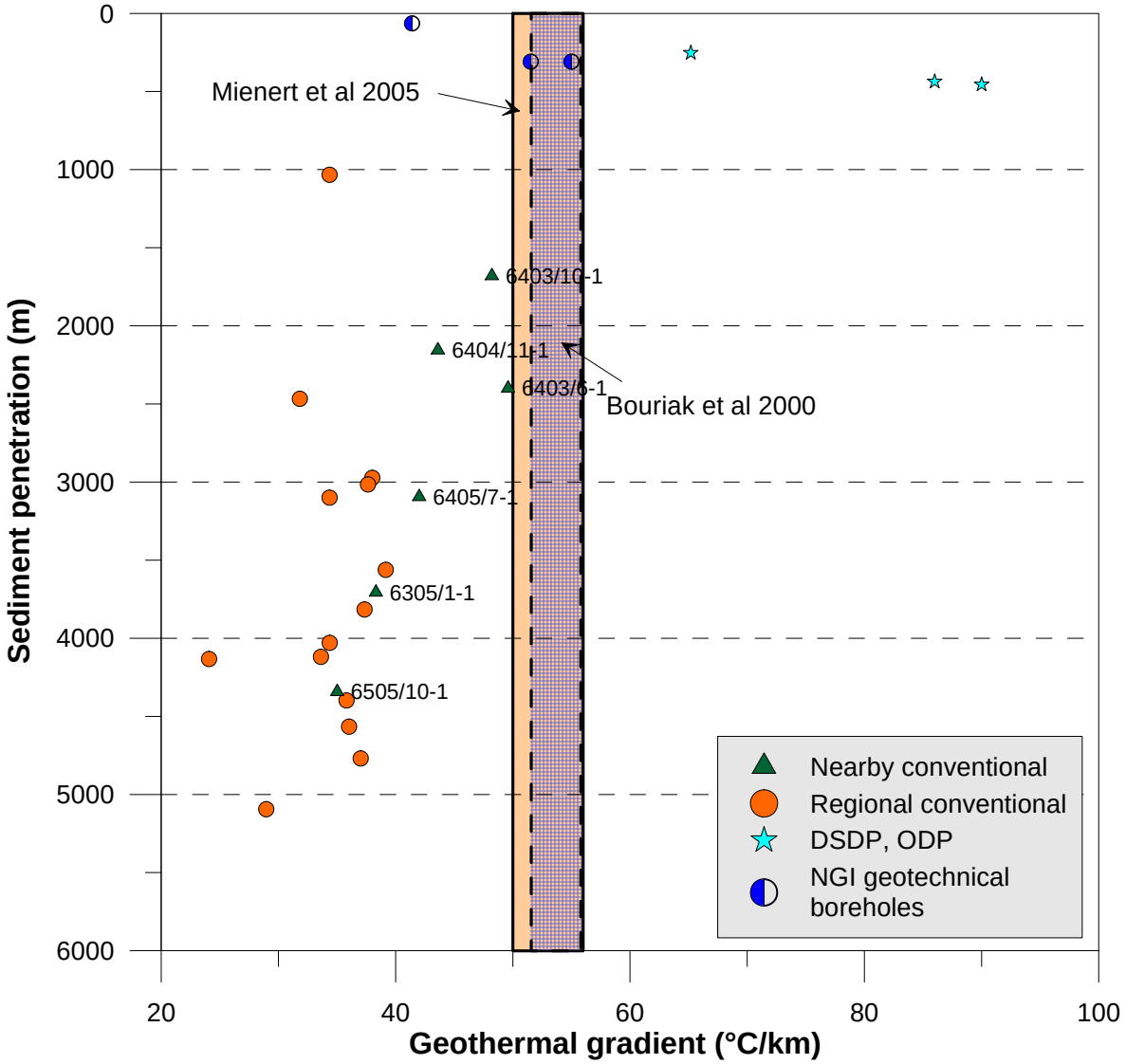


Figure 5.4: Geothermal gradients in the survey area, plotted against the sediment penetration of the respective holes. Note that deeper holes generally have a geothermal gradient lower than 40°C/km, while a large range exists for the shallow DSDP/ODP/geotechnical boreholes. Data from Talwani *et al.* (1974), The Shipboard Scientific Party (1974), Eldholm *et al.* (1987), NGI (1997), Bouriak *et al.* (2000), Mienert *et al.* (2005a), Pribnov *et al.* (2000), Gosnold (2008) and NPD (2009d).

linear geothermal gradient through the HSZ (Figure 5.5). The geothermal gradient of 51.5°C/km coincides with that of the BSR-inferred values of Bouriak *et al.* (2000) and Mienert *et al.* (2005a). In deeper waters, with a significantly thicker HSZ, a slightly lower geothermal gradient as measured in conventional boreholes should be applied. This applies particularly if the BHSZ is to be modeled at water depths exceeding 1000 to 1500 m.

In this case, a regional geothermal gradient of 50°C/km, with an uncertainty range of ±5°C/km, was applied for modeling the HSZ.

### 5.1.3 Gas sourcing and composition

It is important to gain an understanding on possible gas sources within the study area, because the composition of the hydrate forming gas exerts an effect on the hydrate phase boundary (HPB). Interstitial gas may either be formed *in situ* by biogenic gas generation or migrated to the area from a source system, often associated with thermogenic gas generation.

Gas samples from nearby conventional boreholes are available for determining the origin of the gas phase, clearly showing the thermogenic nature of the sampled gas (Figure 5.6). In contrast, ODP site 644 displays a strongly biogenic signature. While this site is geographically more distant to the study area than the conventional wells[6], its shallow penetration (see Table 5.2) makes it the only well to sample gas from the modeled HSZ. Furthermore, examining the wetness index of C1/(C2+C3) in relation to the sampling depth (Figure 5.7) reveals a natural increase in relative methane concentration at shallower depths. This may be partially related to gas fractionation during its ascent (Dahl, pers. comm. 2008). The total amount of gas present provides a means of quantifying possible gas accumulations underneath permeability barriers.

It is a reasonable assumption to define two end member hydrate-forming compositions for modeling the Nyegga HSZ:

1. A pure methane system.

[6]ODP site 644 lies 240 km to the north of the centre of the study site.

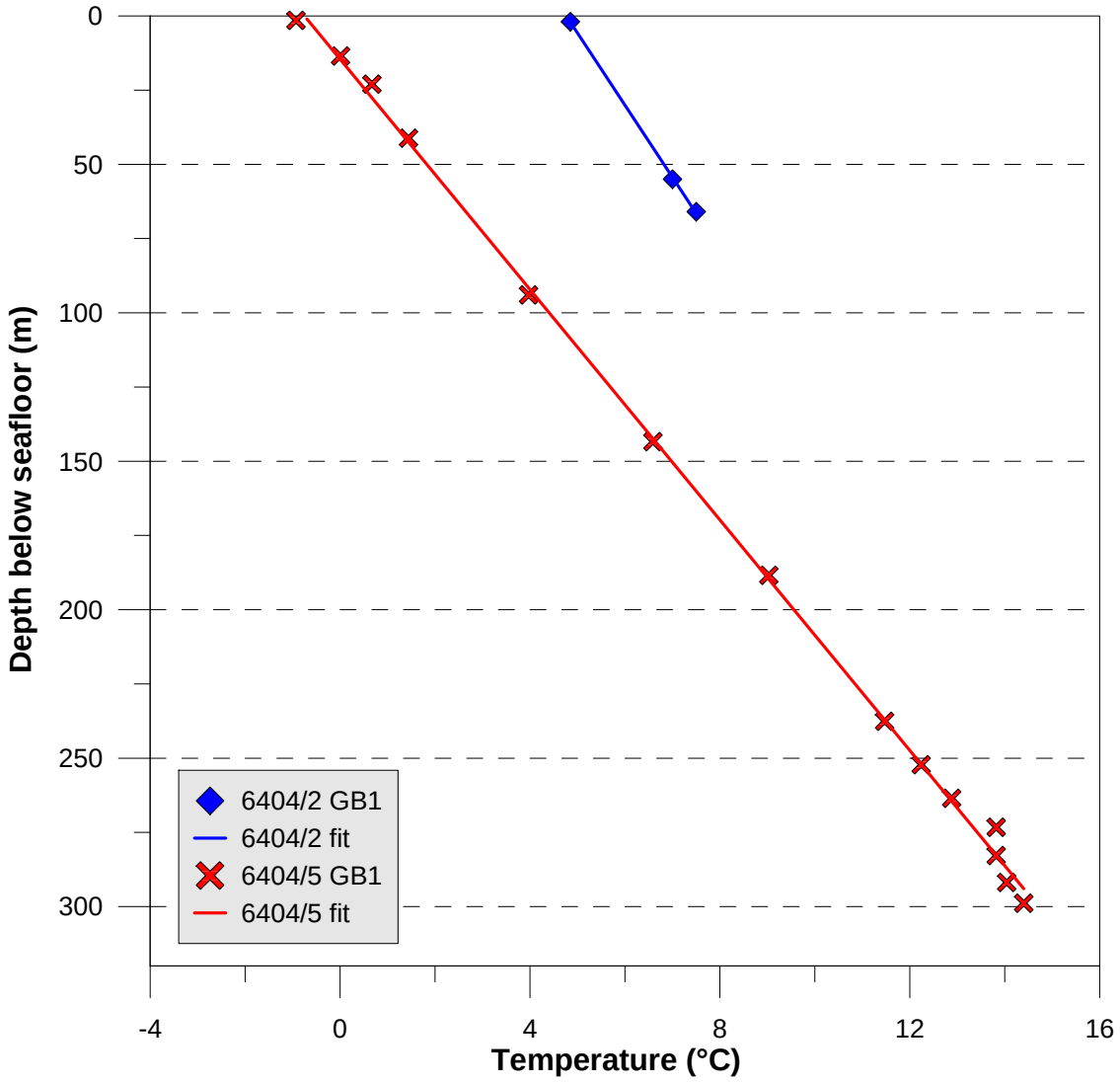


Figure 5.5: Geothermal gradients in the two NGI geotechnical boreholes in the study area. The data points represent down-hole temperature measurements, and gives a geothermal gradient of 51.5 to 55°C/km for the 6404/5 GB1 borehole. Data from NGI (1997).

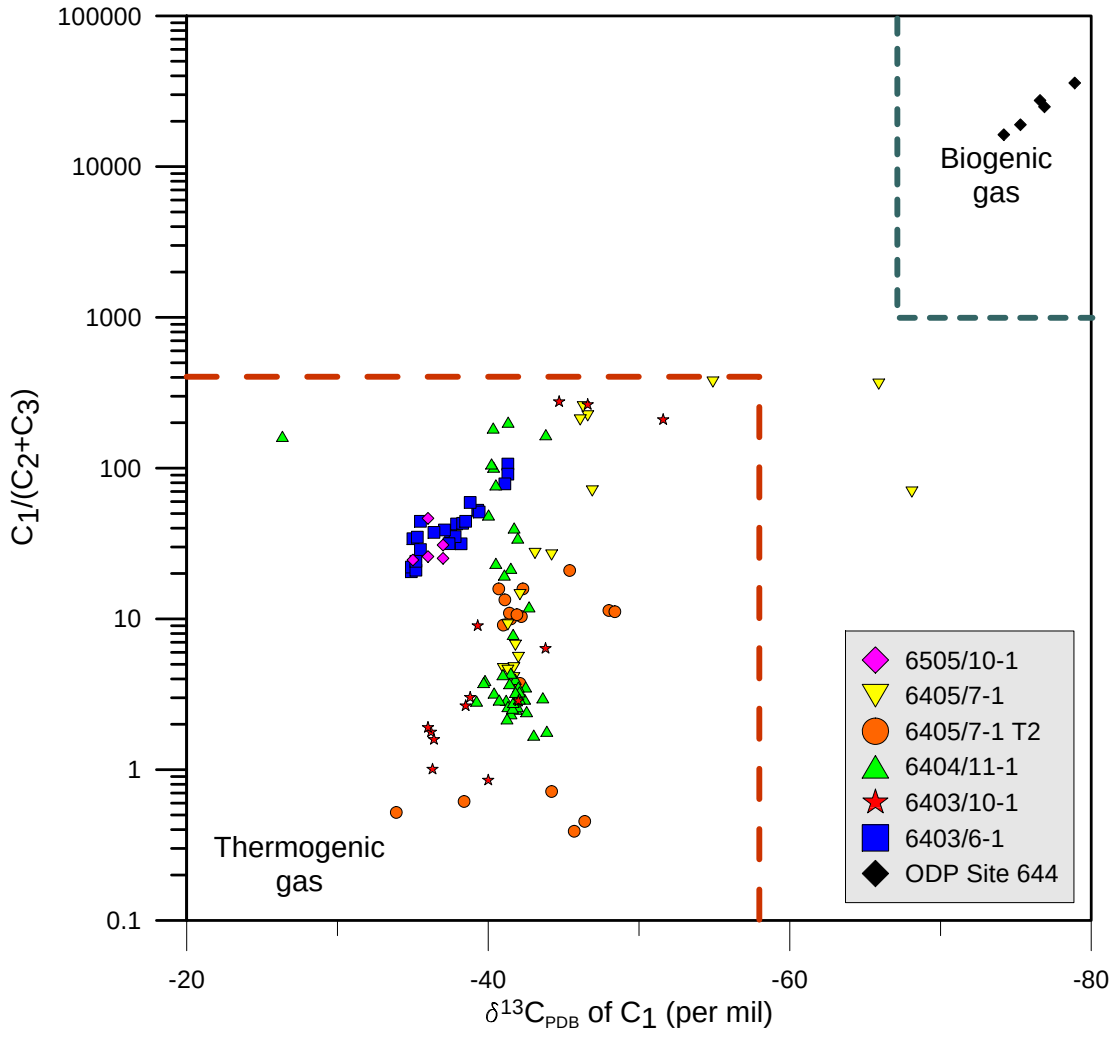


Figure 5.6: Plot of C1/(C2+C3) versus isotopic composition of C1 to distinguish biogenic and thermogenic gas. The thermogenic and biogenic cut-offs are based on Sloan and Koh (2008). Gas analysis data from conventional wells (NPD 2009d) and ODP wells (Vuletich *et al.* 1989). For location of the wells, please refer to Figure 4.3.

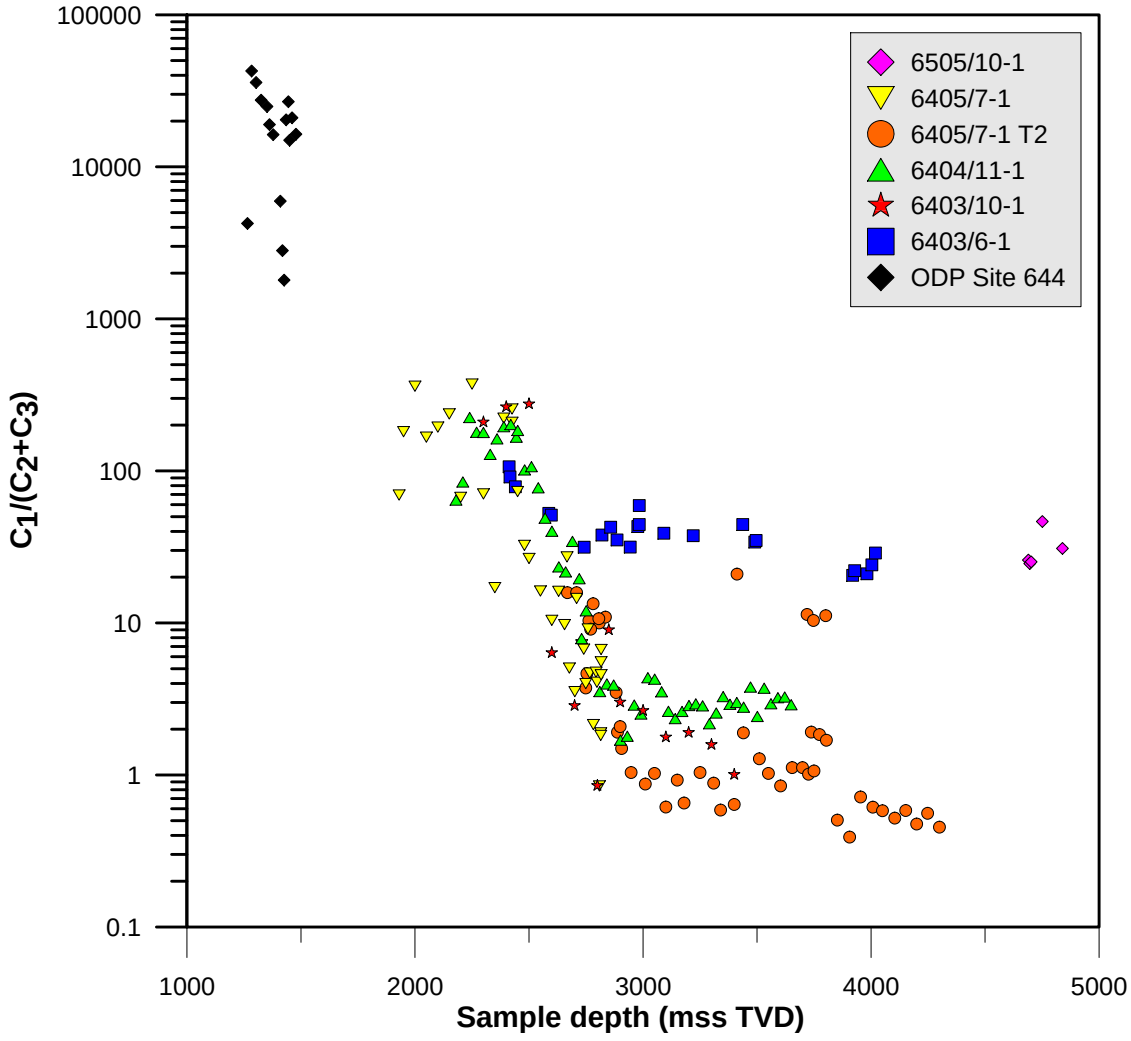


Figure 5.7: Plot of C1/(C2+C3) versus sampling depth to illustrate the increased significance of biogenic methane at shallow subsurface depths. The general decrease in the wetness ratio at shallower levels is thought to be caused by natural gas fractionation during ascent. Data from NPD (2009d) and Vuletich *et al.* (1989). For location of the wells, please refer to Figure 4.3.

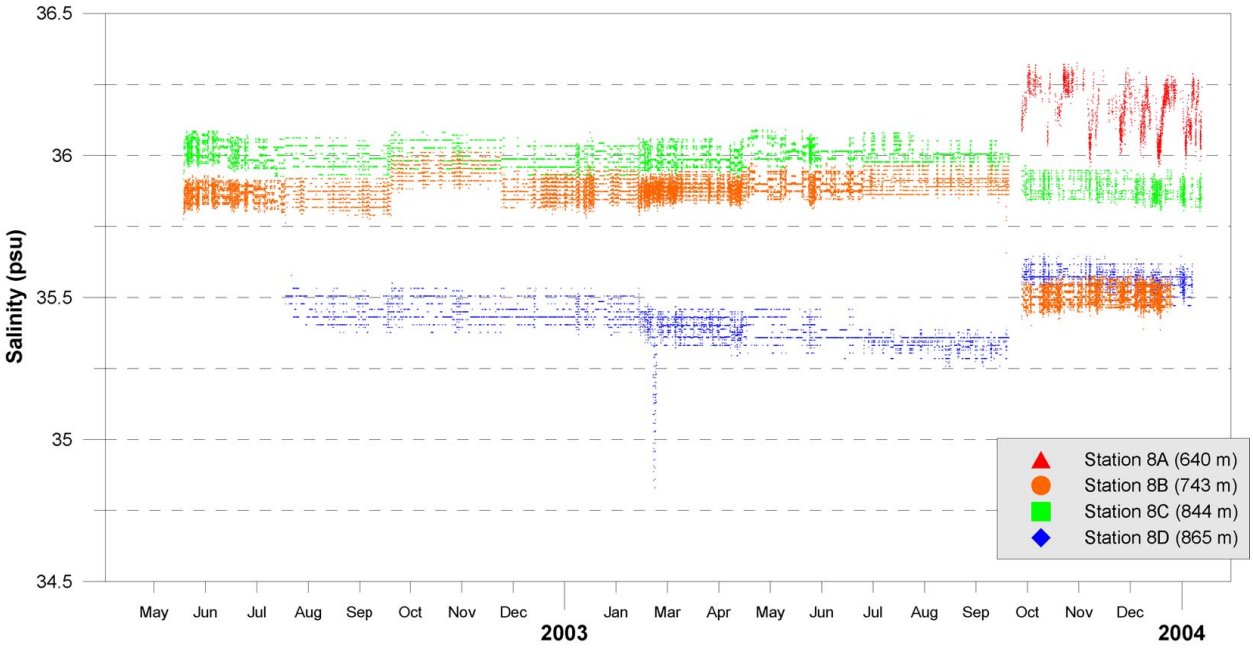


Figure 5.8: Time-series of salinity in the Norwegian Sea. The water depth at the site is 874 m. Data courtesy of Fugro Geos.

2. A methane system with a 5% ethane component.

Furthermore, the salt content of the pore water exerts an effect on the HPB. Increasing salinity of the pore water depresses the HPB, in contrast to the lifting effect of adding a thermogenic gas component (Riedel *et al.* 2006b;a). However, in the study area bottom water salinities (Station 8D on Figure 5.8) appear to be constant at ~35.5 psu[7]. Probable calibration of tools in October 2003 appears to have a larger effect than any natural phenomenon, and an average salinity value of 35.5 practical salinity units (psu) was used to construct the HPBs.

Knowing the hydrate former composition, and assuming both sea- and freshwater aqueous components, phase boundaries can be calculated and plotted using either HWHydrate (Mohammadi 2001) or CSMGEM (Sloan and Koh 2008, Figure 5.9).

[7]psu = practical salinity units

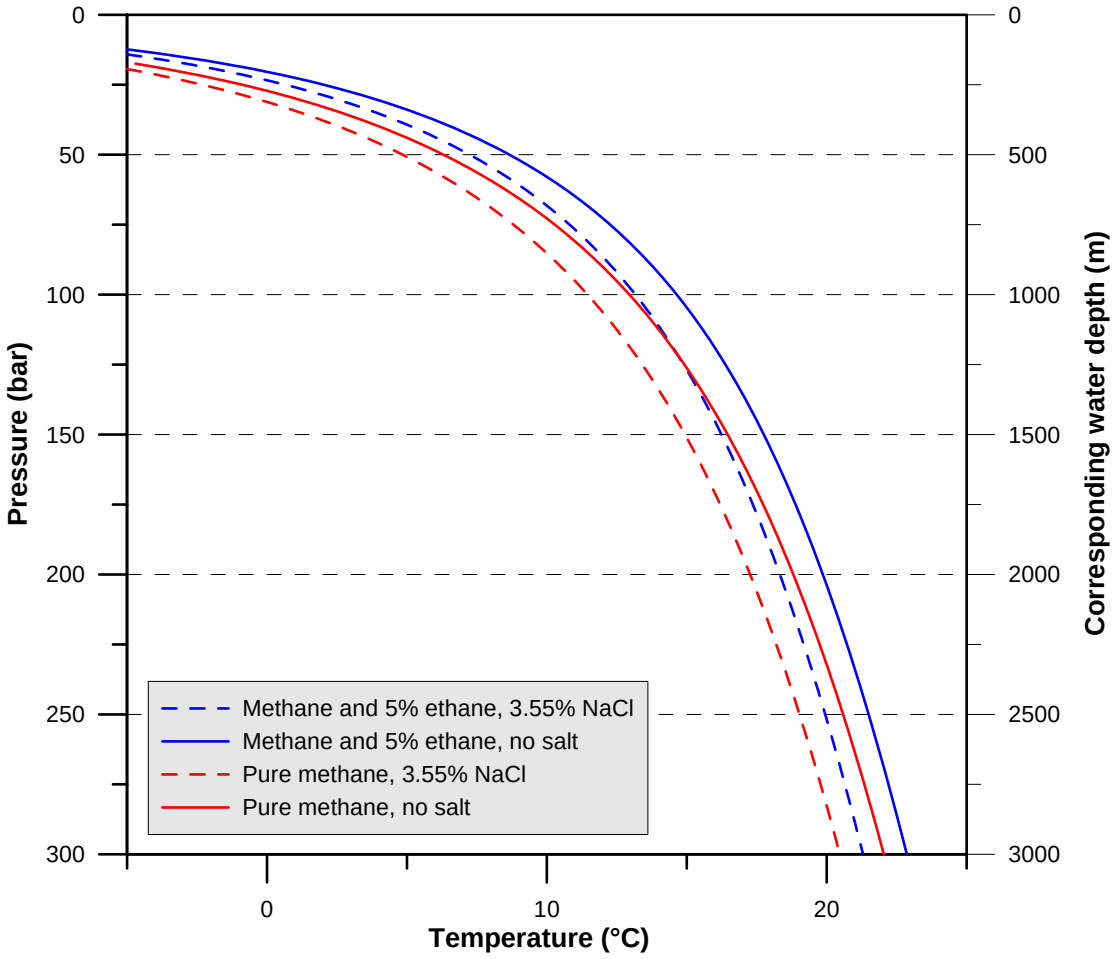


Figure 5.9: Two end member hydrate phase boundaries used for modeling the Nyegga hydrate stability zone (HSZ). Dashed lines indicate the effect of saline pore water. Calculated using HWHydrate (Mohammadi 2001). Note that a water fraction of 20% and 0.1°C steps were used in the hydrate phase boundary (HPB) modeling.

### 5.1.4 Thermobaric modeling

Thermobaric modeling is fundamental in defining the hydrate stability zone (HSZ) and thereby providing indirect evidence for the occurrence of gas hydrates (Milkov and Sassen 2000). Modeling of the HSZ and comparison with the BSR corresponding to the BHSZ can provide further evidence for a hydrate-related BSR.

The thermobaric model is defined on the basis of P-T[8] relationships of the HPB[9], the GG[10] and the OTG[11], as illustrated by Figure 5.10 a, b and c. The model's mathematical restrictions require the characterisation of those three parameters using exponential and linear best-fit lines, which is particularly unsuitable for the OTG (Figure 5.10b). The model's coarse resolution[12] introduces an uncertainty in line with the ability of representing the input data.

The actual model (Figure 5.10d) predicts the theoretical uppermost occurrence of gas hydrates at the intersection of the OTG and the HPB (at approximately 450 m in this case). The water depth for a particular point is then used to tie the geothermal gradient (GG) to the model, with the intersection of the GG and the HPB defining the BHSZ. In the illustrated case, at 750 m water depth, the predicted thickness of the HSZ is approximately 235 m.

To appreciate the effect of substituting the various input parameters to the uncertainties discussed above, a matrix of model runs was constructed. The modeled 2D extent of the HSZ was superimposed on a depth-converted[13] profile of seismic 2D line JMF97-215 (Figures 5.11 and 5.12).

## 5.2 Seismic interpretation

Nine seismic horizons have been interpreted within the Naust Formation (Figure 5.22).

[8] P-T = pressure-temperature
[9] HPB = hydrate phase boundary
[10] GG = geothermal gradient
[11] OTG = oceanic thermal gradient
[12] The model was, due to computational constraints, restricted to a 1000 m vertical resolution and a 10 m horizontal resolution. This is deemed a suitable compromise to represent the 1° slope angle prevalent in the study area.
[13] For the sake of simplicity, only a 1500 m/s water velocity was used in this simple exercise.

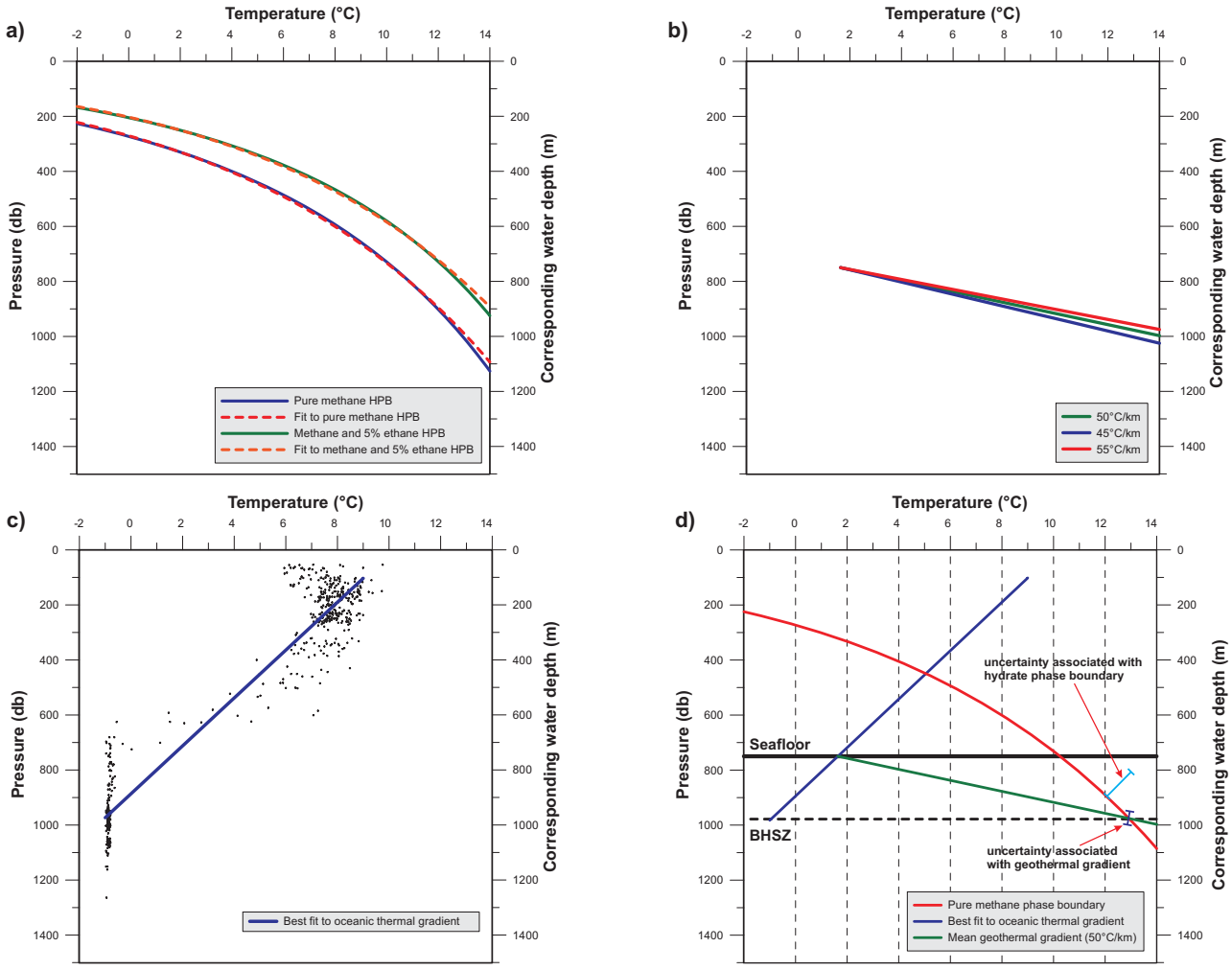


Figure 5.10: An example of the input parameters used to define the thermobaric hydrate stability zone (HSZ) model. (A) The calculated and modeled hydrate phase boundary, using both a pure methane and a methane+ethane case. (B) Range of three geothermal gradients applied in the model. (C) Oceanic thermal gradients applied in the modeling. (D) The complete system plotted on the P-T diagram, using a case with a 750 m water depth. Note the uncertainties associated with changing the hydrate phase boundary and the geothermal gradient. The oceanic thermal gradient fit overestimates the temperature in this case (at 750 m). The model is kept on the same scale to allow for comparison of the effect of the various parameters.

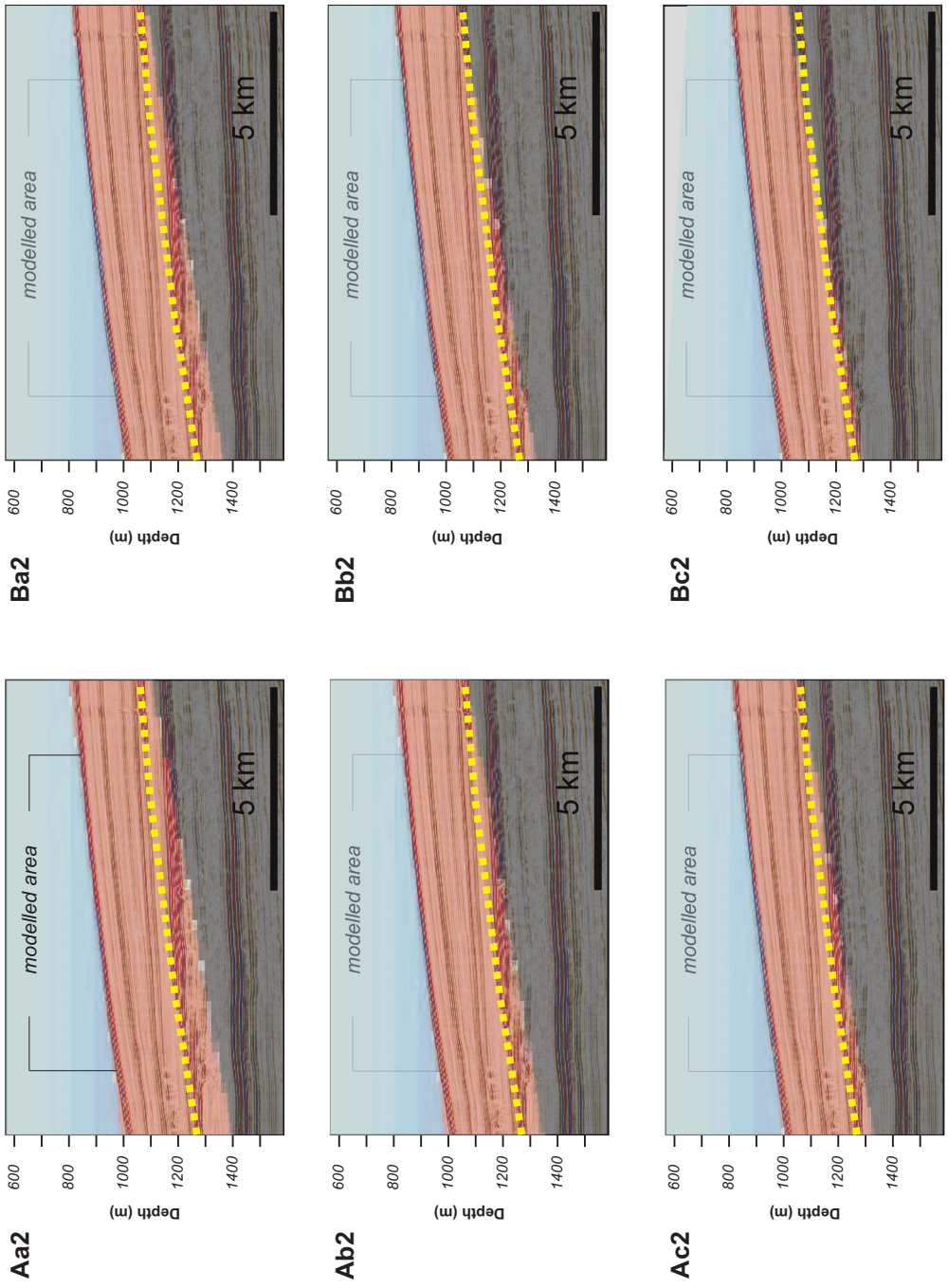


Figure 5.11: Modeled HSZ extent compared to the bottom simulating reflection (BSR, dashed yellow line) as observed on 2D line JMF97-215. For model names and represented properties, please refer to Table 5.3.

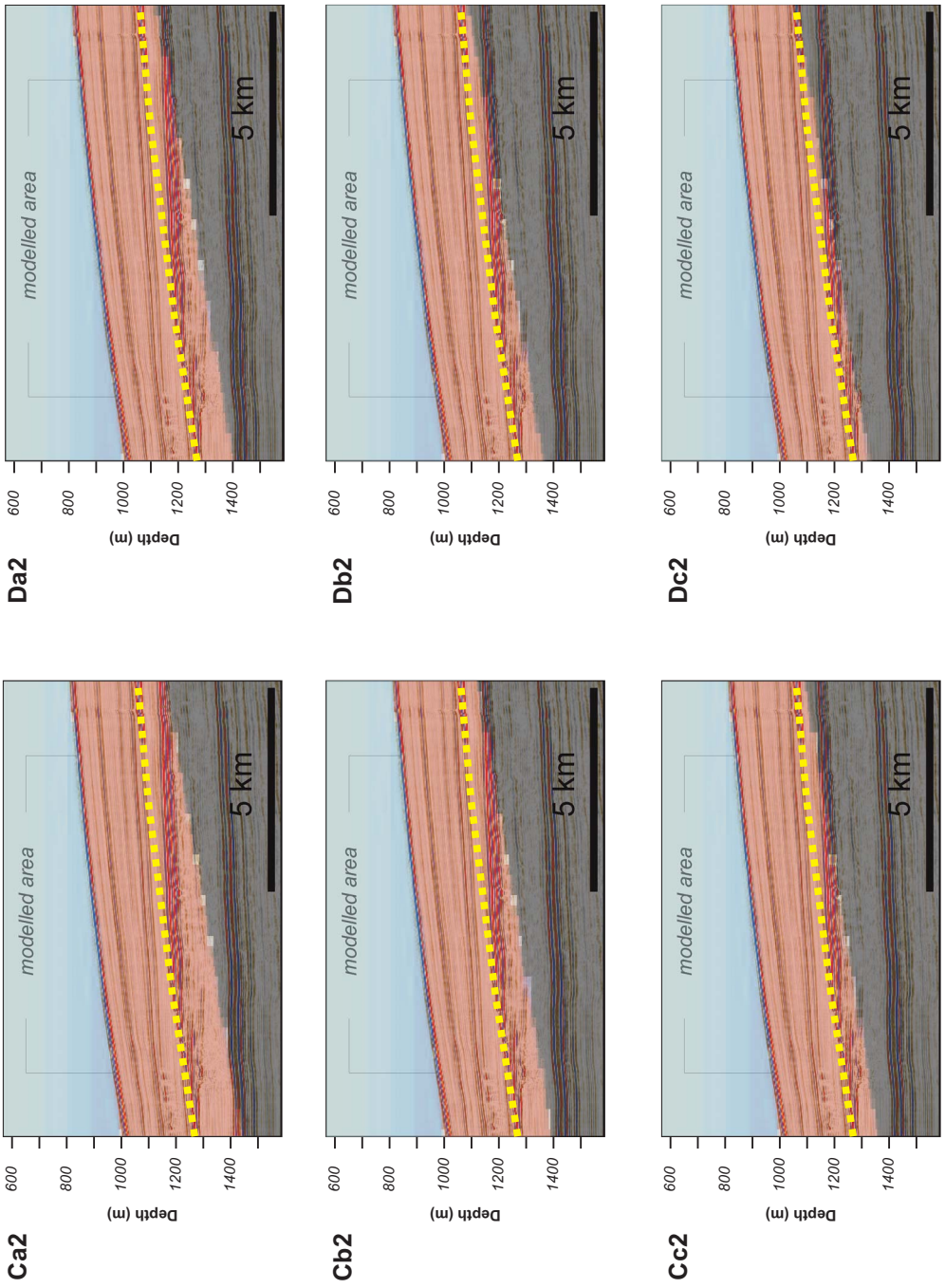


Figure 5.12: Modeled HSZ extent compared to the bottom simulating reflection (BSR, dashed yellow line) as observed on 2D line JMF97-215. For model names and represented properties, please refer to Table 5.3.

| | | | | Hydrate Phase Boundary | | | |
|---|---|---|---|---|---|---|---|
| | | | | Pure Methane | | Methane + 5% ethane | |
| | | | | Fresh pore water | Saline pore water | Fresh pore water | Saline pore water |
| Geothermal gradient | Low (45°C/km) | Oceanic thermal gradient | *Colder* | *Aa1* | *Ba1* | *Ca1* | *Da1* |
| | | | **Average** | **Aa2** | **Ba2** | **Ca2** | **Da2** |
| | | | *Warmer* | *Aa3* | *Ba3* | *Ca3* | *Da3* |
| | Medium (50°C/km) | Oceanic thermal gradient | *Colder* | *Ab1* | *Bb1* | *Cb1* | *Db1* |
| | | | **Average** | **Ab2** | **Bb2** | **Cb2** | **Db2** |
| | | | *Warmer* | *Ab3* | *Bb3* | *Cb3* | *Db3* |
| | High (55°C/km) | Oceanic thermal gradient | *Colder* | *Ac1* | *Bc1* | *Cc1* | *Dc1* |
| | | | **Average** | **Ac2** | **Bc2** | **Cc2** | **Dc2** |
| | | | *Warmer* | *Ac3* | *Bc3* | *Cc3* | *Dc3* |

Table 5.3: Summary of variables defining the 36 cases used for modeling the areal extent of the Nyegga hydrate stability zone (HSZ). Please note that only the bold cases are shown in Figures 5.11 and 5.12, primarily because the oceanic thermal gradient cannot be adequately modeled. A constant slope angle of 0.25 degrees is used in all cases, based on the seafloor slope angle of seismic line JMF97-215.

### 5.2.1 Seafloor

The seafloor reflection (Figure 5.13), while arguably the easiest to interpret, is a key horizon for this study. As such, it defines the top of the 3D subregional model, as well as providing important input for depth conversion. Furthermore, particularly in areas of 3D seismic coverage, hydrate-related features (e.g. pockmarks) can be interpreted on the seafloor. The same data can be used for optimising the location of possible development structures onto the seafloor. Finally, the depth to seafloor provides an idea of the setting of the various CTD stations used in this study.

### 5.2.2 Internal Naust Formation reflectors

Five regionally extensive Intra-Naust reflectors were interpreted, primarily as input data for the depth conversion. The interpretation itself was initially tied to Steinar Hustoft's high-resolution study of the GH2001 3D dataset, and extended with the help of the JMF97 2D survey across the area of interest. For the sake of clarity and traceability, Steinar Hustoft's horizon nomenclature is preserved with minor modifications:

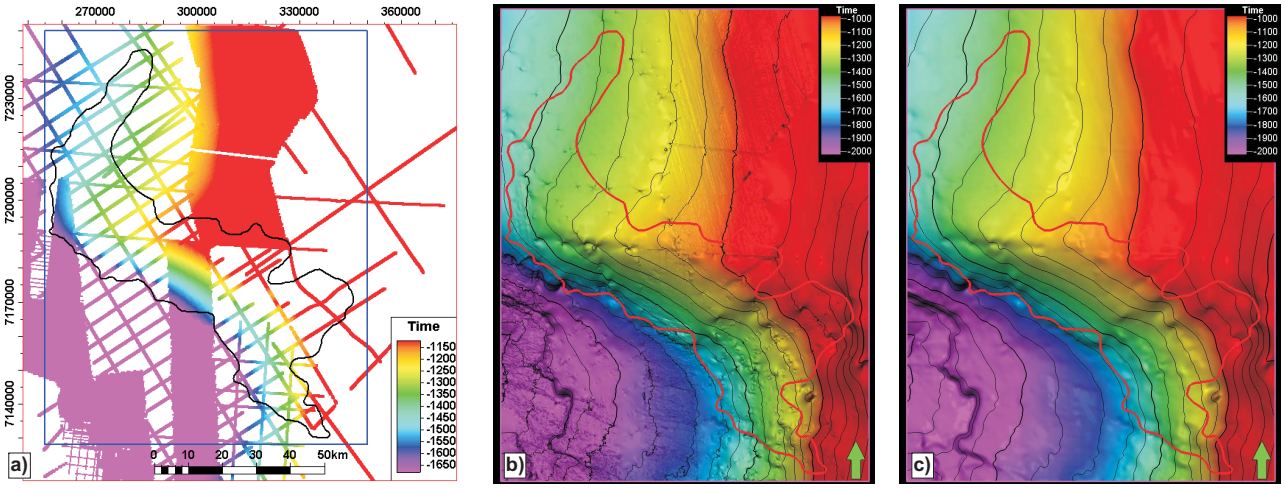


Figure 5.13: Interpretation of the seafloor horizon. (A) Interpreted horizon. (B) Time grid of horizon. (C) Smoothed time grid of horizon.

- KS SH5
- KS SH10
- KS SH13 (near TNS)
- KS SH20 (near TNU)
- KS base model (near TNW)

All interpreted horizons were gridded over a manually defined area that contained adequate interpretation (refer to the dashed line on figures 5.14, 5.15, 5.16, 5.17, 5.18). Convergent interpolation was used for gridding the 100*100 m surfaces.

### 5.2.3 GDF top and base

A glacigenic debris flow (GDF) partially overlaps the BSR-area at its northern edge (Figure 5.19). Bünz *et al.* (2003) hypothesize that the low-porosity sediments of the GDF are unsuitable hydrate host rocks and therefore the GDF effectively forms a barrier for hydrate formation. An area of 347 $km^2$ covering the overlap with the GDF is not included in the low case areal calculation.

GDFs also occur in the eastern area, as reflected particularly at OBS station OBS 4Z AF

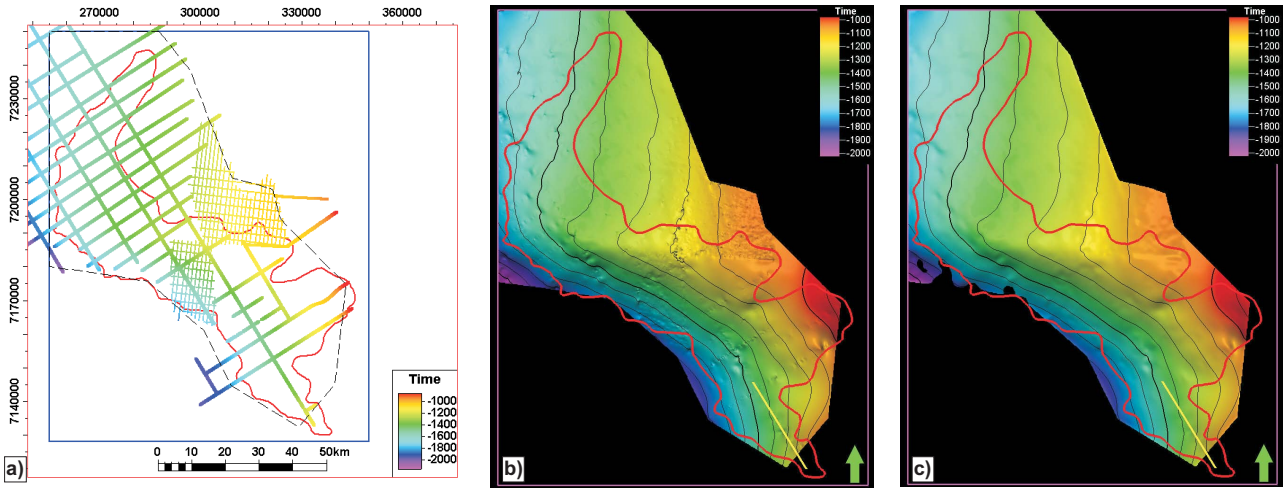


Figure 5.14: Interpretation of the KS SH5 horizon. (A) Interpreted horizon. (B) Time grid of horizon. (C) Smoothed time grid of horizon.

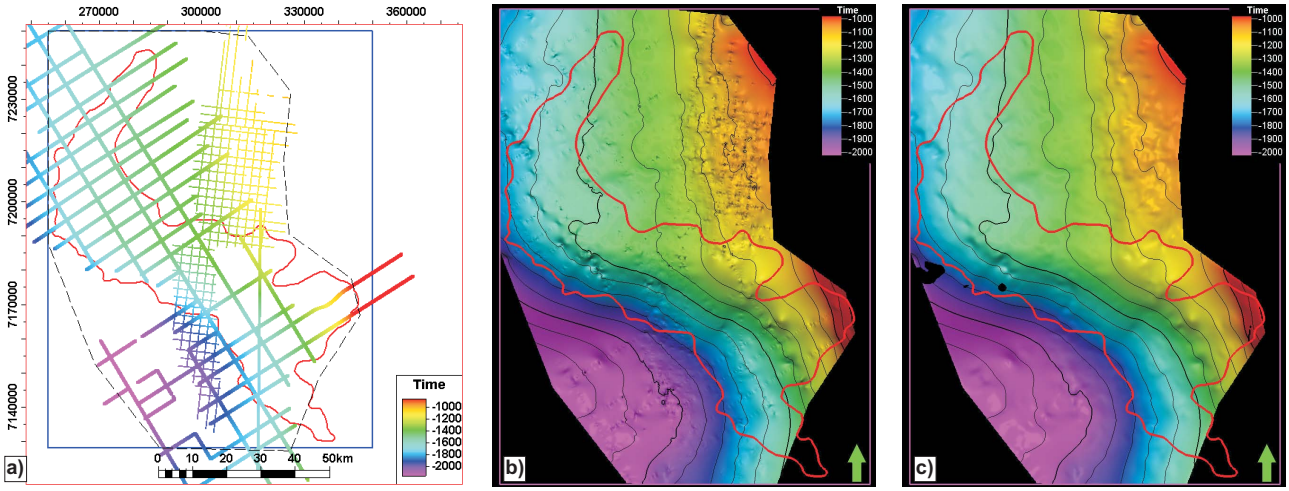


Figure 5.15: Interpretation of the KS SH10 horizon. (A) Interpreted horizon. (B) Time grid of horizon. (C) Smoothed time grid of horizon.

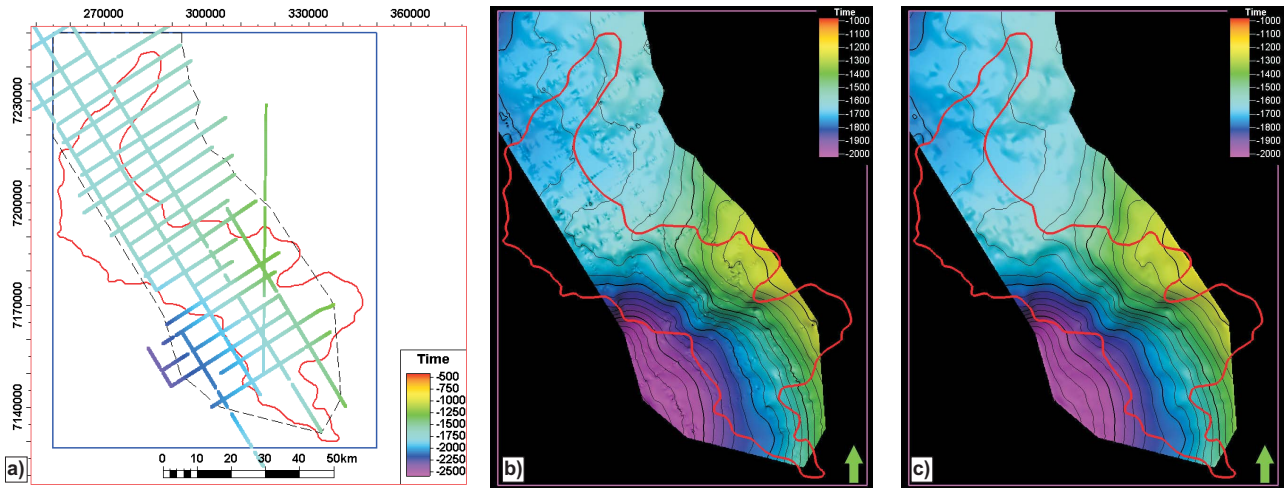


Figure 5.16: Interpretation of the KS SH13 horizon. (A) Interpreted horizon. (B) Time grid of horizon. (C) Smoothed time grid of horizon.

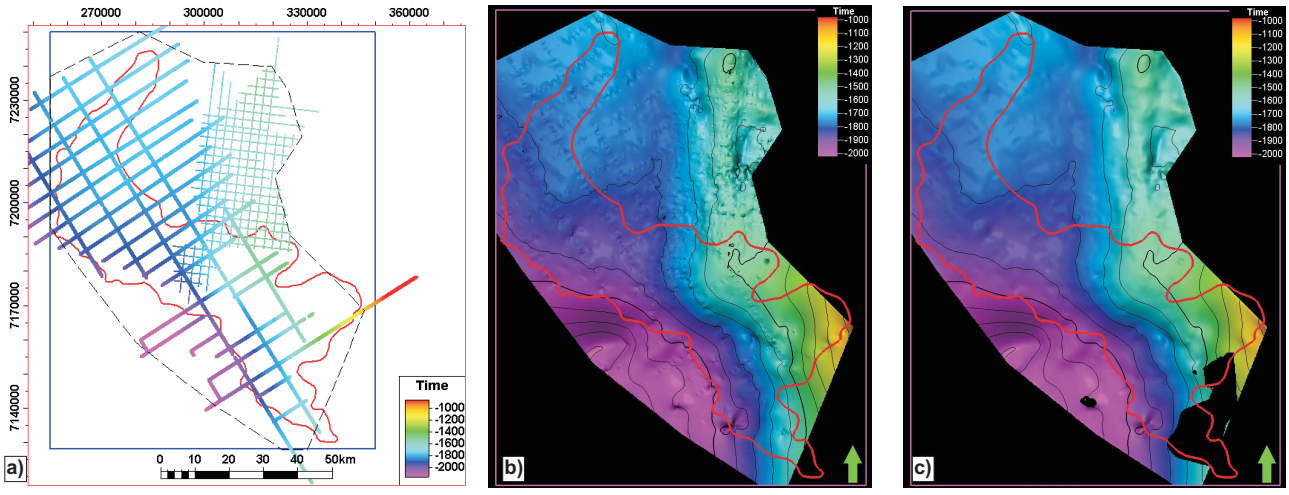


Figure 5.17: Interpretation of the KS S20 horizon. (A) Interpreted horizon. (B) Time grid of horizon. (C) Smoothed time grid of horizon.

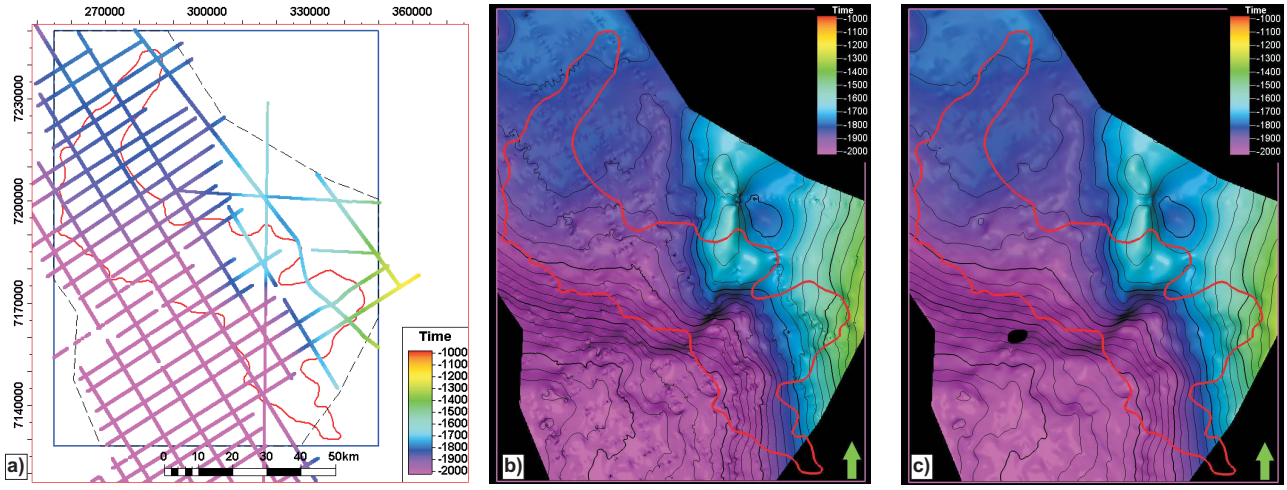


Figure 5.18: Interpretation of the KS baseModel horizon. (A) Interpreted horizon. (B) Time grid of horizon. (C) Smoothed time grid of horizon.

(Faverola *et al.* 2009). Apart from being unsuitable gas hydrate host sediments, GDFs typically have higher interval velocities than the surrounding units and their careful mapping is required in order to achieve an accurate depth conversion model.

### 5.2.4 Bottom simulating reflection

The bottom simulating reflection (BSR) is well defined in the central part of the Nyegga prospect but masked by sloping stratigraphy in the south-eastern part of the prospect and the GDF in the northern part (Figures 5.20 and 5.19). The interpretation is generally consistent with the outline of Bünz *et al.* (2003), though a more conservative approach not including the area around OBS station 6H has led to a slightly smaller BSR coverage ($2254\,km^2$ compared to $3120\,km^2$). OBS station 6H does not give the typical $V_p$ BSR response, and close examination of the seismic reveals a discontinuous BSR.

The BSR is the only true hydrate-related reflection. It has a rather patchy distribution, and is generally defined on the basis of amplitude changes thought to represent the build-up of free gas beneath an impermeable hydrate layer. The hydrate layer thus acts as a top seal for the free

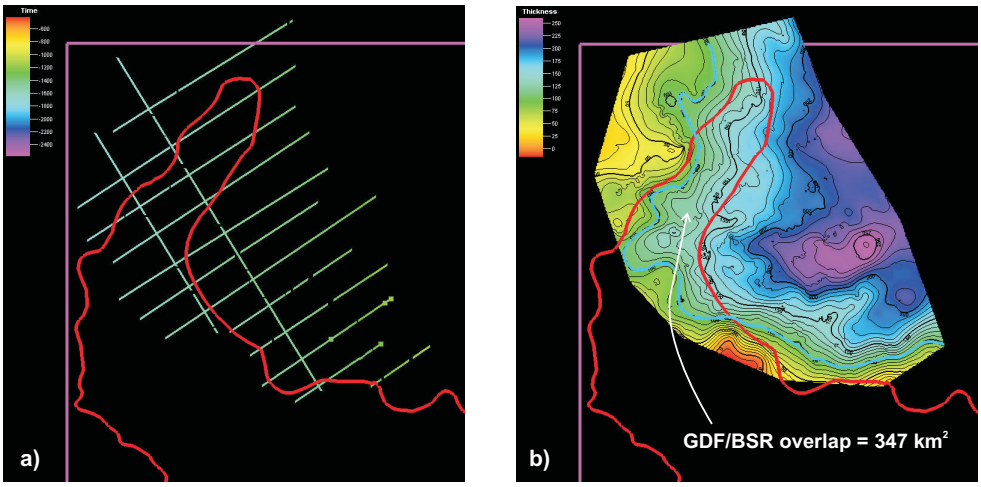


Figure 5.19: Isopach map of the interpreted glacigenic debris flow (GDF), as defined by the KS top GDF and KS base GDF horizons. The blue line emphasizes the 100 ms thickness of the unit.

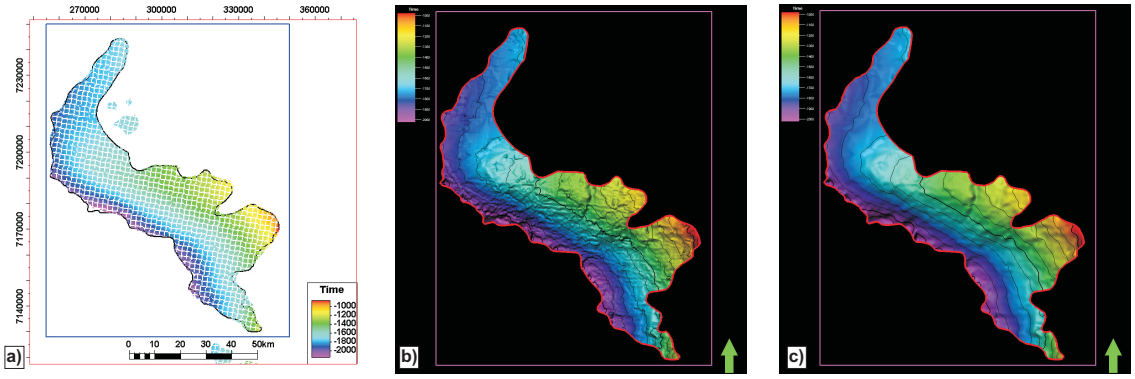


Figure 5.20: Interpretation of the BSR horizon. (A) Interpreted horizon. (B) Time grid of horizon. (C) Smoothed time grid of horizon. The red outline is the BSR outline of Bünz *et al.* (2003).

| | Petrel | GeoX | | |
|---|---|---|---|---|
| | "interpreted" | P90 | P50 | P10 |
| free gas zone GRV ($km^3$) | 64 | 47 | 95 | 163 |
| hydrate zone GRV ($km^3$) | 79 | 46 | 120 | 230 |

Table 5.4: Comparison of the gross rock volume (GRV) calculated in GeoX (using an area * thickness approach) and Petrel (using the Top Hydrate, BSR and Top Free Gas interpretations). While the Petrel calculation is based on a single set of interpretations, the GeoX input is defined by a P90, P50 and P10 range, as calculated on the basis of the BSR areal extent and the column height. The percentiles P90, P50 and P10 relate to the 90%/50%/10% probability of having a GRV of the respective size.

gas segment. Furthermore, the BSR validates the presence of gas hydrates outlined in the HSZ modelling of the previous chapter.

An alternative BSR interpretation that outlines the most obvious central part of the reflection has been conducted to serve as the minimal areal extent in the volumetric calculation. In this part, a bulge in the seafloor seems to provide an accumulation possibility for free gas migrating beneath the BHSZ, and may thus define a sweet spot for gas/hydrate accumulations (Figure 5.21). Figure 5.21 also shows an attempt of interpreting the top of the hydrate zone, and the base of the free gas zone. This is partly possible, particularly where nearby OBS stations provide the necessary constraints but, given the regional nature of the prospect, the poor quality of the JMF97 survey and the wide line spacing (5 by 10 km) it is deemed too inaccurate for use in more than a GeoX quality check (Table 5.4).

## 5.3 Depth conversion

Depth conversion is a necessary step for converting the time-domain interpretations into a depth-domain geomodel in which the prospect's volumes can be calculated. The depth conversion assigns constant interval velocities to subsurface zones defined by the Intra Naust reflectors (Figure 5.22, Table 5.5). Constant interval velocities are defined based on averaging interval velocities at all available OBS stations. The geotechnical borehole 6404/5 GB1 is used to quality-control OBS data

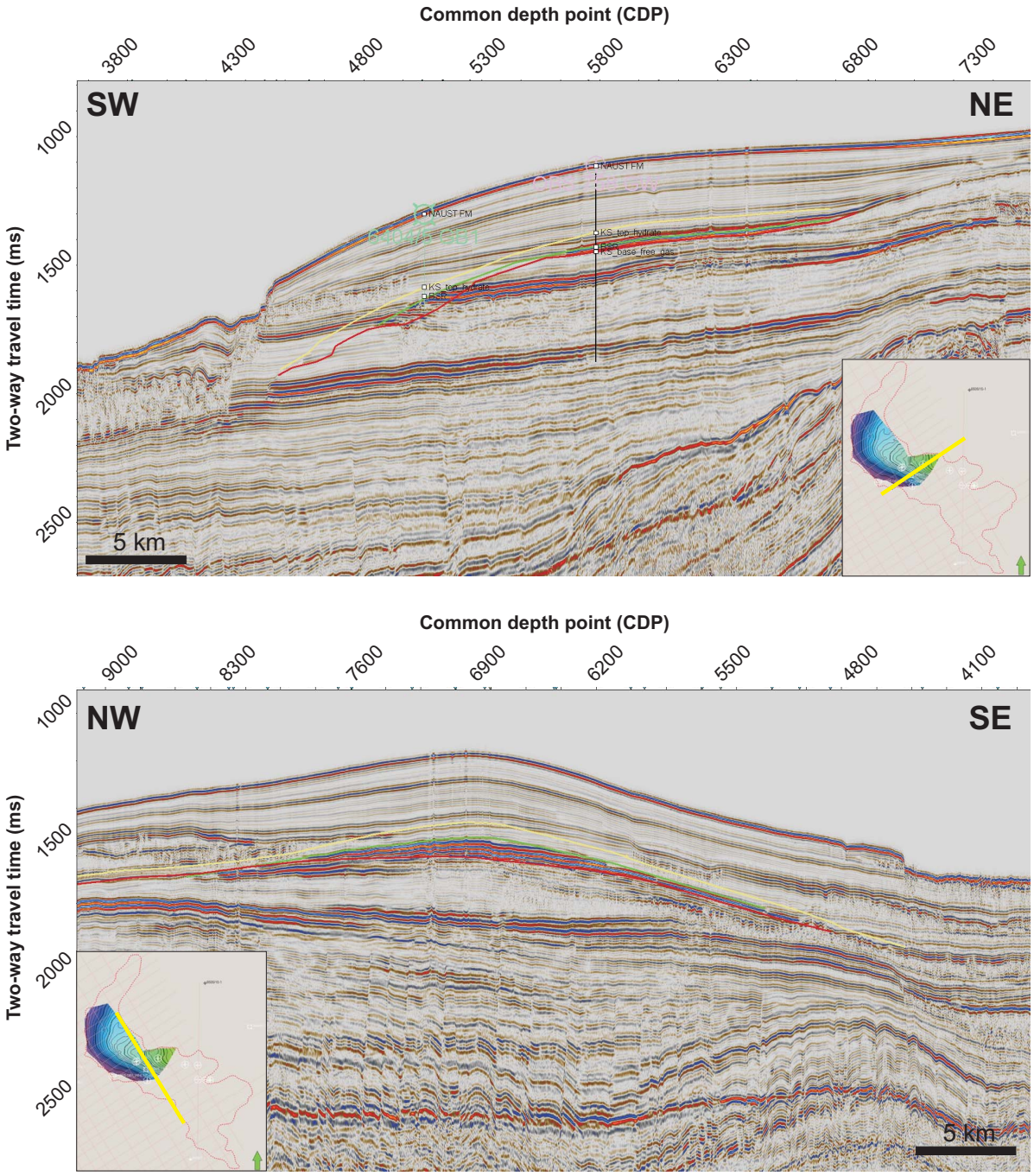


Figure 5.21: An alternative bottom simulating reflection (BSR) interpretation taking only the central part with a clear BSR (green reflector) into account. In addition, the seismic lines illustrate the horizons used to calculate the gross rock volume in Table 5.4: Top Hydrate (yellow) and Base Free Gas (red). The 'well tops' are based on the OBS-derived $V_p$ velocities.

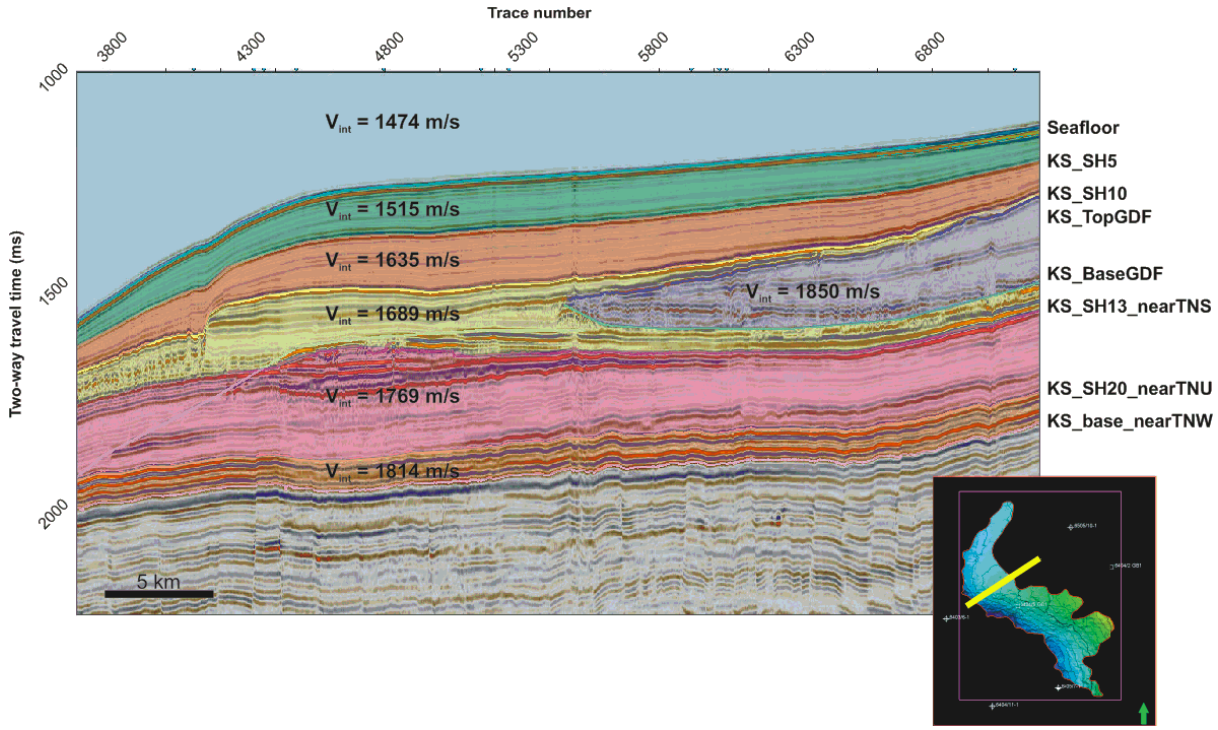


Figure 5.22: Schematic sketch illustrating the linear velocity model applied. The constant interval velocities are based on the ocean bottom seismometer (OBS) stations, and are summarized in Table 5.5.

| | interval velocities (m/s) | | | | | | | | | | |
|---|---|---|---|---|---|---|---|---|---|---|---|
| | OBS 1Z AF | OBS 3H AF | OBS 4Z AF | OBS 5Z AF | OBS6H AF | OBS 758 GW | JM517 | JM523 | JM524 | **Average** | **Range** |
| *Water column* | 1 475 | 1 473 | 1 478 | 1 478 | 1 477 | 1 467 | 1 475 | 1 475 | 1 472 | **1 474** | 11 |
| *upper Naust Fm* | 1 496 | 1 501 | 1 569 | 1 551 | 1 511 | 1 513 | 1 498 | 1 502 | 1 491 | **1 515** | 78 |
| *KS_SH5* | 1 619 | 1 633 | 1 700 | 1 705 | 1 633 | 1 639 | 1 582 | 1 597 | 1 604 | **1 635** | 123 |
| *KS_SH10* | 1 670 | 1 653 | *GDF present* | 1 684 | 1 752 | 1 615 | 1 738 | 1 697 | 1 705 | **1 689** | 136 |
| *KS_SH13 (near TNS)* | 1 726 | 1 761 | 1 687 | | 1 799 | 1 828 | 1 695 | 1 814 | 1 845 | **1 769** | 158 |
| *KS_SH20 (near TNU)* | 1 650 | 1 944 | | | | | 1 864 | 1 793 | 1 820 | **1 814** | 294 |
| *GDF* | | | 1850 | | | | | | | **1 850** | 0 |

Table 5.5: Interval velocities used in the depth conversion, as calculated from the ocean bottom seismometer (OBS) experiments of Bünz *et al.* (2005c), Westbrook *et al.* (2008a) and Faverola *et al.* (2009). The range is simply calculated from the minimal and maximal velocity for each respective interval.

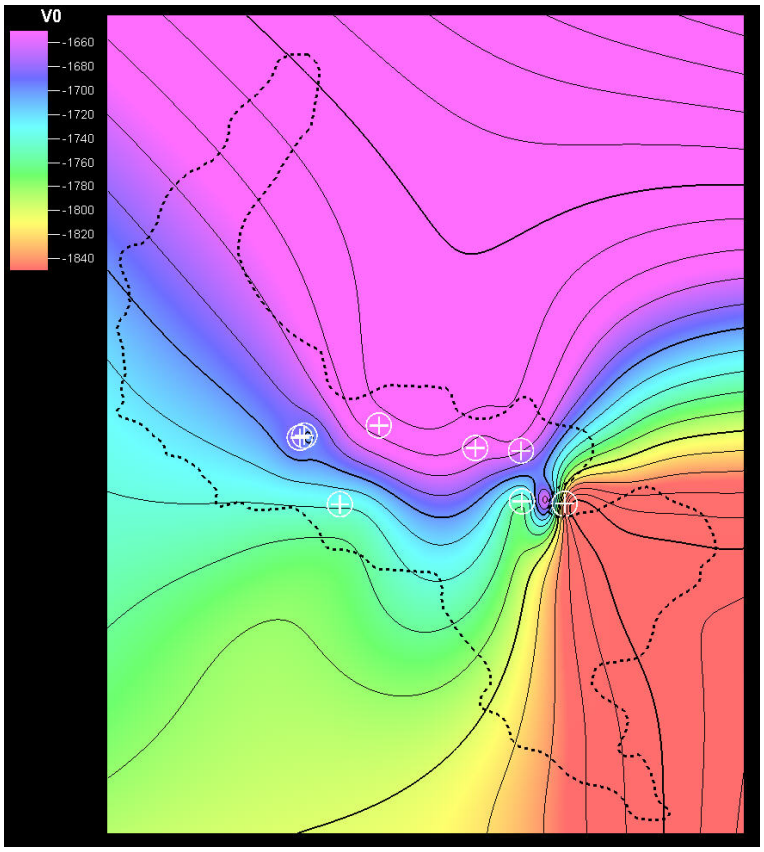


Figure 5.23: Example of lateral velocity variation for the KS SH 13 horizon. The black stippled line represents the Nyegga prospect outline, while the white well symbols indicate the OBS stations from which the map is extracted. Due to the clustering of the OBS data points in the central W-E axis, the velocity map does not reflect the expected subsurface velocity variation and constant interval velocities are thus used.

in the uppermost zones that it actually penetrates.

Due to the limited number of OBS stations in a restricted geographical extent it is deemed unsuitable to grid the velocities between the OBS stations rather than applying an average interval velocity. An example of this problem is illustrated by Figure 5.23, in which the interval velocity for horizon KS SH 13 in the different OBS stations is gridded across the area of interest. Extrapolation away from the data points is clearly erroneous, and while it would be feasible to constrain the extrapolation, an averaged constant interval velocity is considered more accurate and representative at this regional scale.

## 5.4 Volumetric calculation

### 5.4.1 Reservoir parameters

Reservoir parameters used to define the in-place and, to some extent, recoverable volumes reflect the large uncertainty associated with the Nyegga prospect (Table 5.6). Not only are the physical reservoir parameters, such as net-to-gross (NTG), porosity and spatial extent poorly constrained, but the behaviour of the hydrate-free gas system is virtually unknown at the site. The only borehole penetrating the BSR did not recover physical hydrate samples (Mienert and Bryn 1997), let alone constrain the seismic-derived gas saturation values. Previously unpublished wireline data from the geotechnical borehole are of too poor quality to accurately constrain the BSR and any hydrate effect (Figure 5.28). Furthermore, the prospect extends across the better part of 15 blocks on the NCS, an areal extent unheard of in conventional oil and gas exploration. Nonetheless, for a regional study the chosen parameters are deemed adequate.

To account for some of this large uncertainty, a stochastic model was generated. Input parameters were defined by distributions, spanning in both directions from a base case representing the most likely case (Table 5.6 and Figure 5.24). Statistically the base case equates to the mode case, while both the P50 and mean case may be offset due to the skewed distributions used. Percentiles, such as P1, P50 and P99, relate to probabilities of a reservoir parameter being present with the

| | Gas hydrate zone | | | | Reference/Comments |
|---|---|---|---|---|---|
| *Parameter [units]* | Type | Low (P99) | Base | High (P1) | |
| Area of Closure [km2] | StrBeta | **1070** | **2254** | **3120** | Mid case: BSR outline without "tricky" zones, Low case: "Sweet spot" BSR outline, High case: BSR outline |
| Column Height [m] | StrBeta | **10** | **50** | **120** | Based on Bünz et al 2005, Westbrook et al 2008 and Faverola et al 2009. |
| Net/Gross Ratio [decimal] | Norm | **0** | **0.5** | **1** | Based on Hustoft et al 2007 & Bouriak et al 2003. |
| Porosity [decimal] | Norm | **0.49** | **0.55** | **0.61** | Geotechnical borehole 6404/5 GB1 |
| Gas Saturation [decimal] | StrBeta | **0.025** | **0.071** | **0.21** | Based on Bünz et al 2005, Westbrook et al 2008 and Faverola et al 2009. |
| Gas Expans. Factor (1/Bg) [Sm3/m3] | StrBeta | **123** | **164** | **189** | Sloan & Koh 2008 for base case, Schlumberger 2009 for high case, low case using 75% cage occupancy. |
| Recovery factor gas [decimal] | StrBeta | **0.05** | **0.15** | **0.3** | Speculative, yet conservative. |

| | Free gas zone | | | | |
|---|---|---|---|---|---|
| *Parameter [units]* | Type | Low (P99) | Base | High (P1) | |
| Area of Closure [km2] | StrBeta | **1070** | **2254** | **3120** | Mid case: BSR outline without "tricky" zones, Low case: "Sweet spot" BSR outline, High case: BSR outline |
| Column Height [m] | StrBeta | **20** | **40** | **80** | Based on Bünz et al 2005, Westbrook et al 2008 and Faverola et al 2009. |
| Net/Gross Ratio [decimal] | Norm | **0** | **0.5** | **1** | Based on Hustoft et al 2007 & Bouriak et al 2003. |
| Porosity [decimal] | Norm | **0.49** | **0.55** | **0.61** | Geotechnical borehole 6404/5 GB1 |
| Gas Saturation [decimal] | StrBeta | **0.002** | **0.007** | **0.19** | Based on Bünz et al 2005, Westbrook et al 2008 and Faverola et al 2009. |
| Gas Expans. Factor (1/Bg) [Sm3/m3] | Norm | **100** | **120** | **140** | 1/pressure - reservoir at 1200m |
| Recovery factor gas [decimal] | StrBeta | **0.05** | **0.29** | **0.43** | Peon field analogue (NPD 2009) for mid and high case, 5% conservative for low case. |

| | Chimney zone | | | | |
|---|---|---|---|---|---|
| *Parameter [units]* | Type | Low (P99) | Base | High (P1) | |
| Gross Rock Volume [km2-m] | StrBeta | **3452** | **9286** | **15120** | Weibull 2009 direct estimate for low case, extrapolated across the Nyegga prospect in the high case. |
| Net/Gross Ratio [decimal] | Norm | **0** | **0.5** | **1** | Uncertainty with respect to suitable host rock, assumed to be 50:50 chance. |
| Porosity [decimal] | Norm | **0.35** | **0.55** | **0.75** | Mean value from geotech borehole, wider range to account for carbonate formation and fracture-induced porosity. |
| Gas Saturation [decimal] | Norm | **0.05** | **0.2** | **0.35** | Increased to reflect hydrate potential. Max from Stoian et al 2008. |
| Gas Expans. Factor (1/Bg) [Sm3/m3] | StrBeta | **123** | **164** | **189** | Sloan & Koh 2008, Schlumberger, min case using 75% cage occupancy |
| Recovery factor gas [decimal] | StrBeta | **0.05** | **0.15** | **0.3** | As hydrate zone, may be higher. |

Table 5.6: Range of reservoir parameters used in defining the in-place volumes of hydrate-bound methane. Each reservoir parameter is defined by a distribution between a range of possible values used in the stochastic calculation. The mode case will, by definition, have the highest impact in the volumetric calculation and thus represents the most favoured case. Note that StrBeta = Stretched Beta distribution.

respective quality. As an example, the 10-50-120 distribution for the thickness of the hydrate zone gives a 99% probability of a hydrate zone at least 10 m thick being present, yet only a 1% chance that a 120 m thick zone is present in any of the 5000 simulation runs calculated. The shape of the distribution, either Normal or Stretched Beta, then defines which thickness is most likely to be chosen in the calculation (Figure 5.24) . In this example, a 50 m thickness has the highest probability of being picked.

#### 5.4.1.1 Gross rock volume

The chimney structures, described in detail by Weibull (2008), are represented by a gross rock volume calculated from the chimney's diameter and length. Since Weibull's study area does not cover the whole Nyegga prospect, a correction[14] is applied to extrapolate the chimney density across the whole prospect area. This scenario is used for the high case, while the chimney extent as reported by Weibull (2008) in his study area is used as a conservative low case. This is deemed adequate since seismic data indicates chimneys away from the aforementioned study area (Figure 5.25).

#### 5.4.1.2 Area of closure

Spatially, the reservoir is restricted to the BSR-defined lateral extent of the Nyegga prospect (Figure 5.20). The low case is defined by the interpretation of the central part of the BSR, the so-called 'BSR Sweet Spot' (Figure 5.21). For the high case, previous BSR interpretations were used (Bünz *et al.* 2003). The base case is based on the same interpretation, but disregards the zones of uncertain BSR interpretations to the north (Figure 5.19) and south-east.

An upside potential exists in other areas where BSRs have been identified. Seven other areas with BSRs have been mapped in the immediate area around the main Nyegga prospect (Bünz *et al.* 2003), with a combined area of 658 $km^2$. These areas, as well as other hydrate-prone zones on the Norwegian continental shelf, have not been included in the volumetric calculation but represent a

[14]The AOI of Weibull (2008) covers about a quarter of the total BSR area, and a multiplication factor of 4.38 is applied to account for this.

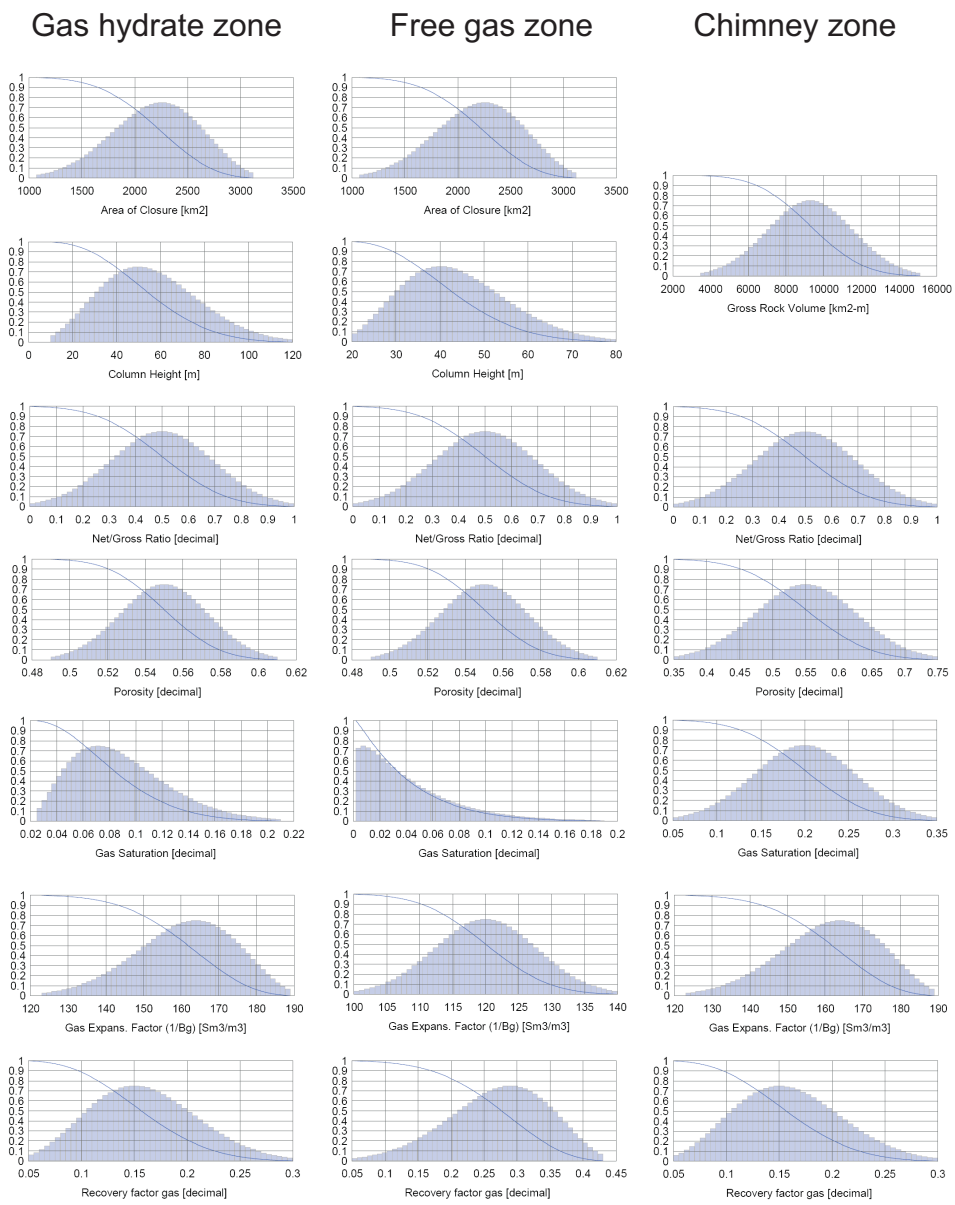


Figure 5.24: A graphical representation of the distributions of the various reservoir parameters for Nyegga's three segments. The graphs illustrate the relative probability of a particular value to be chosen for the stochastic volumetric calculation. The peak of the curve, corresponding to the mode, stands a higher chance of being selected than the outlying points near the P99 and P1 end points. Skewed distribution are used particularly for the gas saturation parameter in order to account for both the relatively large upside potential while keeping a conservative P99 and mode case. Please note that the y-axis is a measure of the probability of the respective reservoir parameter value being chosen in any particular stochastic calculation run.

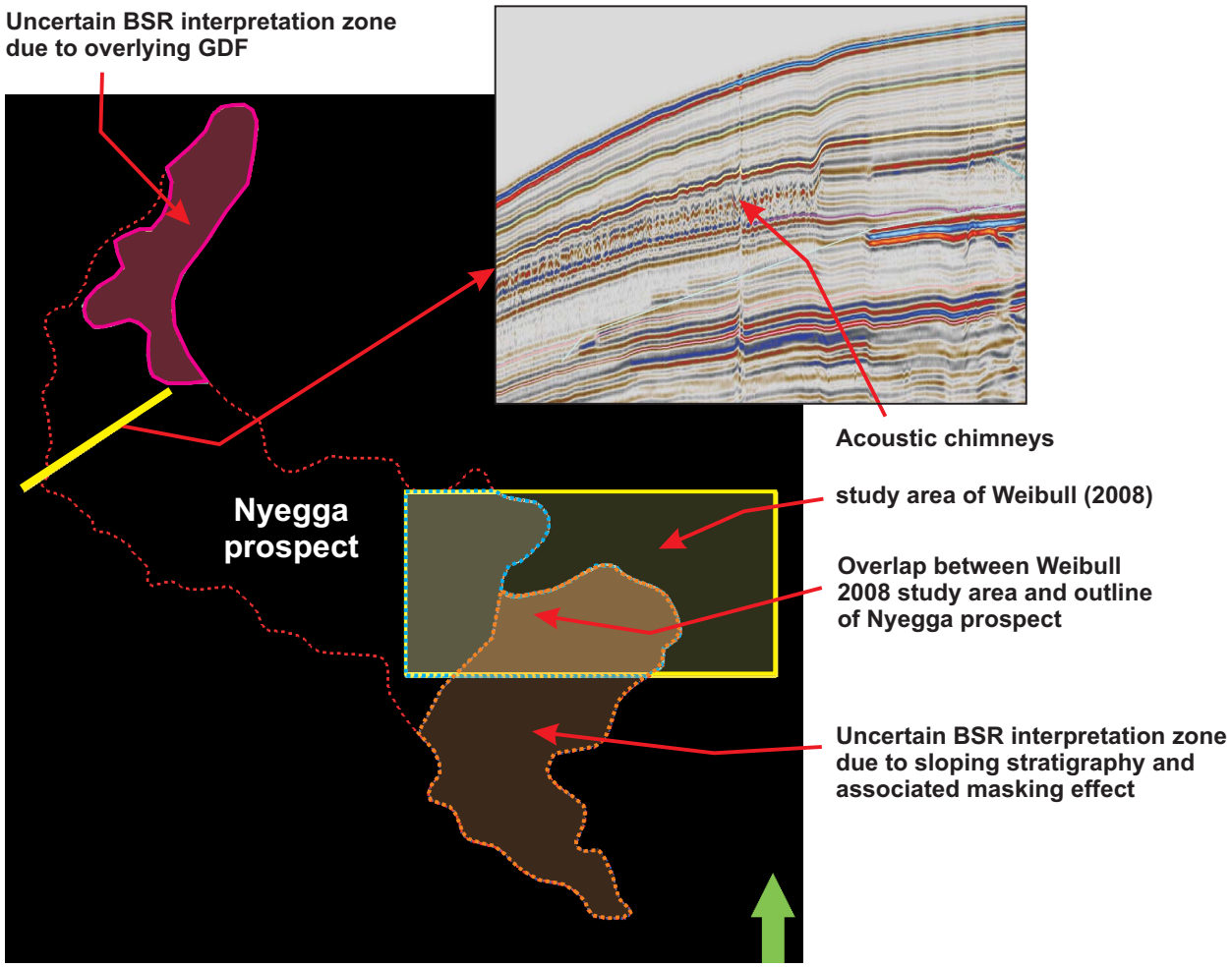


Figure 5.25: Chimney structures in relation to their study site and the Nyegga prospect. The illustrations highlights the extent of the study area of Weibull (2008) compared to the Nyegga prospect outline. Please note that the study area of Weibull (2008) was used as a low case gross rock volume (GRV) in the chimney volume calculation, while an extrapolation over the whole Nyegga prospect was undertaken for both the base and high case. Please also note the two areas of uncertain bottom simulating reflection (BSR) interpretation, which were disregarded in the areal extent base case.

considerable upside potential.

#### 5.4.1.3 Column height

The thicknesses and concentrations of the hydrate system itself, both the solid hydrate-layer and the underlying free gas, is primarily defined by the ocean bottom seismometer (OBS) experiments of Bünz *et al.* (2005c), Westbrook *et al.* (2008a) and Faverola *et al.* (2009).

Utilising P-wave velocities derived from the OBS experiments as interval velocities, it is possible to derive a time-depth relationship at the OBS stations (example shown in Table 5.7) using a simple relationship:

$$TWT_n = Z_{int}/V_p * 2 + TWT_{n-1} \tag{5.1}$$

where:

$TWT_n$ = Two-way-travel-time at top of interval n

$Z_{int}$ = Thickness of interval Z

$V_p$ = P-wave velocity of interval Z

$TWT_{n-1}$ = Two-way-travel-time to top of interval n-1

This allows the OBS-derived P-wave velocities to be plotted directly onto the seismic profiles (Figure 5.26), serving both as a quality-control and for visualising the continuity of the various zones of anomalous velocities. Furthermore, a time-depth relationship allows the plotting of time-domain interpreted horizons onto the OBS depth-domain 'well section' (Figure 5.27).

#### 5.4.1.4 Porosity

Porosity ($\phi$) is derived from the nearby geotechnical borehole 6404/5-GB1 (Figure 5.28), and is restricted to a narrow distribution of **0.49-0.55-0.61**.

Station: OBS 758 GW

| MD | TWT | Average velocity (m/s) | Interval velocity (m/s) |
|---|---|---|---|
| 804.6 | 1113 | 1445.82 | 1482 |
| 832 | 1149.98 | 1446.99 | 1501 |
| 857.6 | 1184.09 | 1448.54 | 1548 |
| 886.2 | 1221.04 | 1451.55 | 1595 |
| 936.3 | 1283.86 | 1458.57 | 1629 |
| 977.5 | 1334.44 | 1465.03 | 1631 |
| 1008.7 | 1372.7 | 1469.66 | 1693 |
| 1032.6 | 1400.94 | 1474.16 | 1716 |
| 1055.8 | 1427.98 | 1478.74 | 1337 |
| 1067.6 | 1445.63 | 1477.01 | 1713 |
| 1100.7 | 1484.27 | 1483.15 | 1724 |
| 1133.1 | 1521.86 | 1489.1 | 1522 |
| 1163.6 | 1561.94 | 1489.94 | 1642 |
| 1233.3 | 1646.83 | 1497.78 | 1939 |
| 1417.9 | 1837.24 | 1543.51 | 1757 |
| 1451.7 | 1875.72 | 1547.89 | |

Table 5.7: Example of interval velocity calculation, using the OBS 758 GW station. The interval pick is based on layer boundaries for this particular example. For the other stations, please refer to the attached electronic appendix.

| Station | Water depth (m) | Depth to BSR (mbsl) | Hydrate zone | Free gas thickness | Hydrate saturation | Free gas saturation | Comments | Reference |
|---|---|---|---|---|---|---|---|---|
| 6404/5 GB1 | 960 | 1220 | 25 | 15 to >40 | ? | ? | Free gas zone poorly imaged by borehole ending 50m below the BSR | 6404/5 GB1 borehole |
| OBS 758 | | 1052 | max 120 | 18m | 12-20% | | Two additional gas layers at 1128 (30m thick) and 1415 (35m thick) | Westbrook et al 2008 |
| JM516 | 965 | 1245 | 47 | | 6-12% | 0.7-14% | Low hydrate estimate = hydrate in frame, high-estimate = hydrate as pore fill. Low gas estimate = homogeneous distribution, high gas estimate = patchy distribution. | Bünz et al 2005 |
| JM517 | 945 | 1225 | 56 | 46-90 | 11-21% | 0.9-19% | | |
| JM523 | 921 | 1201 | 42 | 50-85 | 4-8% | 0.9-18% | | |
| JM524 | 919 | 1199 | 32 | 60-68 | 2.5-5% | 0.7-14% | | |
| 1Z | 708 | 956 | 70 | 37 | | 0.55-15% | | |
| *3H* | 740 | 998 | 71 | 29 | | 0.5-14% | | |
| *4Z* | 706 | no BSR | | | | | Gas trapped beneath GDF, 0.3-8% | Faverola et al 2009 |
| *5Z* | 733 | no BSR | | | | | Gas trapped beneath GDF, 0.2-5.5% | |
| *6H* | 765 | no BSR | | | | | No LVZ1 seen on OBS data | |
| **GeoX input** | | | **10 - 50 -120** | **20 - 40 - 80** | **2.5 - 7.1 - 21** | **0.2 - 0.7 - 19** | | |

Table 5.8: Summary of the column height and saturation values derived from the 6404/5 GB1 borehole as well as the ocean bottom seismometer (OBS) sites of Bünz *et al.* (2005c), Westbrook *et al.* (2008a) and Faverola *et al.* (2009).

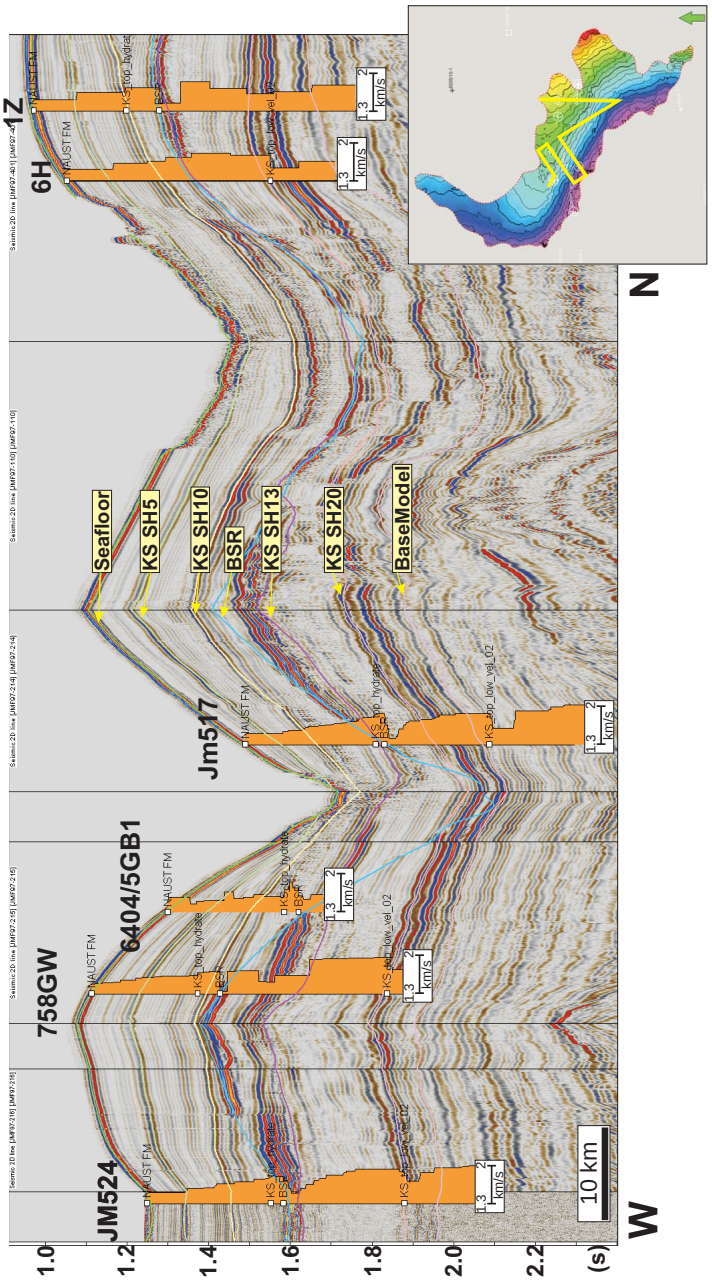


Figure 5.26: OBS-derived P-wave velocities as displayed on a composite seismic line. The illustration also provides an overview of the interpreted horizons. Note particularly the cross-cutting nature of the bottom simulating reflection (BSR). Furthermore, the P-wave velocity at OBS station 6H indicates no free gas layer at the expected BSR layer, leading to the reduction of the BSR-extent of Bünz *et al.* (2003) in the volume calculation. Well tops are based on the OBS data. OBS data from Bünz *et al.* (2005c),Westbrook *et al.* (2008a) and Faverola *et al.* (2009).

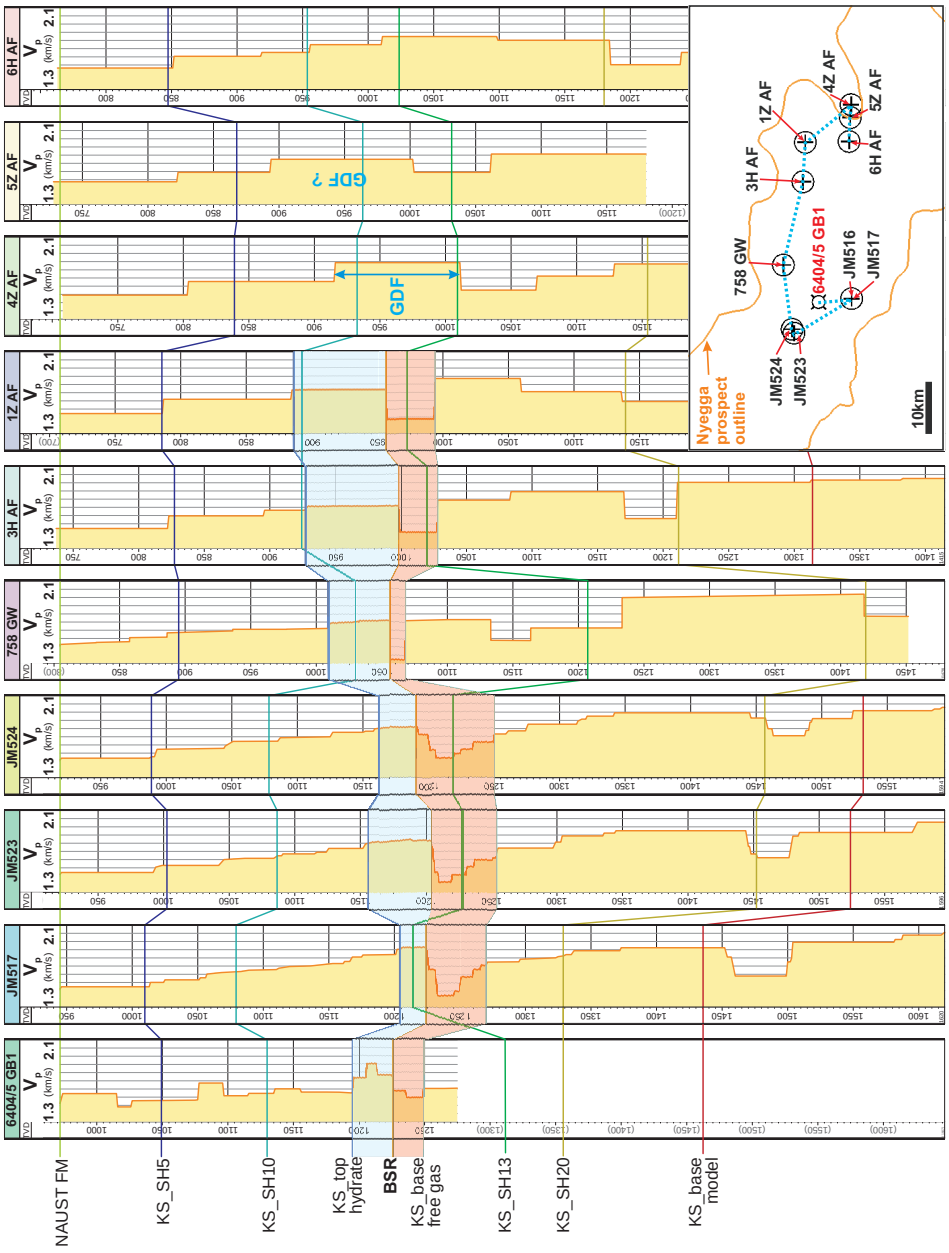


Figure 5.27: Summary of OBS data from Bünz *et al.* (2005c),Westbrook *et al.* (2008a) and Faverola *et al.* (2009) compared to the 6404/5 GB1 measured P-wave velocity. The bottom simulating reflection (BSR) well top is defined on the basis of the onset of the low velocity anomaly on the OBS data, and is notably absent at stations 4Z, 5Z and 6H. The remaining tops are defined by the intersection of the interpreted horizons with the 'well path' of the OBS stations. The BSR separates the hydrate zone (blue), interpreted as the higher velocity package above the BSR, from an underlying low-velocity free gas zone (red).

For the chimney zone, porosity is assigned a broader range centered upon the same base case, namely **0.35-0.55-0.75**. This range is designed to account for the possibility of increased authigenic carbonate formation lowering the porosity, particularly in the uppermost chimney zones. On the other hand, increased fracture porosity could be generated by increased fluid flux.

#### 5.4.1.5 Net to gross

Hustoft *et al.* (2007) illustrate a series of porous and permeable zones suitable for hydrate formation.

A quick estimate suggest that this 'reservoir' accounts for approximately 50% of the area of interest. The preference of hydrates to form in these zones is further manifested by the discontinuous nature of the BSR, being well defined in areas of hydrates forming and absent in areas of no hydrate forming.

An attempt was made, as explained above, to account for the difference in GRV when simply extrapolating a constant column from the BSR or when interpreting the top of the hydrate zone and the base of the free gas zone (Table 5.4). This was motivated by the hypothesis that porous (i.e. high net reservoir) strata are seen on the seismic due to their higher amplitudes (Bouriak *et al.* 2003). In that sense, one could assume a 100% NTG in such zones, and assign a lower (perhaps close to zero) for the seemingly impermeable layers in between. However, the large line spacing and low quality of the critical JMF97 survey hamper this approach beyond the quick quality-check illustrated by the GRV calculation listed in Table 5.4.

A wide NTG range of **0-1** is used to account for the large uncertainty due to limited ground truth.

#### 5.4.1.6 Gas saturation

**5.4.1.6.1 Hydrate and free gas zone** As summarized by Table 5.8, gas saturations at the Nyegga prospect are low, on the order of 1-2% of the pore space. This is similar to other Class 4 hydrate reservoirs, as the $< 1\%$ saturation reported from the Cascadia margin by Milkov *et al.* (2003). At Cascadia, Riedel *et al.* (2005) outline four essentially independent methods for estimating

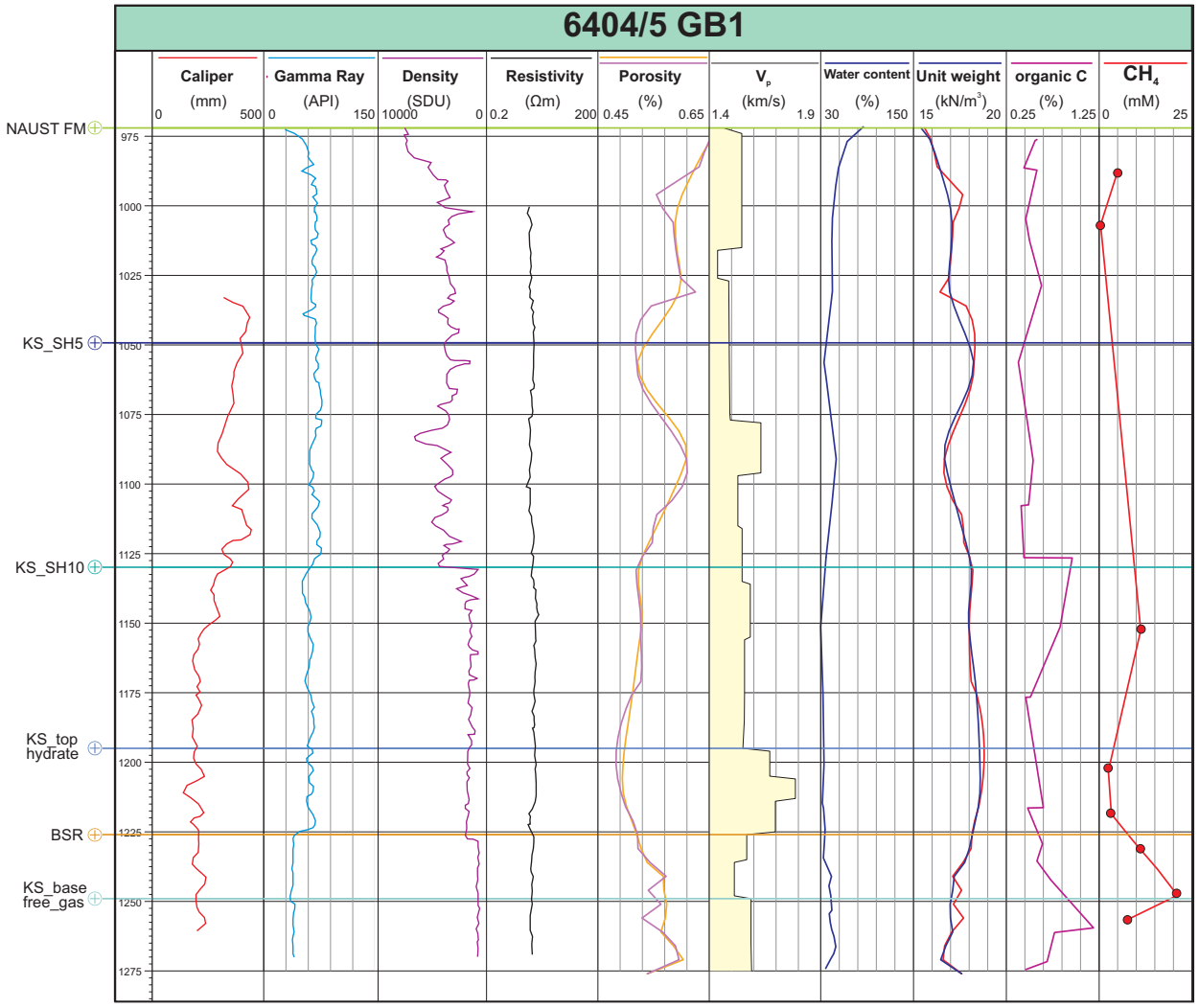


Figure 5.28: Wireline and measured data from the 6404/GB5 geotechnical borehole. Unfortunately, poor data quality makes the wireline data of limited use. The porosity measurements (5th track), however, are useful and provide constraints for the reservoir. Vertical seismic profiling (VSP), shown in the 6th track, appears to indicate a slightly higher velocity in a 30 m interval above the BSR, a zone that has been interpreted as the solid gas hydrate zone. Porosity and unit weight is calculated using two methods, which are plotted on the same track. Data is provided by StatoilHydro, and is the property of the Norwegian Deepwater Programme. Wireline logs are digitalised by hand and inaccuracies need to be considered.

the hydrate concentration, yet still come up with a large uncertainty of <5% to >25% of hydrate saturation. Similar saturations have been obtained through an MCS analysis at the Korean Ulleung Basin, where Stoian (2008) calculated a 1-4% gas saturation.

Even for well studied hydrate deposits where ground truth is available, gas saturations vary widely. As an example, Ruppel *et al.* (2008) outline Gulf of Mexico hydrate saturations of 1.5-6%, 1-12% and $>20\%$ depending on which method for calculation is used (Claypool 2006, Cook *et al.* 2008, Kastner *et al.* 2008).

At the Nyegga prospect, depending on the model of hydrate formation used, a heterogeneous hydrate saturation of up to 10-20% was calculated. Concentrations of up to 12% were predicted using a frame-only model, while concentrations of up to 20% were predicted for the frame-and-pore model (Westbrook *et al.* 2008a).

With this uncertainty in mind, a broad yet conservative gas saturation range from **0.025** (P99) to **0.035** (mode) to **0.21** (P1) for the hydrate zone and from **0.007** (P99) to **0.01** (mode) to **0.18** (P1) for the free gas zone was assigned.

High values of **0.21** and **0.18** are deemed to represent possible 'sweet spots' where high and focused fluid flux forms higher concentration hydrate deposits.

**5.4.1.6.2 Chimney structures** Chimney structures are expected to contain higher saturations of gas hydrates than the hydrate zone, due to the focused fluid flux thought to form them.

It follows that the Nyegga chimney structures have been assigned a more optimistic hydrate saturation range of **0.05-0.2-0.35**. To account for the uncertainty in whether the chimneys actually contain hydrate, as raised by Paull *et al.* (2008a), cases were calculated without the chimney component. The chimney zone hydrate is thus considered an upside of the Nyegga prospect.

#### 5.4.1.7 Gas expansion factor

Gas compressibility is defined by the relative amount of hydrate-bound gas compared to the same gas at STP. The base case assumes full cage occupancy, with 164 units of methane held within one

unit of hydrate (Sloan and Koh 2008). The low case assumes a cage with a 75% cage occupancy. The high case is based on the 189 units of methane reported by Schlumberger (2009). This gives a slightly skewed stretched beta distribution of **123-164-189**.

For the free gas zone, compressibility is assumed to be 1/pressure. Given that the prospect lies only a few hundred meters beneath the seafloor at ~1200 m depth, and assuming hydrostatic pressure, a gas expansion factor range of **100-120-140** was used.

#### 5.4.1.8 Gas recovery factor

Recovery factors, when it comes to conventional oil and gas fields, are typically based on the reservoir engineer's simulation runs and/or past experience. In this case, neither are possible and the recovery factor arguably remains the critical parameter to relate the calculated in-place resources to producible reserves.

The broad recovery factor range for the three different zones is given by Table 5.6. It is important to note that this study focuses on the calculation of in-place resources at the Nyegga prospect, and any discussion of its recovery is highly speculative. This is even more valid for the chimney zone, which, due to its presence away from the methane hydrate phase boundary, would require a different recovery strategy than the depressurisation envisioned for the regional hydrate zone.

### 5.4.2 Deterministic approach

A deterministic case, using the base case reservoir parameters, was calculated in GeoX. The simple calculation follows the illustration of Figure 4.7 and Equation 4.1. Since the gross rock volume (GRV) is the critical parameter, it was calculated by two constrasting methods in Petrel and GeoX (Table 5.4). While the Petrel method calculates the volume on a depth-converted 3D grid, the GeoX method defines the GRV based on the prospect area and thickness of the gas hydrate and free gas zones.

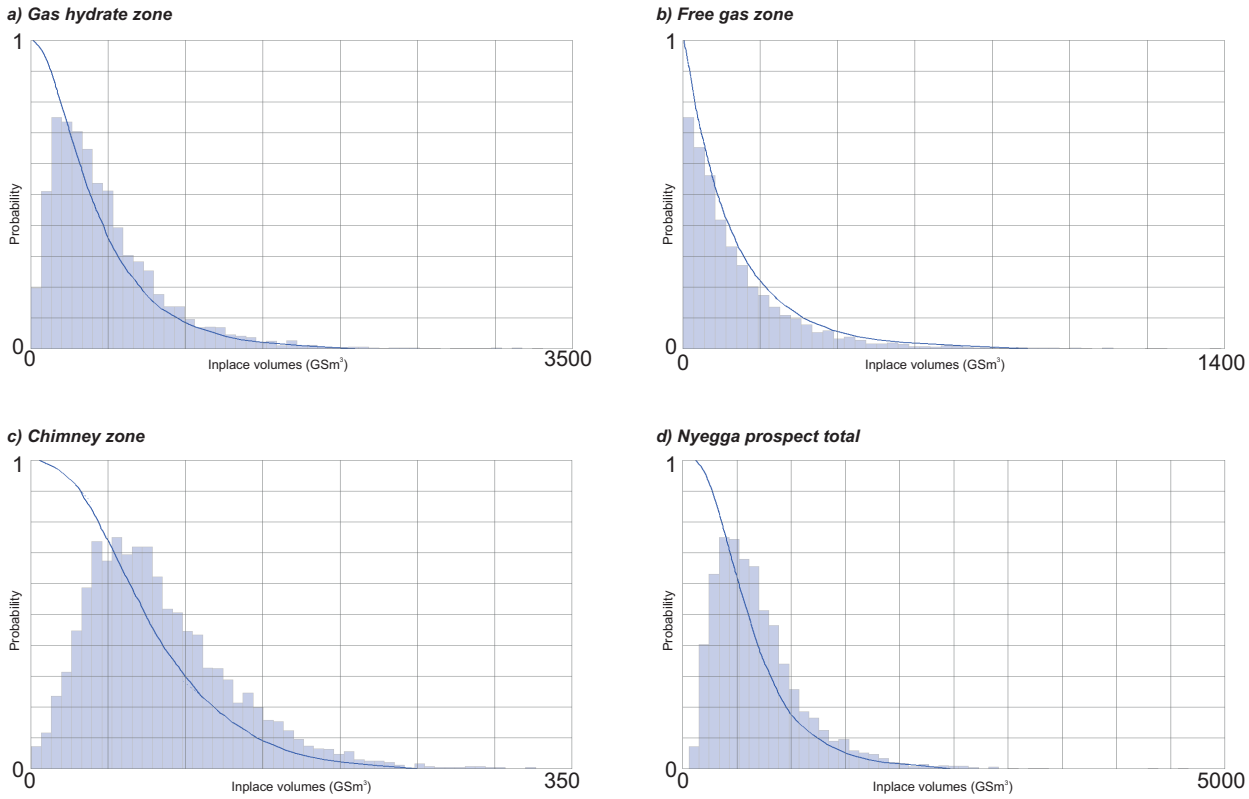


Figure 5.29: The spread of in-place resources for the Nyegga prospect. (A) Gas hydrate zone. (B) Free gas zone. (C) Chimney zone. (D) The whole Nyegga prospect, including all the three zones. Note the highly skewed distributions for both the gas hydrate and free gas zones, driven particularly by the skewed input distributions for column height and gas saturation.

### 5.4.3 Stochastic approach

GeoX is an industry-standard tool to assist in prospect evaluation and volumetric calculations. Due to its flexibility with respect to segment description and setup, all three Nyegga segments can accurately be represented in one complete prospect analysis. The stochastic model, setup with 5 000 runs, used the distributions illustrated by Figure 5.24 as input to produce a range of probable in-place (Figure 5.29) and recoverable resources (Table 5.9). Furthermore, the results also illustrate which segments contributed most gas (Figure 5.30).

The variance diagram illustrates which parameters have the biggest influence on the result (Figure 5.31). The variance is quite simply a measure of statistical dispersion, and illustrates the

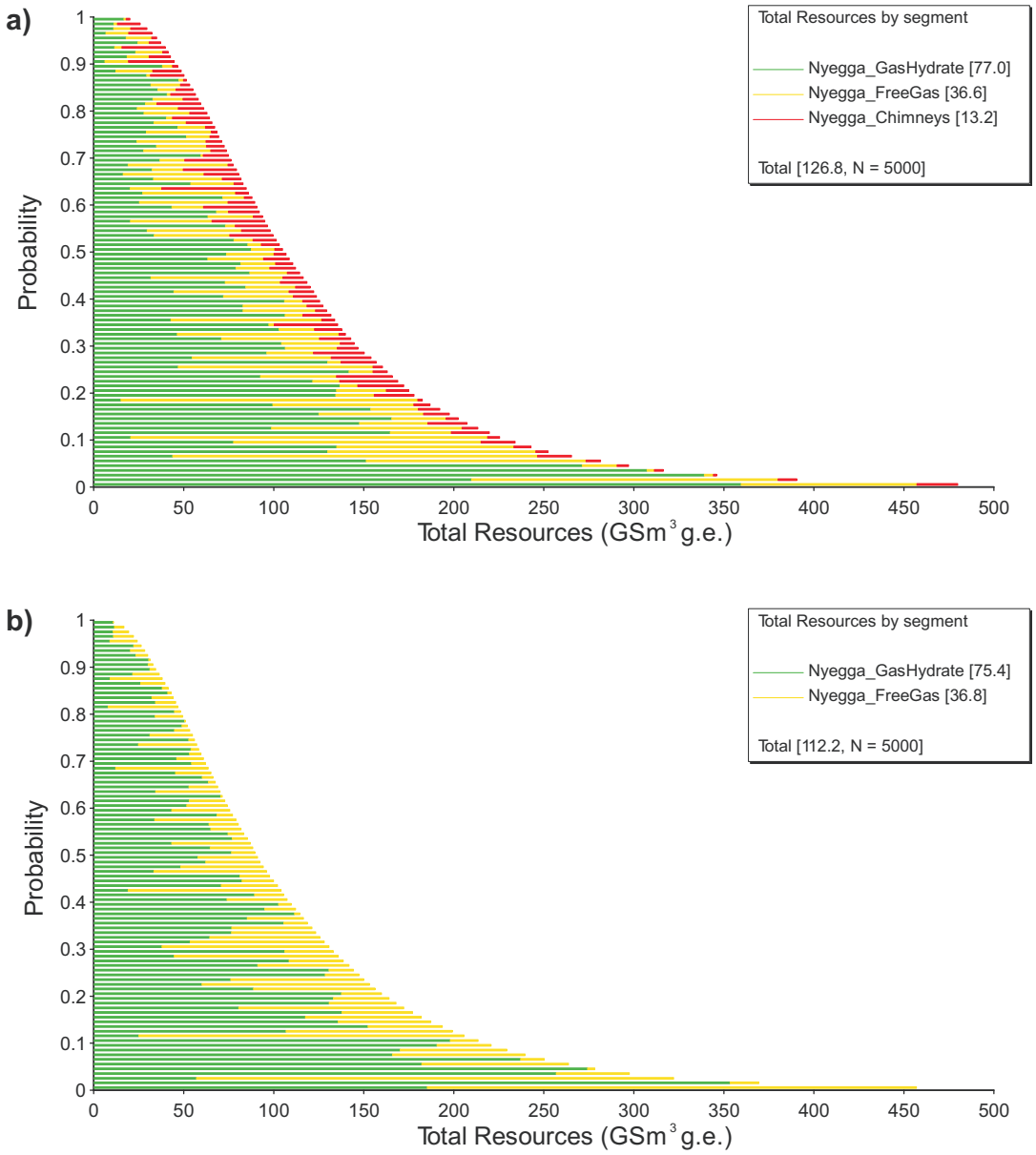


Figure 5.30: Total recoverable resources for the Nyegga prospect, grouped into the three different segments of gas occurrence. (A) Nyegga resources in the hydrate, free gas and chimney zone, (B) Nyegga resources only in the hydrate and free gas zone. The graphs illustrate the significance of the gas hydrate zone, comprising 68% of the total resources in the mean case. The free gas (20%) and chimney zones (12%) contribute minor volumes, though a substantial volume is held in the free gas zone in the P10 case.

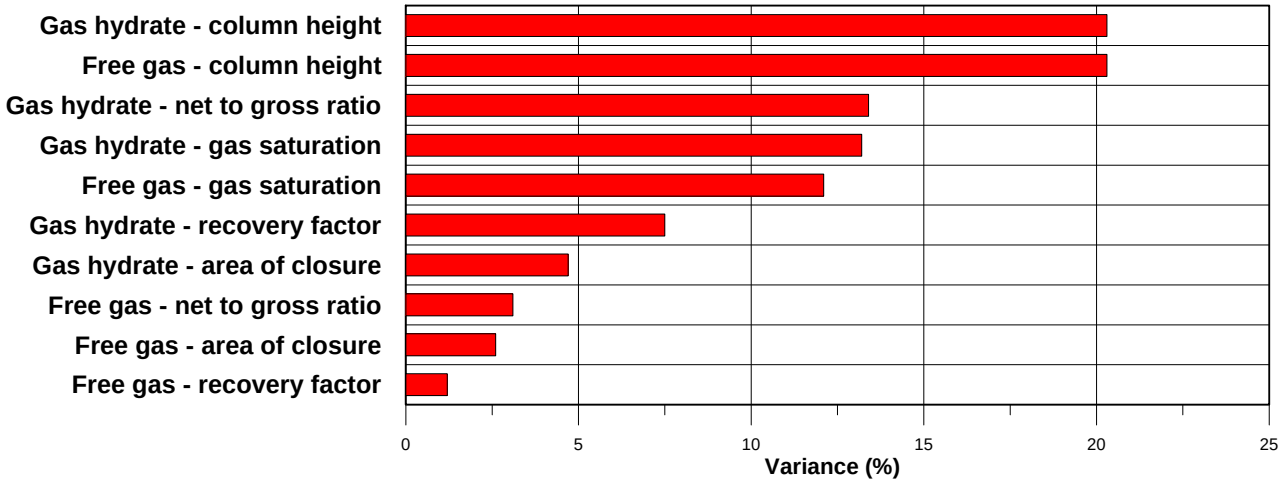


Figure 5.31: A variance diagram showing the relative importance of the various reservoir parameters on the result. Note the dominance of the uncertainty related to the column height and gas saturation in the free gas and gas hydrate zones.

parameters with the largest spread that contribute the most to the final result.

### 5.4.4 In-place gas volumes

Volumes of in-place gas, even in the most pessimistic P90[15] case, amount to 150-180 $GSm^3$, depending on whether the chimney zone is included or not. Out of the three segments, the gas hydrate zone contains the majority of resources (68% of the total mean case), followed by the free gas zone (20%) and the chimney zone (12%, Table 5.9, Figure 5.30).

As the volumes already indicated, the gas hydrate and free gas zones seem to be the most important constituents of the prospect. This is also obvious from the variance diagram (Figure 5.31), where the parameters assigned to the aforementioned zones dominate. In this case, the column height of the gas hydrate and free gas zonez has the highest effect on the calculation, but three other parameters have a variance value $> 10$. Due to the relatively minor volumes calculated for the chimney zone, its resersvoir parameters do not have a major effect on the total in-place volumes.

[15]The P10, P50 and P90 cases calculated by the stochastic calculation represent probabilities of the particular volume to be present in the prospect. In this case, a P90 of $121GSm^3$ represents a 90% chance that $180GSm^3$ of gas will be present at the Nyegga prospect.

| | | Deterministic | Stochastic | | | |
|---|---|---|---|---|---|---|
| **Gas hydrate zone** | unit | | Mean | P90 | P50 | P10 |
| Gross rock volume | $GSm^3$ | 112.7 | 122.4 | 58.5 | 116.0 | 195.6 |
| Net rock volume | $GSm^3$ | 56.4 | 61.0 | 21.2 | 52.5 | 109.7 |
| HC pore volume | $GSm^3$ | 2.2 | 3.0 | 0.8 | 2.4 | 5.9 |
| **Gas inititally in place (GIIP)** | **$GSm^3$** | **360.9** | **478.2** | **130.6** | **384.9** | **945.4** |
| Recoverable gas | $GSm^3$ | 54.1 | 76.4 | 18.4 | 58.0 | 156.7 |
| | tcf | 1.91 | 2.70 | 0.65 | 2.05 | 5.53 |
| **Free gas zone** | | | | | | |
| Gross rock volume | $GSm^3$ | 90.2 | 95.7 | 58.2 | 91.3 | 138.6 |
| Net rock volume | $GSm^3$ | 45.1 | 48.0 | 20.4 | 44.3 | 81.5 |
| HC pore volume | $GSm^3$ | 0.2 | 1.1 | 0.1 | 0.8 | 2.6 |
| **Gas inititally in place (GIIP)** | **$GSm^3$** | **20.8** | **136.9** | **17.6** | **90.1** | **311.3** |
| Recoverable gas | $GSm^3$ | 6.0 | 37.7 | 4.1 | 23.5 | 88.7 |
| | tcf | 0.21 | 1.33 | 0.14 | 0.83 | 3.13 |
| **Chimney zone** | | | | | | |
| Gross rock volume | $GSm^3$ | 9.2 | 9.3 | 3.5 | 9.3 | 15.1 |
| Net rock volume | $GSm^3$ | 4.6 | 4.7 | 2.2 | 4.5 | 7.5 |
| HC pore volume | $GSm^3$ | 0.5 | 0.5 | 0.3 | 0.5 | 0.9 |
| **Gas inititally in place (GIIP)** | **$GSm^3$** | **83.8** | **83.0** | **32.3** | **74.1** | **146.2** |
| Recoverable gas | $GSm^3$ | 12.6 | 13.2 | 4.3 | 11.2 | 24.7 |
| | tcf | 0.44 | 0.47 | 0.15 | 0.40 | 0.87 |
| **Nyegga without chimneys** | | | | | | |
| **Gas inititally in place (GIIP)** | **$GSm^3$** | **381.7** | **615.1** | **148.2** | **475.0** | **1256.7** |
| | tcf | 13.5 | 21.7 | 5.2 | 16.8 | 44.4 |
| Recoverable gas | $GSm^3$ | 60.1 | 114.1 | 22.5 | 81.5 | 245.4 |
| | tcf | 2.1 | 4.0 | 0.8 | 2.9 | 8.7 |
| **Nyegga total (all 3 segments)** | | | | | | |
| **Gas inititally in place (GIIP)** | **$GSm^3$** | **465.5** | **698.1** | **180.5** | **549.1** | **1402.9** |
| | tcf | 16.4 | 24.7 | 6.4 | 19.4 | 49.5 |
| Recoverable gas | $GSm^3$ | 72.7 | 127.3 | 26.8 | 92.7 | 270.1 |
| | tcf | 2.6 | 4.5 | 0.9 | 3.3 | 9.5 |

*Please note $GSm^3 = 10^9$ standard cubic metres, $tcf = 10^{12}$ standard cubic feet*

Table 5.9: Results of in-place volumes of hydrate-bound methane at Nyegga. Intermediate volumes are given for comparison. To calculate the deterministic volume, only the base case reservoir parameters were used. In contrast, wide distributions were used to generate the stochastic spread. Please note that the recoverable volumes are speculative and not based on a reservoir simulation.

# Chapter 6

# Development concept & Economics

A potential Nyegga development is dependant on defining a technically feasible and commercially sound method of producing the gas.

A first look at the 'nearby' conventional hydrocarbon production and processing facilities reveals that the closest field with spare capacity is Kristin (Table 6.1, Figure 6.2). However, Kristin has been designed to produce a high pressure-high temperature field, and modifications to allow for the processing of Nyegga gas would require substantial investments. Furthermore, gas offtake via the Åsgard Transport System (ATS) pipeline would probably be delayed due to low capacity in the system. Future developments in the area are currently too small for development, though a possible Nyegga development would allow for the tie-in of minor discoveries such as Midnattsol (6405/10-1). Perhaps the most likely candidate for tie-in of a gas pipeline is the Ormen Lange field and its multiphase pipeline to shore. Tying the gas offtake into the Ormen Lange system would save about 100 km of pipeline compared to a direct Nyegga to shore pipeline and thus reduce costs.

Depressurisation, by the production of the free gas zone, coupled with thermal stimulation, achieved by the injection of hot brines, are deemed to give the best production results, based on reservoir simulations of analogue reservoirs (Moridis and Collett 2003, Moridis and Sloan 2007). The chimney zone would most likely require a different approach, due to its setting away from the

| Field/Discovery | Distance to Nyegga prospect | Hydrocarbon type | Development concept | Peak gas production ($Mm^3/d$) | Production timing | Processing capacity | | Expected abandonment |
|---|---|---|---|---|---|---|---|---|
| | | | | | | *Gas ($Mm^3/d$)* | *Water ('000 b/d)* | |
| *nearby fields* | | | | | | | | |
| **Ormen Lange** | 135 km | Gas | subsea to shore (Nyhamn) | 59.5 (2010) | 2007-2040 (plateau down after 2020) | | | 2040 |
| **Njord** | 123 km | Oil/Gas | floating steel-hulled drilling and production vessel, Njord A. Oil is offloaded into the floating storage unit (FSU) Njord B and exported with shuttle tankers | 5.0 (2008) | 1997-2017 | 9.9 | 16 | 2021 |
| **Tyrihans** | 105 km | Gas/condensate | four subsea templates tied back via a multiphase pipeline to the Kristin facilities | 9.3 (2017) | 2009-2026 (gas 2012-2026) | N/A | N/A | 2026 |
| **Kristin** | 83 km | Gas/condensate | subsea wells tied back to a semi-submersible floating production platform | 12.1 (2008) | 2005-2026 | 18 | | 2026 |
| **Åsgard (Midgard, Smørbukk and Smørbukk Sør)** | 133 km | Gas/condensate | subsea, tied to floating production-storage-offtake (FPSO) Åsgard A, Semi-sub Åsgard B and FSU Åsgard C | 31.3 (2007) | 1999-2027 | 17+53.8 | 40+95 | 2027 |
| *nearby discoveries* | | | | | | | | |
| **6405/10-1** | 79 km | Gas | New discovery of 1.9GSm$^3$ gas, yet to be evaluated | | | | | |
| **6405/7-1 Ellida** | 48 km | Oil | Development is not very likely (NPD 2009) | | | | | |
| **6306/5-1** | 140 km | Gas | Development is not very likely (NPD 2009) | | | | | |
| **6406/11-1 S** | 113 km | Oil | Development is not very likely (NPD 2009) | | | | | |

Table 6.1: Listing of developments in the area. The closest field, Kristin, is deemed unsuitable for a possible Nyegga tie-back due to its low processing capacity. In addition, the Haltenbanken fields of Njord, Tyrihans and Åsgard struggle with enough capacity in the gas offtake pipeline system. An alternative tie-back would be the Ormen Lange-Nyhamn pipeline, or pipeline extending from Nyegga to shore. Note also that most of the nearby conventional discoveries are too minor to provide incentive for a combined development. Source WoodMackenzie (2008b).

hydrate phase boundary where depressurisation is optimal.

## 6.1 Concept selection

The major requirements for the Nyegga development are deemed to be:

- Flexibility to deal with unexpected developments during hydrate production
- Safety, both in terms of personnel and the environment, needs to be top priority throughout
- Gas offtake should be handled in a cost-effective way, reusing existing facilities if possible
- Proven and tested solutions should be prioritised, particularly with respect to the substantial water depth

In lieu of these requirements, a stand-alone development with gas offtake via Ormen Lange was chosen as the preferred development concept. The stand-alone solution would include at least one floating production-storage-offload (FPSO) that allows the tie-in of multiple subsea templates. Both gas producers and water injectors will be utilised to maximise the recovery from the Nyegga field. All subsea templates would be tied to the FPSO, where the gas would be offloaded via a new pipeline directly to shore or via a tie to the Ormen Lange facilities. The development concept somewhat resembles Exxon's Saxi development off Africa, with the main difference of gas production and offtake via a pipeline or on-board compression. The major reason for using the FPSO instead of any seafloor-based structures is the ability to handle the substantial water depth of approximately 1000 m (Figure 6.1).

For estimating the number of wells required, a simple assumption of one production well per $20\,km^2$ is used. This compromise between using the least wells possible, for commercial reasons, and trying to achieve the maximum recovery is deemed adequate given the current technical and geological understanding. Even so, this works out as slightly more than 110 wells to cover the mode areal coverage of $2250\,km^2$. At a day rate of deep-water rigs on the order of 500 000 USD/day (Shute 2009) and assuming a conservative 20 days per well, just the drilling cost (1.1 billion USD) would be substantial, even if the shallow target depth would offset some of the cost. Most critical, however, would be the feasibility of using only one production well per $20\,km^2$. Thermal stimulation wells would likely also be required for improving the recovery factor.

Apart from the drilling cost, the major CAPEX[1] expenses would relate to the construction of the FPSO, the gas offtake pipeline and the multitude of subsea templates. The increased capacity requirement on the gas offtake route may furthermore require modifications at the Ormen Lange/Nyhamna facilities. OPEX[2] costs would be related to gas processing at Nyhamna, as well as day to day operations of the Nyegga development project.

[1]CAPEX = capital expenditure
[2]OPEX = operational expenditure

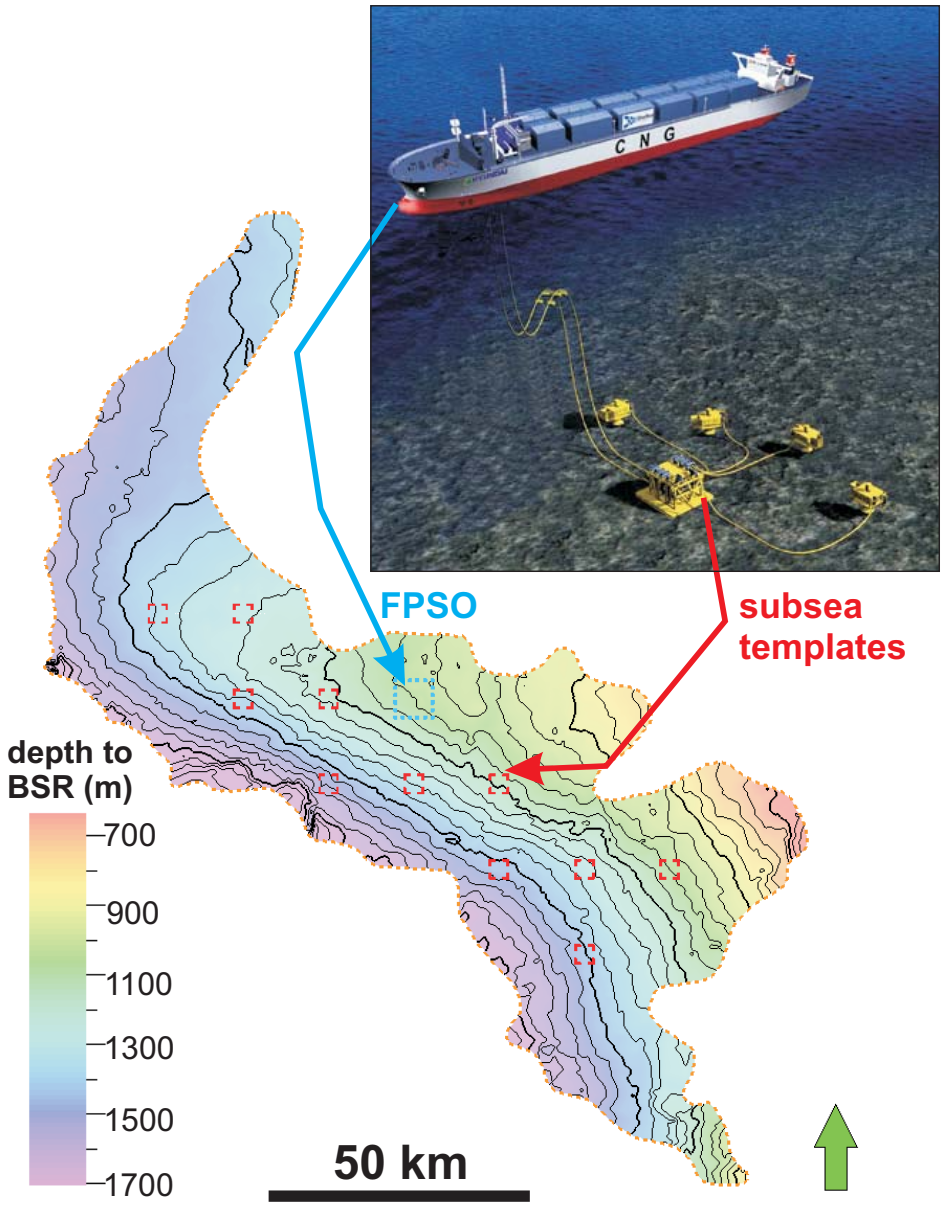


Figure 6.1: Depth map of the Nyegga prospect and proposed infrastructure. A floating production-storage-offtake (FPSO, marked blue on the map) solution is suitable given the substantial water depth of 800-1400 m at the prospect. Subsea templates (red), spread across the whole prospect and controlled from the FPSO using umbilicals, serve as the control point for the numerous wells required to produce the Nyegga deposit. In this scenario, it is assumed that each of the 11 subsea templates will control 10 production wells. Figure compiled using an image from EPMag (2009).

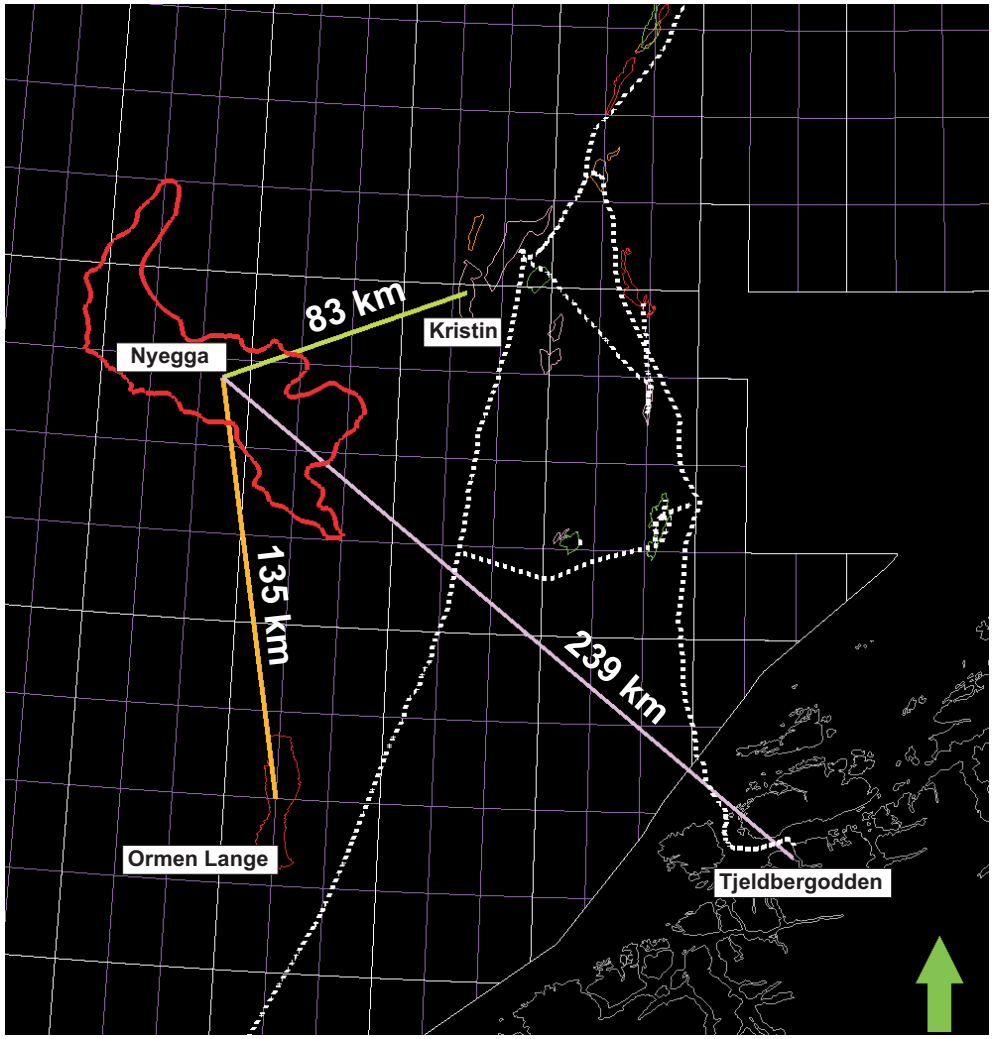


Figure 6.2: Distance from the Nyegga prospect to existing infrastructure. The stippled white lines indicate existing pipeline systems. Two preferred gas offtake scenarios exist. A direct to shore solution would require a $>200$ km pipeline to Tjeldbergodden, while a 135 km pipeline would be sufficient to transport the gas to Ormen Lange and its export pipeline system.

| Nyegga without chimneys | | Mean | P90 | P50 | P10 |
|---|---|---|---|---|---|
| In-place gas (GIIP) | $GSm^3$ | **615.1** | **148.2** | **475.0** | **1256.7** |
| Recoverable gas | $GSm^3$ | 114.1 | 22.5 | 81.5 | 245.4 |
| Value | GNOK | 168.9 | 33.3 | 120.6 | 363.2 |
| | GUSD | 29.6 | 5.8 | 21.2 | 63.7 |

| Nyegga with chimneys | | Mean | P90 | P50 | P10 |
|---|---|---|---|---|---|
| In-place gas (GIIP) | $GSm^3$ | **698.1** | **180.5** | **549.1** | **1402.9** |
| Recoverable gas | $GSm^3$ | 24.7 | 6.4 | 19.4 | 49.5 |
| Value | GNOK | 36.5 | 9.4 | 28.7 | 73.3 |
| | GUSD | 6.4 | 1.7 | 5.0 | 12.9 |

Table 6.2: An overview of the economic value of the Nyegga prospect, both including and excluding the chimney zone. Assumptions based on NPD (2009), particularly important for the exchange rate of 5,7 NOK/USD and the gas price of 1,48 NOK/$Sm^3$.

## 6.2 Economics

The conservative case, assuming only the gas hydrate and free gas zones, has a mean value around 30 billion USD (Table 6.2). The upside potential of the chimney zone represents an additional value of 6.8 billion USD.

Due to the uncertainty related to the ultimately recoverable reserves and the difficulty in estimating the development costs of the Nyegga prospect, a full technical economical evaluation was deemed premature at this stage.

# Chapter 7

# Discussion

## 7.1 Seismic interpretation

Seismic interpretation across the Nyegga prospect is consistent, but dependant on the seismic data quality. The conventional survey JMF97, used as the key survey due to its coverage of the Nyegga prospect, has a large 5 by 10 km line spacing and a too low frequency to image the shallow subsurface optimally. Nonetheless, the bottom simulating reflection (BSR) interpretation is generally consistent with that of Bünz *et al.* (2003). Internal Naust Formation reflectors were mapped with reasonable confidence, and served as an important input to the depth conversion. Furthermore, $V_p$ variations in the subsurface observed on the ocean bottom seismometer (OBS) data could be compared to the lateral extent of the Naust Formation zones.

Closer examination of the OBS-derived $V_p$ velocity data suggests a general trend of gradual velocity increase with depth in the uppermost 2 zones (KS SH5, KS SH10, Figure 5.27). The discontinuous presence of both free gas zones and glacigenic debris flows (GDFs) cause velocity anomalies at sub-BSR levels. The uppermost low velocity zones tend to be associated with the BSR (if present), probably due to the build up of free gas below an impermeable hydrate zone.

It is notable that the lower low velocity zone, as imaged by the nearby OBS stations JM517 and JM523, does not follow the seismic reflectors but is present alternatively in both the KS SH13

and KS SH20 zones. The higher range of velocities in the deeper layers (up to 16% for the KS SH20 zone) is thought to be primarily caused by the presence of gas rather than lithological variation. This hypothesis is primarily based on seismic information, which does not appear to hint at any obvious lithological changes over the short distance between the OBS stations. The main exception to this hypothesis are the high-velocity GDFs readily identified on seismic profiles.

At Nyegga, acoustic chimneys are the primary disturbance within the sediments of the hydrate stability zone, modeled to cover at least the uppermost 250 m (at 750 m water depth) and significantly more at deeper levels. This contrasts with New Zealand's Hikurangi margin, where focussed fluid flux has been attributed to causing a local upwarping of the BSR (Pecher *et al.* 2009). At the Hikurangi margin free gas, directed primarily through faults and permeable layers (Crutchley *et al.* 2009), migrates towards the seafloor where it is associated with methane seeps (Jones *et al.* 2009). At the Nyegga province, more diffuse fluid migration is hypothesised by Hustoft *et al.* (2007), who conclude that pipes are formed from the expulsion of originally overpressured sediments. Nonetheless, both sites indicate that focussed fluid flux has the ability of directing free gas upwards through a 'plumbing' system.

## 7.2 Hydrate stability modeling

The thermobaric model compares well with the interpreted BSR.

All model results indicate the BHSZ within 200 m of the BSR (Figures 5.11 and 5.12). Most models seem to overestimate the hydrate stability zone (HSZ) extent, though this could be a partial artifact of the simple depth conversion or the poor representation of the oceanic thermal gradient. The best fit is obtained by model run 'Bc2', obtained from a pure methane system with a salt water component and the highest geothermal gradient. This is not surprising given the strong evidence for prevalent biogenic methane sourcing, high interaction of pore waters with oceanic waters at shallow sub-seafloor depths and corresponding geothermal gradients.

As shown previously, for example by Senger *et al.* (2006), the HSZ is thickest under cold condi-

tions, caused both by a cold water mass and a low geothermal gradient. Furthermore, the addition of higher-order hydrocarbons such as ethane promotes the formation of hydrates at shallower depths. At Nyegga, a combination of a predominantly cool water mass (-1℃at the depth of interest) with relatively high geothermal gradients (50℃/km on average) combine to define a stability zone 250-400 m thick (Figures 5.11 and 5.12). Reasoned variation in the hydrate phase boundary and the geothermal gradient indicates a larger impact of a possible ethane component than the variation assigned to the geothermal gradient (Figure 5.10).

The model provides evidence that the observed BSR is likely caused by gas hydrates lying above a free gas zone at the level of the BHSZ.

## 7.3 Challenges to hydrate production

The Nyegga hydrates are heterogeneous and of low saturation, occurring over a wide area of more than 2000 $km^2$ (Table 5.6). Furthermore, their shallow location within an unconsolidated reservoir make their production technically challenging. On the positive side, the Nyegga hydrate zone is underlain by a free gas zone, implying boundary pressure-temperature (P-T) conditions which require limited energy input to dissociate the solid hydrate.

The low-saturation large-area Nyegga prospect poses serious technical issues with respect to its production. Depressurisation, presently thought to be the most effective hydrate production strategy, is dependant on reducing pressure through the production of the free gas zone underlying the hydrate zone (Collett 2008). At Nyegga, this free gas zone appears to be of very low concentration and limited thickness and it is uncertain if its production would be technically feasible. It is particularly uncertain whether the pressure drawdown caused by the production of the free gas zone would be significant enough to initiate dissociation of the overlying hydrate. Regardless of the implemented production strategy, a large number of wells would be required to tap the large area, further decreasing the commerciality of the project.

Production of the free gas zone may in itself be hampered by low reservoir pressure, resulting

in limited flow rates. However, while the prospect lies a mere 300 m below the seafloor, the water depth in excess of 900 m should provide adequate gas compression at reservoir depth. Furthermore, both StatoilHydro, with its recently appraised Peon discovery (WoodMackenzie 2009, NPD 2009a), and Chevron, with its producing A&B Shallow Gas field in the Dutch sector of the North Sea (WoodMackenzie 2008c), are developing technologies to increase recovery. Such technologies could be adapted to the production of the free gas zone. Both these fields incidentally lie at even lower pressures (30-60 bar) than predicted for the Nyegga prospect at 1200 m depth (120 bar[1]). Erichsen (2009) suggests a recovery factor of 60%[2] for the Peon discovery, lying at a depth of 580 m. The recent formation test has shown that producing gas at these low pressures is technologically feasible[3], though gas saturations at Peon are likely to be an order of magnitude larger than at the Nyegga prospect.

Production of the hydrate zone itself is likely to use the knowledge gained during extensive production tests in permafrost areas. Collett (2008) outlines the production tests conducted at the Canadian study site at Mallik, as well as the potential contribution of hydrates to the final recoverable resources at the Western Siberia gas field of Messoyakha. These permafrost hydrate deposits, often associated with conventional gas fields, are suitable candidates for early extraction, particularly due to their large saturation. It must be stressed that the production characteristics of a Nyegga-type deposit are likely to be very different from a Mallik-type deposit but the indirect advantages of understanding the behaviour of hydrate during its production is important in developing any hydrate resource, both in permfrost and marine environments.

A reservoir simulation, using hydrate-specific simulators such as TOUGH+HYDRATE (Moridis and Sloan 2007, Moridis and Kowalsky 2006, Pruess 2004), would nonetheless be required to argue whether production of the free gas zone would depressurize the Nyegga system enough for dissociation to occur.

[1] This assumes a hydrostatic pressure within the uppermost 300 m of the sediments

[2] In-place volumes of $35 GSm^3$ give recoverable resources of $21 GSm^3$

[3] According to the NPD press release from the 23.7.2009, the formation test flowed $1.03\, MSm^3$ of gas per day through a 104/64 inch nozzle. Ultimately recoverable resources are thought to be on the order of 10-15 $GSm^3$, giving a recovery factor of 29-43%.

## 7.4 Comparison with other hydrate provinces

Regional hydrate assessments have been conducted in a wide range of settings. In the marine environment, most of these were based on the delineation of the bottom simulating reflection (BSR) and subsequent extrapolation of poorly constrained reservoir parameters across the area. To ease comparison between very different hydrate provinces, a resource density was calculated based on the reported in-place resources and the areal extent of the BSR (Table 7.1, Figure 7.1). The range of those, from $0.005\,GSm^3$ per $km^2$ to $2.129 GSm^3$ per $km^2$, represents both the uncertainty range with estimating hydrate-bound volumes and the geological differences between these provinces. On the one side, $0.005\,GSm^3$ per $km^2$ resembles the average methane hydrate resource density extrapolated across the whole Earth landmass. On the other side, $2.129\,GSm^3$ per $km^2$ is a reasonable resource density seen in Norwegian conventional gas fields.

The Nyegga prospect, with a range of $0.08\,GSm^3$ per $km^2$ to $0.62\,GSm^3$ per $km^2$, plots in between these two end-members. In terms of its areal extent, it is a fraction of the other hydrate provinces, most closely related to the West Svalbard margin investigated by Hustoft *et al.* (2009). Its mean resource density ($0.24\,GSm^3/km^2$) is comparable to both the West Svalbard site ($0.34\,GSm^3/km^2$, Hustoft *et al.* (2009)) and the Nankai Trough ($0.23\,GSm^3/km^2$, Ichikawa and Yonezawa (2002)). Nyegga's low case, $0.08\,GSm^3/km^2$, nonetheless resembles the resource density calculated for the whole ocean ($0.06\,GSm^3/km^2$), using estimates of MacDonald (1990). Compared to geologically similar provinces, distinguished by large areas of low saturations, Nyegga seems to have a slightly higher resource density that the regional Gulf of Mexico site, yet a lower resource density than both the Blake Ridge and New Zealand's Fiordland and Hikurangi provinces.

Comparing the recent investigations of the marine Gulf of Mexico ($1.31\,GSm^3/km^2$ in the mean case) system by the Minerals Management Service (MMS 2008) to the assessment of the Alaskan North Slope ($0.02\,GSm^3/km^2$ in the mean case) by the USGS (Collett *et al.* 2008) highlights the insignificance of the permafrost deposits compared to the marine provinces. Nonetheless, production tests are being undertaken on permafrost hydrate, where easier logistics and a well developed

| | Province | Area ($km^2$) | In-place resources ($GSm^3$ g.e.) min | mean | max | Resource density ($GSm^3/km^2$) min | ave | max | Reference |
|---|---|---|---|---|---|---|---|---|---|
| | **Nyegga (all three zones)** | **2 254** | **180** | **549** | **1 402** | **0.080** | **0.244** | **0.622** | This study |
| | **Nyegga (hydrate and free gas)** | **2 254** | **148** | **475** | **1 256** | **0.066** | **0.211** | **0.557** | This study |
| Hydrate prospects/ provinces | Barents Sea | 27 | 0.190 | | 0.380 | 0.007 | | 0.014 | Laberg et al 1998 |
| | West Svalbard | 3 000 | | 1 035 | | | 0.345 | | Hustoft 2009 |
| | Gulf of Mexico regional | 22 500 | 2 000 | | 3 000 | 0.089 | | 0.133 | Milkov and Sassen 2001 |
| | Gulf of Mexico "sweet spots" | 23 000 | 8 000 | | 11 000 | 0.348 | | 0.478 | Milkov and Sassen 2001 |
| | Niger Delta | 568 | | 951 | | | 1.674 | | Hovland 1997 |
| | Hikurangi and Fjordland margins, NZ | 50 000 | | 20 000 | | | 0.400 | | Pecher et al 2004 |
| | Fiordland margin "sweet spots" | 352 | | 48 | | | 0.136 | | Fohrmann 2009, Gorman 2008 |
| | Alaskan North Slope | 144 764 | 715 | 2 406 | 4 469 | 0.005 | 0.017 | 0.031 | Collett et al 2008 |
| | Gulf of Mexico | 457 933 | 314 000 | 607 000 | 975 000 | 0.686 | 1.326 | 2.129 | MMS 2008 |
| | Nankai Trough | 32 000 | | 7 400 | 60 000 | | 0.231 | 1.875 | Ichikawa and Yonezawa 2002 |
| | Blake Ridge | 26 000 | | 28 000 | | | 1.077 | | Milkov and Sassen 2002 |
| | Håkon Mosby Mud Volcano | 1.8 | | 0.300 | | | 0.167 | | Milkov and Sassen 2002 |
| | South Shetland Margin, Antarctica | 1 362 | | 2 360 | | | 1.733 | | Lodolo et al 2002 |
| Norwegian gas fields | Ormen Lange (recoverable) | 345 | | 396 | | | 1.148 | | NPD 2009, Woodmac 2009 |
| | Kristin (recoverable) | 84 | | 64 | | | 0.756 | | NPD 2009, Woodmac 2009 |
| | Troll (recoverable) | 700 | | 1 361 | | | 1.944 | | NPD 2009, Woodmac 2009 |
| | Peon (recoverable) | 80 | | 12.5 | | | 0.156 | | NPD 2009, Woodmac 2009 |
| Globe | Ocean | 361 132 000 | | 21 000 000 | | | 0.058 | | MacDonald 1990 |
| | Land | 148 940 000 | | 740 000 | | | 0.005 | | MacDonald 1990 |
| | Total | 510 072 000 | | 20 000 000 | | | 0.039 | | Collett 2002 |

Table 7.1: Comparison of the resource density at the Nyegga prospect and other hydrate and conventional deposits worldwide. Data from Milkov and Sassen (2001), Pecher *et al.* (2004), Laberg *et al.* (1998), MMS (2008), Hustoft *et al.* (2009), Collett *et al.* (2008), Hovland *et al.* (1997), MacDonald (1990), Collett (2002), Ichikawa and Yonezawa (2002), Milkov and Sassen (2002), Lodolo *et al.* (2002), Fohrmann (2009), Gorman (2008) and NPD (2009d). For ease of comparison, the data presented here is also plotted in Figure 7.1.

infrastructure make such projects economically feasible.

A further way of putting the results of the Nyegga volumetric calculation is through bench-marking it against similar hydrate provinces worldwide (Table 7.2). Using the classification of Milkov and Sassen (2002) as a base, the Nyegga prospect resembles the stratigraphic accumulations of the Gulf of Mexico, the Blake Ridge and the Nankai Trough. These are aerially much more extensive than the Nyegga prospect, but all have a similarly low hydrate concentration and thus a similar resource density. The chimney zones at Nyegga would, in this bench-marking context, be more structurally defined, resembling the higher-flux provinces of the Håkon Mosby mud volcano and the Hydrate Ridge.

With respect to production, higher concentration structural accumulations are likely candidates

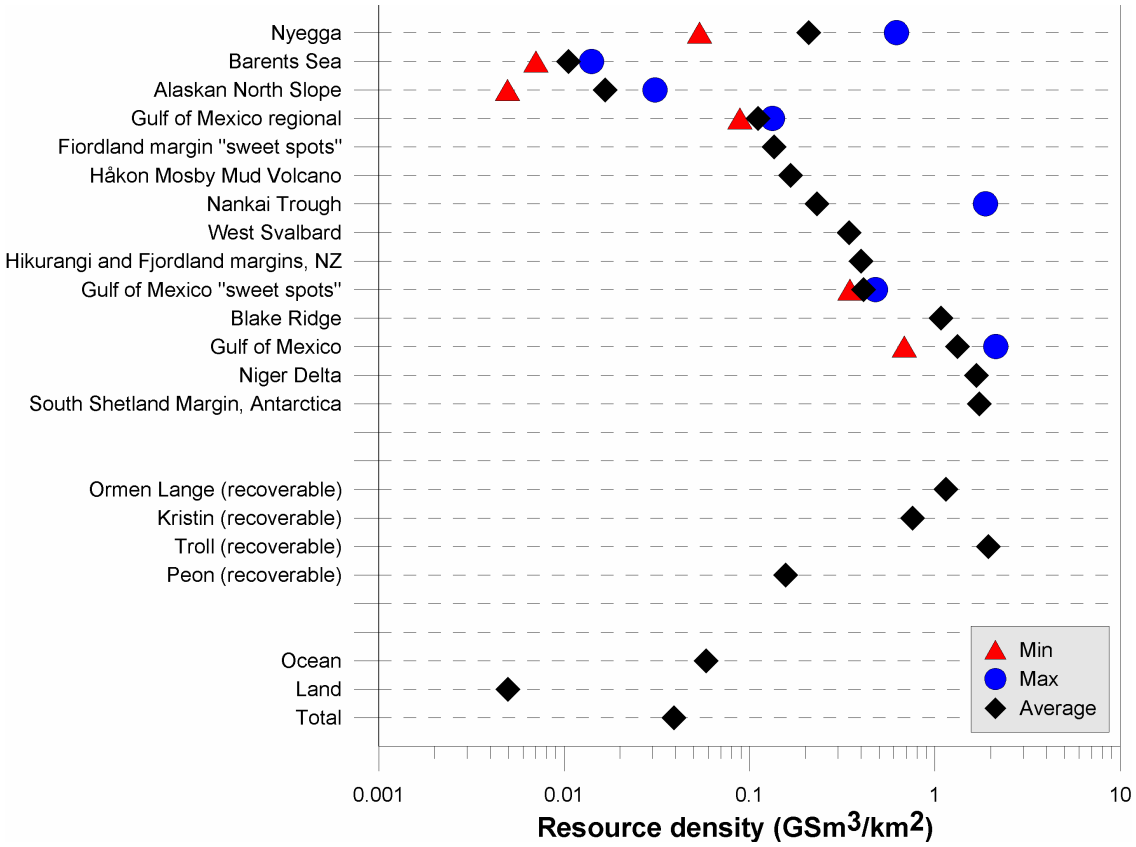


Figure 7.1: Graphical comparison of the resource density at the Nyegga prospect and other hydrate and conventional deposits worldwide. The diamonds indicate the average resource density, while the minimum and maximum resource densities are represented by triangles and circles, respectively. Note particularly the low resource density in the Alaskan North Slope permafrost province. Data source identical to Table 7.1.

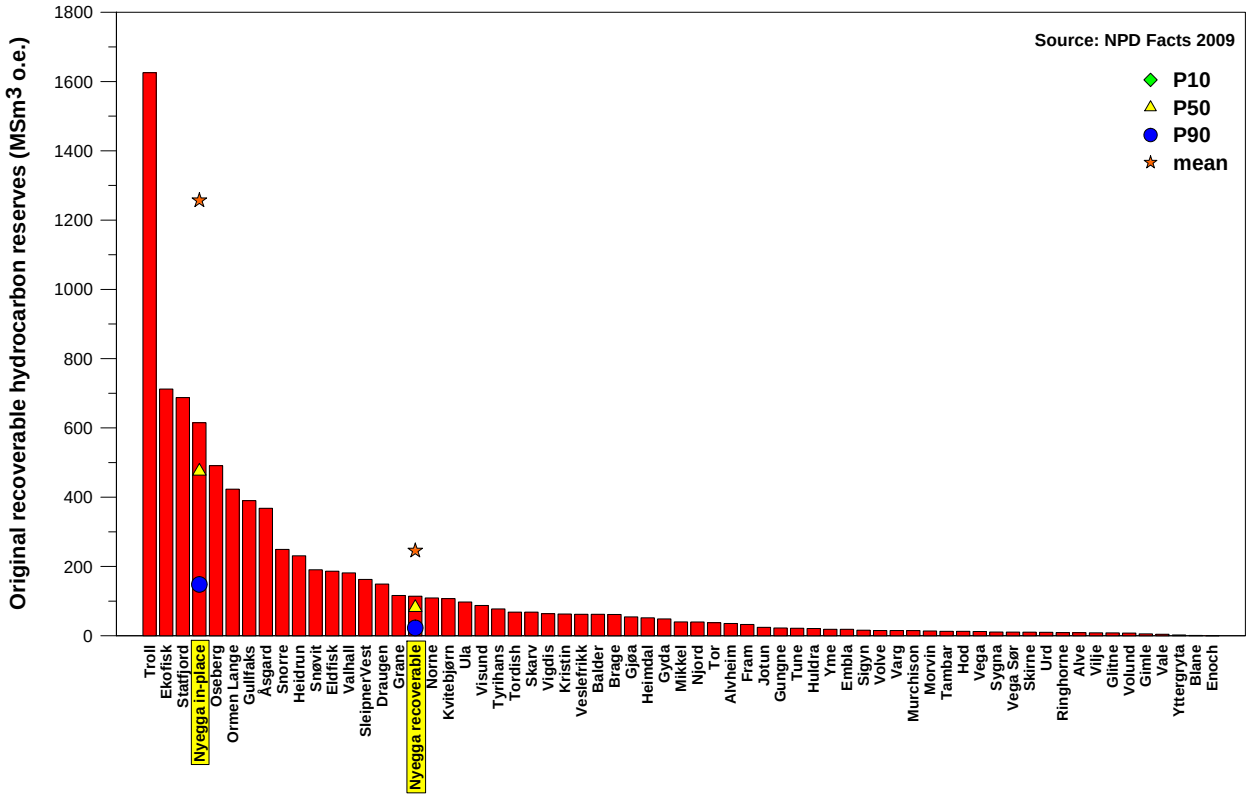


Figure 7.2: Graph illustrating the originally recoverable reserves of all the Norwegian fields, coupled with the in-place and recoverable results for the Nyegga prospect (excluding the chimney zone). Conventional field data from NPD (2009d).

for future development, particularly if the infrastructure is well developed as in the Gulf of Mexico (Milkov and Sassen 2002). Nonetheless, even if the resource density is much lower in the permafrost provinces, the fractional price of field experiments onshore compared to offshore are likely to keep the attention focused on the permafrost hydrate in the near future.

## 7.5 Comparison with conventional gas fields

The conservative recoverable reserves of the 2-segment Nyegga prospect would make it Norway's 16th largest field in the mean case (Figure 7.2).

In absolute value, the mean gas initially in-place (GIIP) numbers of ~650 $GSm^3$ roughly cor-

| Characteristics | Structural accumulations/provinces | | |
|---|---|---|---|
| | Northwestern Gulf of Mexico[a] | Hydrate Ridge[b] | Haakon Mosby mud volcano[c] |
| Water depth (m) | 440–2500 | 700–1000 | 1250–1260 |
| Areal extent ($km^2$) | 23 000 | 375 | 1.8 |
| Subsurface depth of gas hydrate occurrence (m) | 0–1900 (data from cores and modeling) | 0–200 (data from cores and BSR) | 0–160 (data from cores and modeling) |
| Gas hydrate origin | From thermogenic, bacterial, and mixed gas rapidly migrated from depth below | | |
| Gas hydrate concentration (vol%) | Average 20–30, up to 100 | Up to 20–60 | Up to 25 |
| Resource ($m^3$) | $8–11 \times 10^{12}$ | Not reported | $3 \times 10^8$ |
| Average resource density ($m^3/km^2$) | $4–5 \times 10^8$ | Not reported | $1.7 \times 10^8$ |
| Permeability | High (fracture) | High (fracture) | High (fracture) |
| Recovery factor | High | High | High |
| Development costs | Low | Low to average | Average to high |
| Production costs | Low | Low | Low |
| Infrastructure | Well developed | None | None |
| Economic potential | High | Average to high | Low |

| Characteristics | Stratigraphic accumulations/provinces | | | **Nyegga prospect** |
|---|---|---|---|---|
| | Northwestern Gulf of Mexico[a] | Blake Ridge[d] | Nankai Trough[e] | |
| Water depth (m) | 615–2500 | 1000–4000 | 700–3500 | 600-1700 |
| Areal extent ($km^2$) | 22 500 | 26 000 | 32 000 | 2240 |
| Subsurface depth of gas hydrate occurrence (m) | 20–1500 (data from one well and modeling) | 58–620 (data from 18 wells and BSR) | 50–500 (data from one well and BSR) | 0-700 (data from cores and modeling) |
| Gas hydrate origin | Mainly from bacterial methane generated in situ or slowly supplied from depth below | | | Predominantly biogenic |
| Gas hydrate concentration (vol%) | Up to 1–2 | Average 2, up to 14 | Average 10 (?), up to 30 | Average 1-2% of pore space, up to 18% |
| Resource ($m^3$) | $2–3 \times 10^{12}$ | $2.8 \times 10^{13}$ | Up to $6 \times 10^{13}$ [f] | $3.8 * 10^{11}$ |
| Average resource density ($m^3/km^2$) | $1 \times 10^8$ | $12 \times 10^8$ | Up to $18.4 \times 10^8$ | $0.5\text{-}6 * 10^8$ |
| Permeability | Low (matrix) | Low (matrix) | Low to high (matrix) | unknown |
| Recovery factor | Low | Low | Low to high | unknown |
| Development costs | High | High | High | average to high |
| Production costs | High | High | Average to high | average to high |
| Infrastructure | Well developed | None | None | limited |
| Economic potential | Low | Low | Average to high | low to moderate |

[a] Data from Milkov and Sassen (2001a), Pflaum et al. (1986), and Sassen et al. (1999a,b).
[b] Data from Suess et al. (1999, 2001) and Trehu et al. (1999).
[c] Data from Bogdanov et al. (1999) and Ginsburg et al. (1999).
[d] Data from Dickens et al. (1997), Hollister and Ewing (1972), Paull et al. (1996, 2000), Sheridan and Gradstein (1983), and Keigwin et al. (1998).
[e] Data from Matsumoto et al. (2001), Takahashi et al. (2001), and Matsumoto (personal communication).
[f] The value is roughly calculated from the estimates of gas hydrate concentration around the Nankai Trough exploratory well and the areal extent of BSR distribution (Matsumoto, personal communication).

Table 7.2: Comparison of the Nyegga prospect with other hydrate deposits worldwide. Note the similarity of the Nyegga prospect to the large but low saturation stratigraphic deposits at Blake Ridge, the Nankai Trough and the Gulf of Mexico. Figure modified from Milkov and Sassen (2002).

responds to the size of the Ormen Lange field (recoverable reserves of 393.70 $GSm^3$ gas). However, when compared to the area it covers, the Nyegga prospect has a considerably lower recoverable resource density (0.24 $GSm^3/km^2$, Table 7.1) compared to Troll (1.94 $GSm^3/km^2$), Kristin (0.76 $GSm^3/km^2$) and Ormen Lange (1.15 $GSm^3/km^2$; WoodMackenzie (2008b;a), NPD (2009d)). A discovery on the NCS with a lower energy per unit area density is Peon, whose 12.5 $GSm^3$ recoverable resources are spread over 80 $km^2$ (0.16 $GSm^3/km^2$).

## 7.6 Significance of Nyegga in-place volumes

The large in-place volumes of hydrate at Nyegga have several implications. While this thesis has focused on quantifying the energy potential of the prospect, it is worth noting that natural gas hydrate dissociation may lead to the release of some of the hydrate-bound methane. In that sense, an in-place estimation provides key information for studies dealing with possible methane fluxes to the ocean and/or atmosphere. Both the absolute GIIP volumes, as well as regional resource densities can be used to estimate the amount of hydrate-bound gas liable that could potentially dissociate.

Arguably more relevant in the short-term is the growing possibility that future conventional boreholes will penetrate the Nyegga prospect, or other BSR areas, when targeting deeper conventional prospects. Its large areal extent, and location fully covered by the blocks nominated for the 21st licensing round (NPD 2009d), make this possibility quite likely.

A recent presentation by Peters *et al.* (2008) outlined the work undertaken by Shell in mitigating against the increased risk of drilling through hydrate-saturated sediments. In essence, circulating mud fluids are shown to dissociate the hydrate proximal to the borehole and cause increased borehole instability. While avoiding hydrates may be possible in some cases, the increased cost of drilling from highly deviated positions means that drilling through hydrates is becoming one of the challenges of deep water exploration. On the other hand, the positive by-product of such boreholes is the ability of collecting much needed ground truth data to allow better characterization of

Nyegga-like hydrate provinces.

# Chapter 8

# Conclusions

## 8.1 Accomplishments

This thesis had one primary objective, namely to ***provide a best technical estimate for the total in-place natural gas encaged within the gas hydrates of the Nyegga area and discuss the possibility of its potential economic extraction.*** This objective has been fulfilled, with the in-place volumes listed in Table 5.9. Arguably more importantly than the results themselves is, however, the process of calculating these, and the uncertainties building up in this exercise.

This uncertainty is exemplified by the large spread in the P90 to P10 in-place resources, as well as the large spread of the input parameters. As discussed in the previous section, more data need to be acquired in order to reduce the uncertainty. Nonetheless, based on the currently available data it appears that the Nyegga prospect holds a substantial volume of predominantly hydrate-bound gas.

In summary, the major findings of this thesis are:

- Modelling of the constraining parameters confirms that the bottom simulating reflection (BSR) widespread at the Nyegga study site appears to be hydrate-related.
- A gas hydrate prospect, called Nyegga and spanning across 1000-3000$km^2$, is defined by the

extent of the largest continuous BSR.

- The gas hydrate resource, $698 GSm^3$ in the mean case, appears to be significant for a prospect on the Norwegian continental margin, potentially holding approximately the same amount of hydrocarbons as the Ormen Lange field.
- The resource density of the Nyegga prospect, $0.24\, GSm^3/km^2$, is generally in line with that calculated for other hydrate provinces, though the large spread of the estimates emphasizes the large uncertainties involved.
- Large uncertainty in calculated in-place volumes is primarily due to the lateral variations in reservoir parameters, with the 3D reservoir extent and gas saturation being the most important with respect to the final in-place volumes.
- Using the employed reservoir parameters, it appears that the gas hydrate and free gas zones contribute most to the total in-place resources. Chimneys, assuming that they're at least partially hydrate-filled, contribute as localized high saturation hydrate accumulations.
- Employing a simplistic yet conservative recovery factor, the hydrate resources of the Nyegga prospect have a value of 36 billion USD.
- Bench-marking of the Nyegga prospect against other hydrate provinces highlights its immaturity with respect to near-term development.
- Apart from their economic value, the hydrate-held methane could, under changing pressure-temperature conditions, potentially be released into the ocean and/or the atmosphere. Further work is required to test this hypothesis.
- An appraisal programme designed to ground truth the various geophysical models is required to better define the prospect and constrain reservoir parameters.
- It is questionable whether the Nyegga resource will ever be commercially produced, given its low saturation and large lateral extent.

## 8.2 Future research

The integrated approach in defining the Nyegga in-place volumes has demonstrated the large uncertainty in evaluating such fields. Nonetheless, it has also provided some directions on how to address the limitations of the current data set. A hypothetical appraisal work programme is thus proposed:

- Acquisition of high-resolution high-frequency 2D seismic lines across the whole Nyegga prospect, with a 1 by 2 km line spacing. This would allow for higher-resolution seismic interpretation, especially useful in area where the BSR is masked by the dipping stratigraphy.
- Velocity analysis of selected profiles with the objective of determining lateral variation in hydrate and free gas concentration.
- Acquisition of additional ocean bottom seismometer (OBS) experiments, particularly in the northern and southern edges of the prospect. This would allow the determination of subsurface velocity variation, and allow for the calculation of hydrate and free gas saturation. An OBS station substantially distant from the BSR would be included to allow for the comparison to a background velocity.
- Acquisition of 10 ocean bottom cable (OBC) profiles across the Nyegga prospect, for better constraining the lateral hydrate and free gas extent.
- Acquisition of high-resolution high-frequency 3D seismic across the central part of the Nyegga prospect. A 3D survey is key to accurately interpret the three-dimensional fluid flow 'plumbing' system known at Nyegga. Any well placement could furthermore be optimized to zones modeled to contain the highest hydrate concentrations.
- Acquisition of 10 electromagnetic profiles across the Nyegga prospect, for use in determining hydrate saturation and confirming the seismic data.
- Drilling of 5-10 boreholes penetrating the BSR and 200 m of sub-BSR sediments, with focus on collecting as much data around the BSR as possible. Pressure-coring of the hydrate zone

is fundamental to provide input parameters to e.g. saturation determination from seismic-derived $V_p$-velocities.

- Reservoir simulation, based on the acquired data, to determine the production rate achievable at Nyegga and optimise the production strategy accordingly.

# References

**Abdalla, B. K. and Abdullatef, N. A.** (2005). Simulation and economic evaluation of natural gas hydrates [NGH] as an alternative to liquefied natural gas [LNG]. In *Catalysis Today*, **vol. 106** (1-4): pp. 256–258.

**Alendal, G., Berntsen, J., Engum, E., Furnes, G. K., Kleiven, G. and Eided, L. I.** (2005). Influence from "Ocean Weather" on near seabed currents and events at Ormen Lange. In *Marine and Petroleum Geology*, **vol. 22**: pp. 21–31.

**Aloisi, G., Pierre, C., Rouchy, J.-M., Foucher, J.-P. and Woodside, J.** (2000). Methane-related authigenic carbonates of eastern Mediterranean Sea mud volcanoes and their possible relation to gas hydrate destabilisation. In *Earth and Planetary Science Letters*, **vol. 184** (1): pp. 321 – 338.

**Andreassen, K., Hart, P. E. and Grantz, A.** (1995). Seismic studies of a bottom simulating reflection related to gas hydrate beneath the continental margin of the Beaufort Sea. In *Journal of Geophysical Research*, **vol. 100** (B7): pp. 12,659–12,674.

**Andreassen, K., Hart, P. E. and MacKay, M.** (1997). Amplitude versus offset modeling of the bottom simulating reflection associated with submarine gas hydrates. In *Marine Geology Gas in Marine Sediments, Geology/Geochemistry/Microbiology*, **vol. 137** (1-2): pp. 25–40.

**Andreassen, K., Mienert, J., Bryn, P. and Singh, S.** (2000). A Double Gas-Hydrate Related Bottom Simulating Reflector at the Norwegian Continental Margin. In *Annals of the New York Academy of Sciences*, **vol. 912** (1): pp. 126–135.

**Asher, G. B., Sloan, E. D. and Graboski, M. S.** (1986). A computer-controlled transient needle-probe thermal conductivity instrument for liquids. In *International Journal of Thermophysics*, **vol. 7** (2): pp. 285–294.

**Bathe, M., Vagle, S., Saunders, G. A. and Lambson, E. F.** (1984). Ultrasonic wave velocities in the structure II clathrate hydrate THF-17H 2 OJ Mater. In *Journal of Materials Science Letters*, **vol. 3** (904).

**Beauchamp, B.** (2004). Natural gas hydrates: myths, facts and issues. In *Comptes Rendus Geosciences*, **vol. 336** (9): pp. 751–765.

**Bentley, R. W.** (2002). Global oil & gas depletion: an overview. In *Energy Policy*, **vol. 30** (3): pp. 189–205.

**Berg, K., Solheim, A. and Bryn, P.** (2005). The Pleistocene to recent geological development of the Ormen Lange area. In *Marine and Petroleum Geology*, **vol. 22** (1-2): pp. 45–56.

**Berndt, C., Büenz, S. and Mienert, J.** (2003). Polygonal fault systems on the mid-Norwegian margin: A long-term source for fluid flow, vol. 216. Geological Society of London, pp. 283–290.

**Berndt, C., Bünz, S., Clayton, T., Mienert, J. and Saunders, M.** (2004a). Seismic character of bottom simulating reflectors: examples from the mid-Norwegian margin. In *Marine and Petroleum Geology*, **vol. 21** (6): pp. 723–733.

**Berndt, C., Mienert, J., Vanneste, M. and Bunz, S.** (2004b). Gas hydrate dissociation and sea floor collapse in the wake of the Storegga Slide, Norway. In **Wandas, B., Eide, E., Gradstein, F. and Nystuen, J.**, eds., *Onshore-offshore relationships on the North Atlantic Margin*, Special Publication. Elsevier, Amsterdam, p. 18.

**Beyer, A., Rathlau, R. and Schenke, H. W.** (2005). Multibeam bathymetry of the Håkon Mosby Mud Volcano. In *Marine Geophysical Researches*, **vol. 26**: pp. 61–75.

**Bil, K.** (2003). Economic Perspectives of Methane from Hydrate. In **Max, M.**, ed., *Natural Gas Hydrate in Oceanic and Permafrost Environments*. Kluwer Academic Publishers, pp. 349–360.

**Bjørnseth, H., Grant, S., Hansen, E., Hossack, J., Roberts, D. and Thompson, M.** (1997). Structural evolution of the Voring Basin, Norway, during the Late Cretaceous and Palaeogene. In *Journal of the Geological Society*, **vol. 154** (3): pp. 559–563.

**Boetius, A., Ravenchlag, K., Schubert, C., Rickert, D., Widdel, F., Gieseke, A., Amann, R., Jorgensen, B., Witte, U. and Pfannkuche, O.** (2000). A marine microbial consortium apparently mediating anaerobic oxidation of methane. In *Nature*, **vol. 407**: pp. 623–626.

**Bohrmann, G., Greinert, J., Suess, E. and Torres, M.** (1998). Authigenic carbonates from the Cascadia subduction zone and their relation to gas hydrate stability. In *Geology*, **vol. 26** (7): pp. 647–650.

**Bohrmann, G., Ivanov, M., Foucher, J.-P., Spiess, V., Bialas, J., Greinert, J., Weinrebe, W., Abegg, F., Aloisi, G., Artemov, Y., Blinova, V., Drews, M., Heidersdorf, F., Krabbenhüft, A., Klaucke, I., Krastel, S., Leder, T., Polikarpov, I., Saburova, M., Schmale, O., Seifert, R., Volkonskaya, A. and Zillmer, M.** (2003). Mud volcanoes and gas hydrates in the Black Sea: new data from Dvurechenskii and Odessa mud volcanoes. In *Geo-Marine Letters*, **vol. 23** (3 - 4): pp. 239–249.

**Bojanowski, M.** (2007). Oligocene cold-seep carbonates from the Carpathians and their inferred relation to gas hydrates. In *Facies*, **vol. 53**: pp. 347–360.

**Bondevik, S., Løvholt, F., Harbitz, C., Mangerud, J., Dawson, A. and Inge Svendsen, J.** (2005). The Storegga Slide tsunami–comparing field observations with numerical simulations. In *Marine and Petroleum Geology*, **vol. 22** (1-2): pp. 195–208.

**Borowski, W. S.** (2004). A review of methane and gas hydrates in the dynamic, stratified system of the Blake Ridge region, offshore southeastern North America. In *Chemical Geology*, **vol. 205** (3-4): pp. 311–346.

**Borowski, W. S., Paull, C. K. and Ussler, W.** (1996). Marine pore-water sulfate profiles indicate in situ methane flux from underlying gas hydrate. In *Geology*, **vol. 24** (7): pp. 655–658.

**Borowski, W. S., Paull, C. K. and Ussler, W.** (1999). Global and local variations of interstitial sulfate gradients in deep-water, continental margin sediments: Sensitivity to underlying methane and gas hydrates. In *Marine Geology*, **vol. 159** (1-4): pp. 131–154.

**Boswell, R., Hunter, R., Collett, T. S., Digert, S., Hancock, S. H., Weeks, M. and Team, M. E. S.** (2008). Investigation of gas hydrate-bearing sandstone reservoirs at the "Mount Elbert" stratigraphic test well, Milne Point, Alaska. In *Proceedings of the 6th International Conference on Gas Hydrates, Vancouver, Canada*. p. 9.

**Boswell, R., Kleinberg, R., Collett, T. and Frye, M.** (2007). Exploration Priorities for Marine Gas Hydrate Resources. In *Fire in the Ice newsletter*, **vol. Summer**: pp. 11–13.

**Bouriak, S., Vanneste, M. and Saoutkine, A.** (2000). Inferred gas hydrates and clay diapirs near the Storegga Slide on the southern edge of the Vøring Plateau, offshore Norway. In *Marine Geology*, **vol. 163** (1-4): pp. 125–148.

**Bouriak, S., Volkonskaia, A. and Galaktionov, V.** (2003). Strata-bounded gas hydrate BSR below deposits of the Storegga Slide and at the southern edge of the Voring Plateau. In *Marine Geology*, **vol. 195** (1-4): pp. 301–318.

**BP** (2008). BP Statistical Review of World Energy. Tech. Rep., British Petroleum.

**Braathen, A.** (2009). The Longyearbyen $CO_2$ Lab. UNIS handbook, available at http://co2-ccs.unis.no/.

**Bradner, T.** (2009). Conoco works with DOE on gas hydrates test. Published as article in Alaskan Journal of Commerce, 13/3/2009.

**Brekke, H.** (2000). The tectonic evolution of the Norwegian Sea Continental Margin with emphasis on the Vøring and Møre Basins. In *Geological Society, London, Special Publications*, **vol. 167** (1): pp. 327–378. doi:10.1144/GSL.SP.2000.167.01.13.

**Bryn, P., Berg, K., Forsberg, C. F., Solheim, A. and Kvalstad, T. J.** (2005a). Explaining the Storegga Slide. In *Marine and Petroleum Geology*, **vol. 22** (1-2): pp. 11–19.

**Bryn, P., Berg, K., Stoker, M. S., Haflidason, H. and Solheim, A.** (2005b). Contourites and their relevance for mass wasting along the Mid-Norwegian Margin. In *Marine and Petroleum Geology*, **vol. 22** (1-2): pp. 85–96.

**Bryn, P., Solheim, A., Berg, K., Lien, R., Forsberg, C., Haflidason, H., Ottesen, D. and Rise, L.** (2003). The Storegga Slide Complex; Repeated Large Scale Sliding in Response to Climatic Cyclicity. In **Locat, J. and Mienert, J.**, eds., *Submarine Mass Movements and their Consequences*. Kluwer Academic Publishers, Dordrecht, pp. 215–222.

**Bugge, T., Belderson, R. H. and Kenyon, N. H.** (1988). The Storegga Slide. In *Philosophical Transactions of the Royal Society of London. Series A, Mathematical and Physical Sciences*, **vol. 325** (1586): pp. 357–388.

**Bugge, T., Løfaldli, M., Maisey, G. H., Rokoengen, K., Skaar, F. E. and Thusu, B.** (1975). Geological investigation of a Lower Tertiary-Quaternary core, offshore Trøndelag, Norway. In *Norges Geologiske Undersøkelse*, **vol. 316**: pp. 253–269.

**Bünz, S. and Mienert, J.** (2004). Acoustic imaging of gas hydrate and free gas at the Storegga Slide. In *Journal of Geophysical Research*, **vol. 109** (B04102): p. 15.

**Bünz, S., Mienert, J., Andreassen, K. and Berteussen, K. A.** (2005a). Marine multicomponent seismology in gas hydrate investigations on the Norwegian Margin. In *Fire in the Ice newsletter*, **vol. Spring**: pp. 11–13.

**Bünz, S., Mienert, J., Andreassen, K., Vanneste, M. and Guidard, S.** (2005b). Multicomponent seismic technology in gas hydrate investigation on the Mid-Norwegian margin. In *Proceedings of the Fifth International Conference on Gas Hydrates, June 12-16, 2005. Trondheim, Norway*. p. 4.

**Bünz, S., Mienert, J. and Berndt, C.** (2003). Geological controls on the Storegga gas-hydrate system of the mid-Norwegian continental margin. In *Earth and Planetary Science Letters*, **vol. 209** (3-4): pp. 291–307.

**Bünz, S., Mienert, J., Vanneste, M. and Andreassen, K.** (2005c). Gas hydrates at the Storegga Slide: Constraints from an analysis of multicomponent, wide-angle seismic data. In *Geophysics*, **vol. 70** (5): pp. B19–B34.

**Cameron, I., Handa, Y. and Baker, T.** (1990). Compressive strength and creep behavior of hydrate-consolidated sand. In *Canadian Geotechnical Journal*, **vol. 27**: p. 255.

**Carcione, J. M., Gei, D., Rossi, G. and Madrussani, G.** (2005). Estimation of gas-hydrate concentration and free-gas saturation at the Norwegian-Svalbard continental margin. In *Geophysical Prospecting*, **vol. 53** (6): pp. 803–810.

**Carroll, J. J.** (2003). Natural Gas Hydrates: A Guide for Engineers. Elsevier Science, 270 pp.

**Cartwright, J. and Lonergan, L.** (1996). Volumetric contraction during the compaction of mudrocks: a mechanism for the development of regional-scale polygonal fault systems. In *Basin Research*, **vol. 8** (2): pp. 183–193.

**Chand, S. and Minshull, T. A.** (2003). Seismic constraints on the effects of gas hydrate on sediment physical properties and fluid flow: a review. In *Geofluids*, **vol. 3** (4): pp. 275–289.

**Chapman, N. R., Gettrust, J. F., Walia, R., Hannay, D., Spence, G. D., Wood, W. T. and Hyndman, R. D.** (2002). High-resolution, deep-towed, multichannel seismic survey of deep-sea gas hydrates off western Canada. In *Geophysics*, **vol. 67** (4).

**Chatterji, J. and Griffith, J. E.** (1998). Methods of decomposing gas hydrates. US patent, filed 1996.

**Chatti, I., Delahaye, A., Fournaison, L. and Petitet, J.-P.** (2005). Benefits and drawbacks of clathrate hydrates: a review of their areas of interest. In *Energy Conversion and Management*, **vol. 46** (9-10): pp. 1333–1343.

**CIA** (2008). CIA World Factbook. URL `https://www.cia.gov/library/publications/the-world-factbook/`.

**Claypool, G.** (2006). Gulf of Mexico Gas Hydrate Joint Industry Project (GOMJIP), 2005. The cruise of the drilling vessel Uncle John, Mobile, Alabama to Galveston, Texas, Atwater Valley Blocks 13/14 and Keathley Canyon Block 151, 17 April to 22 May 2005. Tech. Rep., NETL.

**Clennell, M., Hovland, M., Booth, J. S., Henry, P. and Winters, W. J.** (1999). Formation of natural gas hydrates in marine sediments. Conceptual model of gas hydrate growth conditioned by host sediment properties. In *Journal of Geophysical Research*, **vol. 104** (B10): pp. 22,985–23,004.

**Collett, T., Agena, W., Lee, M., Zyrianova, M., Bird, K., Charpentier, T., Houseknect, D., Klett, T., Pollastro, R. and Schenk, C.** (2008). Assessment of Gas Hydrate Resources on the North Slope, Alaska, 2008. USGS Fact Sheet 2008-3073, U.S. Geological Survey. URL `http://pubs.usgs.gov/fs/2008/3073/`.

**Collett, T. S.** (1993). Natural gas hydrates of the Prudhoe Bay-Kuparuk River area, North Slope. In *AAPG Bulletin*, **vol. 77** (5).

**Collett, T. S.** (2002). Energy Resource Potential of Natural Gas Hydrates. In *AAPG Bulletin*, **vol. 86** (11): pp. 1971–1992.

**Collett, T. S.** (2008). Geologic and Enginnering Controls on the Production of Permafrost-associated Gas Hydrate Accumulations. In *Proceedings of the 6th International Conference on Gas Hydrates, Vancouver, Canada*. p. 12.

**Collett, T. S. and Dallimore, S.** (2000). Permafrost-Associated Gas Hydrate. In **Max, M. D.**, ed., *Natural Gas Hydrate in Oceanic and Permafrost Environments*. Kluwer Academic Publishers, Dordrecht, pp. 43–60.

**Collett, T. S. and Ginsburg, G. D.** (1998). Gas Hydrates in the Messoyakha Gas Field of the West Siberian Basin — A Re-Examination of the Geologic Evidence. In *International Journal of Offshore and Polar Engineering*, **vol. 8** (1): p. 21.

**Collett, T. S. and Ladd, J.** (2000). Detection of gas hydrate with downhole logs and assessment of gas hydrate concentrations (saturation) and gas volumes with electrical resistivity log data. In **Paull, C., Matsumoto, R., Wallace, P. and Dillon, W. P.**, eds., *Proceedings of the Ocean Drilling Programme, Scientific Results*, vol. 164. ODP, pp. 179–191.

**Colwell, F., Matsumoto, R. and Reed, D.** (2004). A review of the gas hydrates, geology, and biology of the Nankai Trough. In *Chemical Geology*, **vol. 205** (3-4): pp. 391–404.

**Constable, S. and Weiss, C.** (2006). Mapping thin resistors and hydrocarbons with marine EM methods: Insights from 1D modeling. In *Geophysics*, **vol. 71** (2): pp. G43–G51.

**Cook, A. E., Goldberg, D. and Kleinberg, R. L.** (2008). Fracture-controlled gas hydrate systems in the northern Gulf of Mexico. In *Marine and Petroleum Geology*, **vol. 25** (9): pp. 932–941.

**Crutchley, G. J.** (2004). Marine gas hydrate distribution and submarine slope failure: an example from offshore Fiordland, southwest New Zealand. BSc(Hons), Department of Geology, University of Otago.

**Crutchley, G. J., Pecher, I. A., Gorman, A. R., Henrys, S. A. and Greinert, J.** (2009). Seismic imaging of gas conduits beneath seafloor seep sites in a shallow marine gas hydrate province, Hikurangi Margin, New Zealand. In *Marine Geology*, **vol. In Press, Corrected Proof**: pp. –.

**Curray, J. R.** (1980). The Ipod Programme on Passive Continental Margins. In *Philosophical Transactions of the Royal Society of London. Series A, Mathematical and Physical Sciences*, **vol. 294** (1409, The Evolution of Passive Continental Margins in the Light of Recent Deep Drilling Results): pp. 17–33.

**Dahl, pers. comm.** (2008).

**Dalland, A., Worsley, D. and Ofstad, K.** (1988). A lithostratigraphic scheme for the Mesozoic and Cenozoic succession offshore mid- and northern Norway. In *NPD Bulletin*, **vol. 4**: p. 87.

**Dallimore, S. and Collett, T. S.** (2005). Scientific Results From the Mallik 2002 Gas Hydrate Production Research Well Program, Mackenzie Delta, Northwest Territories. Bulletin of the Geological Survey of Canada.

**Dawe, R. and Thomas, S.** (2007). Energy Sources, Part A: Recovery, Utilization and Environmental Effects. A Large Potential Methane Source – Natural Gas Hydrates. In *Energy Sources*, **vol. 29** (3): pp. 217–229.

**De Blasio, F., Elverhoi, A., Issler, D., Harbitz, C., Bryn, P. and Lien, R.** (2005). On the dynamics of subaqueous clay rich gravity mass flows–the giant Storegga slide, Norway. In *Marine and Petroleum Geology Ormen Lange - an integrated study for the safe development of a deep-water gas field within the Storegga Slide Complex, NE Atlantic continental margin*, **vol. 22** (1-2): pp. 179–186.

**de Forcrand, M.** (1902). Sur la composition des hydrates de gaz. In *Comp Rend*, **vol. 135**: pp. 959–961.

**Demirbas, A.** (2002). Fuel Properties of Hydrogen, Liquefied Petroleum Gas (LPG), and Compressed Natural Gas (CNG) for Transportation. In *Energy Sources*, **vol. 24** (7): pp. 601–610.

**Dickens, G.** (2003). Climate: A Methane Trigger for Rapid Warming? In *Science*, **vol. 299** (5609).

**Dickens, G., O'Neil, J., Rea, D. and Owen, R.** (1995). Dissociation of oceanic methane hydrate as a cause of the carbon isotope excursion at the end of the Paleocene. In *Paleoceanography*, **vol. 10** (6): pp. 965–972.

**Dickens, G. R., Castillo, M. M. and Walker, J. C. G.** (1997). A blast of gas in the latest Paleocene; simulating first-order effects of massive dissociation of oceanic methane hydrate. In *Geology*, **vol. 25** (3): pp. 259–262.

**Dillon, W. P. and Max, M. D.** (2000). Oceanic Gas Hydrate. In **Max, M. D.**, ed., *Natural Gas Hydrate in Oceanic and Permafrost Environments*. Kluwer Academic Publishing, Dordrecht, Germany, pp. 61–76.

**Doré, E. R., A. G. Lundin** (1996). Cenozoic compressional structures on the NE Atlantic margin: nature, origin and potential significance for hydrocarbon exploration. In *Petroleum Geoscience*, **vol. 2** (4): pp. 299–312.

**Driscoll, N. W., Weissel, J. K. and Goff, J. A.** (2000). Potential for large-scale submarine slope failure and tsunami generation along the U.S. mid-Atlantic coast. In *Geology*, **vol. 28** (5): pp. 407–410.

**Ecker, C., Dvorkin, J. and Nur, A. M.** (2000). Estimating the amount of gas hydrate and free gas from marine seismic data. In *Geophysics*, **vol. 65** (2): pp. 565–573.

**EIA** (2003). The Global Liquefied Natural Gas Market: Status & Outlook. Tech. Rep., Energy Information Administration, U.S. Department of Energy.

**EIA** (2008a). Emission coefficients. URL `http://www.eia.doe.gov/oiaf/1605/coefficients.html`.

**EIA** (2008b). International energy outlook 2008. Tech. Rep., Energy Information Administration. URL `http://www.eia.doe.gov/oiaf/ieo/index.html`.

**EIA** (2008c). Natural gas prices. Tech. Rep., Energy Information Administration. URL `http://www.eia.doe.gov/oiaf/ieo/index.html`.

**EIA** (2008d). Weekly All Countries Spot Price FOB Weighted by Estimated Export Volume. URL `http://tonto.eia.doe.gov/dnav/pet/hist/wtotworldw.htm`.

**Eidesmo, T., Ellingsrud, S., MacGregor, L. M., Constable, S., Sinha, M. C., Johansen, S., Kong, F. N. and Westerdahl, H.** (2002). Sea Bed Logging (SBL), a new method for remote and direct identification of hydrocarbon filled layers in deepwater areas. In *First Break*, **vol. 20** (3): pp. 144–152.

**Eldholm, O.** (1970). Seismic refraction measurements on the Norwegian continental shelf between 62°N and 65°N. In *Norsk geologiske tiddskrift*, **vol. 50**: pp. 215–229.

**Eldholm, O., Thiede, J. and Taylor, E.** (1987). Evolution of the Norwegian continental margin: Background and Objectives. In *Proceedings of the Ocean Drilling Programme, Leg 104*. p. 21.

**Ellingsrud, pers. comm.** (2007).

**Ellis, M., Evans, R. L., Hutchinson, D., Hart, P., Gardner, J. and Hagen, R.** (2008). Electromagnetic surveying of seafloor mounds in the northern Gulf of Mexico. In *Marine and Petroleum Geology*, **vol. 25** (9): pp. 960–968.

**Energy Current** (2008). Power from shore for Eni's Goliat. URL `http://www.energycurrent-.com/index.php?id=2&storyid=11559`.

**Englezos, P.** (1993). Clathrate Hydrates. In *Industrial & Engineering Chemistry*, **vol. 32**: pp. 1251–1274.

**Englezos, P., Kalogerakis, N., Dholabhai, P. and Bishnoi, P.** (1987). Kinetics of gas hydrate formation from mixtures of methane and ethane. In *Chemical engineering science*, **vol. 42** (11): pp. 2659–2666.

**Englezos, P. and Lee, J.** (2005). Gas hydrates: A cleaner source of energy and opportunity for innovative technologies. In *Korean Journal of Chemical Engineering*, **vol. 22** (5): pp. 671–681.

**EPA** (2009). The U.S. Inventory of Greenhouse Gas Emissions and Sinks. Online. URL `http://www.epa.gov/climatechange/emissions/downloads/2007GHGFastFacts.pdf`.

**EPMag** (2009). CNG Stranded Assets. Available online 11.11.2009.

**Erichsen, L.** (2009). The Peon Field, unlocking unconventional reserves in the North Sea. Presented at Bergen SPE "One day seminar" 2009.

**EU Directive** (2008). Proposal for a directive of the European Parliament and of the Council on the promotion of the use of energy from renewable sources. Tech. Rep., Commission of the European Communities.

**Evans, D., King, E. L., Kenyon, N. H., Brett, C. and Wallis, D.** (1996). Evidence for long-term instability in the Storegga Slide region off western Norway. In *Marine Geology*, **vol. 130** (3-4): pp. 281–292.

**Faraday, M. and Davy, H.** (1823). On Fluid Chlorine. In *Philosophical Transactions of the Royal Society of London*, **vol. 113**: pp. 160–165.

**Faverola, A. P., Bünz, S. and Mienert, J.** (2009). Fluid distributions inferred from P-wave velocity and reflection seismic amplitude anomalies beneath the Nyegga pockmark field of the mid-Norwegian margin. In *Marine and Petroleum Geology*, **vol. in press**: p. 15.

**Fiebig, J., Woodland, A., Spangenberg, J. and Oschmann, W.** (2007). Natural evidence for rapid abiogenic hydrothermal generation of $CH_4$. In *Geochimica et Cosmochimica Acta*, **vol. 71**: pp. 3028–3039.

**Fohrmann, M.** (2009). The Occurrence and Distribution of Gas Hydrates on the Puysegur Continental Margin and Slope-Stability Aspects on Ritchie Banks, Hikurangi Margin, New Zealand. Ph.D. thesis, University of Otago. P. 244.

**Forsberg, C. F. and Locat, J.** (2005). Mineralogical and microstructural development of the sediments on the Mid-Norwegian margin. In *Marine and Petroleum Geology*, **vol. 22** (1-2): pp. 109–122.

**Forster, A., Merriam, D. and Davis, J.** (1997). Spatial analysis of temperature (BHT/DST) data and consequences for heat-flow determination in sedimentary basins. In *Geologische Rundschau*, **vol. 86** (2): pp. 252–261.

**Furevik, T.** (2001). Annual and interannual variability of Atlantic Water temperatures in the Norwegian and Barents Seas: 1980-1996. In *Deep-Sea Research*, **vol. 48**: pp. 383–404.

**Gauer, P., Kvalstad, T. J., Forsberg, C. F., Bryn, P. and Berg, K.** (2005). The last phase of the Storegga Slide: simulation of retrogressive slide dynamics and comparison with slide-scar morphology. In *Marine and Petroleum Geology*, **vol. 22** (1-2): pp. 171–178.

**Gausland, I.** (2000). Impact of seismic surveys on marine life. In *The Leading Edge*, **vol. 19** (8): pp. 903–905. doi:10.1190/1.1438746.

**Gausland, I.** (2003). Seismic surveys impact on fish and fisheries. Tech. Rep., Norwegian Oil Industry Association.

**Gazprom** (2009). Shtokman project. URL `http://www.gazprom.com/eng/articles/article-21712.shtml`.

**Ginsburg, G. D., Milkov, A. V., Soloviev, V. A., Egorov, A. V., Cherkashev, G. A., Vogt, P. R., Crane, K., Lorenson, T. D. and Khutorskoy, M. D.** (1999). Gas hydrate accumulation at the Håkon Mosby Mud Volcano. In *Geo-Marine Letters*, **vol. 19** (1 - 2): pp. 57–67.

**Google Scholar** (2008). Google Scholar. URL `http://scholar.google.com`.

**Gorman, A.** (2008). Seismic characterization of gas hydrates and associated fluid flow on passive and active continental margins: examples from New Zealand. CSEG Luncheon presentation, January 2008.

**Gorman, A. R., Holbrook, W. S., Hornbach, M. J., Hackwith, K. L., Lizarralde, D. and Pecher, I.** (2002). Migration of methane gas through the hydrate stability zone in a low-flux hydrate province. In *Geology*, **vol. 30** (4): pp. 327–330.

**Gosnold, W.** (2008). The Global Heat Flow Database of the International Heat Flow Commission. URL `http://www.heatflow.und.edu/index2.html`.

**Grant, A. and Briggs, A. D.** (2002). Toxicity of sediments from around a North Sea oil platform: are metals or hydrocarbons responsible for ecological impacts? In *Marine Environmental Research*, **vol. 53** (1): pp. 95 – 116.

**Grauls, D.** (2001). Gas hydrates: importance and applications in petroleum exploration. In *Marine and Petroleum Geology*, **vol. 18** (4): pp. 519–523.

**Gray, J. S., Bakke, T., Beck, H. J. and Nilssen, I.** (1999). Managing the Environmental Effects of the Norwegian Oil and Gas Industry: From Conflict to Consensus. In *Marine Pollution Bulletin*, **vol. 38** (7): pp. 525 – 530.

**Grevemeyer, I. and Villinger, H.** (2001). Gas hydrate stability and the assessment of heat flow through continental margins. In *Geophysical Journal International*, **vol. 145** (3): pp. 647–660.

**Gudmundsson, J. S.** (2002). Cold Flow Hydrate Technology. In *4th International Conference on Gas Hydrates, Yokohama*. p. 6.

**Gudmundsson, J. S. and Borrehaug, A.** (1996). Frozen hydrate for transport of natural gas. In **Monfort, J.**, ed., *Proceedings of the Second International Conference on Gas Hydrates*. pp. 415–422.

**Gupta, A.** (2007). Methane hydrate dissociation measurements and modeling: The role of heat transfer and reaction kinetics. Ph.D. thesis, Colorado School of Mines, Golden, Colorado, USA.

**Haacke, R. R., Westbrook, G. K. and Hyndman, R. D.** (2007). Gas hydrate, fluid flow and free gas: Formation of the bottom-simulating reflector. In *Earth and Planetary Science Letters*, **vol. 261**: pp. 407–420.

**Haacke, R. R., Westbrook, G. K. and Riley, M. S.** (2008). Controls on the formation and stability of gas hydrate-related bottom-simulating reflectors (BSRs): A case study from the west Svalbard continental slope. In *Journal of Geophysical Research*, **vol. 113**: p. 17.

**Haflidason, H., Hjelstuen, B. O., Chen, Y., Vaular, E. N., Steen, I. H., Daae, F. L., Todt, C., Hocking, W. and Portnova, D.** (2008). Active seafloor seeps with associated methane and methane hydrate bearing sediments on the Mid-Norwegian margin, Nyegga: a multidisciplinary geological, geochemical and biological study. In *AGU Fall Meeting Abstracts*. p. 1.

**Hammerschmidt, E.** (1934). Formation of Gas Hydrates in Natural Transmission Lines. In *Industrial & Engineering Chemistry*, **vol. 26** (8): pp. 851–855.

**Hancock, S. H., Dallimore, S. R., Collett, T. S., Carle, D., Weatherill, B., Satoh, T. and Inoue, T.** (2005a). Overview of pressure-drawdown production-test results for the JAPEX/JNOC/GSC et al. Mallik 5L-38 gas hydrate production research well. In **S.R., D. and T.S., C.**, eds., *Scientific Results from the Mallik 2002 Gas Hydrate Production Research Well Program, Mackenzie Delta, Northwest Territories, Canada*, vol. Bulletin 585. Geological Society of Canada, p. 16.

**Hancock, S. H., Dallimore, S. R., Collett, T. S., Satoh, T., Inoue, T., Huenges, E., Henninges, J. and Weatherill, B.** (2005b). Overview of thermal-stimulation production-test results for the JAPEX/JNOC/GSC et al. Mallik 5L-38 gas hydrate production research well. In **S.R., D. and T.S., C.**, eds., *Scientific Results from the Mallik 2002 Gas Hydrate Production Research Well Program, Mackenzie Delta, Northwest Territories, Canada*, vol. Bulletin 585. Geological Society of Canada, p. 15.

**Harris, R. E., Miller, G. W. and Richardson, W. J.** (2001). Seal responses to airgun sounds during summer seismic surveys in the Alaskan Beaufort Sea. In *Marine Mammal Science*, **vol. 17**: pp. 795–812.

**Hart, P. E., Hutchinson, D. R., Gardner, J., Carney, R. S. and Fornari, D.** (2008). A photographic and acoustic transect across two deep-water seafloor mounds, Mississippi Canyon, northern Gulf of Mexico. In *Marine and Petroleum Geology*, **vol. 25** (9): pp. 969–976.

**Hassel, A., Knutsen, T., Dalen, J., Skaar, K., Lokkeborg, S., Misund, O. A., Ostensen, O., Fonn, M. and Haugland, E. K.** (2004). Influence of seismic shooting on the lesser sandeel (Ammodytes marinus). In *ICES Journal of Marine Science*, **vol. 61** (7): pp. 1165–1173. doi: 10.1016/j.icesjms.2004.07.008.

**Haugen, K. B., Løvholt, F. and Harbitz, C. B.** (2005). Fundamental mechanisms for tsunami generation by submarine mass flows in idealised geometries. In *Marine and Petroleum Geology*, **vol. 22** (1-2): pp. 209–217.

**Hein, J., Scholl, D., Barron, J., Jones, M. and Miller, J.** (1978). Diagenesis of late Cenozoic diatomaceous deposits and formation of the bottom simulating reflector in the southern Bering Sea. In *Sedimentology*, **vol. 25**: pp. 155–181.

**Henriet, J., Batist, M. D. and Verschuren, M.** (1991). Early fracturing of Palaeogene clays, southernmost North Sea: Relevance to mechanisms of primary hydrocarbon migration. In *Special Publication of the European Association of Petroleum Geoscientists*, **vol. 1**: pp. 217–227.

**Henrys, S., Ellis, S. and Uruski, C.** (2003). Conductive heat flow variations from bottom-simulating reflectors on the Hikurangi margin, New Zealand. In *EOS Transactions*, **vol. 87** (33): pp. 325–330.

**Hesse, R.** (1986). Diagenesis 11. Early diagenetic pore water/sediment interaction: Modern offshore basins. In *Geoscience Canada*, **vol. 13** (3).

**Hjelstuen, B. O., Eldholm, O. and Skogseid, J.** (1999). Cenozoic evolution of the northern Vøring margin. In *Geol Soc Am Bull*, **vol. 111** (12): pp. 1792–1807.

**Hjelstuen, B. O., Haflidason, H., Sejrup, H. P. and Nygård, A.** (2009). Sedimentary and structural control on pockmark development - evidence from the Nyegga pockmark field, NW European margin. In *Geo-Marine Letters*, **vol. author's proof**: p. 10. doi:DOI 10.1007/s00367-009-0172-4.

**Hjelstuen, B. O., Sejrup, H. P., Haflidason, H., Nygård, A., Berstad, I. M. and Knorr, G.** (2004). Late Quaternary seismic stratigraphy and geological development of the south Vøring margin, Norwegian Sea. In *Quaternary Science Reviews*, **vol. 23** (16-17): pp. 1847–1865.

**Hjelstuen, B. O., Sejrup, H. P., Haflidason, H., Nygård, A., Ceramicola, S. and Bryn, P.** (2005). Late Cenozoic glacial history and evolution of the Storegga Slide area and adjacent slide flank regions, Norwegian continental margin. In *Marine and Petroleum Geology*, **vol. 22** (1-2): pp. 57–69.

**Holditch, S. A.** (2006). Tight Gas Sands. In *Journal of Petroleum Technology, SPE Distinguished Author Series*: pp. 86–93.

**Holditch, S. A. and Chianelli, R. R.** (2008). Factors That Will Influence Oil and Gas Supply and Demand in the 21st Century. In *MRS Bulletin*, **vol. 33**: pp. 317–325.

**Holland, M., Schultheiss, P., Roberts, J. and Druce, M.** (2008). Observed gas hydrate morphologies in marine sediments. In *Proceedings of the 6th International Conference on Gas Hydrates (ICGH 2008), Vancouver, British Columbia, Canada, July 6-10, 2008.* p. 7.

**Hornbach, M. J., Holbrook, W. S., Gorman, A. R., Hackwith, K. L., Lizarralde, D. and Pecher, I.** (2003). Direct seismic detection of methane hydrate on the Blake Ridge. In *Geophysics*, **vol. 68** (PART 1): pp. 92–100.

**Hovland, M.** (2002). On the self-sealing nature of marine seeps. In *Continental Shelf Research*, **vol. 22**: pp. 2387–2394.

**Hovland, M., Gallagher, J. W., Clennell, M. B. and Lekvam, K.** (1997). Gas hydrate and free gas volumes in marine sediments: Example from the Niger Delta front. In *Marine and Petroleum Geology*, **vol. 14** (3): pp. 245 – 255.

**Hovland, M. and Svensen, H.** (2006). Submarine pingoes: Indicators of shallow gas hydrates in a pockmark at Nyegga, Norwegian Sea. In *Marine Geology*, **vol. 228** (1-4): pp. 15–23.

**Hovland, M., Svensen, H., Forsberg, C. F., Johansen, H., Fichler, C., Fosså, J. H., Jonsson, R. and Rueslåtten, H.** (2005). Complex pockmarks with carbonate-ridges off mid-Norway: Products of sediment degassing. In *Marine Geology*, **vol. 218** (1-4): pp. 191–206.

**Howe, S., Nanchary, N., Patil, S. L., Ogbe, D., Chukwu, G., Hunter, R. B. and Wilson, S.** (2004). Economic Analysis and Feasibility study of Gas Production from Alaska North Slope Gas Hydrate Resources. In *AAPG Hedberg Conference, Vancouver, BC*. p. 4.

**Huo, Z., Hester, K., Sloan, E. D. and Miller, K. T.** (2003). Methane hydrate nonstoichiometry and phase diagram. In *AIChE Journal*, **vol. 49** (5): pp. 1300–1306.

**Hustoft, S.** (2009). Spatial and temporal analysis of fluid venting systems on the Norwegian-Svabard margin. Ph.D. thesis, University of Tromsø.

**Hustoft, S., Bünz, S., Mienert, J. and Chand, S.** (2009). Gas hydrate reservoir and active methane-venting province in sediments on $<$ 20Ma young oceanic crust in the Fram Strait, offshore NW-Svalbard. In *Earth and Planetary Science Letters*, **vol. 284** (1-2): pp. 12 – 24.

**Hustoft, S., Mienert, J., Bünz, S. and Nouzé, H.** (2007). High-resolution 3D-seismic data indicate focussed fluid migration pathways above polygonal fault systems of the mid-Norwegian margin. In *Marine Geology*, **vol. 245** (1-4): pp. 89–106.

**HWU** (2008). Centre for Gas Hydrate Research, Heriot-Watt University. URL `http://www.pet.hw.ac.uk/research/hydrate/`.

**Hydro** (2003). Ormen lange: Konsekvensutredning feltutbygging og ilandføring. Tech. Rep., Norsk Hydro.

**Hyndman, R. D. and Davis, E. E.** (1992). A Mechanism for the Formation of Methane Hydrate and Seafloor Bottom-Simulating Reflectors by Vertical Fluid Expulsion. In *Journal of Geophysical Research*, **vol. 97**: pp. 7025–7041.

**Hyodo, M., Nakata, Y., Yoshimoto, N. and Ebinuma, T.** (2005). Basic research on the mechanical behavior of methane hydrate-sediments mixture. In *Journal of the Japanese Geotechnical Society of Soils and Foundations*, **vol. 45** (1): pp. 75–85.

**ICES** (2008). Ices oceanographic database and services. URL `http://www.ices.dk/ocean/`.

**Ichikawa, Y. and Yonezawa, T.** (2002). The outline of the MH21 program and the R&D plan of methane hydrate development system for offshore Japan. Provided by Japanese MH21 research program.

**IEA** (2006). World Energy Outlook. Tech. Rep., International Energy Agency.

**IEA** (2008). Key World Energy Statistics. Tech. Rep., International Energy Agency.

**Ilahi, M.** (2005). Evaluation of Cold Flow Concepts. Master's thesis, University of Trondheim.

**IMR** (2008). Norwegian Marine Data Centre at the Institute of Marine Research. Data provided by Øyvin Strand.

**Islam, M. R.** (1994). A new recovery technique for gas production from Alaskan gas hydrates. In *Journal of petroleum science & engineering*, **vol. 11** (4): pp. 267–281.

**Ivanov, M., Blinova, V., Kozlova, E., Westbrook, G., Mazzini, A., Minshull, T. and Nouzé, H.** (2007). First Sampling of Gas Hydrate From the Vøring Plateau. In *EOS Transactions*, **vol. 88** (19).

**Johansen, O.** (2002). Regional konsekvesutredning, Norskehavet underlagsrapport: Dypvannsutslipp - Oppdatering av kunnskapsstatus. Tech. Rep., SINTEF.

**Johnson, A. H. and Max, M. D.** (2006). The path to commercial hydrate gas production. In *The Leading Edge*, **vol. 25** (5): pp. 648–651.

**Johnson, J., Goldfinger, C. and Suess, E.** (2003). Geophysical constraints on the surface distribution of authigenic carbonates across the Hydrate Ridge region, Cascadia margin. In *Marine Geology*, **vol. 202**: pp. 79–120.

**Jones, A., Greinert, J., Bowden, D., Klaucke, I., Petersen, C., Netzeband, G. and Weinrebe, W.** (2009). Acoustic and visual characterisation of methane-rich seabed seeps at Omakere Ridge on the Hikurangi Margin, New Zealand. In *Marine Geology*, **vol. In Press, Corrected Proof**: pp. –.

**Jose, T., Minshull, T., Westbrook, G. and Berndt, C.** (2007). A Geophysical Study of a Pockmark in the Nyegga Region, Norwegian Sea. In *B43E-1653, AGU Fall meeting 2007*. p. 1.

**Juichiro, A., Hidekazu, T. and Asahiko, T.** (2002). Distribution of methane hydrate BSRs and its implication for the prism growth in the Nankai Trough. In *Marine Geology*, **vol. 187** (1-2): pp. 177–191.

**Kanda, H.** (2006). Economic study of natural gas hydrate transportation with natural gas hydrate (NGH) pellets. In *Proceedings of the 23rd World Gas Conference, Amsterdam*. p. 11.

**Kastner, M., Claypool, G. and Robertson, G.** (2008). Geochemical constraints on the origin of the pore fluids and gas hydrate distribution at Atwater Valley and Keathley Canyon, northern Gulf of Mexico. In *Marine and Petroleum Geology*, **vol. 25** (9): pp. 860–872.

**Katzman, R., Holbrook, W. S. and Paull, C.** (1994). Combined vertical-incidence and wide-angle seismic study of a gas hydrate zone, Blake Ridge. In *Journal of Geophysical Research*, **vol. 99** (B9): pp. 17,975–17,995.

**Kennett, J., Cannariato, K., Hendy, I. and Behl, R.** (2003). Methane Hydrates in Quaternary Climate Change: The Clathrate Gun Hypothesis, vol. 54. American Geophysical Union.

**Khan, F. I. and Amyotte, P. R.** (2002). Inherent safety in offshore oil and gas activities: a review of the present status and future directions. In *Journal of Loss Prevention in the Process Industries*, **vol. 15** (4): pp. 279 – 289.

**Klauda, J. and Sandler, S.** (2005). Global Distribution of Methane Hydrate in Ocean Sediment. In *Energy Fuels*, **vol. 19** (2): pp. 459–470.

**Klitgaard-Kristensen, D., Sejrup, H. P. and Haflidason, H.** (2001). The last 18 kyr fluctuations in Norwegian Sea surface conditions and implications for the magnitude of climatic change: Evidence from the North Sea. In *Paleoceanography*, **vol. 16**: pp. 455–467. doi: 10.1029/1999PA000495.

**Kobayashi, R. and Katz, D. L.** (1949). Methane hydrate at high pressures. In *Petroleum Transactions, American Institute for Mechanical Engineers*: pp. 66–70.

**Korenaga, J., Holbrook, W. S., Singh, S. C. and Minshull, T. A.** (1997). Natural gas hydrates on the southeast U.S. Margin: Constraints from full waveform and travel time inversions of wide-angle seismic data. In *J. Geophys. Res.*, **vol. 102**: pp. 15,345–15,365.

**Kvalstad, T. J., Andresen, L., Forsberg, C. F., Berg, K., Bryn, P. and Wangen, M.** (2005). The Storegga slide: evaluation of triggering sources and slide mechanics. In *Marine and Petroleum Geology*, **vol. 22** (1-2): pp. 245–256.

**Kvamme, B., Graue, A., Buanes, T., Kuznetsova, T. and Ersland, G.** (2007). Storage of CO2 in natural gas hydrate reservoirs and the effect of hydrate as an extra sealing in cold aquifers. In *International Journal of Greenhouse Gas Control*, **vol. 1** (2): pp. 236–246.

**Kvenvolden, K. and Barnard, L.** (1983). Hydrates of natural gas in continental margins. In **Watkins, J. and Drake, C.**, eds., *Studies in Continental Margin Geology, AAPG Memoir*, vol. 34. AAPG, pp. 631–640.

**Kvenvolden, K. and Loreson, T.** (2001). The global occurrence of natural gas hydrate. In **Paull, C. and Dillon, W.**, eds., *Natural Gas Hydrates: Occurrence, Distribution and Dynamics*, vol. 124 of *AGU Monograph Series*. American Geophysical Union, pp. 3–18.

**Kvenvolden, K. A.** (1995). A review of the geochemistry of methane in natural gas hydrate. In *Organic Geochemistry*, **vol. 23** (11-12): pp. 997–1008.

**Kvenvolden, K. A.** (1998). Estimates of the methane content of world-wide gas-hydrate deposits. In *JNOC Methane hydrates: resources in the near future? Workshop Panel Discussion Proceedings*. 20 to 22 October, Chiba City, Japan, pp. 1–8.

**Kvenvolden, K. A.** (1999). Potential effects of gas hydrate on human welfare. In *PNAS*, **vol. 96** (7): pp. 3420–3426.

**Kvenvolden, K. A.** (2000). Gas Hydrate and Humans. In *Annals of the New York Academy of Sciences*, **vol. 912** (1): pp. 17–22.

**Kvenvolden, K. A.** (2002). Methane hydrate in the global organic carbon cycle. In *Terra Nova*, **vol. 14** (5): pp. 302–306.

**Laberg, J. S., Andreassen, K. and Knutsen, S.-M.** (1998). Inferred gas hydrate on the Barents Sea shelf – a model for its formation and a volume estimate. In *Geo-Marine Letters*, **vol. 18** (1): pp. 26–33.

**Laberg, J. S., Dahlgren, T., Vorren, T. O., Haflidason, H. and Bryn, P.** (2001). Seismic analyses of Cenozoic contourite drift development in the Northern Norwegian Sea. In *Marine Geophysical Researches*, **vol. 22** (5): pp. 401–416.

**Laberg, J. S., Vorren, T. O. and Knutsen, S.-M.** (2002). The Lofoten Drift, Norwegian Sea. In *Geological Society, London, Memoirs*, **vol. 22** (1): pp. 57–64.

**Lapham, L. L., Chanton, J., Martens, C. S., Sleeper, K. and Woolsey, J. R.** (2008). Microbial activity in surficial sediments overlying acoustic wipeout zones at a Gulf of Mexico cold seep. In *Geochemistry, Geophysics, Geosystems*, **vol. 9**: pp. 1–17.

**Larsen, E. and Sejrup, H.** (1990). Weichselian land-sea interactions: Western Norway-Norwegian sea. In *Quaternary Science Reviews*, **vol. 9**: pp. 85–97.

**Larsen, R.** (2008). SATURN Cold Flow - transport av brønnstrøm uten kjemikalier og oppvarming. In *NPF Seminar, Oslo, 25.9.2008*. p. 15.

**Lederhos, J. P., Long, J. P., Sum, A., Christiansen, R. L. and Sloan, E. D.** (1996). Effective kinetic inhibitors for natural gas hydrates. In *Chemical Engineering Science*, **vol. 51** (8): pp. 1221–1229.

**Lee, M.** (2000). Gas Hydrates Amount Estimated from Acoustic Logs at the Blake Ridge, Sites 994, 995 and 997. In **Paull, C., Matsumoto, R., Wallace, P. and Dillon, W. P.**, eds., *Proceedings of the Ocean Drilling Programme, Scientific Results*, vol. 164. ODP, College Shetation, TX., pp. 193–198.

**Lee, M. W. and Collett, T. S.** (2001). Elastic properties of gas hydrate-bearing sediments. In *Geophysics*, **vol. 66**: p. 3.

**Lee, S.-Y. and Holder, G. D.** (2001). Methane hydrates potential as a future energy source. In *Fuel Processing Technology*, **vol. 71** (1-3): pp. 181–186.

**Leynaud, D., Sultan, N. and Mienert, J.** (2007). The role of sedimentation rate and permeability in the slope stability of the formerly glaciated Norwegian continental margin: the Storegga slide model. In *Landslides*, **vol. 4**: pp. 297–309.

**Lindzen, R. S.** (1990). Some Coolness Concerning Global Warming. In *Bulletin of the American Meteorological Society*, **vol. 71**: pp. 288–299.

**Locat, J. and Lee, H.** (2002). Submarine landslides: Advances and challenges. In *Canadian Geotechnical Journal*, **vol. 39** (1): pp. 193–213.

**Locat, J. and Lee, H.** (2005). Subaqueous debris flows. In **Jakob, M. and Hungr, O.**, eds., *Debris-flow Hazards and Related Phenomena*. Springer/Praxis, Heidelberg, p. 739.

**Lodolo, E., Camerlenghi, A., Madrussani, G., Tinivella, U. and Rossi, G.** (2002). Assessment of gas hydrate and free gas distribution on the South Shetland margin (Antarctica) based on multichannel seismic reflection data. In *Geophysical Journal International*, **vol. 148** (1): pp. 103–119.

**Lorenson, T. D., Claypool, G. E. and Dougherty, J. A.** (2008). Natural gas geochemistry of sediments drilled on the 2005 Gulf of Mexico JIP cruise. In *Marine and Petroleum Geology*, **vol. 25** (9): pp. 873–883.

**Løvholt, F., Harbitz, C. B. and Haugen, K. B.** (2005). A parametric study of tsunamis generated by submarine slides in the Ormen Lange/Storegga area off western Norway. In *Marine and Petroleum Geology*, **vol. 22** (1-2): pp. 219–231.

**Lundin, E. and Doré, A. G.** (2002). Mid-Cenozoic post-breakup deformation in the 'passive' margins bordering the Norwegian-Greenland Sea. In *Marine and Petroleum Geology*, **vol. 19** (1): pp. 79–93.

**MacDonald, G.** (1990). The future of methane as an energy resource. In *Annual Review of Energy*, **vol. 15**: pp. 53–83.

**Makogon, Y.** (1965). Hydrate formation in gas bearing strata under permafrost. In *Gazovaya promyshlennost*.

**Makogon, Y., Holditch, S. and Makogon, T.** (2004). Proven reserves and basics for development of gas hydrate deposits. In *AAPG Hedberg Conference*. Vancouver, BC, Canada, p. 3.

**Makogon, Y. F., Holditch, S. A. and Makogon, T. Y.** (2007). Natural gas-hydrates – A potential energy source for the 21st Century. In *Journal of Petroleum Science and Engineering*, **vol. 56** (1-3): pp. 14–31.

**Mao, W. L., Mao, H.-k., Goncharov, A. F., Struzhkin, V. V., Guo, Q., Hu, J., Shu, J., Hemley, R. J., Somayazulu, M. and Zhao, Y.** (2002). Hydrogen Clusters in Clathrate Hydrate. In *Science*, **vol. 297** (5590): pp. 2247–2249.

**Martin, R. A., Nesbitt, E. A. and Campbell, K. A.** (2009). The effects of anaerobic methane oxidation on benthic foraminiferal assemblages and stable isotopes on the hikurangi margin of eastern new zealand. In *Marine Geology*, **vol. In Press, Corrected Proof**: pp. –.

**Maslin, M. and Thomas, E.** (2003a). Balancing the deglacial global carbon budget: the hydrate factor. In *Quaternary Science Reviews*, **vol. 22**: pp. 1729–1736.

**Maslin, M. and Thomas, E.** (2003b). The Clathrate Gun is firing blanks: evidence from balancing the deglacial global carbon budget. In *EGS-AGU-EUG Joint Assembly*. Nice, France, pp. 12,015–.

**Max, M., Johnson, A. and Dillon, W.** (2006). Economic Geology of Natural Gas Hydrate, vol. 9 of *Coastal Systems and Continental Margins*. Springer, Dordrecht, 341 pp.

**Max, M. D. and Lowrie, A.** (1996). Oceanic methane hydrates: A "Frontier" gas resource. In *Journal of Petroleum Geology*, **vol. 19** (1): pp. 41–56.

**Mazzini, A., Svensen, H., Hovland, M. and Planke, S.** (2006). Comparison and implications from strikingly different authigenic carbonates in a Nyegga complex pockmark, G11, Norwegian Sea. In *Marine Geology*, **vol. 231** (1-4): pp. 89–102.

**McCauley, R., Fewtrell, J., Duncan, A., Jenner, C., Jenner, M.-N., Penrose, J., Prince, R., Adhitya, A., Murdoch, J. and McCabe, K.** (2000). Marine Seismic Surveys - A Study of Environmental Implications. In *APPEA JOURNAL*, **vol. 1**: pp. 692–708.

**McCauley, R. D., Fewtrell, J. and Popper, A. N.** (2003). High intensity anthropogenic sound damages fish ears. In *The Journal of the Acoustical Society of America*, **vol. 113** (1): pp. 638–642. doi:10.1121/1.1527962.

**McGrail, B., Schaef, H., White, M., Zhu, T., Kulkami, A., Hunter, R., S.L.Patil, Owen, A. and Martin, P.** (2007). Using Carbon Dioxide to Enhance Recovery of Methane from Gas Hydrate Reservoirs: Final Summary Report. Tech. Rep. PNNL-17035, Pacific Northwest National Laboratory.

**Mehta, A., Hebert, P., Cadena, E. and Weatherman, J.** (2003). Fulfilling the Promise of Low-Dosage Hydrate Inhibitors: Journey From Academic Curiosity to Successful Field Implementation. In *SPE Production and Facilities*, **vol. 18** (1): pp. 73–79.

**MH21** (2008). Impacts of the second on-shore methane hydrate production test results on the Japanese resource development. Provided by Japanese MH21 research program.

**Mienert, J., Andreassen, K., Posewang, J. and Lukas, D.** (2000). Changes of the Hydrate Stability Zone of the Norwegian Margin from Glacial to Interglacial Times. In *Annals of the New York Academy of Sciences*, **vol. 912** (1): pp. 200–210.

**Mienert, J. and Bryn, P.** (1997). Gas hydrate drilling conducted on the European margin. In *Eos Transactions*, **vol. 78** (49): pp. 567–567.

**Mienert, J., Bünz, S., Guidard, S., Vanneste, M. and Berndt, C.** (2005a). Ocean bottom seismometer investigations in the Ormen Lange area offshore mid-Norway provide evidence for shallow gas layers in subsurface sediments. In *Marine and Petroleum Geology*, **vol. 22** (1-2): pp. 287–297.

**Mienert, J. and Posewang, J.** (1999). Evidence of shallow- and deep-water gas hydrate destabilizations in North Atlantic polar continental margin sediments. In *Geo-Marine Letters*, **vol. 19** (1-2): pp. 143–149.

**Mienert, J., Vanneste, M., Bünz, S., Andreassen, K., Haflidason, H. and Sejrup, H. P.** (2005b). Ocean warming and gas hydrate stability on the mid-Norwegian margin at the Storegga Slide. In *Marine and Petroleum Geology*, **vol. 22** (1-2): pp. 233–244.

**Milkov, A. and Sassen, R.** (2001). Estimate of gas hydrate resource, northwestern Gulf of Mexico continental slope. In *Marine Geology*, **vol. 179**: pp. 71–83.

**Milkov, A. V.** (2004). Global estimates of hydrate-bound gas in marine sediments: how much is really out there? In *Earth-Science Reviews*, **vol. 66** (3-4): pp. 183–197.

**Milkov, A. V., Claypool, G. E., Lee, Y.-J., Xu, W., Dickens, G. R., Borowski, W. S. and ODP Leg 204 Scientific Party** (2003). In situ methane concentrations at Hydrate Ridge, offshore Oregon: New constraints on the global gas hydrate inventory from an active margin. In *Geology*, **vol. 31** (10): pp. 833–836.

**Milkov, A. V. and Sassen, R.** (2000). Thickness of the gas hydrate stability zone, Gulf of Mexico continental slope. In *Marine and Petroleum Geology*, **vol. 17** (9): pp. 981 – 991. ISSN 0264-8172. doi:DOI: 10.1016/S0264-8172(00)00051-9.

**Milkov, A. V. and Sassen, R.** (2002). Economic geology of offshore gas hydrate accumulations and provinces. In *Marine and Petroleum Geology*, **vol. 19** (1): pp. 1–11.

**Milkov, A. V., Sassen, R., Novikova, I. and Mikhailov, E.** (2000). Gas Hydrates at Minimum Stability Water Depths in the Gulf of Mexico: Significance to Geohazard Assessment. In *Gulf Coast Association of Geological Societies Transactions*, **vol. L**: pp. 217–224.

**Minshull, S., Spence, T. and Singh, G.** (1993). Velocity Structure of a Gas Hydrate Reflector. In *Science*, **vol. 260** (5105): pp. 204–207.

**Minshull, T. A., Singh, S. C. and Westbrook, G. K.** (1994). Seismic velocity structure at a gas hydrate reflector, offshore western Colombia, from full waveform inversion. In *Journal of Geophysical Research*, **vol. 99** (B3): pp. 4715–4734.

**MMS** (2008). Preliminary Evaluation of In-Place Gas Hydrate Resources: Gulf of Mexico Outer Continental Shelf. Tech. Rep., U.S. Department of the Interior, Minerals Management Service, Resource Evaluation Division.

**Moessner, pers. comm.** (2008). Personal communication.

**Mohammadi, A. H.** (2001). HWHydrate - software for calculating phase equilibria using hydrates.

**Moridis, G. J. and Collett, T. S.** (2003). Strategies for gas production from hydrate accumulations under various geological and reservoir conditions. In *Proceedings, TOUGH Symposium 2003, Lawrence Berkeley National Laboratory, Berkeley, California, May 12 to 14, 2003*. p. 8.

**Moridis, G. J. and Kowalsky, M.** (2006). Depressurization-induced gas production from Class 1 and Class 2 hydrate deposits. In *Proceedings, TOUGH Symposium 2006, Lawrence Berkeley National Laboratory, Berkeley, California, May 15 to 17, 2006*. p. 8.

**Moridis, G. J. and Sloan, E. D.** (2007). Gas production potential of disperse low-saturation hydrate accumulations in oceanic sediments. In *Energy Conversion and Management*, **vol. 48** (6): pp. 1834–1849.

**MPE/NPD** (2008). Facts: The Norwegian Petroleum Sector 2008. Tech. Rep., Ministry of Petroleum and Energy Norwegian Petroleum Directorate.

**Nadim, F., Kvalstad, T. J. and Guttormsen, T.** (2005). Quantification of risks associated with seabed instability at Ormen Lange. In *Marine and Petroleum Geology*, **vol. 22** (1-2): pp. 311–318.

**NGI** (1997). Møre and Vøring Soil Investigation 1997 Part B - Geotechnical Data. Tech. Rep., Norwegian Geotechnical Institute.

**Ning, F., Jiang, G. and Zhang, L.** (2008). Comprehensive utilization of geothermal and solar energy to exploit gas hydrates buried in oceanic sediments. In *Proceedings of the 6th International Conference on Gas Hydrates (ICGH 2008), Vancouver, British Columbia, Canada, July 6-10, 2008.* p. 6.

**Norske Shell** (1987). Draugen-Feltet Konsekvensutredning. Tech. Rep., Norske Shell.

**NPD** (2005). The petroleum resources on the Norwegian Continental Shelf. Tech. Rep., Norwegian Petroleum Directorate.

**NPD** (2007). Resource report 2007. URL `http://www.npd.no/English/-Produkter+og+tjenester/Publikasjoner/Ressursrapporter/2007/coverpage.htm`.

**NPD** (2009). 20. konsesjonsrunde Veiledning til Søknad om Utvinningstillatelse.

**NPD** (2009a). Drilling on shallow gas discovery in the North Sea - 35/2-2. online, 23.7.2009.

**NPD** (2009b). Forskning om fisk og seismikk. Available online, 28.10.2009. URL `http://www.npd-.no/no/Nyheter/Nyheter/2009/Fo% -rskning-om-fisk-og-seismikk/`.

**NPD** (2009c). Resource report 2009. URL `http://www.npd.no/en/Publications/Resource--Reports/2009/`.

**NPD** (2009d). The NPD's Fact-pages. URL `http://www.npd.no/engelsk/cwi/pbl/en/index-.htm`.

**NPR** (2007). National Petroleum Report. Tech. Rep., The National Petroleum Council. URL `http://www.npc.org/`.

**Numasawa, M., Yamamoto, K., Yasuda, M., Fujii, T., Fujii, K., Dallimore, S. R., Wright, J. F., Nixon, F. M., Imasato, Y., Cho, B., Ikegami, T., Sugiyama, H., Mizuta, T., Kurihara, M. and Masuda, Y.** (2008). Objectives and operation overview of the 2007 JOGMEC/NRCAN/AURORA Mallik 2L-38 gas hydrate production test. In *Proceedings of the 6th International Conference on Gas Hydrates (ICGH 2008), Vancouver, British Columbia, Canada, July 6-10, 2008.* p. 10.

**Ohgaki, K., Katano, K. and Moritoki, K.** (1994). Exploitation of CH4 Hydrates under the Nankai Trough in Combination with CO2 Storage. In *Kagaku Kogaku Ronbunshu*, **vol. 20**: pp. 121–123.

**OLF** (2003). Regional konsekvensutredning for petroleumsvirksomheten i Norskehavet. Tech. Rep., Oljeindustriens Landsforening.

**Olsgard, F. and Gray, J.** (1995). A comprehensive analysis of the effects of offshore oil and gas exploration and production on the benthic communities of the Norwegian continental shelf. In *Marine Ecology Progress Series*, **vol. 122**: pp. 277–306.

**OPEC** (2008). Organization of the petroleum exporting countries. URL `http://www.opec.org/-home/`.

**Padden, M. and Weissert, H.** (2001). Evidence for Late Jurassic release of methane from gas hydrate. In *Geology*, **vol. 29** (3): pp. 223–226.

**Parameswaran, V., Paradis, M. and Handa, Y.** (1989). Strength of frozen sand containing tetrahydrofuran hydrate. In *Canadian Geotechnical Journal*, **vol. 26**: p. 479.

**Paull, C. and Matsumoto, R.** (1995). Leg 164 Overview. In **Paull, C., Matsumoto, R., Wallace, P. and Dillon, W. P.**, eds., *Proceedings of the Ocean Drilling Programme, Scientific Results*, vol. 164. ODP, p. 8.

**Paull, C., Ussler, W., Holbrook, W., Hill, T., Keaten, R., Mienert, J., Haflidason, H., Johnson, J., Winters, W. and Lorenson, T.** (2008a). Origin of pockmarks and chimney structures on the flanks of the Storegga Slide, offshore Norway. In *Geo-Marine Letters*, **vol. 28** (1): pp. 43–51.

**Paull, C., Ussler III, W., Lorenson, T., Winters, W. and Dougherty, J.** (2005). Geochemical constraints on the distribution of gas hydrates in the Gulf of Mexico. In *Geo-Marine Letters*, **vol. 25** (5): pp. 273–280.

**Paull, C. K., Normark, W. R., Ussler III, W., Caress, D. W. and Keaten, R.** (2008b). Association among active seafloor deformation, mound formation, and gas hydrate growth and accumulation within the seafloor of the Santa Monica Basin, offshore California. In *Marine Geology*, **vol. 250** (3-4): pp. 258–275.

**Paull, pers. comm.** (2008).

**Pecher, I., Henrys, S., Gorman, A. and Fohrmann, M.** (2004). Gas Hydrates on the Hikurangi and Fiordland Margins, New Zealand. In *AAPG Hedberg Conference*. Vancouver, BC, Canada, p. 4.

**Pecher, I. A., Henrys, S. A., Wood, W. T., Kukowski, N., Crutchley, G. J., Fohrmann, M., Kilner, J., Senger, K., Gorman, A. R., Coffin, R. B., Greinert, J. and Faure, K.** (2009). Focussed Fluid Flow on the Hikurangi Margin, New Zealand - Evidence from Possible Local Upwarping of the Base of Gas Hydrate Stability. In *Marine Geology*, **vol. In Press, Accepted Manuscript**: pp. –.

**Perttila, M., Kankaanpaa, H., Kotilainen, A., Laine, A., Lehtoranta, J., Leivuori, M., Myrberg, K. and Stipa, T.** (2006). Implementation of the northern european gas pipeline project - data inventory and further need for data for environmental impact assessment. Tech. Rep., MERI: Report Series of the Finnish Institute of Marine Research No. 58.

**Peters, D., Hatton, G., Mehta, A. and Hadley, C.** (2008). Gas hydrate geohazards in shallow sediments and their impact on the design of subsea systems. In *Proceedings of the 6th International Conference on Gas Hydrates*. p. 7.

**Peterson, C. H., Kennicutt II, M. C., Green, R. H., Montagna, P., Harper, D. E., Powell, E. N. and Roscigno, P. F.** (1996). Ecological consequences of environmental perturbations associated with offshore hydrocarbon production: a perspective on long-term exposures in the Gulf of Mexico. In *Can. J. Fish. Aquat. Sci.*, **vol. 53**: pp. 2637–2654.

**Posewang, J. and Mienert, J.** (1999a). High-resolution seismic studies of gas hydrates west of Svalbard. In *Geo-Marine Letters*, **vol. 19** (1 - 2): pp. 150–156.

**Posewang, J. and Mienert, J.** (1999b). The enigma of double BSRs: indicators for changes in the hydrate stability field? In *Geo-Marine Letters*, **vol. 19** (1 - 2): pp. 157–163.

**Pribnov, D., Kinoshita, M. and Stein, C.** (2000). Thermal Data Collection and Heat Flow Recalculations for Ocean Drilling Program Legs 101-180. Tech. Rep., Institute for Joint Geoscientific Research (GGA). URL `http://www-odp.tamu.edu/publications/heatflow/`.

**Pruess, K.** (2004). The TOUGH Codes–A Family of Simulation Tools for Multiphase Flow and Transport Processes in Permeable Media. In *Vadose Zone J*, **vol. 3** (3): pp. 738–746.

**Rasmussen, E., Frantzen, J.-H., Holbaek-Hanssen, L. E., Thorstensen, L. and Weibull, W.** (2007). Jan Mayen's High Resolution 3-D Seismic Acquisition System. Tech. Rep., University of Tromsø.

**Ravnas, R., Nottvedt, A., Steel, R. J. and Windelstad, J.** (2000). Syn-rift sedimentary architectures in the Northern North Sea. In *Geological Society, London, Special Publications*, **vol. 167** (1): pp. 133–177.

**Riedel, M., Collett, T., Malone, M., Akiba, F., Blanc-Valleron, M., Ellis, M., Guerin, G., Hashimoto, Y., Heuer, V., Higashi, Y., Holland, M., Jackson, P., Kaneko, M., Kastner, M., Kim, J., Kitajima, H., Long, P., Malinverno, A., Myers, G., Palekar, L., Pohlman, J., Schultheiss, P., Teichert, B., Torres, M., Trhu, A., Wang, J., Worthmann, U. and Yoshioka, H.** (2006a). Gas Hydrate Transcet Across Northern Cascadia Margin. In *Geophysical Research Letters*, **vol. 30** (2): pp. 325–330.

**Riedel, M., Collett, T., Malone, M. and the Expedition 311 Scientists** (2005). Proceedings of the Integrated Ocean Drilling Program Volume 311 Expedition Reports Cascadia Margin Gas Hydrates. Integrated Ocean Drilling Program Management International, Inc., for the Integrated Ocean Drilling Program.

**Riedel, M., Long, P. E. and Collett, T. S.** (2006b). Estimates of in situ gas hydrate concentration from resistivity monitoring of gas hydrate bearing sediments during temperature equilibration. In *Marine Geology*, **vol. 227** (3-4): pp. 215–225.

**Ripmeester, J. A., Tse, J. S., Ratcliffe, C. I. and Powell, B. M.** (1987). A new clathrate hydrate structure. In *Nature*, **vol. 325** (6100): pp. 135–136.

**Rise, L., Ottesen, D., Berg, K. and Lundin, E.** (2005). Large-scale development of the mid-Norwegian margin during the last 3 million years. In *Marine and Petroleum Geology*, **vol. 22** (1-2): pp. 33–44.

**Rise, L., Ottesen, D., Longva, O., Solheim, A., Andersen, E. and Ayers, S.** (2006). The Sklinnadjupet slide and its relation to the Elsterian glaciation on the mid-Norwegian margin. In *Marine and Petroleum Geology*, **vol. 23** (5): pp. 569 – 583.

**Rokoengen, K., Rise, L., Bryn, P., Frengstad, B., Gustavsen, B., Nygaard, E. and Sættem, J.** (1995). Upper Cenozoic stratigraphy on the mid-Norwegian continental shelf. In *Norsk Geologisk Tidsskrift*, **vol. 75** (2-3): p. 88.

**Root, T., Price, J., Hall, K., Schneider, S., Rosenzweig, C. and Pounds, J.** (2003). Fingerprints of global warming on wild animals and plants. In *Nature*, **vol. 421**: pp. 57–60.

**Ruppel, C.** (2007). Tapping Methane Hydrates for Unconventional Natural Gas. In *Elements*, **vol. 3** (3): pp. 193–199.

**Ruppel, C., Boswell, R. and Jones, E.** (2008). Scientific results from Gulf of Mexico Gas Hydrates Joint Industry Project Leg IIÂ drilling: Introduction and overview. In *Marine and Petroleum Geology*, **vol. 25** (9): pp. 819–829.

**Sassen, R., Joye, S., Sweet, S. T., DeFreitas, D. A., Milkov, A. V. and MacDonald, I. R.** (1999). Thermogenic gas hydrates and hydrocarbon gases in complex chemosynthetic communities, Gulf of Mexico continental slope. In *Organic Geochemistry*, **vol. 30** (7): pp. 485 – 497.

**Sauter, E. J., Muyakshin, S. I., Charlou, J.-L., Schlüter, M., Boetius, A., Jerosch, K., Damm, E., Foucher, J.-P. and Klages, M.** (2006). Methane discharge from a deep-sea submarine mud volcano into the upper water column by gas hydrate-coated methane bubbles. In *Earth and Planetary Science Letters*, **vol. 243** (3-4): pp. 354–365.

**Schlumberger** (2009). SEED - Fire and Ice: The Story of Gas Hydrates. URL `http://www.seed.slb.com/content.aspx?id=2444`.

**Scholl, D. and Hart, P.** (1993). Velocity and amplitude structures on seismic-reflection profiles - possibly massive gas-hydrate deposits and underlying gas accumulations in the Bering Sea Basin.

**Schultheiss, P. J., Francis, T. J. G., Holland, M., Roberts, J. A., Amann, H., Thjunjoto, Parkes, R. J., Martin, D., Rothfuss, M., Tyunder, F. and Jackson, P. D.** (2006).

Pressure coring, logging and subsampling with the HYACINTH system. In *Geological Society, London, Special Publications*, **vol. 267** (1): pp. 151–163.

**Schwalenberg, K., Haeckel, M., Poort, J. and Jegen, M.** (2009a). Evaluation of gas hydrate deposits in an active seep area using marine controlled source electromagnetics: Results from Opouawe Bank, Hikurangi Margin, New Zealand. In *Marine Geology*, **vol. In Press, Corrected Proof**: pp. –.

**Schwalenberg, K., Scholl, C., Mir, R., Edwards, R. N. and Willoughby, E. C.** (2005a). Gas hydrate assessment using a marine bottom-towed controlled source electromagnetic system: latest results from Cascadia. In *21. Kolloquium Elektromagnetische Tiefenforschung, Haus Wohldenberg, Holle, 3.-7.10.2005,*. p. 10.

**Schwalenberg, K., Willoughby, E., Mir, R. and Edwards, R. N.** (2005b). Marine gas hydrate electromagnetic signatures in Cascadia and their correlation with seismic blank zones. In *First Break*, **vol. 23**.

**Schwalenberg, K., Wood, W., Pecher, I., Hamdan, L., Henrys, S., Jegen, M. and Coffin, R.** (2009b). Preliminary Interpretation of Electromagnetic, Heat flow, Seismic, and Geochemical Data for Gas Hydrate Distribution across the Porangahau Ridge, New Zealand. In *Marine Geology*, **vol. In Press, Accepted Manuscript**: pp. –.

**Sejrup, H. P., Aarseth, I., Haflidason, H., Løvlie, R., Bratten, A., Tjøstheim, G. and Forsberg, C. G.** (1995). Quaternary of the Norwegian Channel: glaciation history and palaeoceanography. In *Norsk geologisk tidsskrift*, **vol. 75** (3-4): p. 65.

**Sejrup, H. P., Haflidason, H., Hjelstuen, B. O., Nygård, A., Bryn, P. and Lien, R.** (2004). Pleistocene development of the SE Nordic Seas margin. In *Marine Geology*, **vol. 213** (1-4): pp. 169–200.

**Sellevoll, M. A.** (1975). Seismic refraction measurements and continuous seismic profiling on the continental margin of Norway between 60o and 69oN. In *Norges Geologiske Undersøkelse*, **vol. 316**: pp. 219–235.

**Selley, R. C.** (1998). Elements of Petroleum Geology. Academic Press.

**Senger, K., Gorman, A. and Fohrmann, M.** (2006). Defining the Hydrate Stability Zone in Low Geothermal Gradient Systems: An example from the Canterbury Slope, New Zealand. Presented at the 5th International Workshop on Methane Hydrates, Edinburgh, U.K.

**Sherwood Lollar, B., Lacrampe-Couloume, G., Slater, G., Ward, J., Moser, D., Gihring, T., Lin, L. H. and Onstott, T.** (2006). Unravelling abiogenic and biogenic sources of methane in the Earth's deep surface. In *Chemical Geology*, **vol. 226**: pp. 328–339.

**Shimizu, H., Kumazaki, T., Kume, T. and Sasaki, S.** (2002). Elasticity of single-crystal methane hydrate at high pressure. In *Phys. Rev. B*, **vol. 65** (21): p. 212,102. doi: 10.1103/PhysRevB.65.212102.

**Shpakov, V. P., Tse, J. S., Tulk, C. A., Kvamme, B. and Belosludov, V. R.** (1988). Elastic moduli calculation and instability in structure I methane clathrate hydrate. In *Chemical Physics Letters*, **vol. 282** (2): pp. 107–114.

**Shute, T.** (2009). Checking in on Deepwater Demand. URL `http://www.fool.com/investing/general/2009/09/30/checking-in-on-deepwater-demand.aspx`.

**Singh, P., Panda, M. and Stokes, P. J.** (2008). Characterization and Quantification of the Methane Hydrate Resource Potential associated with the Barrow Gas Fields. DOE Award No: DE-FC26-06NT42962, University of Alaska - Fairbanks.

**Singh, S. C., Minshull, T. A. and Spence, G. D.** (1993). Velocity structure of a gas hydrate reflector. In *Science*, **vol. 260** (5105): pp. 204 – 207.

**Sloan, E.** (1998a). Gas Hydrates: Review of Physical/Chemical Properties. In *Energy Fuels*, **vol. 12** (2): pp. 191–196.

**Sloan, E. D.** (1998b). Clathrate Hydrates of Natural Gases. Marcel Dekker, New York, NY.

**Sloan, E. D.** (2000). Hydrate Engineering. Tech. Rep., Society of Petroleum Engineers.

**Sloan, E. D.** (2003a). Fundamental principles and applications of natural gas hydrates. In *Nature*, **vol. 426** (6964): pp. 353–363.

**Sloan, E. D.** (2003b). Seven Industrial Hydrate Flow Assurance Lessons from 1993-2003. Tech. Rep., Centre of Hydrate Research.

**Sloan, E. D. and Fleyfel, F.** (1992). Hydrate dissociation enthalpy and guest size. In *Fluid phase equilibria*, **vol. 76**.

**Sloan, E. D. and Koh, C.** (2008). Clathrate Hydrates of Natural Gases, Third Edition. No. 119 in Chemical Industries. CRC Press, Taylor & Francis group, 721 pp.

**Solheim, A., Berg, K., Forsberg, C. and Bryn, P.** (2005a). The Storegga Slide complex: repetitive large scale sliding with similar cause and development. In *Marine and Petroleum Geology*, **vol. 22** (1-2): pp. 97–107.

**Solheim, A., Bryn, P., Sejrup, H., Mienert, J. and Berg, K.** (2005b). Ormen Lange–an integrated study for the safe development of a deep-water gas field within the Storegga Slide Complex, NE Atlantic continental margin; executive summary. In *Marine and Petroleum Geology*, **vol. 22** (1-2): pp. 1–9.

**Solheim, A. and Elverhoi, A.** (1993). Gas-related sea floor craters in the Barents Sea. In *Geo-Marine Letters*, **vol. 13** (4): pp. 235–243.

**Statoil** (2001). Kosekvensutredning - Kristin. Tech. Rep., Statoil.

**Stern, L. A., Kirby, S. H. and Durham, W. B.** (1996). Peculiarities of Methane Clathrate Hydrate Formation and Solid-State Deformation, Including Possible Superheating of Water Ice. In *Science*, **vol. 273** (5283): pp. 1843–1848.

**Stoian, I.** (2008). Seismic studies of gas hydrate in the Ulleung Basin, East Sea, offshore Korea. Master's thesis, School of Earth and Ocean Sciences, University of Victoria.

**Stoian, I., Park, K.-P., Yoo, D.-G., Haacke, R., Hyndman, R., Riedel, M. and Spence, G.** (2008). Seismic reflection blank zone in the Ulleung basin, offshore Korea, associated with high concentrations of gas hydrate. In *Proceedings of the 6th International Conference on Gas Hydrates, Vancouver, Canada*. p. 9.

**Stoker, M. S., Praeg, D., Hjelstuen, B. O., Laberg, J. S., Nielsen, T. and Shannon, P. M.** (2005). Neogene stratigraphy and the sedimentary and oceanographic development of the NW European Atlantic margin. In *Marine and Petroleum Geology*, **vol. 22** (9-10): pp. 977–1005.

**Stow, D. A. V., Faugeres, J.-C., Howe, J., Pudsey, C. and Viana, A.** (2002). Bottom currents, contourites and deep-sea sediment drifts: current state-of-the-art. In **Stow, D. A. V., Pudsey, C. J., Howe, J., Faugeres, J.-C. and Viana, A.**, eds., *Deep-Water Contourite Systems: Modern Drifts and Ancient Series, Seismic and Sedimentary Characteristics*, Geological Society Memoir No. 22. Geological Society, pp. 7–20.

**Sultan, N., Cochonat, P., Foucher, J.-P. and Mienert, J.** (2004). Effect of gas hydrates melting on seafloor slope instability. In *Marine Geology*, **vol. 213** (1-4): pp. 379–401.

**Sung, W. and Kang, H.** (2003). Experimental Investigation of Production Behaviors of Methane Hydrate Saturated in Porous Rock. In *Energy Sources, Part A: Recovery, Utilization, and Environmental Effects*, **vol. 27**: p. 13.

**Sung, W., Lee, H., Lee, H. and Lee, C.** (2002). Numerical Study for Production Performances of a Methane Hydrate Reservoir Stimulated by Inhibitor Injection. In *Energy Sources*, **vol. 24**: pp. 499–512.

**Talukder, A., Bialas, J., Klaeschen, D., Buerk, D., Brueckmann, W., Reston, T. and Breitzke, M.** (2007). High-resolution, deep tow, multichannel seismic and sidescan sonar survey of the submarine mounds and associated BSR off Nicaragua pacific margin. In *Marine Geology*, **vol. 241** (1-4): pp. 33–43.

**Talwani, M., Udintsev, G. B. and White, S. M.** (1974). Introduction and explanatory notes, Leg 38, Deep Sea Drilling Project. In *Initial Reports of the Deep Sea Drilling Project, Volume XXXVIII, covering Leg 38 of the cruises of the Drilling Vessel Glomar Challenger Dublin, Ireland to Amsterdam, The Netherlands, August-September 1974*. University of California, p. 17.

**Tang, L. G., Xiao, R., Huang, C., Feng, Z. P. and Fan, S. S.** (2005). Experimental Investigation of Production Behavior of Gas Hydrate under Thermal Stimulation in Unconsolidated Sediment. In *Energy & Fuels*, **vol. 19**: pp. 2402–2407.

**Tappin, D. R., Watts, P., McMurtry, G. M., Lafoy, Y. and Matsumoto, T.** (2001). The Sissano, Papua New Guinea tsunami of July 1998 – offshore evidence on the source mechanism. In *Marine Geology*, **vol. 175** (1-4): pp. 1–23.

**The Shipboard Scientific Party** (1974). SITES 338-343. In *Initial Reports of the Deep Sea Drilling Project, Volume XXXVIII, covering Leg 38 of the cruises of the Drilling Vessel Glomar Challenger Dublin, Ireland to Amsterdam, The Netherlands, August-September 1974*. University of California, p. 237.

**Tinivella, U., Accaino, F. and Della Vedova, B.** (2008). Gas hydrates and active mud volcanism on the South Shetland continental margin, Antarctic Peninsula. In *Geo-Marine Letters*, **vol. 28** (2): pp. 97–106.

**Townend, J.** (1997). Estimates of conductive heat flow through bottom-simulating reflectors on the Hikurangi and southwest Fiordland continental margins, New Zealand. In *Marine Geology*, **vol. 141**: pp. 209–220.

**Trans Canada** (2008). TransCanada's Alaska Pipeline Project. URL `http://www.transcanada-.com/`.

**Tréhu, A., Torres, M., Bohrmann, G. and Colwell, F.** (2006). 1. Leg 204 Synthesis: Gas Hydrate Distribution and Dynamics in the Central Cascadia Accretionary Complex. In *Scientific Proceedings of the Ocean Drilling Program, Leg 204*. p. 75.

**van Balen, R. T. and Skar, T.** (2000). The influence of faults and intraplate stresses on the overpressure evolution of the Halten Terrace, mid-Norwegian margin. In *Tectonophysics*, **vol. 320** (3-4): pp. 331–345.

**Vanneste, M., Guidard, S. and Mienert, J.** (2005). Bottom-simulating reflections and geothermal gradients across the western Svalbard margin. In *Terra Nova*, **vol. 17** (6): pp. 510–516.

**Vanneste, M., Poort, J., Batist, M. D. and Klerkx, J.** (2002). Atypical heat-flow near gas hydrate irregularities and cold seeps in the Baikal Rift Zone. In *Marine and Petroleum Geology*, **vol. 19** (10): pp. 1257 – 1274. ISSN 0264-8172. doi:DOI: 10.1016/S0264-8172(03)00019-9.

**Victor, D. G.** (2001). The Collapse of the Kyoto Protocol and the Struggle to Slow Global Warming. Princeton University Press, 224 pp. ISBN: 978-1-4008-2406-9.

**Villard, M.** (1896). Dissolution des liquides et des solids dans les gaz. In *J. De Phys. Theor. et Appl.*, **vol. 5**: p. 453.

**von Stackelberg, M. and Jahns, W.** (1954). Feste gashydrate. In *Zeitschrift für Elektrochemie*.

**von Stackelberg, M. and Müller, H.** (1951). On the structure of gas hydrates. In *Journal of chemical physics*.

**Vuletich, A. K., Threlkeld, C. N. and Claypool, G. E.** (1989). Isotopic composition of gases and interstital fluids in sediment of the Vøring plateau, ODP Leg 104, Site 644. In **Eldholm, O., Thiede, J. and Taylor, E.**, eds., *Proceedings of the Ocean Drilling Program, Scientific Results*, vol. 104. p. 21.

**Waite, W. F., Gilbert, L. Y., Winters, W. J. and Mason, D. H.** (2006). Estimating thermal diffusivity and specific heat from needle probe thermal conductivity data. In *Review of Scientific Instruments*, **vol. 77**.

**Walsh, M., Hancock, S., Wilson, S., Patil, S., Moridis, G., Boswell, R., Collett, T., Koh, C. and Sloan, D.** (2008). Preliminary report on the economics of gas production from natural gas hydrates. In *Proceedings of the 6th International Conference on Gas Hydrates (ICGH 2008), Vancouver, British Columbia, Canada, July 6-10, 2008.* p. 11.

**Walters, R., Barnes, P., Lewis, K., Goff, J. and Fleming, J.** (2006). Locally generated tsunami along the Kaikoura coastal margin: Part 2. Submarine landslides. In *New Zealand Journal of Marine and Freshwater Research*, **vol. 40**: pp. 17–28.

**Weibull, W.** (2008). Geological Fluid Flow Systems at Nyegga of the Mid-Norwegian Margin. Master's thesis, University of Tromsø. P 145.

**Westbrook, G., Chand, S., Rossi, G., Long, C., Bünz, S., Camerlenghi, A., Carcione, J., Dean, S., Foucher, J.-P., Flueh, E., Gei, D., Haacke, R., Madrussani, G., Mienert, J., Minshull, T., Nouzé, H., Peacock, S., Reston, T., Vanneste, M. and Zillmer, M.** (2008a). Estimation of gas hydrate concentration from multi-component seismic data at sites on the continental margins of NW Svalbard and the Storegga region of Norway. In *Marine and Petroleum Geology*, **vol. 25** (8): pp. 744 – 758.

**Westbrook, G., Exley, R., Minshull, T., Nouzé, H., Gailler, A., Jose, T., Ker, S. and Plaza, A.** (2008b). High-resolution 3D seismic investigations of hydrate-bearing fluid-escape chimneys in the Nyegga region of the Vøring Plateau, Norway. In *Proceedings of the 6th International Conference on Gas Hydrates (ICGH 2008), Vancouver, British Columbia, Canada, July 6-10, 2008.* p. 12.

**Westbrook, G. K.** (2004). Techniques for the Quantification of Methane Hydrate in European Continental Margins - HYDRATECH - Final Report. Tech. Rep., HYDRATECH Consortium.

**Whalley, E.** (1980). Speed of longitudinal sound in clathrate hydrates. In *Journal of Geophysical Research*, **vol. 85** (B5): pp. 2539–2542.

**Whiffen, B. L., Kiefte, H. and Clouter, M. J.** (1982). Determination of acoustic velocities in xenon and methane hydrates by Brillouin spectroscopy. In *Geophysical Research Letters*, **vol. 9**: pp. 645–648.

**White, M., McGrail, B. and Zhu, T.** (2005). Assessment of Current Technologies for Producing Natural Accumulations of Gas Hydrate. Tech. Rep. DOE Award No. DE-FC26-05NT42666, Batelle Pacific Northwest Division.

**Williams, T. E., Millheim, K. and Liddell, B.** (2005). Methane Hydrate Production from Alaskan Permafrost. Tech. Rep. DE-FC26-01NT41331, Maurer Technology and Anadarko Petroleum.

**Winters, W., Waite, W., Mason, D. and Kumar, P.** (2008). Physical properties of repressurized samples recovered during the 2006 national gas hydrate program expedition offshore India. In *Proceedings of the 6th International Conference on Gas Hydrates (ICGH 2008), Vancouver, British Columbia, Canada, July 6-10, 2008.* p. 10.

**Winters, W. J., Dallimore, S. R., Collett, T. S., Katsube, T. J., Jenner, K. A., Cranston, R. E., Wright, J. F., Nixon, F. M. and Uchida, T.** (1999). Physical properties of sediments from the JAPEX/JNOC/GSC Mallik 2L-38 gas hydrate research well. In *Scientific Results from JAPEX/JNOC/GSC Mallik 2L-38 Gas Hydrate Research Well, Mackenzie Delta, Northwest Territories, Canada*. Geological Survey of Canada, Bulletin 544, pp. 95–100.

**Winters, W. J., Waite, W. F., Hutchinson, D. R. and Mason, D. H.** (2005). Physical property studies in the USGS GHASTLI laboratory. In *Fire in the Ice Newsletter*, **vol. Spring**.

**Winters, W. J., Waite, W. F., Mason, D. H., Gilbert, L. Y. and Pecher, I. A.** (2007). Methane gas hydrate effect on sediment acoustic and strength properties. In *Journal of Petroleum Science and Engineering*, **vol. 56** (1-3): pp. 127–135.

**Wood, W. T. and Gettrust, J. F.** (2001). Deep-tow seismic investigations of methane hydrates. In *Geophysical monograph*, **vol. 124**: pp. 165–178.

**WoodMackenzie** (2008a). Wood Mackenzie Europe (North West) Upstream Service - Frigg.

**WoodMackenzie** (2008b). Wood Mackenzie Europe (North West) Upstream Service - Ormen Lange.

**WoodMackenzie** (2008c). Wood Mackenzie Europe (North West) Upstream Service - Shallow Gas A & B.

**WoodMackenzie** (2009). Wood Mackenzie Europe (North West) Upstream Service - Peon.

**World Bank Group** (2004). Regulation of Associated Gas Flaring and Venting: A Global Overview and Lessons from International Experience. Tech. Rep., The World Bank.

**Yakushev, V.** (2008). Current view of upstream gas industry on gas hydrate studies. In *Vulnerability and Opportunity of Methane Hydrates Workshop, 13-14 March 2008, Laxenburg, Austria.* p. 1.

**Yuan, J. and Edwards, R.** (2000). The assessment of marine gas hydrates through electrical remote sounding: Hydrate without a BSR? In *Geophysical Research Letters*, **vol. 27** (16): pp. 2397–2400.

**Yuan, T., Spence, G., Hyndman, R., Minshull, T. and Singh, S.** (1999). Seismic velocity studies of a gas hydrate bottom-simulating reflector on the northern Cascadia continental margin: Amplitude modeling and full waveform inversion. In *Journal of Geophysical Research*, **vol. 104** (B1): pp. 1179–1192.

**Zatsepina, O. and Buffett, B.** (1998). Thermodynamic conditions for the stability of gas hydrate in the seafloor. In *Journal of Geophysical Research - Solid Earth*, **vol. 103** (10): pp. 127–151.

**Zillmer, M., Flueh, E. R. and Petersen, J.** (2005). Seismic investigation of a bottom simulating reflector and quantification of gas hydrate in the Black Sea. In *Geophysical Journal International*, **vol. 161** (3): pp. 662–678. ISSN 1365-246X.

**Zitha, P. L., He, Y. and Rudolph, S.** (2008). Gas hydrates as energy resource: will they deliver? In *Vulnerability and Opportunity of Methane Hydrates Workshop, 13-14 March 2008, Laxenburg, Austria*. p. 1.

# List of Figures

# List of Tables

# List of Abbreviations

**AVO** amplitude versus offset : A geophysical method for determining pore fluids, based on the difference between near and far offset of a seismic data set.

**APA** awards in pre-defined areas : A system for awarding acreage to oil & gas companies on the NCS, in use since 2003.

**BHSZ** base of the hydrate stability zone

**BSR** bottom simulating reflection : A seismic reflection observed at the interface of a hydrate layer and underlying free gas.

**BTU** British thermal unit : A unit employed in gas sales.

**CAPEX** capital expenditure : Costs accrued during the manufacture of production, storage and offloading facilities. Can include abandonment costs at end of field life.

**CTD** Conductivity-Temperature-Depth : The oceanographer's most important tool, designed to allow the determination of various water masses based on their physical properties.

**dd** decimal degrees

**DLF** distributed low flux : A type of gas hydrate, typically occurring in low saturations over a wide area.

**DSDP** Deep Sea Drilling Programme

**EIA** environmental impact assessment

**EMGS** Electro-Magnetic Geo Services : Norwegian company, originating as a spinoff from Statoil, responsible for the commercialisation of the EM method.

**FHF** focussed high flux : A type of gas hydrate, typically occurring in high saturations in a locally constrained area.

**GDF** glacigenic debris flow

**GDP** gross domestic product

**GIIP** Gas initially in place : The amount of gas, quoted at standard atmospheric pressure, held in a reservoir.

**GG** geothermal gradient : The gradient describing the subsurface change in temperature with depth.

**GWC** gas water contact : The density-driven fluid interface between underlying water and overlying gas.

**GHOZ** gas hydrate occurrence zone : Similar to the HSZ, though typically restricted to the zones where hydrate seems to be present.

**HPB** hydrate phase boundary : A physical boundary defining at which pressure-temperature conditions gas hydrate will form and/or dissociate.

**HCPV** Hydrocarbon pore volume : The amount of pore space filled with hydrocarbons.

**HSE** Health, Safety & Environment

**HSZ** hydrate stability zone : The zone, defined on the basis of pressure-temperature conditions and the hydrate phase boundary, in which gas hydrates may potentionally form.

**IODP** Integrated Ocean Drilling Programme

**IPOD** International Programme for Ocean Drilling

**LNG** Liqufied natural gas

**MEG** monoethylene glycol : An inhibitor frequently used to prevent hydrate blockages in pipelines.

**MDT** Modular Formation Dynamics Tester : Equipment used to test how much hydrocarbons a reservoir may produce.

**My** million years

**NAC** Norwegian Atlantic Current

**NCC** Norwegian Coastal Current

**NCM** Norwegian continental margin

**NCS** Norwegian continental shelf : The Norwegian continental shelf is typically subdivided into the Norwegian sector of the North Sea, the Norwegian Sea and the Barents Sea.

**NSDW** Norwegian Sea Deep Water

**NSAIW** Norwegian Sea Arctic Intermediate Water

**NGI** Norwegian Geotechnical Institute

**NTNU** Norwegian University of Science and Technology

**OBS** ocean bottom seismometer : Equipment used to measure P- and S-waves propagating through the subsurface.

**OBC** ocean bottom cable : Technique of collecting information on both P- and S-waves by deploying a cable with multi-component hydrophones on the seabed.

**ODP** Ocean Drilling Programme

**OTG** oceanic thermal gradient : An acronym to describe the rate at which temperature changes with depth for a given water column.

**OPEC** Organization of the Petroleum Exporting Countries

**OPEX** operational expenditure : Costs accrued during the day-by-day operation of a field.

**P-T** pressure-temperature

**psu** practical salinity units

**ppm** parts per million

**PDO** plan for development & operation : A technical document submitted by an operator to Norwegian authorities in conjunction with a request to develop a field.

**SINTEF** The Foundation for Scientific and Industrial Research

**SMI** sulfate methane interface : The depth to which methane-reducing bacteria break down gas hydrates.

**THF** tetrohydrofuran : A synthetic gas hydrate manufactured to allow laboratory experiments on hydrate properties.

**UTM** Universal Transverse Mercator : A geographic coordinate system.

# Appendices

# Appendix A

# Health, Safety and Environment evaluation

The Nyegga development would be as much a political statement as a technical challenge. Similar to the Shtokman development in the eastern Barents Sea (Gazprom 2009), development of a hydrate resource on the Norwegian shelf is as much a question of proving that it is possible and establish the knowledge base of extracting further hydrate resources. Nonetheless, the project would also be under immense pressure to prove that safe and prudent methods exist for developing marine hydrate resources with a minimal impact on the environment.

## A.1 Environmental impact of oil & gas activities

Direct impact of oil & gas activities fundamentally relates to environmental effects during data acquisition (notably sesimic shooting) as well as release of harmful chemicals (e.g. oil spills, cuttings disposal) in the vicinity of production facilities.

The effect of seismic acquisition, specifically the high-pressure air released by operation of the airgun, on fish stocks and marine mammals is still disputed (McCauley *et al.* 2000; 2003, Harris *et al.* 2001). Direct short-term damage is, especially compared to the early days of seismic shooting using chemical explosives, not considered an environmental problem, but the longer-term impact on fish behaviour is still poorly understood (Gausland 2003). A field experiment by Hassel *et al.* (2004) suggests a low impact of seismic shooting on the behaviour of lesser sand eel, and no effect on their abundance. Direct damage to fish stocks is expected within a radius of 5 m of the source, resulting on a stock-level per day mortality rate of $< 0.018\%$, deemed insignificant considering the natural species mortality rate of 5-15% (Gausland 2003). The effect on behaviour changes of fish stocks is more difficult to determine, being affected by external factors such as physical conditions of the sea, food supply chains and the behavioural pattern of the species present. However, it is generally agreed that behavioural impact is restricted to a maximum radius of 1-2 km of an ongoing seismic survey (Gausland 2000; 2003). A recent survey, conducted during the seismic acquisition of the Norwegian Petroleum Directorate off Lofoten, has an objective of monitoring the status of the fish stocks prior, during and after the acquisitions (NPD 2009b). Results are expected in early

2010.

Oil & gas activities typically result in localised sediment contamination within 1-3 km of a platform (Olsgard and Gray 1995, Gray *et al.* 1999). Hydrocarbons, essentially sourced from cuttings extracted when using oil-based muds, are deemed responsible for increasing toxicity (Grant and Briggs 2002). Norwegian authorities banned the discharge of oil-based drilling mud and cuttings in 1993, and none of the above has since been intentionally discharged to sea (Gray *et al.* 1999). Even though long-term effects are observed both in sediments and local benthic organisms, larger inverterbrates and fish appear to be generally unaffected, perhaps due to their higher mobility (Peterson *et al.* 1996).

## A.2 The Norwegian Sea

A very comprehensive regional environmental impact assessment (EIA) was conducted for the Norwegian Sea in 2003 (OLF 2003). In addition, field-based environmental impact assessments are available for numerous oil & gas fields in the Norwegian Sea, including Ormen Lange (Hydro 2003), Kristin (Statoil 2001) and Draugen (Norske Shell 1987). The regional EIA covers topics well beyond the scope of this thesis, including the usage of environmentally-friendly technologies (such as sub-sea separation and reinjection of produced water, measures addressing energy efficiency and the 'power from shore' concept), the consequences of atmospheric and marine emissions of gases, chemicals and produced water (Figure A.1[1]), scenarios for sudden and catastrophic oil spills and its impact on tourism in coastal Norway, the conflict with the Norwegian fishery industry, consequences on cultural artifacts (e.g. shipwrecks) as well as the effect of oil & gas activities on the Norwegian society. Of most interest, however, is the spatial definition of specially sensitive ecosystems where oil & gas activities should be highly restricted.

The Ormen Lange EIA is a 211 page document that underlines the point that 'The development, operation and subsequent abandonmnet of Ormen Lange will be addressed with Health, Safety & Environment (HSE) in mind at all times'. While the document was critisised for being vague, especially with regards to strict monitoring of the 1200 km long Langeled export pipeline (Perttila *et al.* 2006), it provides a solid overview of the key chalenges with developing Ormen Lange in a safe and environmentally-friendly fashion. In addition, it provides an overview of the measures taken to reduce negative side effects of the development. Coral reefs, occurring in abundance in the Storegga area, have been considered and avoided when pipeline routes were planned. The consequences of the development, including documentation of the planned air and ocean emissions, is in line with international and Norwegian law (Hydro 2003). Modelling of sudden releases of gas or condensate show limited effect on the environment, given the condensate's low residence time and rapid dilution in the water column. Leakage of inhibitors such as MEG from the Nyhamna pipeline is considered to have a low probability, and, due to the MEG's low toxicity and solubility, have a minor environmental effect (Hydro 2003). Socio-economic consequences include a need of 43 000 man work years in Norway alone, as well as a 15 GNOK[2] direct Norwegian share in investment

[1] Brønntesting = Well testing, Supplybåter = Supply boats, Fakkel = Flaring, Dieselmotorer = Diesel engines, Turbiner = Gas-powered power plants on platforms, Skyttletankere = Shuttle tankers, Lagring = Storage, Lasting = Loading, Kaldventilering og diffuse utslipp = Diffusive emissions.

[2] The figure is given in 2002-NOK, and is equivalent to 56% of the total investment.

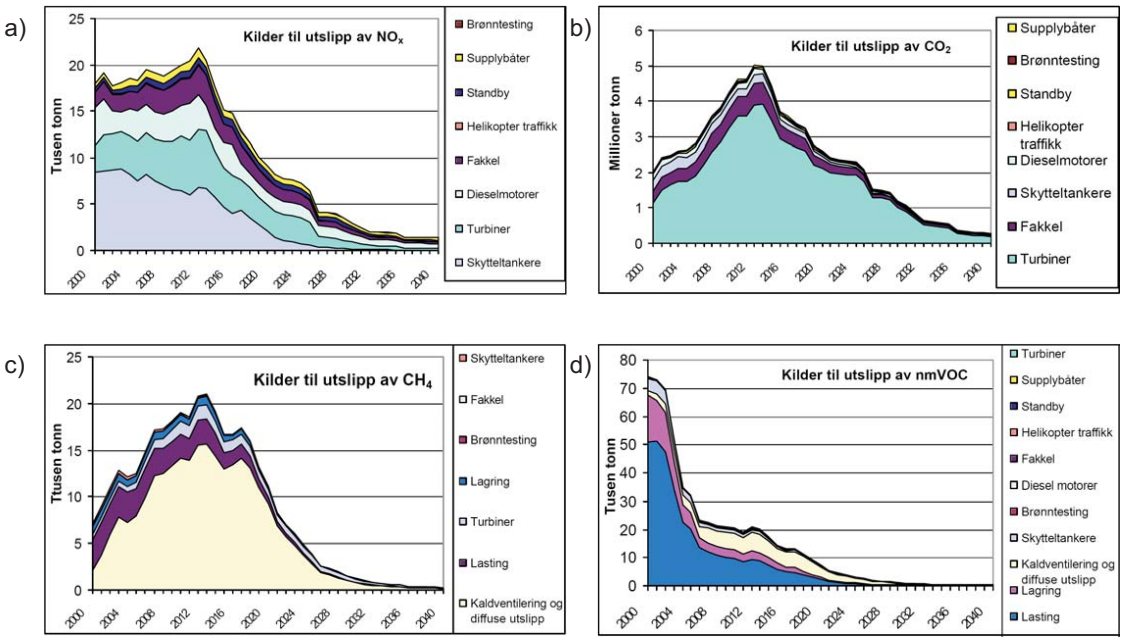


Figure A.1: Sources of harmful emissions from oil & gas activities in the Norwegian Sea, as identified by OLF (2003). Data includes planned emissions from 8 planned developments as well as exploration drilling. a) NOx emissions, b) CO2 emissions, c) CH4 emissions and d) nmVOC emissions. Please refer to the text for Norwegian translations.

(Hydro 2003).

## A.3 Hazards identified

The need for a platform, particularly for the injection of warm brine, needs to consider platform placement with regard to the high-risk zones associated with the wellheads (Khan and Amyotte 2002).

Uncontrolled gas, and associated condensate, leakage from wellheads has been identified as a potential hazard by OLF (2003). Johansen (2002) model such rising plumes and conclude that gas plumes are unlikely to reach the surface, especially for deep-water fields such as Ormen Lange. This is due to a collection of phenomena, including the inhibition of upward gas motion through increased pressure, consequences of oceanic currents and biological break-down of hydrocarbons. Under modelled conditions, which represent only one instance in a dynamically changing setting, the gas plume stabilised approximately 500 m from source and never reached the ocean surface (Figure A.2).

The uncertain nature of hydrate production, related primarily due to the lack of experience, may make drilling into the HSZ a risk. Experience gained from hydrate-drilling on the Alaskan North Slope (Boswell *et al.* 2008, Numasawa *et al.* 2008) as well as the Nankai Trough (Colwell *et al.* 2004), will somewhat reduce the risk but it is vital to prepare for the unexpected prior to the operation.

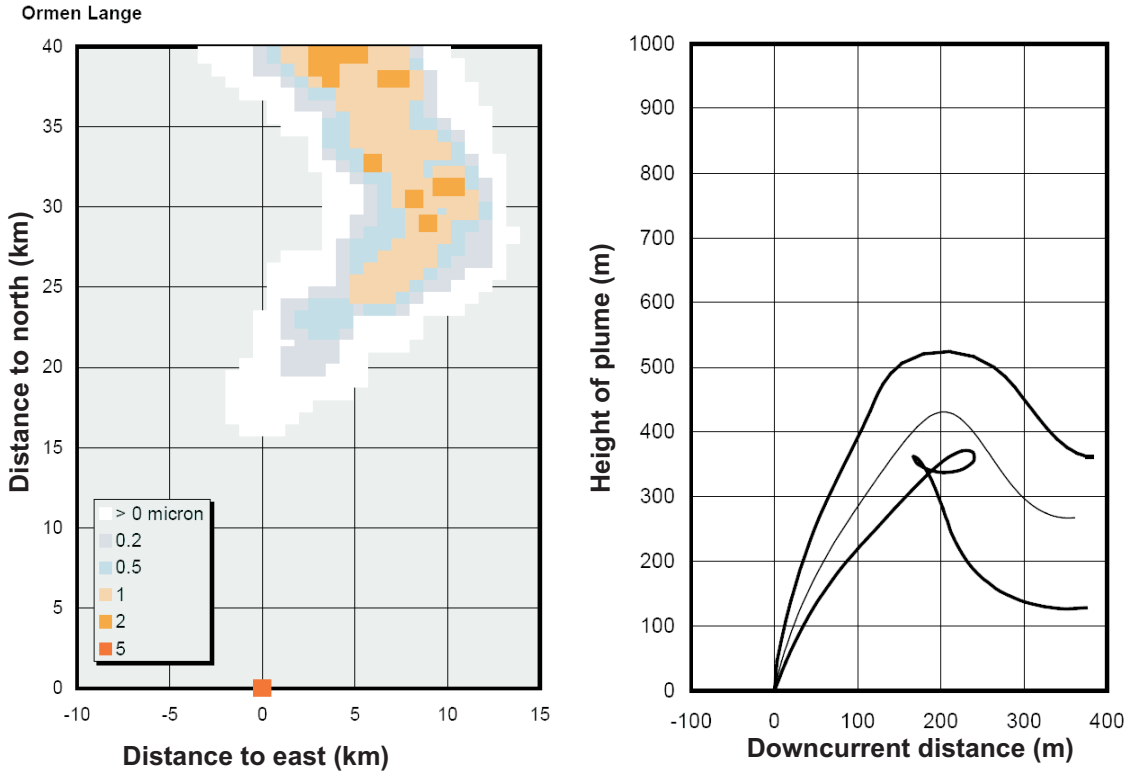


Figure A.2: Gas leakage modelling at Ormen Lange. The scenario presented attempts to model a gas blowout at the location of the Ormen Lange field. The left diagram shows the areal extent of the thin ($< 0.6\mu$ m) condensate layer at the ocean surface following release of 442 $m^3$ /day for 11 hours. The right figure shows the location of the gas plume within the water column. In essence, these figures illustrate that the modelled blowout scenario will have minimal impact at these quantities, and the natural breakdown of hydrocarbons will quickly disperse the hydrocarbons. Figure modified from Johansen (2002).

# Appendix B

# Accompanying data

The appendix contains a collection of material relevant to this thesis that does not fit into the main body of the work. Most useful information, including all data, high-resolution plots and software, can be found on the accompanying DVD. It is strongly recommended to view this thesis in its electronic version to fully appreciate the various coloured figures.

The accompanying DVD includes the following folders:

- Bibtex: contains the full bibliography in BibTex format.
- Content: including the high-resolution .pdf of the thesis as well as the .tex files containing the actual text.
- Conversion factors: includes a conversion factor overview sheet, from www.npd.no.
- Figures: contains high-resolution versions of the figures, mostly in .pdf format.
- HSZ model: a storage place for the MatLab code used in the HSZ modelling.
- Interpretation: files including the seismic interpretation and gridded horizons.
- Petrel: includes the Petrel project of the Nyegga prospect.
- Volumetric cases: summary sheets of the various zones for which volumes were calculated.